Synthesis and Exploration of New Gold(III) Complexes

Franziska Stefanie Ihlefeldt

Master's Thesis, Department of Chemistry

UNIVERSITETET I OSLO

15.05.2015

2015

Synthesis and Exploration of New Gold(III) Complexes

Franziska Stefanie Ihlefeldt

http://www.duo.uio.no/

Trykk: Reprosentralen, Universitetet i Oslo

Preface

The work presented in this master's thesis was carried out at the Department of Chemistry, University of Oslo, in the research group of Professor Mats Tilset. I truly enjoyed being a part of this group for these two years, not only because of the fun and exciting gold(III) chemistry I was working with, but also the great people who added so much more to my life in Norway.

First of all I would like to thank my supervisor Mats Tilset for welcoming me into his group with open arms and offering me such an interesting topic to work on under excellent supervision. A big thank you also goes to Marte Sofie Holmsen for all her help and feedback while writing this thesis and for organizing our movie and soup nights. Thanks for the [Au]some time!

Thanks to crystallographer Sigurd Øien-Ødegaard for always taking the time to look through my attempts at crystallization and splitting off the bad twin where it was needed. I also want to thank the theoretical chemists Ainara Nova and especially David Balcells for guiding me through the field of computational chemistry. For the experiments presented in this thesis NMR and MS data are indispensable, so I want to thank Frode Rise and Dirk Petersen for taking such a great care of the NMR facilities and offering immediate help if any kind of problem occurred and also Osamu Sekiguchi for recording all my mass spectra.

I would like to thank past and present members of the Tilset group, catalysis group and people from the 2nd and 3rd floor, especially Eirin Langseth for introducing me to the lab and Knut Hylland for being a splendid office mate and for all our conversations about chemistry and the world. For manifold fruitful discussions I would like to thank Richard H. Heyn.

Last but not least I want to thank my family and friends, my parents in particular, for supporting me throughout my journey in Norway and for always being there.

Tusen takk! Danke schön!

Oslo, May 2015
Franziska Stefanie Ihlefeldt

Abstract

The interest in organogold compounds has seen a great development during the last years. Gold(III) complexes are investigated as potential anti-cancer drugs and homogeneous catalysts for organic transformations. Nucleophilic additions to alkenes are of high practical value but also very challenging. Gold(III)-mediated methods for these reactions are underdeveloped, but alkyl gold(III) complexes are assumed to be important intermediates in the catalytic process. Here, the synthesis of a number of novel alkyl gold(III) complexes, that have been characterized by NMR spectroscopy, mass spectrometry and X-ray crystallography, is presented. A DFT geometry optimization of the structure of one of the new alkyl gold(III) complexes and its isomers was performed to shed light on the stabilities of different isomers. Geometry optimization of the solid-state structure was performed and a good agreement between the X-ray and DFT structure was found. Some unexpected products were obtained and possible mechanisms regarding the formation were proposed and discussed.

Abbreviations

°C	degrees Celsius
µ	micro
ax	axial
br.	broad (NMR)
cal	calorie(s)
COSY	correlated spectroscopy (NMR)
d	day(s)
d	doublet (NMR)
D	deviation
dd	doublet of doublets (NMR)
ddt	doublet of doublets of triplets (NMR)
DFT	Density Functional Theory
DMSO	dimethyl sulfoxide
dt	doublet of triplets (NMR)
eq	equatorial
eq.	equivalents
ESI	electrospray ionization
Et	ethyl
et al.	*et alii*
g	gram(s)
h	hour(s)
HMBC	heteronuclear multiple-bond correlation (NMR)
HR	high resolution
HSQC	heteronuclear single-quantum correlation (NMR)
Hz	Hertz
J	coupling constant (NMR)
l	liter(s)
m	milli
m	multiplet (NMR)
m/z	mass-to-charge ratio
Me	methyl

min	minutes
MS	Mass Spectrometry
MW	microwave
NMR	Nuclear Magnetic Resonance
NOESY	Nuclear Overhauser Eect Spectroscopy (NMR)
ORTEP	Oak Ridge Thermal Ellipsoid Plot
ppm	parts per million
rel	relative
RMSD	root-mean-square deviation
rt	room temperature
s	singlet (NMR)
t	triplet (NMR)
td	triplet of doublets (NMR)
TFA	trifluoroacetic acid
TFE	trifluoroethanol
tpy	2-(*p*-tolyl)pyridin
Å	Ångstrøm
δ	chemical shift (NMR)

Overview of key compounds

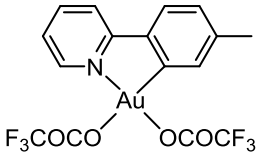

1

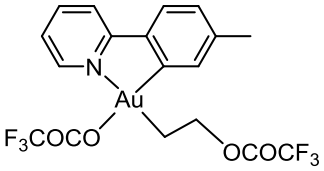

2

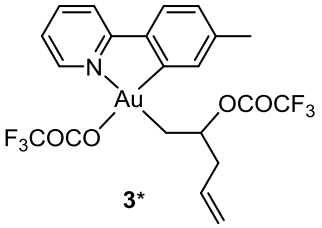

3*

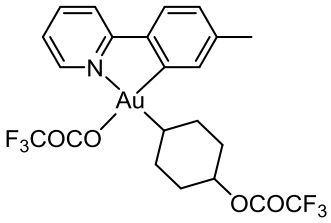

4*

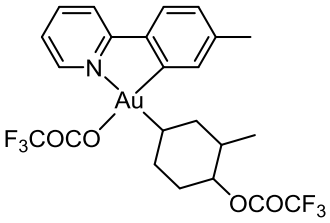

5*

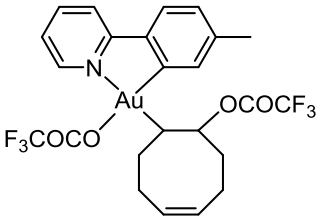

6*

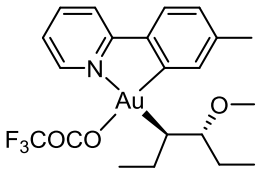

7* (*R*,*R*) and (*S*,*S*)

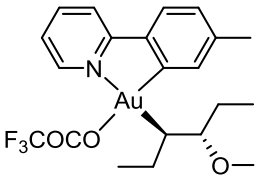

8* (*R*,*S*) and (*S*,*R*)

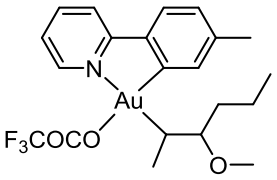

9*

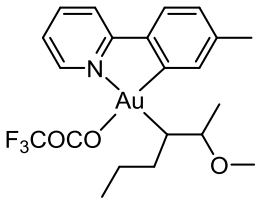

10*

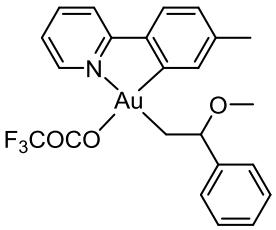

11*

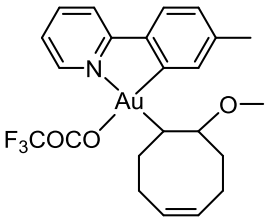

12*

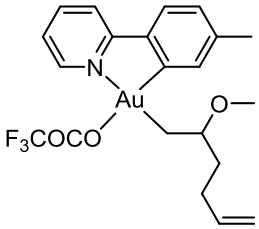

13*

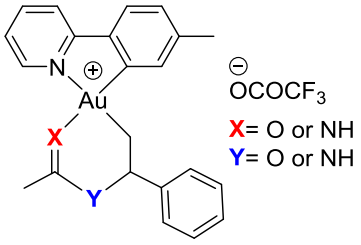

14*

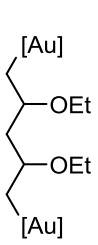

15*

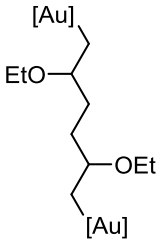

16*

* = new compounds

[Au]: $Au(OCOCF_3)(tpy)$

Aim of the project

The use of gold compounds as catalysts has seen an impressive development in recent years. In the last few years, the focus of the Tilset group has shifted towards gold(III) chemistry. Efficient synthesis protocols for cyclometalated gold(III) complexes have been the starting point for many novel complexes including the first crystallographically characterized gold(III) alkene complex shown below.[1],[2],[3]

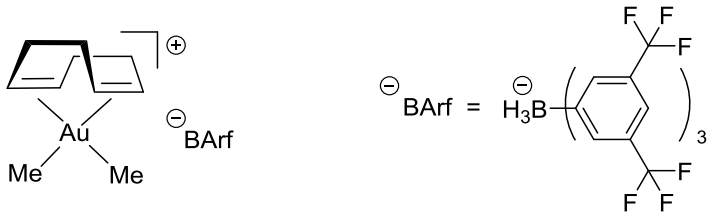

The reactivity of gold complexes is examined with particular emphasis on properties of relevance for catalytic reactions. The Tilset group focuses on gold(III) compounds, as the chemistry of such species remains less investigated than the more commonly encountered gold(I) compounds in catalysis.[4] The research on this gold chemistry has been the topic of several master's and PhD theses in our group.[5],[6] Gold is particularly well known for its ability to catalyze transformations of unsaturated organic molecules, such as alkenes and alkynes. The Tilset group very recently described the gold(III)-mediated nucleophilic attack of trifluoroacetate at ethylene, shown below.[7]

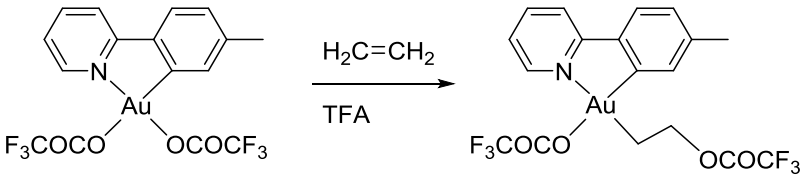

The aim of this project was to investigate the reactivity of $Au(OCOCF_3)_2(tpy)$ towards a wide variety of different alkenes and dienes, including synthesis and characterization of the new alkyl gold(III) complexes. The starting point for the experimental work was the recently published, efficient synthesis of $Au(OCOCF_3)_2(tpy)$.[7]

Contents

1 Introduction

1.1 General Introduction to Gold

Gold is one of the most popular and well-known native metals. It can be found in nature as nuggets or veins in a rock matrix, but also occurs in very low concentrations in seawater.[8] Gold is known for its value and special properties since the earliest of time. It was always associated with wealth, power and beauty. Already in prehistoric time it was collected and processed. Old civilizations such as Aztec, Inca and Egyptian amassed huge amounts of gold. The coffin of Tutankhamun (Egyptian pharaoh 1415-1403 B.C.) contained 112 kg of gold.[9] The fact that some of the oldest gold artifacts found in Mesopotamia date from 6000 B.C.[10] proves the immense durability of this precious metal. Because of its ductility and unusual stability is gold an outstanding material for crafting jewelry.

Nowadays, the usage of gold is not only bound to handcrafts anymore. Due to its high electrical conductivity and corrosion resistance, gold coating finds great applications in the electronics manufacturing industry[11] such as electrical connectors in mobile devices and computers. Also astronauts benefit from the thin gold layer on their space helmet visor. The gold coat reflects the electromagnetic radiation of the sun and protects the user against the effects of radiant energy. Gold also plays an important part in the fields of dental care and medicine.[12],[13] In contrast to gold in its ionic form, elemental gold is biocompatible and has even an E-number[i], E175, which allows its use as food additive. However, since metallic gold is inert to all body fluids, it has no taste, provides no nutrition and leaves the body unaltered. Gold has therefore an advantage as drug candidate compared to for example nickel, because as a result of the highly positive normal potential of gold ($E° = +1.691$ V[10]) the main degradation pathway of gold complexes leads to non-toxic metallic gold. Gold drugs have shown effectiveness against bronchial asthma and different kinds of arthritis.[12] One example being auranofin (**17**, Figure 1), a monomeric gold(I) complex, used to treat rheumatoid arthritis.[14] Cisplatin (*cis*-$PtCl_2(NH_3)_2$) is the renowned anti-cancer drug but interest towards alternative

[i] E numbers are codes for substances approved as food additives for use within the European Union ("E" stands for "Europe").

compounds still retains, since cisplatin is highly toxic to patients and new agents with improved specificity and decreased toxic side effects are needed.[15] The square-planar geometry of Pt(II) is significant for its anti-tumor activity. Special interest is given to the exploration of anti-cancer properties of gold(III) derivatives, since Au(III) is isoelectronic with Pt(II) and therefore likely to show similar activity. Studied compounds are amongst others the neutral monomeric gold(III) complex **18** and the cationic dinuclear gold(III) species **19** (Figure 1) with structures related to the gold(III) complexes that will be presented in this thesis. Complex **18** shows compared to cisplatin higher activity against a leukemia cell line and complex **19**·$(PF_6)_2$ is cytotoxic against certain cisplatin-resistant tumor cells.[16],[17]

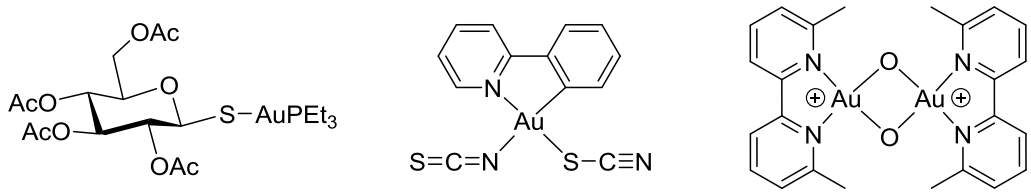

17 **18** **19**

Figure 1: Anti-arthritic gold(I) drug auranofin (**17**)[14],[15] and two organogold(III) complexes **18** and **19**·$(PF_6)_2$ with cytotoxic[16],[17] properties.

In addition to the potential applications in medicine, several organogold(III) complexes show luminescence properties and are studied as luminophors in organic light emitting diodes (OLEDs), which are used to create digital displays in devices such as television screens or mobile phones.[18]

The potential of gold chemistry kept unexplored for a long time, probably because the misconception that gold was a noble immutable element has hindered any progress. But the interest in gold is renewed, with catalysis as its centerpiece.[19] Gold is now an element of major importance in heterogeneous as well as homogeneous catalysis showing exceptional activity for a lot of diverse reactions.[20],[21] Gold catalysis occurs often under much milder reaction conditions than required by other catalysts and that makes it so desirable to work with, even though the origin of this enhanced activity provides still basis for discussion.[22],[23],[24] There are even efforts made to bridge the gap between homogeneous and heterogeneous gold catalysis in order to shed light on the nature of the active gold species involved in the reaction.[25]

1.2 Homogeneous Gold Catalysis

Kharasch *et al.* reported the first C-H bond activation *via* gold(III) already in 1931 but it took many years until further research was conducted in this direction.[26] So the rather young field of homogeneous gold catalysis remained almost silent up to the report by Hashmi *et al.* about the rediscovery of $AuCl_3$ as an effective catalyst for the synthesis of furans.[27] Homogeneous gold catalysis is of high interest in organic synthesis with applications in total synthesis, asymmetric synthesis and C−H activation reactions.[28],[29],[30]

Activation of cumulated, conjugated, or isolated C-C multiple bonds is the most common reactivity mode in gold-catalyzed organic reactions.[21],[22],[31] The ability of gold to behave as a soft and carbophilic Lewis acid allows it to activate unsaturated functionalities such as alkenes, alkynes, allenes but also carbonyls and imines for the attack of a nucleophile.[32],[19] That enables the formation of C-C, C-O, C-N, and C-S bonds under mild conditions. Scheme 1 displays a general catalytic cycle for a gold(I) or gold(III) catalyzed nucleophilic addition to a C-C multiple bond. It is believed that first the gold catalyst **20** interacts with the π-system of the alkene or alkyne to form the intermediate complex **21**, followed by nucleophilic attack yielding the gold alkyl or vinyl complex **22**, respectively. There is much evidence that the nucleophile diastereoselectively adds *anti* to gold to give **22**, but in the cases of norbornenes as well as gold silyl complexes *syn* addition was reported.[19],[33],[34] In the last step protodeauration of the organogold intermediate **22** gives the product and regenerates the gold catalyst **20**.[19]

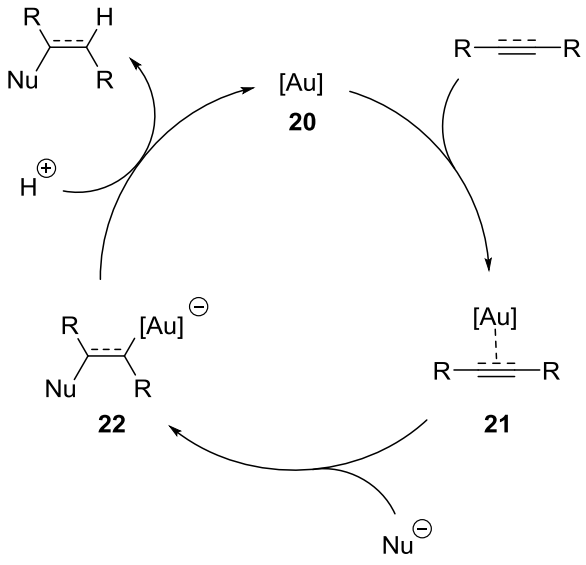

Scheme 1: General mechanistic scheme for gold-catalyzed activation of C-C multiple bonds.[19]

The peculiar π-affinity of gold is not the only factor responsible for its activity and effectiveness. In contrast to most Lewis acids gold is way less oxophilic which holds many advantages. It was recognized quite early that most of the reactions tolerate oxygen, water, alcohols and acidic protons, so neither air nor humidity need to be excluded.[21],[35] That stands in sharp contrast to most air- and moisture-sensitive Lewis acids or transition metal transformations.[36] Also the high tolerance of functional groups, the fine-tunability, for example through varying counter ions, and the ability for asymmetric synthesis have contributed to the success of gold(I) and gold(III) in organic synthesis.[37],[38] Nevertheless, from the catalytic point of view, there are still limitations in the stability of the homogeneous gold catalysts, which tend to precipitate inactive metallic gold with time and therefore have the handicap of catalyst recovery.[32] It should be also mentioned that many gold catalyzed reactions require the presence of silver salts.[22],[24] It has been largely assumed that all of these reactions are catalyzed merely by the gold cation if the silver salt did not catalyze the reaction itself. But it was shown by Shi and co-workers that the presence of silver clearly influenced the gold complexes in solution.[39] The appearance of the complexes formed by mixing gold and silver cations is still under investigation.[40]

While the knowledge about gold(I) catalysts has reached an advanced level, gold(III) catalysis is mainly limited to the use of inorganic gold(III) salts.[41],[42],[43] Most of the organic transformations are catalyzed by rather simple and commercially available gold(III) compounds like $AuCl_3$ and $HAuCl_4 \cdot 3H_2O$.[4] One example being the cycloisomerization of allenyl ketone **23** to the furan derivative **24** catalyzed by $AuCl_3$ (Scheme 2).[27]

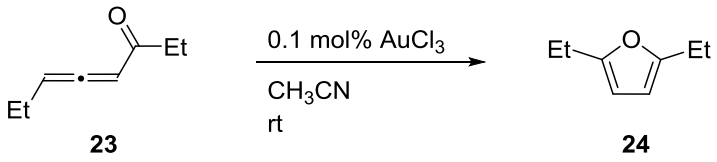

23 **24**

Scheme 2: $AuCl_3$-catalyzed cycloisomerization of allenyl ketone **23**.[27]

The assumed mechanism for $AuCl_3$-catalyzed activation and cyclization of substituted allenes involves π-complexation of an allene unit at the gold(III) center in the first step, followed by nucleophilic attack *via* an internal nucleophile, and protodeauration in the final step, giving the heterocyclic product as well as regenerating the catalyst.[4]

However, the simple binary gold(III) halides as well as tetrachloroauric acid are sensitive to air and moisture. It is therefore desirable to use gold(III) complexes with auxiliary ligands since they are easier to handle due to less sensitivity to air and water, the tolerance towards a larger variety of solvents as well as the possibility to store the complexes without decomposition for a long time.[4] The complexation of gold(III) catalysts might also lead to certain selectivities or significantly different reaction rates in the transformation of the substrates. The latter was impressively demonstrated by Che and co-workers with a report about synthesizing furans *via* cycloisomerization of allenones catalyzed by different gold(III) agents.[44] Scheme 3 depicts the transformation of allenone **25** using a catalyst loading of 1 mol% gold(III) porphyrin **27**, yielding 88% of the furan derivative **26**. Whereas the $AuCl_3$-catalyzed reaction yielded under the exact same reaction conditions only 49% of the heterocyclic product **26**.[44]

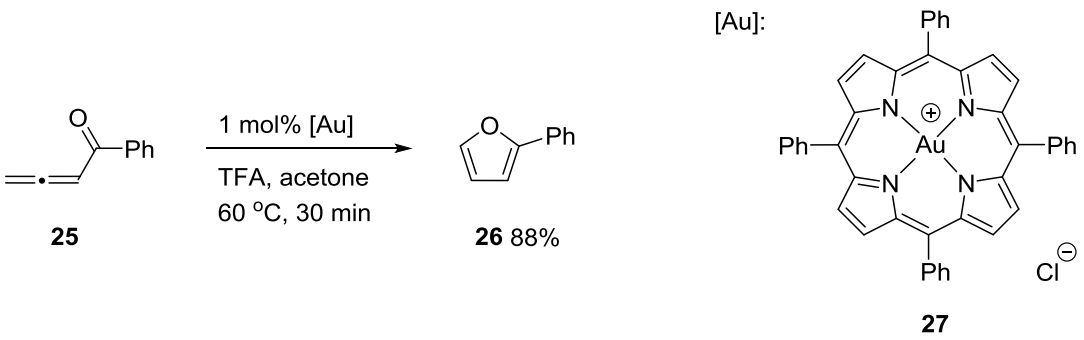

Scheme 3: Cycloisomerization of allenone **25** catalyzed by gold(III) porphyrin **27**.[44]

As shown above, even though $AuCl_3$ and the other rather simple gold(III) catalysts are noted to be reactive catalysts, the efforts to develop more robust and highly chemoselective gold(III) catalysts are worthwhile and recompense in improved yields.

1.3 Synthesis of Cyclometalated Gold(III) Complexes

The key step in the synthesis of new cyclometalated gold(III) complexes is *cyclometalation*, a term first introduced by Trofimenko[45] in 1973. If a ligand in a transition metal complex undergoes an, in general, intramolecular metalation forming a chelate ring that contains a metal-carbon σ-bond, the reaction is called cyclometalation (Scheme 4).

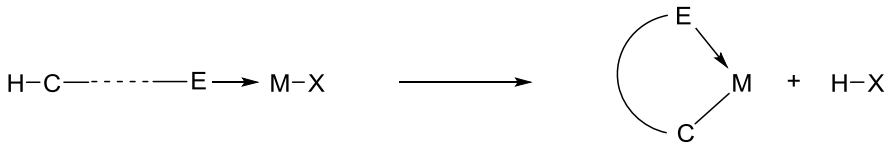

Scheme 4: General scheme for cyclometalation. E: donor atom, M: transition metal, X: leaving group.[46]

Due to direct interaction of the ligand with the metal substrate and hydrogen elimination supported by a suitable leaving group the metal-carbon σ-bond is formed. However, in most cases the reaction proceeds *via* an intermediate ligand-metal complex where the metal-carbon σ-bond is not formed yet.[46]

Until the late 1980's cyclometalation of gold(III) complexes by direct reaction of a ligand with a gold compound was relatively uncommon. Most prevalent was, and still is, the formation of cyclometalated gold(III) complexes *via* transmetalation from organomercury(II) compounds.[47],[48] The transfer of the organic group from Hg to Au is probably one of the most versatile methods for the synthesis of cycloaurated gold(III) complexes.[49] It is often supported by the use of NMe_4Cl to encourage precipitation of $[NMe_4]_2[Hg_2Cl_6]$, shifting the equilibrium in favor of the organogold complex.[50] Nevertheless, the use of highly toxic organomercury(II) compounds[51] is rather unattractive and hampers the potential use as chemotherapeutics.

Direct metalation is a great method to avoid the use of severely toxic organomercury(II) compounds and time consuming preparation of any organometal reagents needed for transmetalation. Constable and Leese published in 1989 the preparation of the cycloaurated complexes $AuCl_2$(ppy) (**30**) by transmetalation from the organomercury derivative, giving 90% yield, as well as by direct auration, giving 80% yield from $AuCl_3$(ppyH) (**29**).[52] The reaction of 2-phenylpyridine (**28**) with $H[AuCl_4]$ gives the square-planar *N*-bonded $AuCl_3$(ppyH) (**29**) that yields the cyclometalated gold(III) complex **34** after heating in an $MeCN/H_2O$ solution at reflux temperature (Scheme 5).

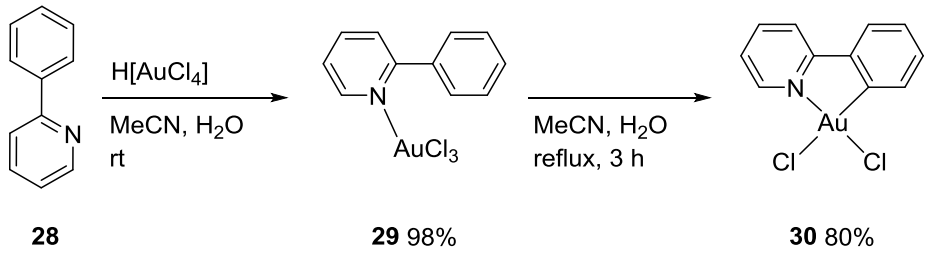

28 **29** 98% **30** 80%

Scheme 5: Synthesis of $AuCl_2$(ppy) (**30**) reported by Constable and Leese.[52]

Other researchers, including our group, had problems reproducing the results of the mercury-free reaction pathway presented by Constable and Leese.[50],[53] Eisenberg and co-workers reported quantitative recovery of $AuCl_3$(ppyH) (**29**) when the thermolysis reaction was attempted.[54] They indicated that the reflux temperature of the MeCN/H_2O solution might have been too low for what is required to activate the ortho C-H bond and form the cyclometalated complex, $AuCl_2$(ppy) (**30**).[54]

12 years later Henderson *et al.* followed the same method for the cycloauration as reported by Constable *et al.* but used 2-(*p*-tolyl)pyridine (**31**) instead of 2-phenylpyridine (**28**) (Scheme 6).[55] The methyl group in the gold(III) 2-(*p*-tolyl)pyridine derivative **33** unambiguously differentiates between the pyridyl and phenyl rings, for example by reducing the possibility of crystallographic disorder in X-ray crystal structure determination,[50] and is therefore a very useful starting material in the study of cyclometalated gold(III) complexes.

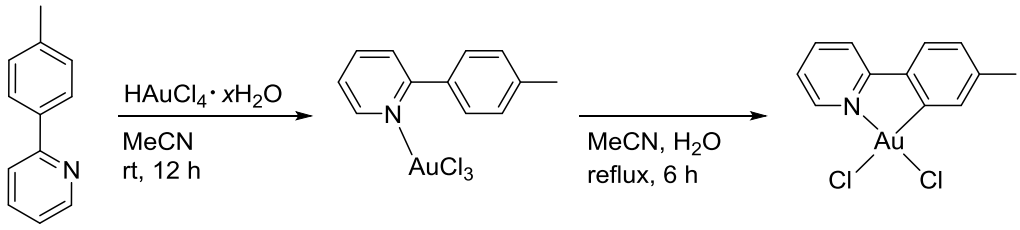

31 **32** 73% **33** 38%

Scheme 6: Synthesis of $AuCl_2$(tpy) (**33**) reported by Henderson *et al.* [55]

The poor yield of 38% of $AuCl_2$(tpy) (**33**) could neither be improved by changing the MeCN/H_2O ratio of the solvent mixture, nor by switching to a solvent with a higher boiling point (propionitrile). The latter led instead to some decomposition of the gold(III) complex to metallic gold.[55]

The synthesis methods for cyclometalated gold(III) complexes presented so far either contain undesirable toxic transition metal complexes, require long reaction times or give only poor yields. That leaves not only space for improvements but downright demands for further enhancement. A former postdoctoral researcher in our group, Dr. Anthony P. Shaw, addressed the problem and developed a procedure for direct cycloauration using microwave technology as a different form of heating.[1] Microwave-assisted synthesis has been widely used in inorganic and organic chemistry.[56],[57] It has been shown that microwave heating significantly reduces reaction times, increases product yields, and improves product purities by reducing undesired side reactions compared to conventional heating methods.[58] The microwave technology enables the use of temperatures above the boiling point of the solvent and a microwave oven equipped with a thermocouple ensures good temperature control.[59] Even though this method has been successfully used in the transition metal-catalyzed synthesis of organic compounds, there are still relative few reports of microwave-assisted syntheses of transition metal complexes.[60],[61],[62]

The same starting materials as Henderson *et al.* used for obtaining $AuCl_2$(tpy) (**33**) *via* direct auration[55] were used in the reported microwave-assisted synthesis, only the solvent was changed from an MeCN/H_2O mixture to pure water.[1] 2-(*p*-tolyl)pyridine (**31**), the gold acid, $HAuCl_4 \cdot 3H_2O$, and water were combined and the aqueous suspension was heated to 160 °C in a sealed vessel in a microwave oven, yielding 87% of the desired cyclometalated gold(III) complex **33** (Scheme 7). Microwave heating reduced the reaction time substantial while the obtained yield of pure product was more than doubled compared to the method using conventional heating.

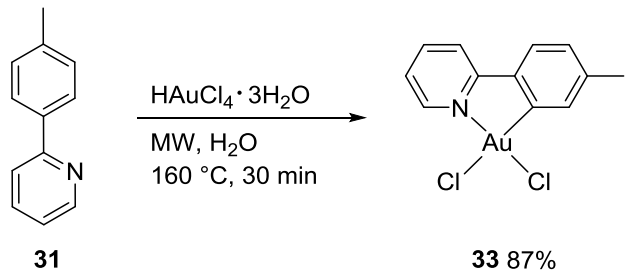

31 **33** 87%

Scheme 7: Microwave-assisted synthesis yielding $AuCl_2$(tpy) (**33**).[1]

Several other neutral and cationic cyclometalated gold(III) complexes could be obtained through a method that gives higher yields and cleaner products without any use of

mercury. In addition to the cyclometalated gold(III) complexes bearing chelated C-N ligands, some complexes bearing bipyridin (bipy) ligands were also synthesized using the microwave-assisted procedure. Amongst others were the cationic cyclometalated gold(III) complexes **34** and **35** (Figure 2) that have not been reported previously.[1]

34 **35**

Figure 2: Cationic cyclometalated gold(III) complexes **34** and **35** synthesized using microwave technology.[1]

The basis of the work presented in this thesis is the synthesis of the starting material, $Au(OCOCF_3)_2(tpy)$ (**1**), which was used for all the reactions presented herein. The microwave-assisted synthesis of $Au(OCOCF_3)_2(tpy)$ (**1**) was developed by a former doctoral student in our group, Dr. Eirin Langseth.[2] 2-(*p*-tolyl)pyridine (**31**), gold acetate, trifluoroacetic acid (TFA) and water were combined and the aqueous suspension was heated to 120 °C in a sealed vessel in a microwave oven, yielding 94% of the desired cyclometalated gold(III) complex **1** (Scheme 8). It was also an alternative route explored, using the less expensive gold hydroxide, $Au(OH)_3$, as starting material. But it turned out that the synthesis with gold hydroxide is less reliable and therefore less favorable than with gold acetate.[5]

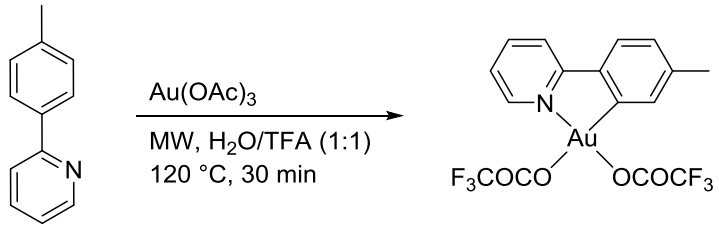

31 **1** 94%

Scheme 8: Microwave-assisted synthesis of $Au(OCOCF_3)_2(tpy)$ (**1**).[2]

1.4 Gold(III) Alkene Complexes

Gold(III) catalysis is currently considered as a hot topic in organic synthesis.[24],[4] It is important to gain insight in the mechanism and knowledge about all steps involved in the catalytic cycle to provide a better understanding of the matter and subsequential to improve its applications. An unsaturated hydrocarbon function is in most reactions the prime target of the catalysis and it is commonly believed that the acceptor properties of a coordinatively unsaturated gold(III) species are essential for the activation of these multiple bonds.[21],[63],[64] Analogous to gold(I) chemistry, gold(III) π-adducts of olefins are assumed to be key intermediates in the catalytic functionalization of alkenes.[65] But in contrast to the plenty characterized representative examples for the primary attack of gold(I) catalysts at unsaturated organic substrates to give isolable π-coordinated intermediates of a gold(I) unit, there is only little experimental evidence for this π-coordination of a gold(III) unit.[66],[67] First structural evidence has been provided by Bochmann and co-workers in 2013 when they reported the first solution characterization of a series of gold(III) alkene complexes bearing the C^N^C pincer ligand, the ethylene complex **36** depicted in Figure 3.[68] The complexes could be prepared by protonolysis of a gold hydroxide as well as by acetate abstraction, all in the presence of the desired alkene. The report was closely followed by the Tilset group, presenting the first crystallographically characterized Au(III) alkene complex **37** (Figure 3).[3] The complex was synthesized by protonolysis of a gold alkyl compound in the presence of 1,5-cyclooctadiene. These new structural insights into gold(III) chemistry validate the inclusion of alkene complexes in mechanistic proposals and will add to better understanding of mechanisms that potentially involve Au(III) alkene complexes.

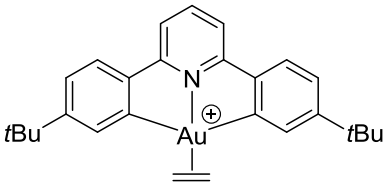

36

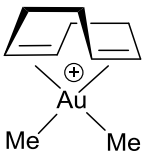

37

Figure 3: First reported gold(III) alkene complexes that were solution characterized, **36**·$(C_6F_5)_3BOCOCF_3$, as well as crystallographically characterized, **37**·B[3,5-$C_6H_3(CF_3)_2]_4$.[68],[3]

1.5 Alkyl Gold(III) Complexes - Nucleophilic Addition to Alkenes

Olefin functionalizations are of high practical value.[69] However, metal-promoted nucleophilic additions to inactivated C-C multiple bonds are considered as very challenging and there are only few reports concerning gold(III)-mediated alkene functionalizations.[67],[70] In order to explore these reactions it is not enough to unambiguous demonstrate the existence of the π-coordinated gold(III) olefin complexes, it is important to analyze the alkyl gold(III) complex furnished from the nucleophilic attack at the activated C-C double bond. These experiments provide evidence and information for the elementary step of gold-mediated nucleophilic addition to alkenes.[69],[71]

In 2013 Rezsnyak *et al.* reported the first direct reactions of alkenes with gold(III) that occur without reduction of the gold(III) and lead to alkyl gold(III) complexes.[70] They investigated the reactivity of different gold(III) complexes towards ethylene and propylene in water at moderate temperatures and with pressures less than one atmosphere. As depicted in Scheme 9, the difunctionalized organic products ethylene glycol (**39**) and chloroethanol (**40**) were the major observed products in the reaction of $HAuCl_4$ with ethylene at 70 °C, while the use of **41**·Cl or **41**·PF_6 as gold agent yielded quantitatively the β-hydroxyalkyl gold(III) complexes **42**·Cl and **42**·PF_6, respectively.[70]

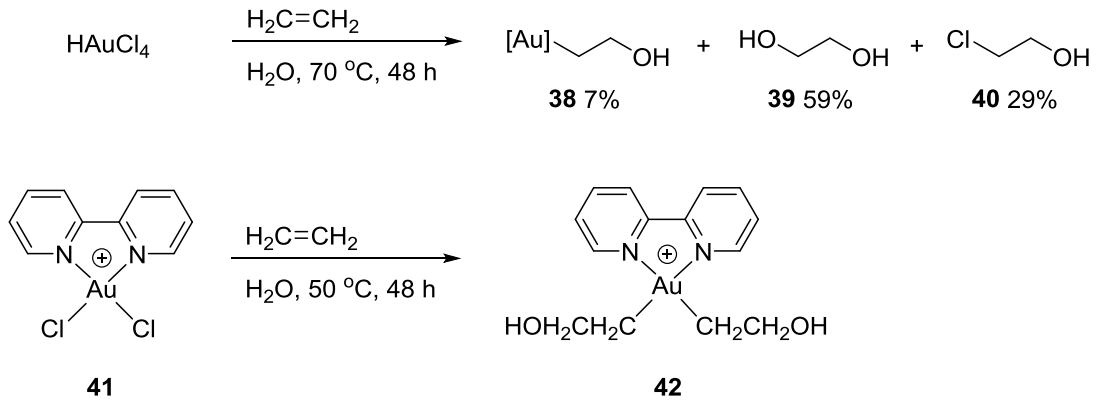

Scheme 9: Selected examples of gold(III) complexes reacting with ethylene.[70] Counteranion Cl^- or PF_6^-.

To obtain stereochemical information about the site of the nucleophilic attack Rezsnyak *et al.* studied the reactivity of the gold(III) complexes towards propylene (Scheme 10).[70] With $HAuCl_4$ as gold(III) complex isopropanol and acetone were formed as products, consistent with Markovnikov attack by OH^- at the coordinated propylene.

No ethylene glycol or chloroethanol analogues were observed. The use of of **41**·Cl or **41**·PF_6 led quantitatively to the β-hydroxyalkyl gold(III) complexes **43**·Cl and **43**·PF_6, respectively.[70] The nucleophilic attack on propylene yielded selectively the Markovnikov product.[70]

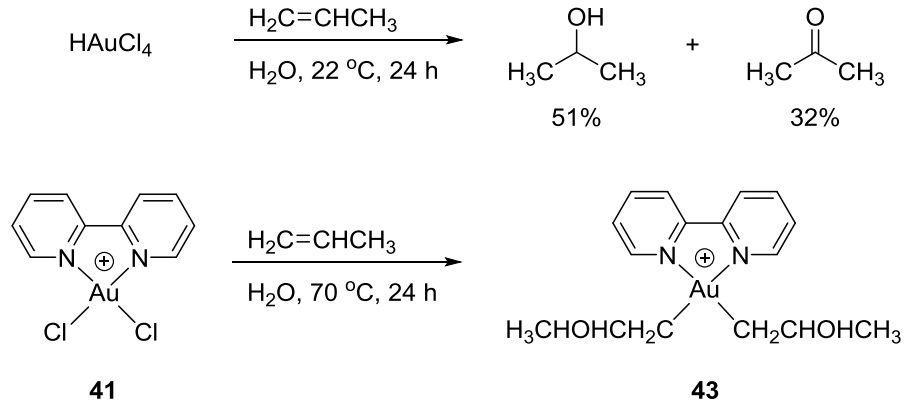

Scheme 10: Selected examples of gold(III) complexes reacting with propylene.[70] Counteranion Cl^- or PF_6^-.

Changing the counter anion in complex **41** altered its solublity in water but seemed to make no appreciable difference regarding the reaction outcome for the reactions with ethylene or propylene.[70] Regarding the products formed from reactions with gold(III) agent **41**, it is noteworthy that the bis(β-hydroxyalkyl) gold(III) complex was selectively formed. This indicates an unusual stability of the bis(β-hydroxyalkyl) gold(III) complex over the mono β-hydroxyalkyl gold(III) complex, which was not observed at any time.[70]

Bochmann and co-workers demonstrated a gold(III)-mediated nucleophilic addition at ethylene at room temperature, using the gold(III) complex **44** bearing a C^N^C pincer ligand (Scheme 11).[68] Corresponding to the observations made by Rezsnyak *et al.*, the alkyl gold(III) complex **45** was assumedly formed by a nucleophilic attack of trifluoroacetate at the π-coordinated ethylene.[68],[70]

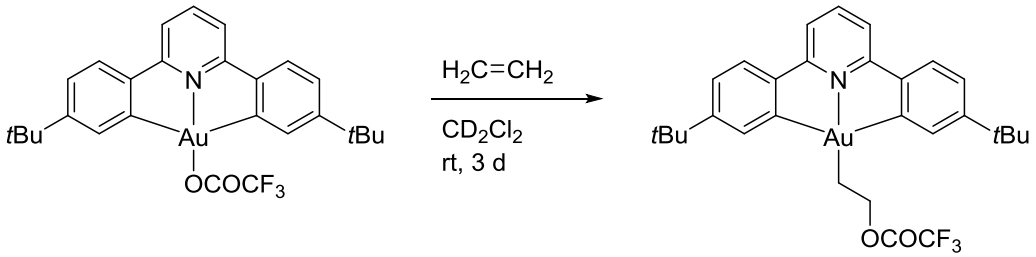

44 **45** 95%

Scheme 11: Reaction of gold(III) complex **44** with ethylene.[68]

Bourissou and co-workers very recently reported the first migratory insertion of alkenes into a gold-carbon bond.[72] They investigated the reaction of the cyclometalated gold(III) dimethyl complex **46** with $B(C_6F_5)_3$ at -80 °C in the presence of different alkenes followed by trapping with Lewis bases or nBu$_4$NCl.[72] Approaches using ethylene or styrene were unsuccessful as NMR monitoring indicated no reaction of either of these alkenes under the given conditions.[72] Whereas, as depicted in Scheme 12, the reaction with the more reactive olefin norbornene followed by addition of nBu$_4$NCl yielded the norbornyl gold(III) complex **47**. Analogous products to **47** could be obtained using the Lewis bases lutidine or pyridine instead of nBu$_4$NCl in the last step.[72]

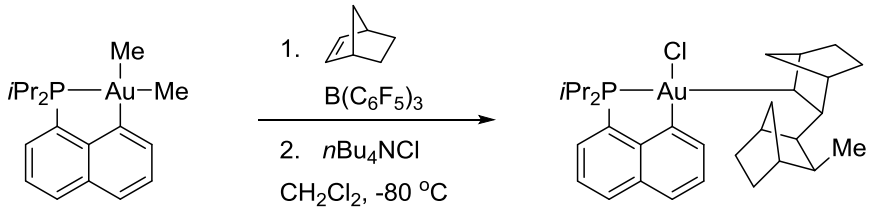

46 **47** 56%

Scheme 12: Formation of norbornyl gold(III) complex **47** upon formal insertion of norbornene into Au-Me bond of **46**.[72]

In contrast to the *anti* addition process that is mostly encountered for gold-mediated nucleophilic attacks at alkenes the formal norbonene insertion reported by Bourissou and co-workers proceeds in a *syn* manner.[21],[72] Bourissou and co-workers assume that the reaction takes place *via* a highly reactive tricoordinate cationic methyl gold(III) intermediate that resulted from methyl group abstraction of **46** through the strong Lewis acid $B(C_6F_5)_3$.[72]

The starting point of the interest of the Tilset group in the reactivity of our complexes towards alkenes was the success of the unambiguous demonstration of the existence of

gold(III) alkene complexes and the great practical value of alkene functionalization.[69],[3] Inspired by the work accomplished by the groups of Rezsnyak[70] and Bochmann[68] the Tilset group investigated the reactivity of $Au(OCOCF_3)_2(tpy)$ (**1**) towards ethylene.[7]

The reaction of $Au(OCOCF_3)_2(tpy)$ (**1**) with ethylene in TFA at room temperature gave after two hours the alkyl gold(III) complex **2** in good yields (Scheme 13).[7] The reaction occurs selectively *trans* to nitrogen, the atom with the weakest *trans* effect in the chelate ligand.[7]

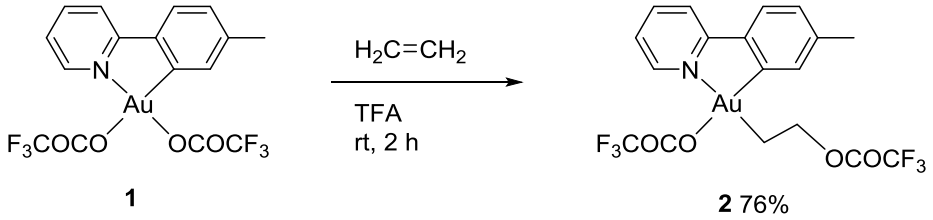

1 **2** 76%

Scheme 13: Reaction of gold(III) complex **1** with ethylene in TFA.[7]

Comparing the ^{1}H-NMR spectra of starting material **1** with product **2** reveals an indicative shift of the singlet signal (labeled with * in Figure 4) from the tpy ligand towards the lower field. Later on the observation of this significant shift while monitoring a reaction of gold(III) complex **1** with an alkene will be considered as strong evidence that a gold(III)-mediated attack of a nucleophile at the olefin took place, yielding an alkyl gold(III) complex.

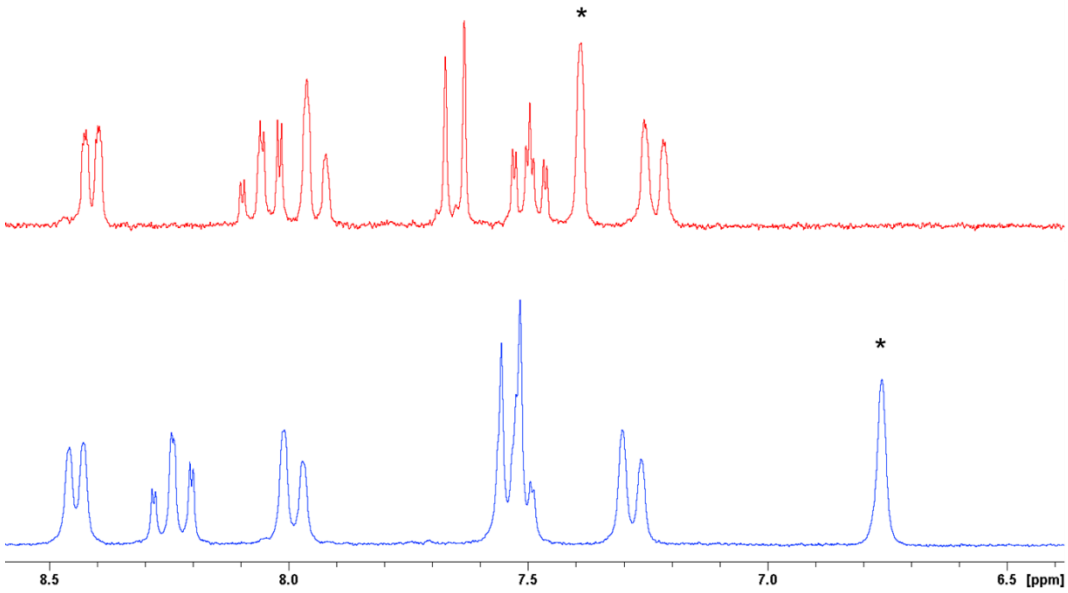

Figure 4: Comparison of the aromatic region in ^{1}H-NMR spectra of **1** (blue) and **2** (red). Indicative shift of singlet (labeled with *) to the lower field.

Langseth *et al.* also reported, supported by experimental as well as computational results, that the formed product in the reaction of $Au(OCOCF_3)_2(tpy)$ (**1**) with *cis*-1,2-dideuterioethylene in TFA arises from an external nucleophilic attack of trifluoroacetate.[7] The reaction gave a single stereoisomer with the observed coupling constant between the two alkyl protons in the range expected for the stereochemistry corresponding to an *anti* addition, which supports an external nucleophilic attack and is consistent with observations made by Rezsnyak *et al.*[7],[70] Experimental and computational data led to the conclusion that the substitution of the trifluoroacetate ligand *trans* to nitrogen with ethylene proceeds in an associative manner, is rate-limiting and followed by an external *anti* attack of the dissociated ligand at the coordinated ethylene.[7]

As depicted in Scheme 14, Tilset and co-workers could also demonstrate that ethylene-d_4 and ethylene undergo an exchange at gold.[7] However, this exchange does not occur through complete reversal of all steps back to **1**, but by an associative ethylene exchange *via* an intermediate, in which two ethylene units are simultaneously bonded to gold.[7]

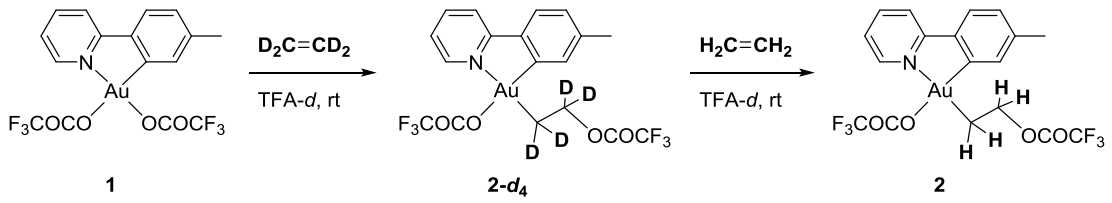

Scheme 14: Ethylene-d_4 and ethylene undergo exchange at Au.[7]

Langseth *et al.* investigated in addition to the reactivity of $Au(OCOCF_3)_2(tpy)$ (**1**) towards ethylene in TFA also its reactivity in trifluoroethanol (TFE).[7] The reaction of $Au(OCOCF_3)_2(tpy)$ (**1**) with ethylene in TFE at room temperature gave after two hours the alkyl gold(III) complex **48** in good yields (Scheme 15).[7]

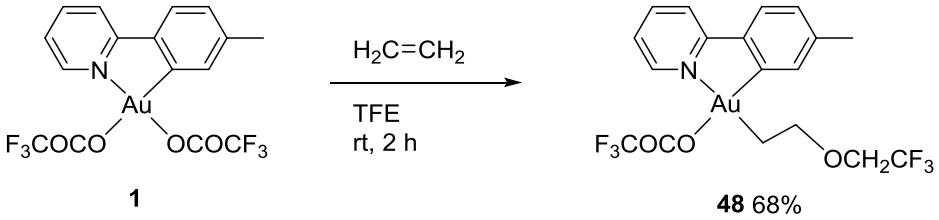

Scheme 15: Reaction of gold(III) complex **1** with ethylene in TFE.[7]

The reaction occurs selectively *trans* to nitrogen, corresponding with the observations made in the reaction using TFA. Monitoring this reaction by ^{1}H-NMR displayed that formation of **48-*d*$_2$** in TFE-d_3 took with 30 minutes considerably longer than formation of **2-*d*** in TFA-*d*, which was completed after 5 minutes.[7]

Observing alkyl gold(III) complex **48**, rather than **2**, as major product in the reaction in TFE led towards investigations regarding reversibility. Dissolution of alkyl gold(III) complex **2** in TFE-d_3 resulted in the formation of alkyl gold(III) complex **48-*d*$_2$**, suggesting a process involving external nucleophilic addition of solvent to an intermediate gold(III) alkene complex (Scheme 16).[7] Analogous, isolated complex **48** was dissolved in TFA-*d* at room temperature, yielding only **2**.[7]

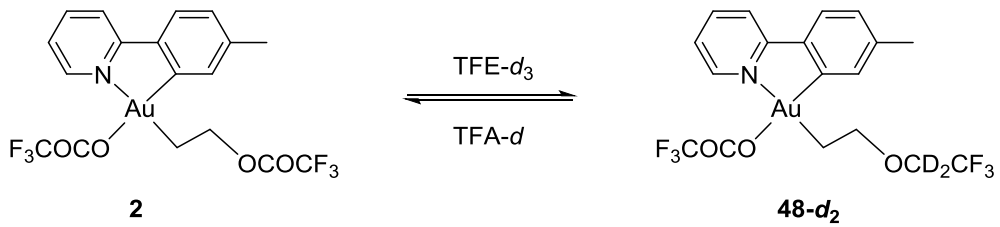

Scheme 16: Interconversion between complexes **2** and **48-*d*$_2$** in solution.[7]

2 Synthesis and Characterization of New Alkyl Gold(III) Complexes

A number of novel alkyl gold(III) complexes, yielding from gold(III)-mediated nucleophilic attack at alkenes, have been synthesized as a part of this project. The synthetic route to these complexes is presented in this chapter and some of the characterization techniques are described with focus on NMR spectroscopy. The single crystal X-ray analyses of eleven new compounds are presented in chapter 3.

2.1 Gold(III)-mediated Nucleophilic Attack at Alkenes – TFA

2.1.1 Internal Alkenes (*Cis* and *Trans*)

Since the gold(III)-mediated nucleophilic attack of TFA at ethylene gave such promising results[7], our group wanted to investigate the reactivity of $Au(OCOCF_3)_2(tpy)$ (**1**) towards substituted alkenes further. Other group members explored reactions using simple, terminal alkenes as well as cycloalkenes.[73],[74] But most of the obtained products were instable and decomposed upon removal of the solvent or could only be observed at low temperatures.[73],[74]

These reactions involved terminal alkenes or cycloalkenes, so it is coherent to explore linear internal alkenes. 2-Hexenes and 3-hexenes were investigated. They were selected because of their similarity to the already investigated 1-hexene[74] as well as their slightly different symmetrical properties compared to each other, which could lead in terms of analyzing the stereo chemistry to a better insight in the reaction mechanism of gold(III)-mediated nucleophilic addition to alkenes.

The reactions were carried out in NMR tubes and monitored by ^{1}H-NMR. The general procedure involved taking a ^{1}H-NMR reference spectrum of the alkene and 1,2-dichloroethane as internal standard in TFA-*d* first, adding $Au(OCOCF_3)_2(tpy)$ (**1**) in a second step and then monitoring the reaction by ^{1}H-NMR over time until no further changes in the spectra could be observed. All four reactions, using *cis*-2-hexene, *trans*-2-hexene, *cis*-3-hexene, and *trans*-3-hexene, proceeded in a similar manner. All alkenes were stable in TFA-*d* and, according to the recorded ^{1}H-NMR spectra, a reaction occurred upon adding the gold(III) complex **1**. However, the main product observed after only a

few hours was the free ligand 2-(*p*-tolyl)pyridine, which indicates decomposition of the gold(III) complex. In none of the cases it was possible to determine the structure of any reaction intermediates.

To clarify the described procedure, the example of *cis*-3-hexene and the examination of its NMR-scale reaction with $Au(OCOCF_3)_2(tpy)$ (**1**) in TFA-*d* at room temperature is given in detail. The ^{1}H-NMR reference spectrum of *cis*-3-hexene and 1,2-dichloroethane in TFA-*d* was recorded and showed that *cis*-3-hexene is stable under the given conditions (Figure 5).

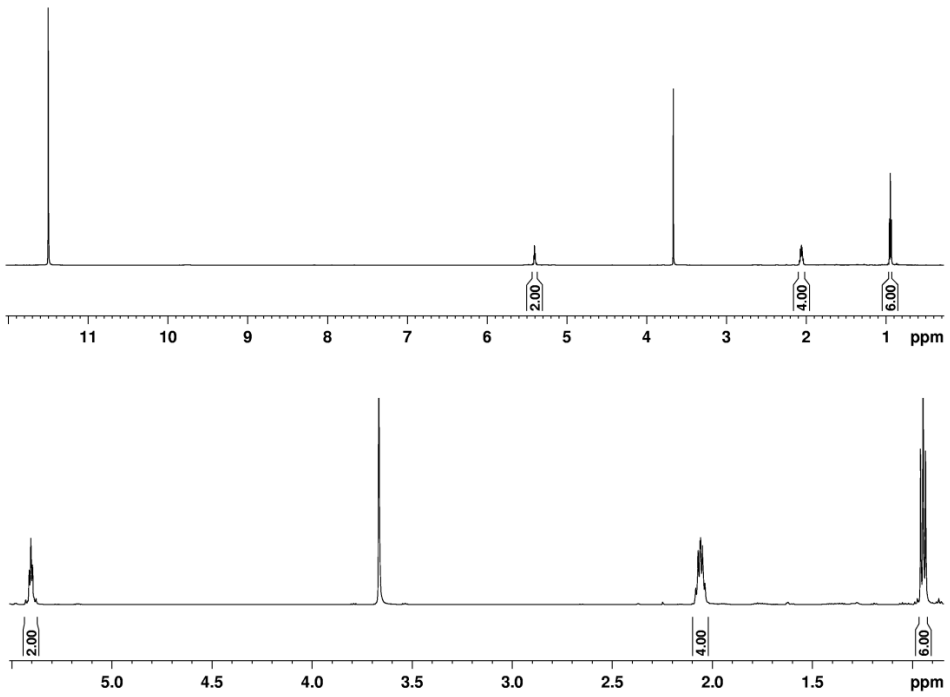

Figure 5: ^{1}H-NMR (600 MHz, TFA-*d*) of *cis*-3-hexene and 1,2-dichloroethane in TFA-*d*. Close-up view in the bottom.

Then $Au(OCOCF_3)_2(tpy)$ (**1**) was added. The main indicator of a reaction with the gold(III) compound **1** taking place is the shift of the characteristic singlet at 6.90 ppm to the lower field. The ^{1}H-NMR spectrum recorded one hour after the addition showed still gold(III) starting material, indicated by the remaining signal at 6.90 ppm, but also complete conversion of the alkene. So, after 1.5 hours another 1.5 eq. *cis*-3-hexene were added, resulting in full conversion of the gold starting material. After 21 hours reaction time one major product could be observed in the ^{1}H-NMR spectrum (Figure 6).

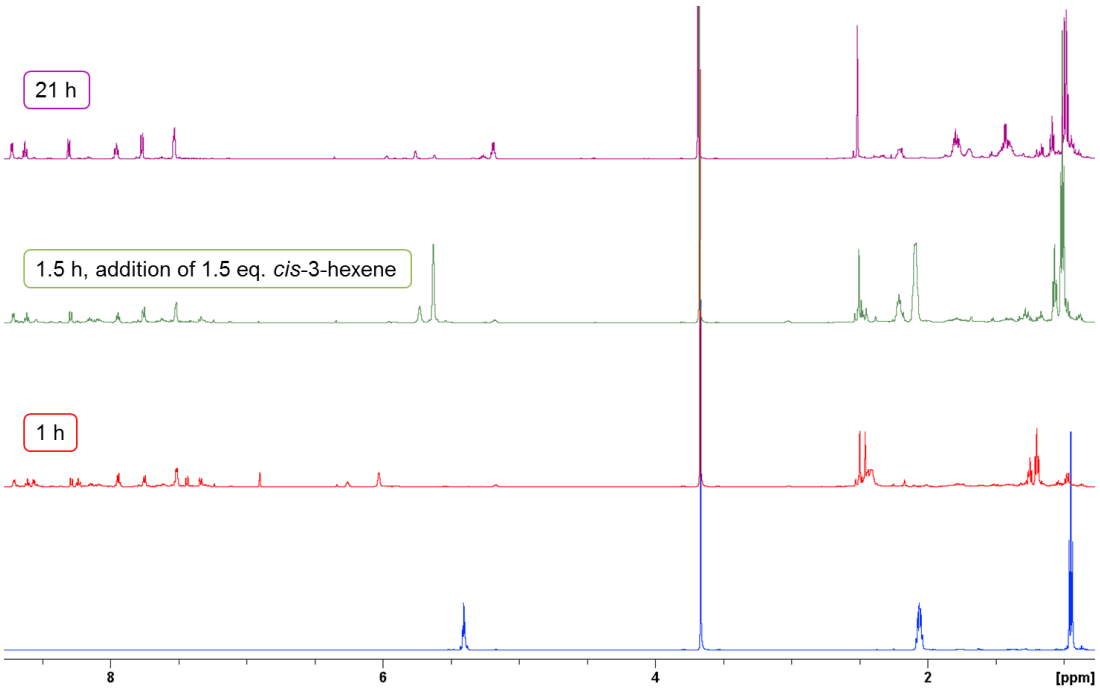

Figure 6: Stacked ^{1}H-NMR (600 MHz, TFA-*d*) following the reaction of *cis*-3-hexene and 1,2-dichloroethane in TFA-*d* with Au(OCOCF$_3$)$_2$(tpy) (**1**).

2D NMR experiments were performed but it was not possible to determine the structure of any intermediate. However, according to the experience gained from the former conducted experiments and the observed indicative shift of the singlet it is assumed that the reaction proceeds *via* intermediate **49**, but because of instability the gold(III) complex decomposes to free ligand **31-*d*** and metallic gold (Scheme 17).

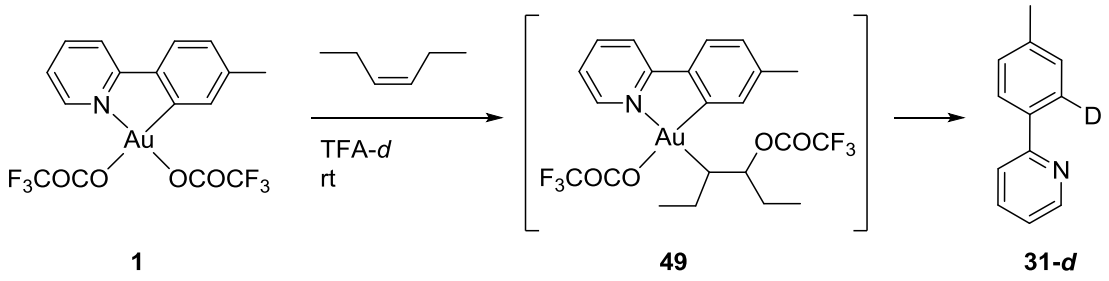

Scheme 17: Assumed reaction pathway in the reaction of gold(III) complex **1** with *cis*-3-hexene in TFA-*d*.

To prove the assumption that the major product observed in the ^{1}H-NMR spectrum is the free ligand the sample was spiked with 0.5 µl 2-(*p*-tolyl)pyridine (**31**). The resulting ^{1}H-NMR spectrum showed significant growth of the peaks belonging to the free ligand while the other peaks stayed unaltered (Figure 7). Also no additional peaks appeared

upon spiking the sample with 2-(*p*-tolyl)pyridine (**31**). This observation suggests that the formed intermediates are not stable under the given conditions and decompose to free ligand as well as metallic gold, as indicated by the formation of a brown mirror at the wall of the NMR tube. The same procedure was followed for the other internal hexenes and resulted in similar outcomes, yielding **31-*d***.

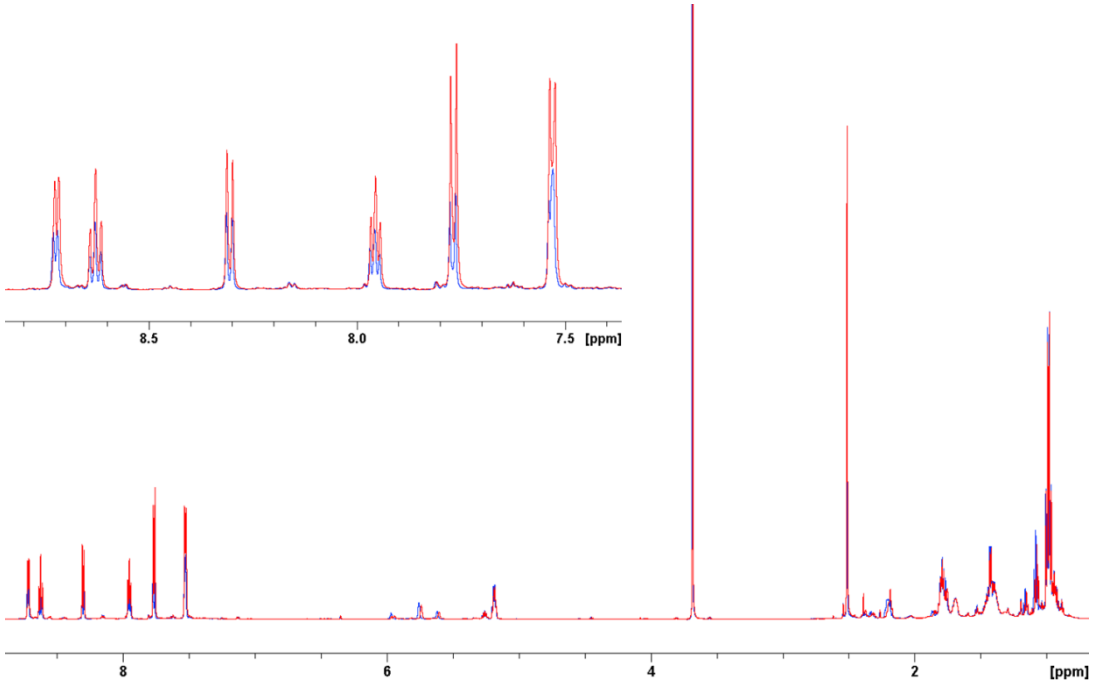

Figure 7: ^{1}H-NMR (600 MHz, TFA-*d*) of *cis*-3-hexene and 1,2-dichloroethane in TFA-*d* with $Au(OCOCF_3)_2(tpy)$ (**1**) (blue) stacked with the ^{1}H-NMR spectrum of the sample spiked with 2-(*p*-tolyl)pyridine (red).

2.1.2 1,4-Pentadiene

After the investigation of different kinds of olefins in the reaction of gold(III)-mediated nucleophilic attack of trifluoroacetate at alkenes, the focus of interest is now shifted towards dienes. While reactions using a variety of alkenes gave interesting results, exploring dienes offers new opportunities besides functionalization of only one double bond. It could be possible to functionalize each double bond, for example by forming a dimer when both double bonds of the diene interact with different gold(III) complexes. 1,4-Pentadiene was chosen because it consists of two terminal double bonds, which seemed so far to lead to more stable products.

The reaction of 1,4-pentadiene with $Au(OCOCF_3)_2(tpy)$ (**1**) in TFA-*d* was first carried out in an NMR tube and monitored by ^{1}H-NMR. The gold(III)starting material was fully converted by ^{1}H-NMR within minutes and the recorded ^{1}H-NMR spectrum showed a clean reaction with one major product formed. In order to isolate the product and ease the determination of its structure the reaction was repeated on larger scale. However, product isolation was not possible because of decomposition upon removal of the solvent. Possible reasons for this instability that was also observed also for other products will be discussed in the end of chapter 2.1.

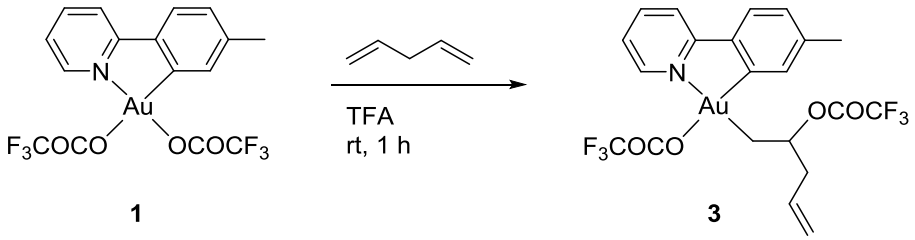

Scheme 18: Reaction of gold(III) complex **1** with 1,4-pentadiene in TFA.

The reaction of $Au(OCOCF_3)_2(tpy)$ (**1**) with 1,4-pentadiene in TFA at room temperature proceeded, analogous to the reactions described so far, in a Markovnikov manner yielding the alkyl gold(III) complex **3** (Scheme 18). Only one double bond of the diene was functionalized in this reaction. The obtained ^{1}H-NMR spectrum of complex **3** (Figure 8) shows the expected peaks from the tpy ligand in the aromatic region, including the shifted singlet signal from the tpy ligand towards the lower field signalizing a gold(III)-mediated nucleophilic attack at 1,4-pentadiene. The small peaks in the aromatic region as well as the TFA residue peak at 9.7 ppm indicate partial decomposition of the product leading to the free ligands trifluoroacetic acid and 2-(*p*-tolyl)pyridine.

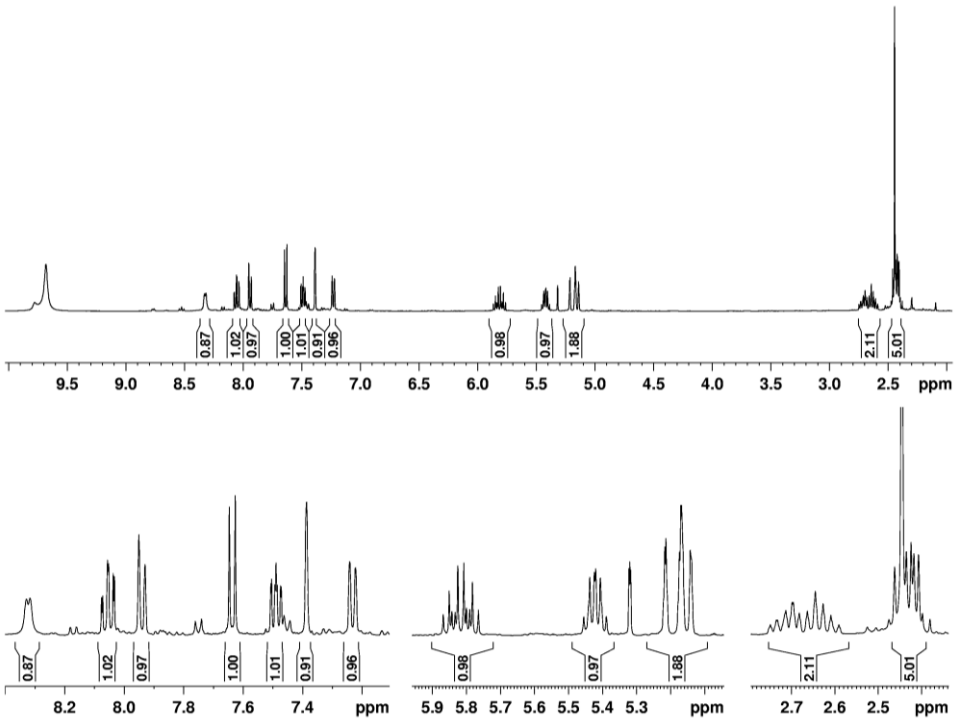

Figure 8: ^{1}H-NMR (400 MHz, CD_2Cl_2) of alkyl gold(III) complex **3**. Close-up views in the bottom. Peak at 9.7 ppm is due to TFA residue.

The doublet of doublets of triplets at 5.82 ppm and the distorted doublet of doublets at 5.24-5.12 ppm are typical shifts for vinylic protons, indicating the existence of a double bond in the molecule. As depicted in Figure 9, the COSY shows that these protons couple with each other. The HSQC shows that the two protons from the distorted doublet of doublets signal are bonded to the same carbon atom, supporting the existence of a double bond. Correspondingly, the two protons close to the gold atom, which overlap with the methyl group signal from the tpy ligand, are bonded to the same carbon and couple with the multiplet at 5.46-5.38 ppm. The proton giving this multiplet is the only proton bonded to its carbon. The shift of this proton is at a lower field compared to the other alkyl shifts and therefore suggests that the trifluoroacetate is bonded to this carbon, too. That leaves the multiplet at 2.75-2.57 ppm as protons of the methylene group next to the terminal double bond, substantiated by them being bonded to the same carbon as well as coupling to the two protons that are each part of a methine group.

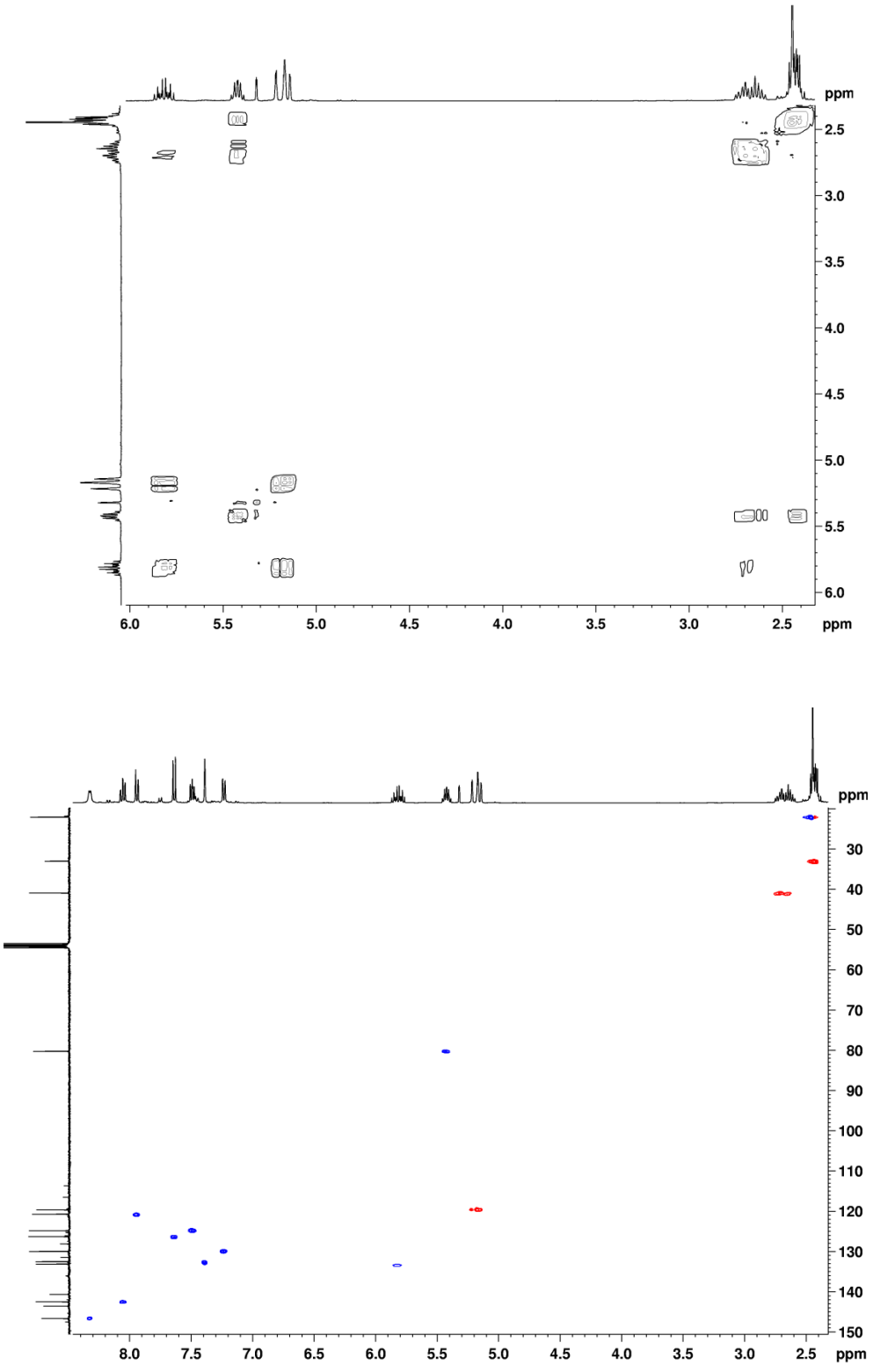

Figure 9: Close-up view of COSY (top) and HSQC (bottom) of complex **3**.

2.1.3 1,5-Hexadiene

Since the reaction with 1,4-pentadiene was successful, reactions with other dienes were also investigated. 1,5-Hexadiene was chosen because of its analogy to the already analyzed 1-hexene, 2-hexenes and 3-hexenes.

The reaction of 1,5-hexadiene with $Au(OCOCF_3)_2(tpy)$ (**1**) in TFA-*d* was first carried out in an NMR tube and monitored by ^{1}H-NMR. The gold(III)starting material was fully converted by ^{1}H-NMR within minutes and the recorded ^{1}H-NMR spectrum showed a clean reaction with one major product formed. In order to isolate the product and ease the determination of its structure the reaction was repeated on larger scale. However, product isolation was not possible because of decomposition upon removal of the solvent, which came along with a rapid color change of a white to a purple solid, indicating gold nanoparticle formation. The reaction was repeated under dry conditions and argon atmosphere. The product was handled in the glove box but the degradation took place anyway, even though significantly slower than under non-inert conditions.

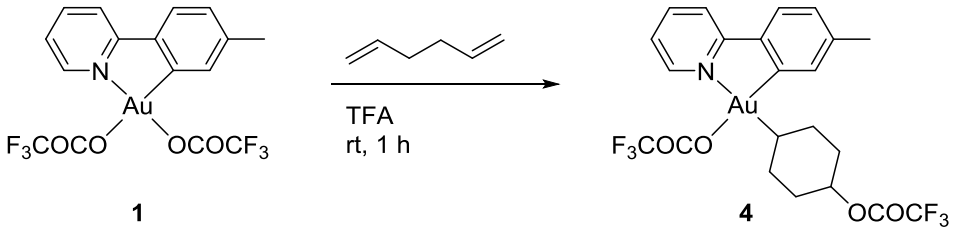

1 **4**

Scheme 19: Reaction of gold(III) complex **1** with 1,5-hexadiene in TFA.

The expected product resulting from functionalization of only one double bond was not observed. Instead, the astonishing and unexpected alkyl gold(III) complex **4** was obtained in the reaction of $Au(OCOCF_3)_2(tpy)$ (**1**) with 1,5-hexadiene in TFA at room temperature (Scheme 19). We assume that the reaction proceeds *via* substitution of the trifluoroacetate ligand *trans* to nitrogen with one double bond of 1,5-hexadiene, followed by cyclization through an intramolecular attack of the non-coordinated double bond at the coordinated one. The dissociated trifluoroacetate then attacks the formed secondary carbocation furnishing product **4** (Figure 10). Formation of six-membered rings is energetic favorable and therefore a strong reaction driving force. However, our observation is contrary to reported reactions of 1,5-hexadiene with Ni(II) or Pd(II) catalysts, which exclusively yield five-membered rings.[75],[76] This reveals the unique properties of gold(III) complexes.

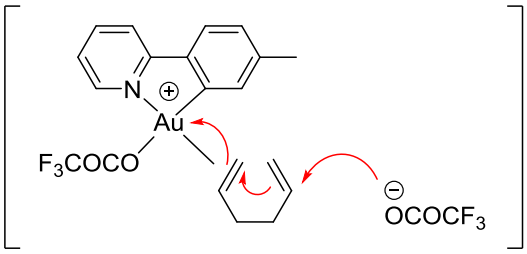

Figure 10: Suggested mechanism for formation of complex **4**.

The obtained ^{1}H-NMR spectrum of complex **4** (Figure 11) shows the expected peaks in the aromatic region resulting from the tpy ligand, including the indicative shift of the singlet signal from the tpy ligand towards the lower field, which is a strong evidence that a gold(III)-mediated attack of a nucleophile to the olefin took place. There are no peaks indicating the existence of a double bond in complex **4**, contrasting the observations made in the reaction with 1,4-pentadiene, which excludes the possibility of the participation of merely one double bond of 1,5-hexadiene in the discussed reaction.

Crystals suitable for single crystal X-ray analysis were obtained by vapor diffusion using CH_2Cl_2 as solvent and *n*-pentane as anti-solvent. The solid-state structure of the selected specimen verifies complex **4**.

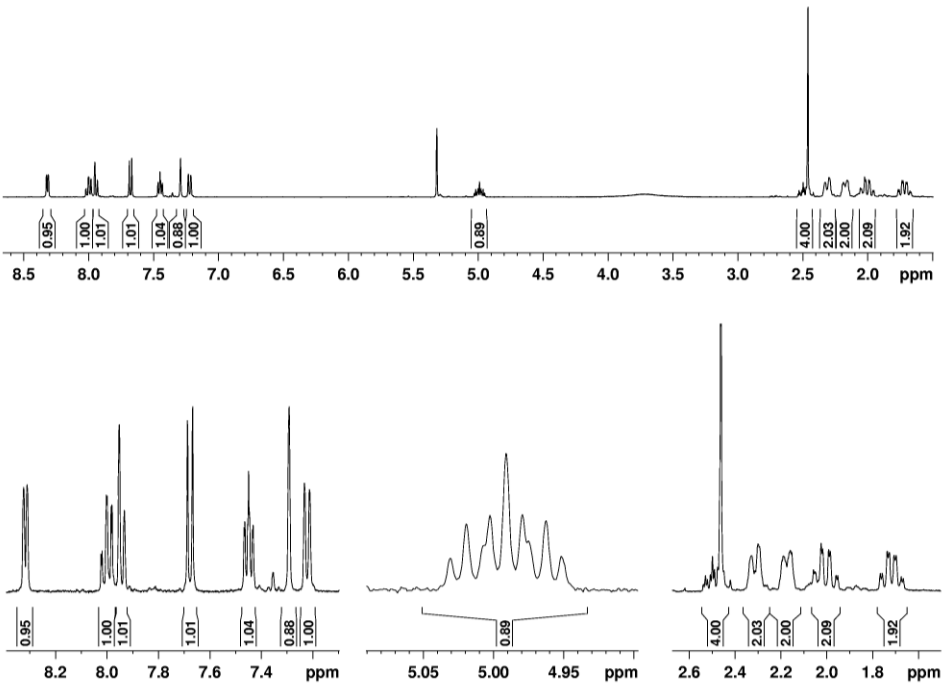

Figure 11: ^{1}H-NMR (400 MHz, CD_2Cl_2) of alkyl gold(III) complex **4**. Close-up views in the bottom. Peak at 3.7 ppm is due to TFA residue.

Presumably, the six-membered ring adopted the most stable chair-conformation with the substituents in equatorial positions to achieve the least steric hindrance and avoid strains. According to this assumption, the protons at 2.5 ppm and 5.0 ppm that are bonded to the same methine group carbon atoms as gold and trifluoroacetate, respectively, occupy axial positions. The six-membered ring possesses mirror symmetry, with the methine group carbon atoms of the ring and their bonded hydrogen atoms lying in the mirror plane, giving two equal sets of proton signals in the ^{1}H-NMR spectrum (Figure 12).

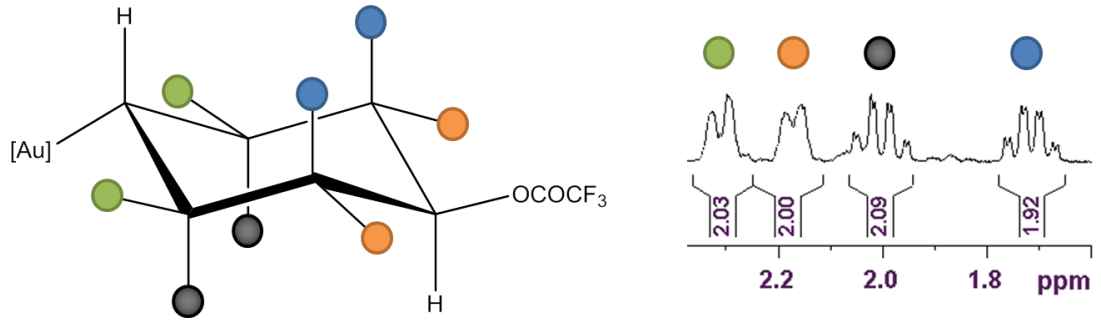

Figure 12: Assignment of proton peaks in the six-membered ring of complex **4**.

As depicted in Figure 14, the HSQC spectrum shows that the orange and blue labeled hydrogens as well as the green and black labeled ones are bonded to the same carbon atom, corresponding with the observed coupling in the COSY to the respective closest hydrogen bonded to the methine group carbon (Figure 12). The hydrogens were assigned to equatorial and axial positions according to the Karplus equation, which predicts large vicinal couplings at H-C-C-H dihedral angles of 180° and 0°, and zero vicinal coupling for dihedral angles at 90° (Figure 13).[77]

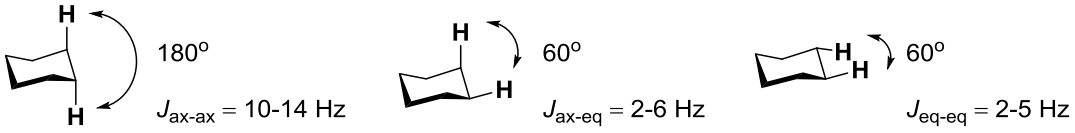

Figure 13: Generalized information regarding vicinal proton-proton couplings in cyclohexane.[78]

So, the proton peaks with the more detailed splitting pattern (black and blue) show larger couplings, indicating diaxial coupling with a dihedral angle of 180° and therefore occupation of an axial position. While the proton peaks with the less detailed splitting pattern (green and orange) show smaller couplings, indicating no diaxial coupling and therefore occupation of an equatorial position (Figure 12, Figure 13).

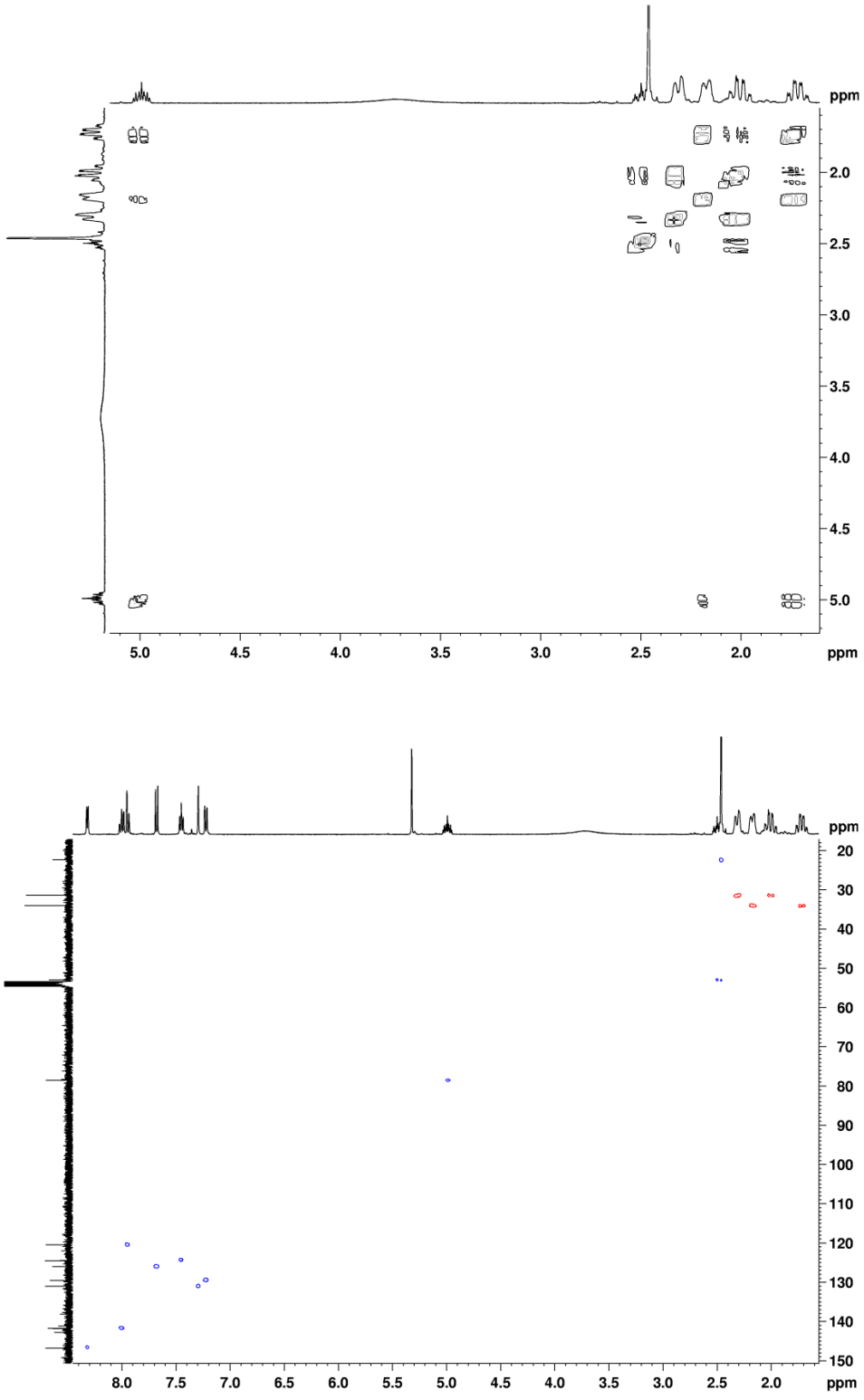

Figure 14: Close-up view of COSY (top) and HSQC (bottom) of complex **4**.

2.1.4 1,5-Heptadiene

The intriguing result of the reaction with 1,5-hexadiene in TFA gives new opportunities for exploration of the reactivity of gold(III) complex **1** towards alkenes. It would be interesting to investigate 1,5-heptadiene as alkene, assumed it comes to a six-membered ring formation as well, to determine the preference of gold coordinating to an internal or terminal alkene. Hence the definite position of the methyl group at the ring is dependent on the reaction mechanism, it provides valuable information about the reactivity of $Au(OCOCF_3)_2(tpy)$ (**1**).

The reaction of 1,5-heptadiene with $Au(OCOCF_3)_2(tpy)$ (**1**) in TFA-*d* was first carried out in an NMR tube and monitored by ^{1}H-NMR. The gold(III) starting material was fully converted by ^{1}H-NMR within minutes and the recorded ^{1}H-NMR spectrum showed a mix of products. The reaction was also repeated on larger scale but product isolation was not possible.

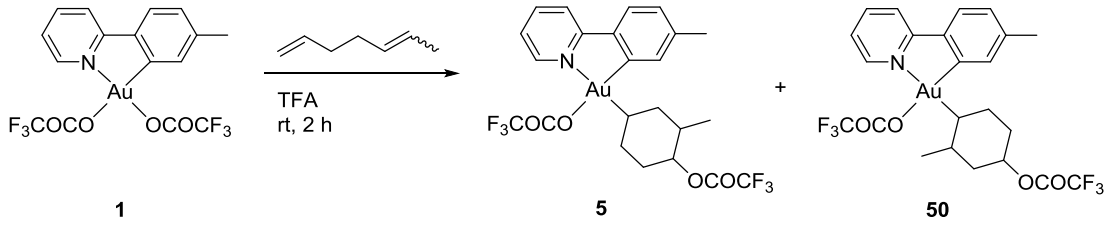

1 **5** **50**

Scheme 20: Assumed products resulting from reaction of gold(III) complex **1** with 1,5-heptadiene in TFA.

The reaction of $Au(OCOCF_3)_2(tpy)$ (**1**) with 1,5-heptadiene TFA at room temperature yielded presumably the alkyl gold(III) complexes **5** and **50**, indicating formation of a six-membered ring corresponding with observations made in the reaction with 1,5-hexadiene (Scheme 20). The obtained ^{1}H-NMR spectrum shows the expected peaks from the tpy ligand in the aromatic region, including the shifted singlet signal from the tpy ligand towards the lower field signalizing a gold(III)-mediated nucleophilic attack at 1,5-heptadiene (Figure 15). However, closer examination of the spectrum reveals the presence of two sets of peaks, some overlapping, in the ratio 2:1, indicating two different products. The peaks in the aliphatic region are similar to the peaks observed for complex **4**, except the additional two sets of doublets at 1.3 ppm and 1.0 ppm.

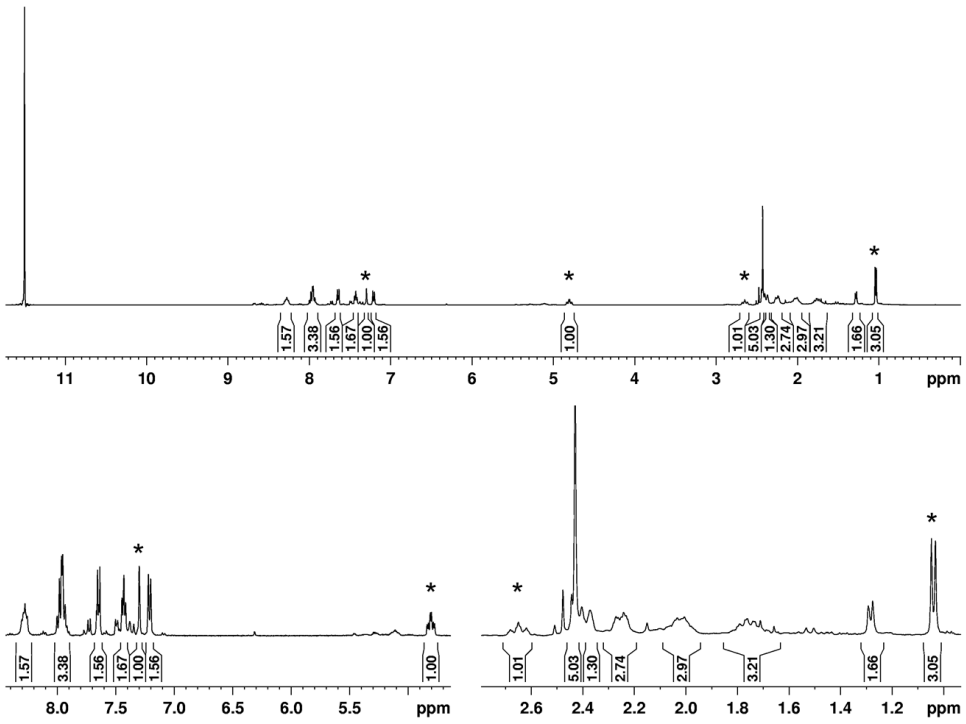

Figure 15: ^{1}H-NMR (400 MHz, TFA-*d*) of reaction products of gold(III) complex **1** and 1,5-heptadiene in TFA. Close-up views in the bottom. (* presumably indicates complex **50**)

The most significant peaks in the recorded ^{1}H-NMR spectrum are the proton peaks of the methyl group bonded to the six-membered ring at 1.3 ppm and 1.0 ppm. It is assumed that the major product (selected peaks labeled with * in Figure 15) is complex **50**, bearing the methyl group close to the gold atom. The correlations shown by COSY and HSQC provide no definite prove for this assumption. However, the supporting evidence they provide is indicated in Figure 16. While the hydrogen bonded to the same carbon as trifluoroacetate at 4.8 ppm couples with the protons bonded to the neighboring carbons of the ring, the methyl group bonded to the ring couples accordingly to a proton bonded to another carbon as the ones described so far. Therefore, it is assumed that the methyl group is positioned close to gold. Furthermore, as shown in the HSQC spectrum, the hydrogen coupling to the methyl group (labeled with * in Figure 16) is the only hydrogen bonded to its carbon. No conclusion can be drawn about the minor isomer with the peak for the methyl group hydrogens at 1.3 ppm.

Crystals suitable for single crystal X-ray analysis were obtained by vapor diffusion using CH_2Cl_2 as solvent and *n*-pentane as anti-solvent. The solid-state structure of the selected specimen verifies complex **5**.

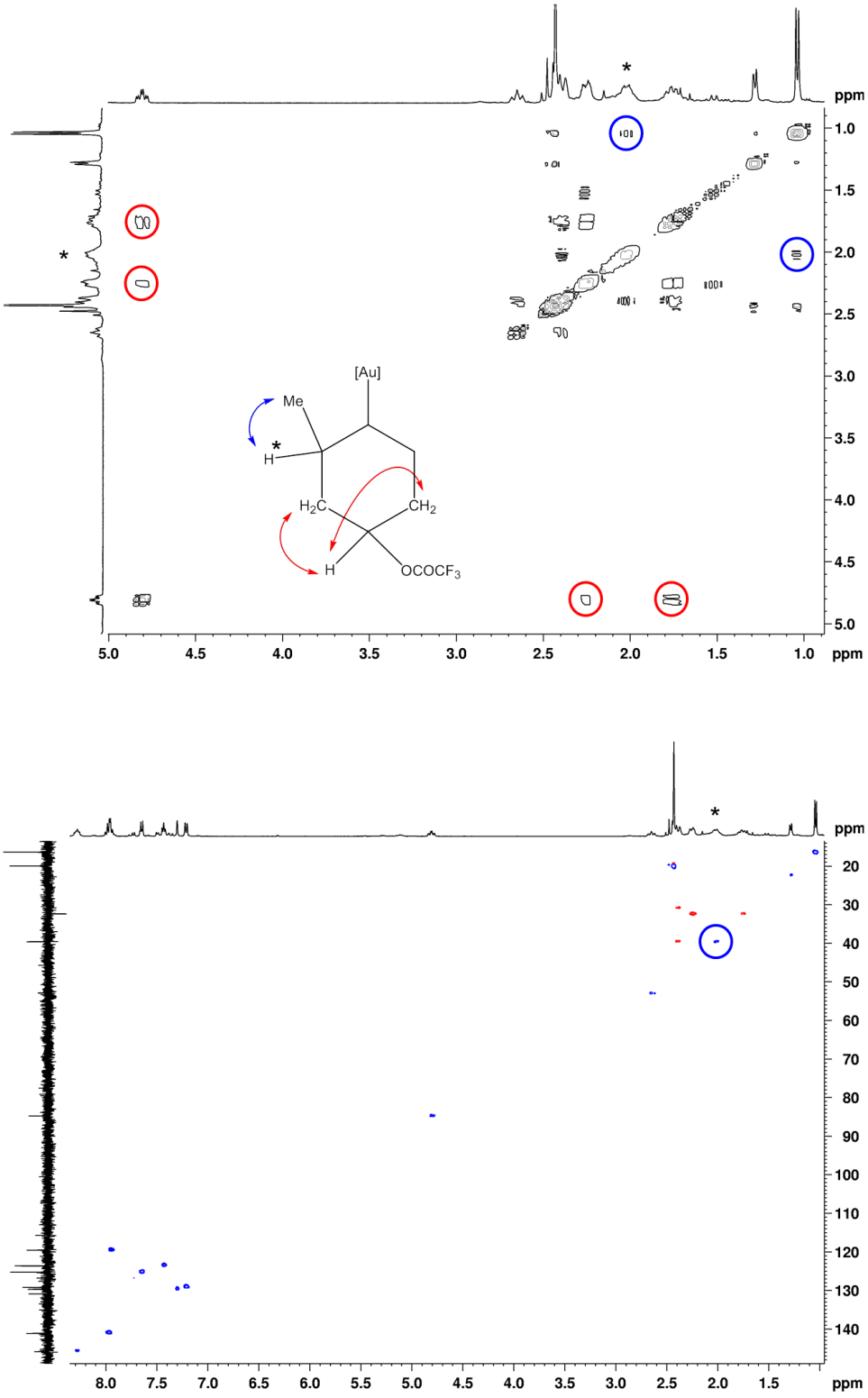

Figure 16: Close-up view of COSY (top) and HSQC (bottom) of reaction products of gold(III) complex **1** and 1,5-heptadiene in TFA.

2.1.5 1,5-Heptadiene (DFT-Calculations)

Since NMR analysis showed presumably complex **50** as major product, while X-ray analysis of a chosen single crystal resulted in structure **5**, density functional theory (DFT) calculations for structure optimization of complexes **5** and **50** were performed to shed light on the stability of different isomers with six-membered rings *trans* to nitrogen (Figure 17).

All calculations were carried out at the DFT level with Gaussian09[79] on the Abel supercomputer[80] at the University of Oslo. For geometry optimizations, all atoms apart from Au were described with the triple-ζ 6-311+G** basis set[81],[82] whereas Au was described with a Stuttgart-Köln basis set including a small-core quasi-relativistic pseudopotential.[83] Geometries were fully optimized without any constraint. Vibrational frequencies were computed to verify that the stationary points found were minima. The calculations were performed in collaboration with Dr. David Balcells, a researcher at the CTCC (Centre for Theoretical and Computational Chemistry) of the University of Oslo.

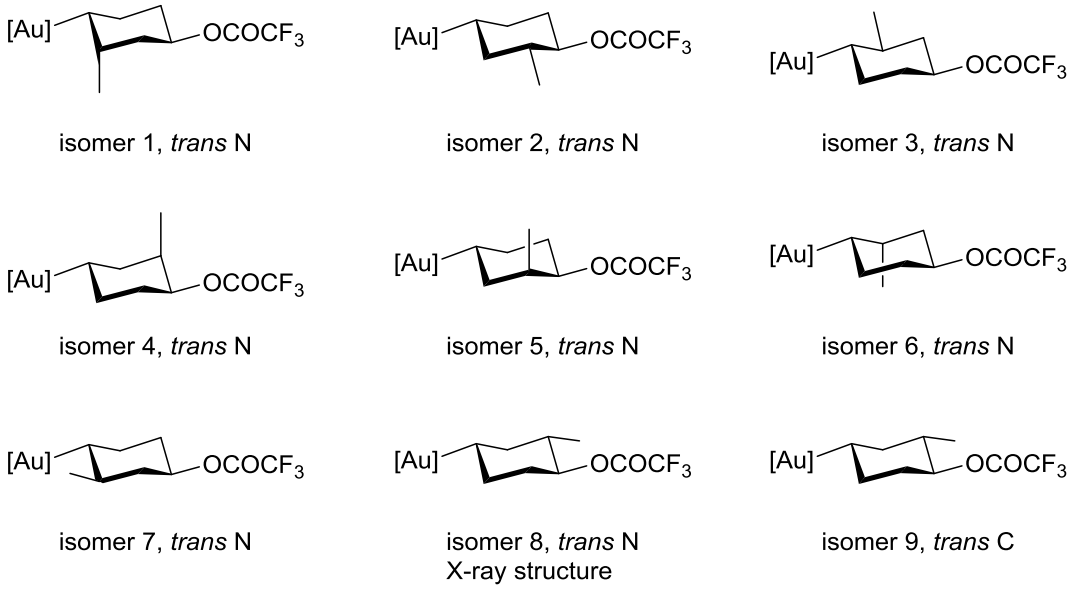

Figure 17: Structure optimization was performed for the shown isomers. *Trans* N and *trans* C indicate the position of the six-membered ring.

The free energy and enthalpy for eight isomers, differing in the position of the methyl group at the ring, as well as for isomer 9 were calculated (Table 1). The values are given relative to the values obtained for the isomer that is equivalent to the solid-state structure. The results of the structure optimization are illustrated in Figure 18. It shows that the crystal structure and isomers 1, 4 and 7 have the lowest free energies, which are quite

similar. As a rule of thumb the difference in free energy becomes significant when it exceeds 1 kcal/mol.[84] It is obvious that the isomer with the six-membered ring located *trans* to carbon, isomer 9, is clearly less stable than the other isomers investigated and supports therefore the observation that all the gold(III)-mediated reaction took place exclusively *trans* to nitrogen. Since the geometries were optimized for a solution in CH_2Cl_2, the assumption drawn from the NMR spectrum that the major isomer observed in solution is complex **50** is supported by the low free energies for isomers 1 and 7, both bearing the methyl group close to the gold atom. The structure based on the crystal, however, bears the methyl group close to the trifluoroacetate and has not the lowest calculated free energy, although the difference in energy is less than 1 kcal/mol. That it was formed anyway can have different reasons. First of all the analysis of one selected specimen gives no information about the composition of the overall sample. Furthermore, for crystal formation the free energy of the complex is not the only important criterion, also interactions between the molecules are crucial factors for crystal packing and these effects are not considered in the structure optimization. In addition it must be considered that the kinetic product possibly crystallizes before the thermodynamic product does, which could also explain the discrepancy between NMR and X-ray analysis.

Table 1: Calculated relative values for the free energy and enthalpy of isomers.

	G_{rel} [kcal/mol]	H_{rel} [kcal/mol]
Isomer 1 (I1)	-0.5	-0.6
Isomer 2 (I2)	3.7	5.1
Isomer 3 (I3)	1.4	1.3
Isomer 4 (I4)	0.2	0.1
Isomer 5 (I5)	2.9	3.5
Isomer 6 (I6)	1.4	1.6
Isomer 7 (I7)	0.2	0.8
Isomer 8 (crystal)	0.0	0.0
Isomer 9 (transC)	22.0	21.3

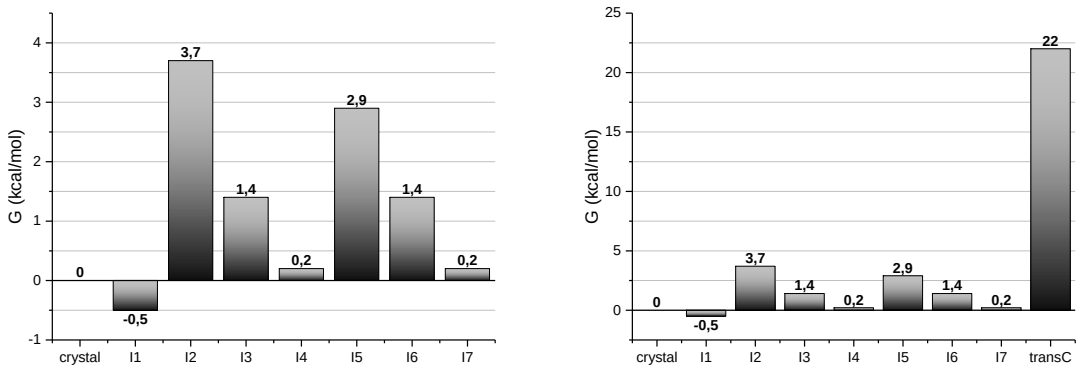

Figure 18: Graph depicting the relative free energy of the isomers.

The obtained solid-state structure was also compared with the geometry optimized in gas phase. The deviations of bond lengths are < 0.1 Å (Table 3) and indicate together with the root-mean-square deviations (RMSD) from the geometry optimized structure (Table 2) a good agreement between the X-ray and DFT structures.

$$RMSD = \sqrt{\frac{\sum_{i=1}^{n}(x_i - y_i)^2}{n}}$$

x = X-ray parameter; y = optimized geometry parameter

Table 2: The root-mean-square deviations (RMSD) from the X-ray structure of complex **5** and the DFT optimized structure. Only the selected bond lengths and angles from Table 3 and Table 4, respectively, were taken into consideration.

	Au-ligand distances (Å)	**Other distances (Å)**	**Angles (°)**
RMSD	0.013	0.038	2.3

Table 3: Deviations (D)[a] from the X-ray structure of complex **5** and the DFT calculated structure.

	X-ray structure	Calculated	
Atoms	**Bond length (Å)**	**Bond length (Å)**	**D[a] (Å)**
Au(1)-N(1)	2.124	2.149	-0.025
Au(1)-C(1)	2.003	2.006	-0.003
Au(1)-O(4)	2.102	2.101	0.001
Au(1)-C(13)	2.052	2.055	-0.003
O(1)-C(16)	1.483	1.455	0.028
C(13)-C(14)	1.523	1.521	0.002
C(13)-C(18)	1.512	1.521	-0.009
C(14)-C(15)	1.537	1.529	0.008
C(15)-C(16)	1.541	1.516	0.025
C(16)-C(17)	1.523	1.519	0.004
C(17)-C(18)	1.527	1.535	-0.008
C(17)-C(19)	1.422	1.522	-0.100

[a] D = x – y; x = X-ray parameter; y = optimized geometry parameter

Table 4: Deviations (D)[a] from the X-ray structure of complex **5** and the DFT calculated structure.

	X-ray structure	Calculated	
Atoms	**Angle (°)**	**Angle (°)**	**D[a] (°)**
C(1)-Au(1)-N(1)	81.5	81.0	0.5
C(1)-Au(1)-O(4)	174.3	170.1	4.2
C(1)-Au(1)-C(13)	93.7	94.1	-0.4
O(4)-Au(1)-N(1)	93.5	89.0	4.5
C(13)-Au(1)-N(1)	174.4	175.0	-0.6
C(13)-Au(1)-O(4)	91.5	95.8	-4.3
C(8)-N(1)-Au(1)	113.4	112.7	0.7
C(2)-C(1)-Au(1)	112.9	113.09	-0.2
C(13)-C(14)-C(15)	109.1	109.3	-0.2
C(16)-C(15)-C(14)	108.4	110.1	-1.7
C(16)-C(17)-C(18)	109.6	109.0	0.6
C(13)-C(18)-C(17)	111.0	111.7	-0.7
O(1)-C(16)-C(17)-C(19)	64.2	61.4	2.8

[a] D = x – y; x = X-ray parameter; y = optimized geometry parameter

2.1.6 1,5-Cyclooctadiene

The reactivity of gold(III) complex **1** towards dienes as well as cycloalkenes was investigated, so it is coherent to explore the reactivity towards cyclic dienes as a next step. 1,5-Cyclooctadiene was chosen due to its flexibility and thus versatility.

The reaction of 1,5-cyclooctadiene with $Au(OCOCF_3)_2(tpy)$ (**1**) in CD_2Cl_2/TFA-*d* (1:1) was first carried out in an NMR tube and monitored by ^{1}H-NMR. The gold(III) starting material was fully converted by ^{1}H-NMR within minutes and the recorded ^{1}H-NMR spectrum showed a clean reaction with one major product formed. In order to isolate the product and ease the determination of its structure the reaction was repeated on larger scale. However, product isolation was not possible because of decomposition upon removal of the solvent.

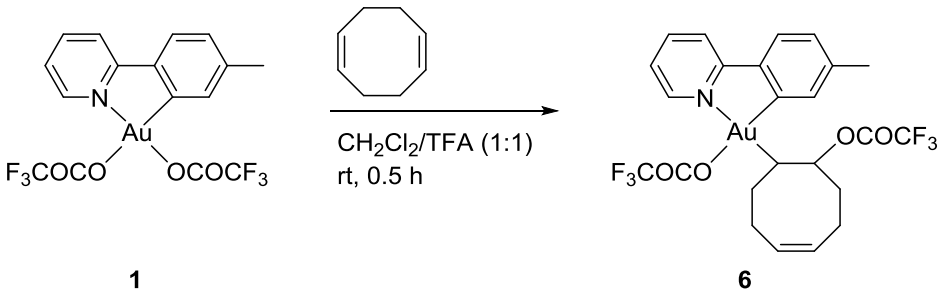

1 **6**

Scheme 21: Reaction of gold(III) complex **1** with 1,5-cyclooctadiene in CH_2Cl_2/TFA (1:1).

The reaction of $Au(OCOCF_3)_2(tpy)$ (**1**) with 1,5-cyclooctadiene in CH_2Cl_2/TFA (1:1) at room temperature yielded the alkyl gold(III) complex **6** (Scheme 21). Only one double bond of the diene was functionalized in this reaction. The obtained ^{1}H-NMR spectrum of complex **6** (Figure 19) shows the expected peaks from the tpy ligand in the aromatic region, including the shifted singlet signal from the tpy ligand towards the lower field signalizing a gold(III)-mediated nucleophilic attack at 1,5-cyclooctadiene. The small peaks in the aliphatic region are due to free 1,5-cyclooctadiene residues and the peak at 9.2 ppm is due to TFA residues. The most significant peaks in the recorded ^{1}H-NMR spectrum of complex **6** are the proton peaks of the hydrogens bonded to the remaining double bond as well as the protons bonded to the other two methine group carbons in the eight-membered ring. The assignment of these peaks (Figure 19) is substantiated by the couplings observed in the COSY and HSQC, showing that the blue labeled

hydrogens as well as the red labeled one couple with each other and that all four hydrogens are bonded to methine group carbon atoms (Figure 20).

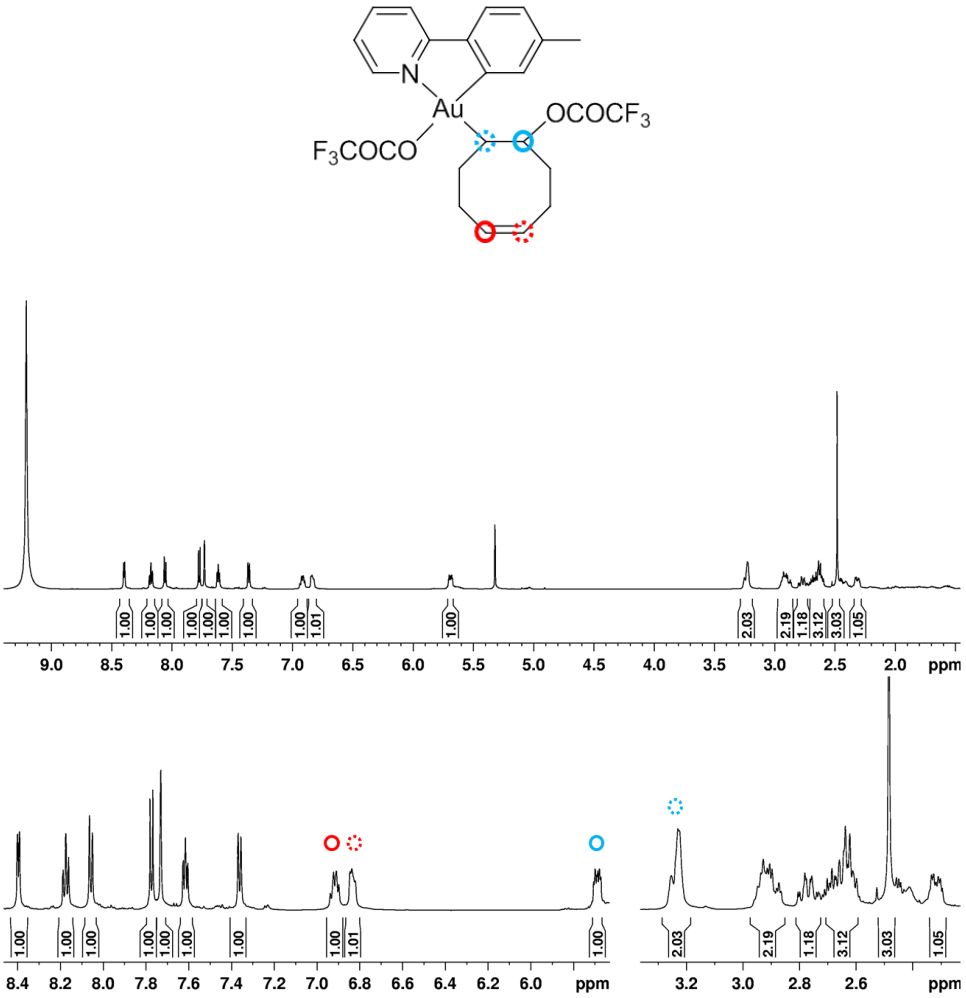

Figure 19: ^{1}H-NMR (600 MHz, CD_2Cl_2) of alkyl gold(III) complex **6**. Close-up views in the bottom. Peak at 9.2 ppm is due to TFA residue.

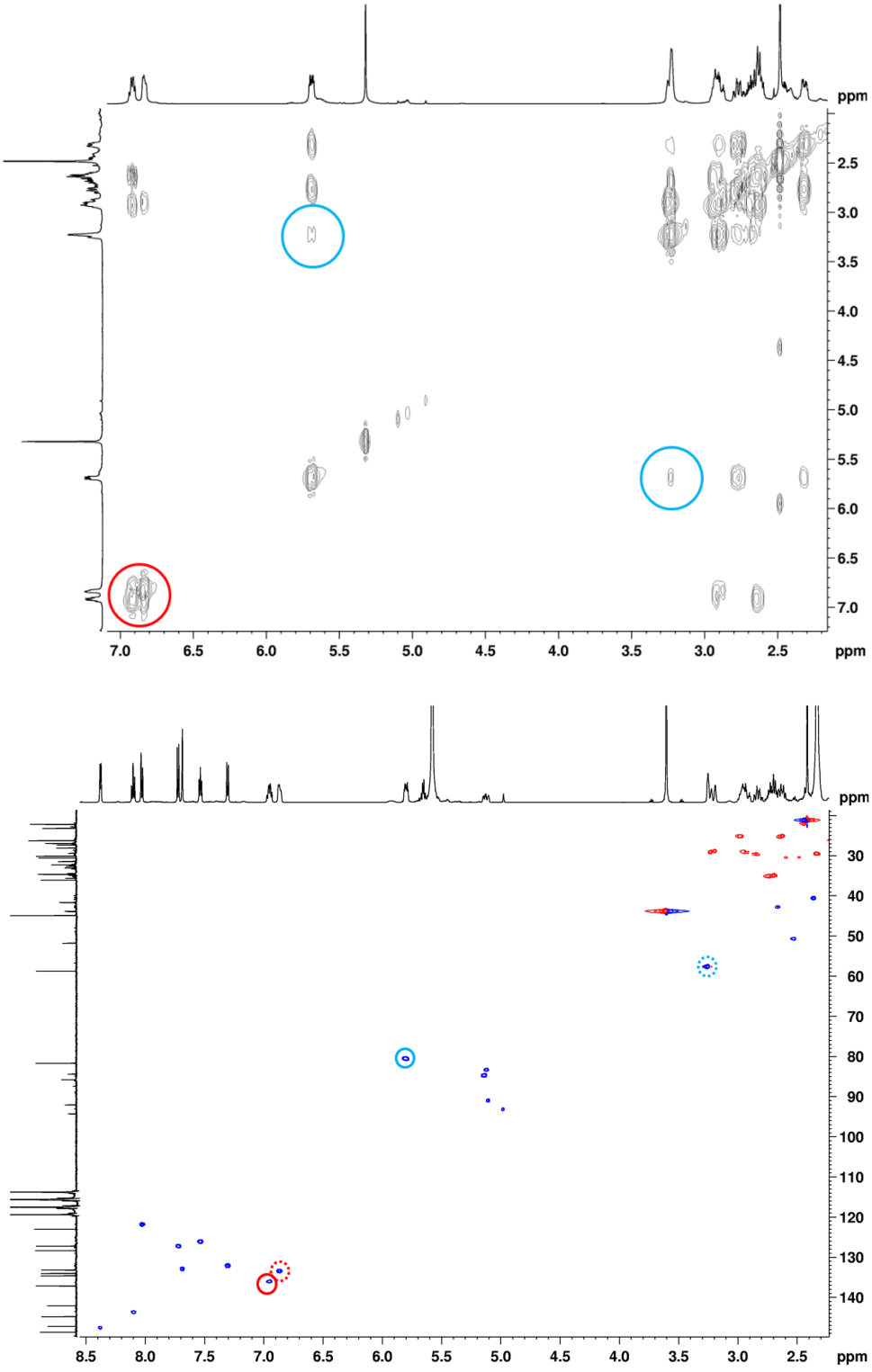

Figure 20: Close-up view of COSY (top) and HSQC (bottom) of complex **6**. HSQC spectrum obtained from small scale experiment, therefore additional peaks from starting material and internal standard.

2.1.7 Instability of Complexes

A major issue for the presented reactions in TFA is the instability of the formed products. Except the alkyl gold(III) complexes **2** and few other investigated complexes, obtained from reactions with relatively small and simple alkenes, all products decompose upon removal of the solvent and could therefore not be isolated.

It is assumed that this instability of the alkyl gold(III) complexes is attributed to the reversibility of the nucleophilic addition of trifluoroacetate as well as the reversibility of the alkene coordination. These reversibilities were indicated by the experiments conducted with ethylene.[7] Since trifluoroacetate is a good leaving group, removing the solvent for isolation might change the equilibrium and therefore forces the reverse reaction to take place, leading eventually to decomposition of the gold(III) complex.

In a follow-up experiment the assumption of reversibility of the ethylene coordination could be supported further. The reaction of alkyl gold(III) complex **2** with the chloride source Bu_4NCl in TFA-*d* yielded $AuCl_2$(tpy) (**33**) (Scheme 22).

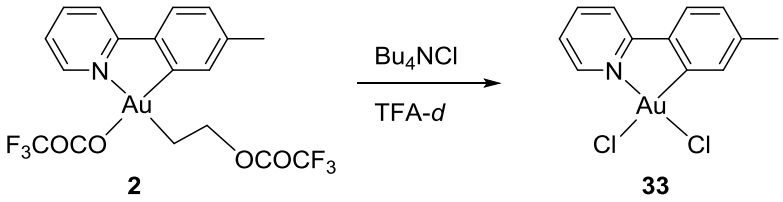

Scheme 22: Reaction of alkyl gold(III) complex **2** with Bu_4NCl in TFA-*d*.

After adding Bu_4NCl to a solution of **2** in TFA-*d* precipitation of a yellow solid was observed immediately. The recorded ^{1}H-NMR spectrum showed no signals in the aromatic region, indicating that no gold(III) complex remained in solution and therefore implying that the reaction proceeded in a quantitative manner (Figure 21). In the next step the solvent was removed *in vacuo*, the residues dissolved in DMSO-d_6 and spiked with $AuCl_2$(tpy) (**33**) to verify the nature of the precipitate. Since **33** is poorly soluble, even in DMSO-d_6, more solvent was added to increase the amount of dissolved complex. As depicted in Figure 22, the resulting ^{1}H-NMR spectrum shows growth of the peaks belonging to the gold(III) complex while the other peaks stay unaltered, except solvent and water peaks due to addition of DMSO-d_6. Also no additional peaks appeared upon spiking the sample with $AuCl_2$(tpy) (**33**), which suggests that the precipitate only contains **33** and the ammonium salts.

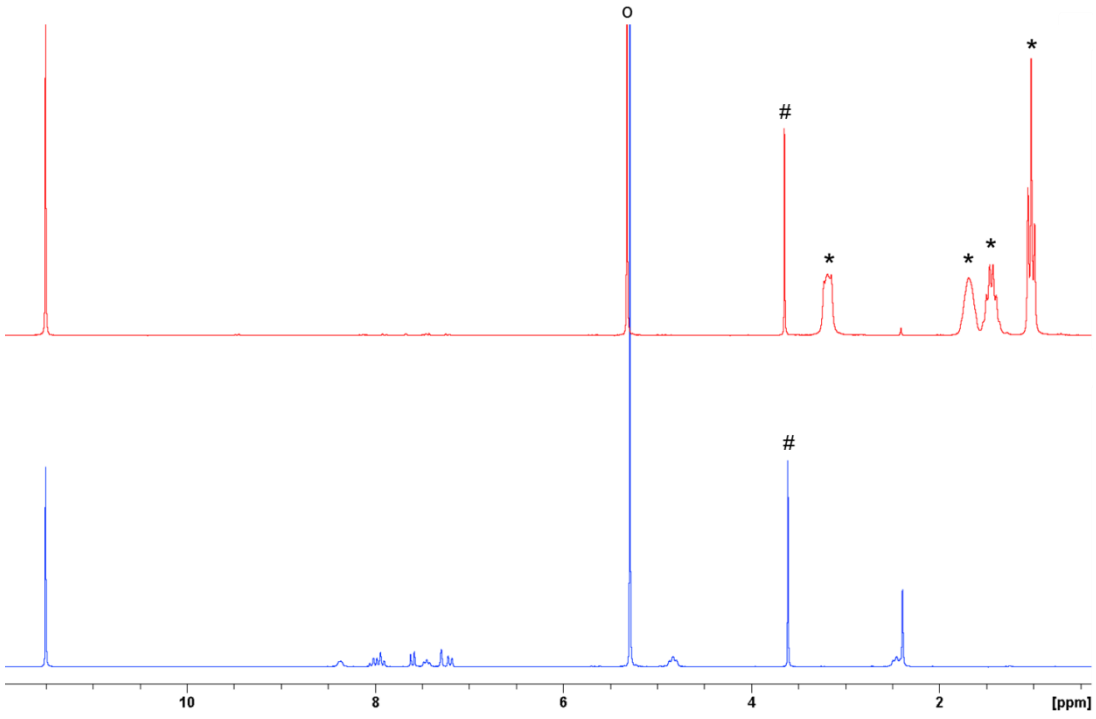

Figure 21: Stacked ^{1}H-NMR (200 MHz, TFA-*d*). Showing the result of the reaction of ethylene (^{o}) with $Au(OCOCF_3)_2(tpy)$ (**1**) in TFA-*d*, with 1,2-dichloroethane($^\#$) as internal standard (blue). Recorded spectrum after addition of Bu_4NCl (ammonium salt peaks are labeled with *) (red).

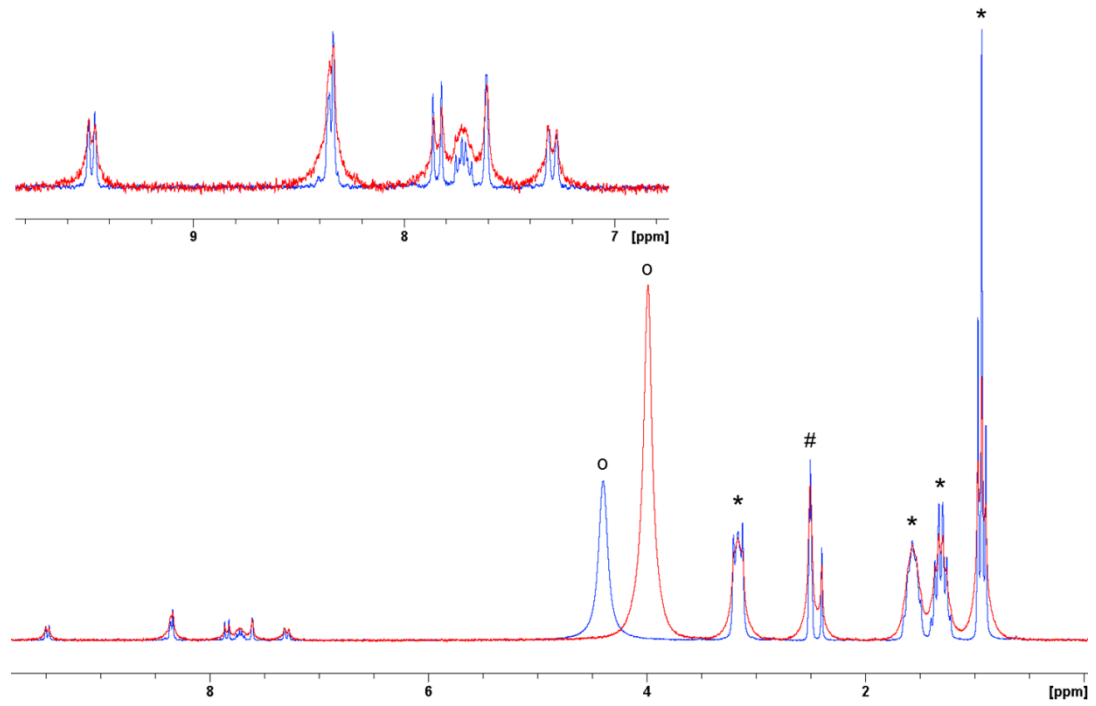

Figure 22: Stacked ^{1}H-NMR (200 MHz, DMSO-d_6 ($^\#$)). Showing the precipitate of the reaction of **2** with Bu_4NCl (ammonium salt peaks are labeled with *) (blue) and the recorded spectrum after spiking with **33** and adding DMSO-d_6 to increase the solubility (red). Water residues are labeled with ^{o}.

2.2 Gold(III)-mediated Nucleophilic Attack at Alkenes – TFE

2.2.1 1,5-Hexadiene

Inspired by the new alkyl gold(III) complex **48** obtained in the reaction of $Au(OCOCF_3)_2(tpy)$ (**1**) with ethylene in TFE, the reaction of 1,5-hexadiene in TFE was investigated in order to explore the influence of another nucleophile towards the six-membered ring formation.

The reaction of 1,5-hexadiene with $Au(OCOCF_3)_2(tpy)$ (**1**) in TFE-d_3 was first carried out in an NMR tube and monitored by ^{1}H-NMR. The gold(III)starting material was fully converted by ^{1}H-NMR within minutes and the recorded ^{1}H-NMR spectrum showed a mix of products. The reaction was also repeated on larger scale but product isolation was not possible.

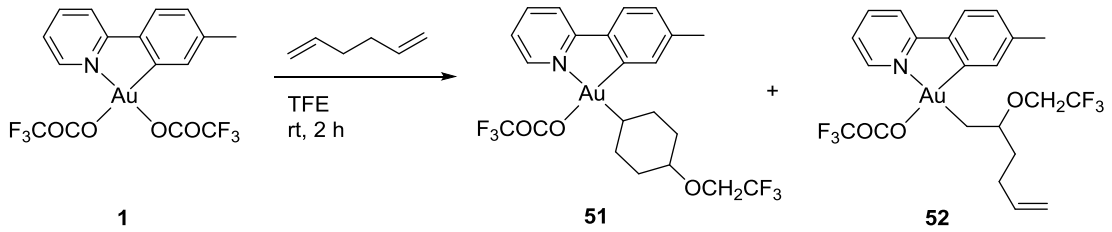

Scheme 23: Assumed products resulting from reaction of gold(III) complex **1** with 1,5-hexadiene in TFE.

The reaction of $Au(OCOCF_3)_2(tpy)$ (**1**) with 1,5-hexadiene in TFE at room temperature yielded after cannula filtration a white precipitate and a solution that presumably contained the alkyl gold(III) complexes **51** and **52** as main products (Scheme 23). The precipitate was only poorly soluble in standard solvents (CD_2Cl_2, MeCN and DMSO), so no good ^{1}H-NMR spectrum could be obtained. However, it is assumed to be a polymer formed through polymerization of the double bonds in the molecule, which would explain the poor solubility. The obtained ^{1}H-NMR spectrum of the remaining solution is depicted in Figure 23. It seems like two major products are observed. One product contains a double bond, showing typical shifts for vinylic protons (labeled with *), similar to the shifts observed in product **3**, resulting from reaction with 1,4-pentadiene in TFA. And the other product seemingly formed a six-membered ring (labeled with °), showing proton shifts similar to product **4**, resulting from reaction with 1,5-hexadiene in TFA. As depicted in Figure 24, these assignments also correspond with the couplings observed in

the COSY and HSQC. Since so many peaks are overlapping, not every signal could be unambiguously assigned but the significant peaks support the assumption of complex formation of **51** and **52** quite well.

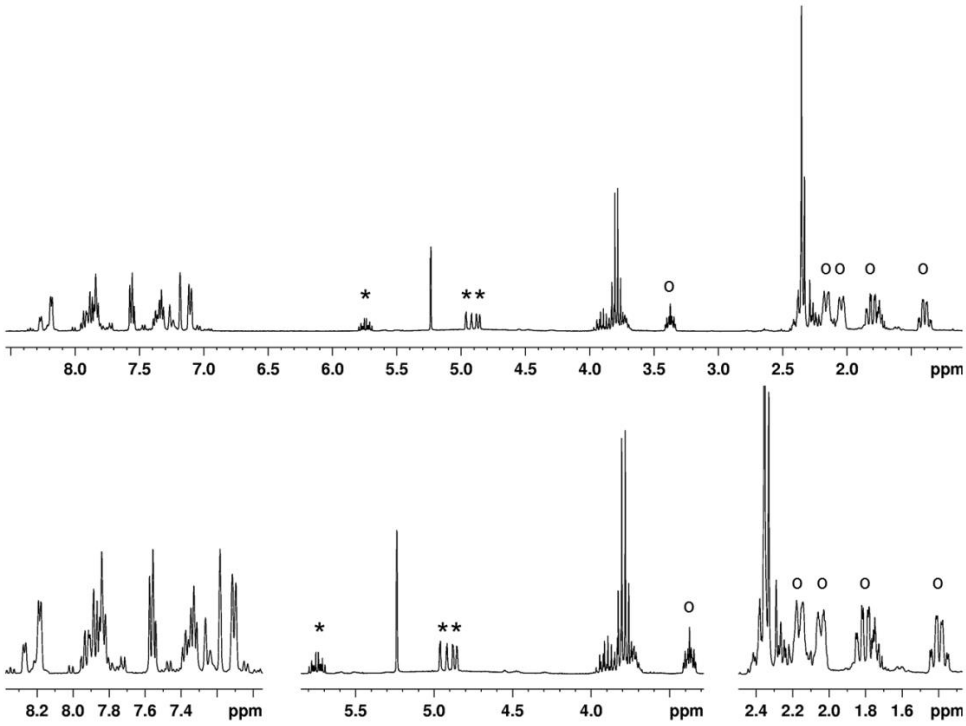

Figure 23: ^{1}H-NMR (400 MHz, CD_2Cl_2) of reaction products of gold(III) complex **1** and 1,5-hexadiene in TFE. Close-up views in the bottom. (* indicates complex **52**, ° indicates complex **51**)

The dependency on the solvent in the formation of the six-membered ring in the reaction with 1,5-hexadiene might be attributed to the different nucleophilicities of TFA and TFE, with TFE being the better nucleophile. In the reaction with 1,5-hexadiene in TFA it is conceivable that after one double bond of the diene is already coordinated to gold, the non-coordinated double bond represents a better nucleophile compared to trifluoroacetate and therefore the diene attacks itself. While it is possible that in the reaction in TFE the nucleophilicities of the non-coordinated double bond and TFE are more equal, so that ring formation as well as functionalization of only one double bond occur in the same reaction, depending on the nucleophile attacking the coordinated double bond.

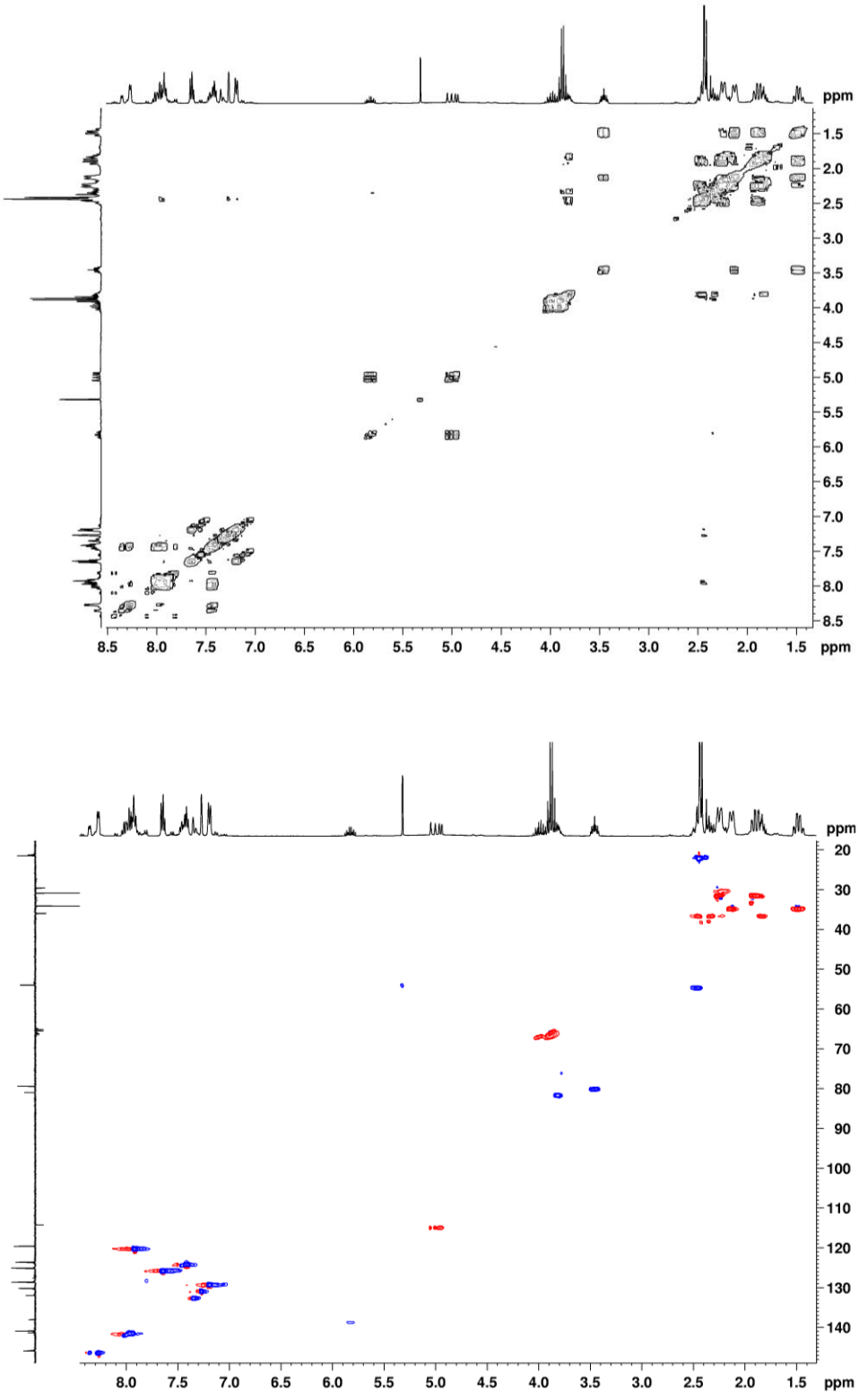

Figure 24: COSY (top) and HSQC (bottom) of the products in the reaction of gold(III) complex **1** with 1,5-hexadiene in TFE.

2.3 Gold(III)-mediated Nucleophilic Attack at Alkenes – EtOH

Changing the solvent to TFE did not improve the isolability of the products, so instability of the products remains a major issue. This problem was addressed by exploring the usage of non-fluorinated solvents in the reactions with ethylene.[73] While full conversion to the expected product was observed after one day in the reaction using EtOH, the reaction in acetic acid took twelve days until completion.[73] For obvious practical reasons further investigations were focused on reactions in EtOH.

Other group members explored reactions using simple, terminal alkenes and managed the first time to isolate some of the products deriving from reactions with those olefins.[73],[74] However, all products contained small impurities that could not be removed.

2.3.1 1,4-Pentadiene, 1,5-Hexadiene

The use of TFE as solvent showed an alteration of the product formation in the reaction with 1,5-hexadiene compared to the reaction using TFA. To investigate these different behaviors further, the reactivity of $Au(OCOCF_3)_2(tpy)$ (**1**) towards dienes in EtOH was explored.

The reaction of $Au(OCOCF_3)_2(tpy)$ (**1**) with 1,4-pentadiene in EtOH at room temperature yielded presumably the alkyl gold(III) complexes **53** and **15** as main products (Scheme 24).

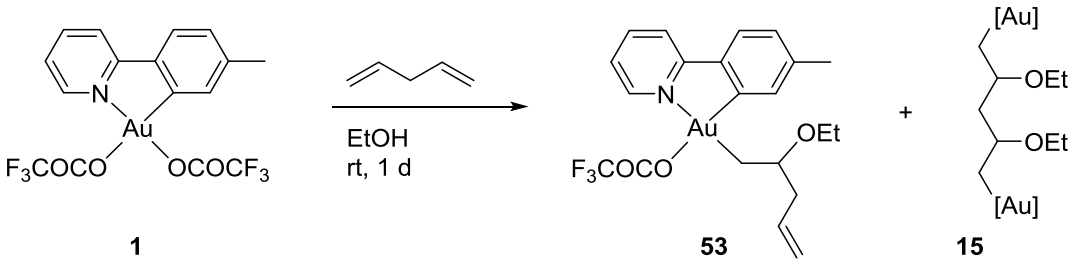

Scheme 24: Assumed products resulting from reaction of gold(III) complex **1** with 1,4-pentadiene in EtOH. [Au]: $Au(OCOCF_3)(tpy)$.

The obtained ^{1}H-NMR spectrum shows a product mixture (Figure 25). One product contains a double bond, showing typical shifts for vinylic protons of a terminal double bond (labeled with * in Figure 25), similar to the shifts observed in product **3**, resulting from the reaction with 1,4-pentadiene in TFA.

Crystals suitable for single crystal X-ray analysis were obtained by vapor diffusion using CH_2Cl_2 as solvent and *n*-pentane as anti-solvent. The solid-state structure of the selected specimen verifies the dimer **15**. This observation is possibly in agreement with the recorded ^{1}H-NMR spectrum that shows two sets of triplets at 1.2 ppm. These triplets originate from the methyl groups of the ethoxy groups in the alkyl gold(III) complexes that have different environments, which is given in complexes **53** and **15**.

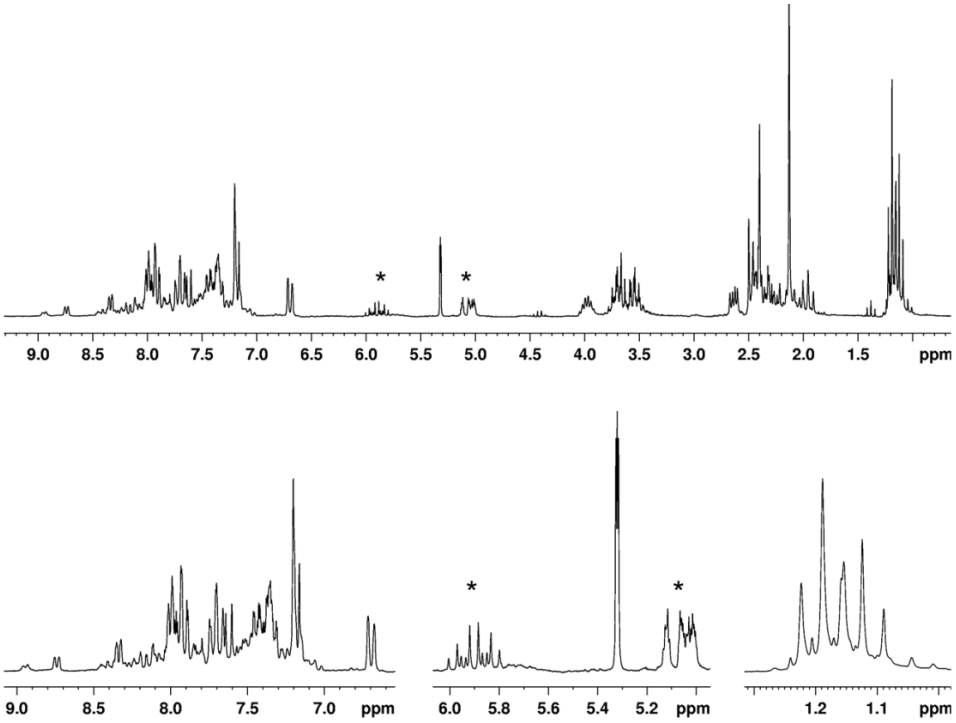

Figure 25: ^{1}H-NMR (200 MHz, CD_2Cl_2) of reaction products of gold(III) complex **1** and 1,4-pentadiene in EtOH. Close-up views in the bottom. (* indicates complex **53**)

The reaction of $Au(OCOCF_3)_2(tpy)$ (**1**) with 1,5-hexadiene in EtOH at room temperature yielded presumably the alkyl gold(III) complexes **54** and **16** as main products (Scheme 25).

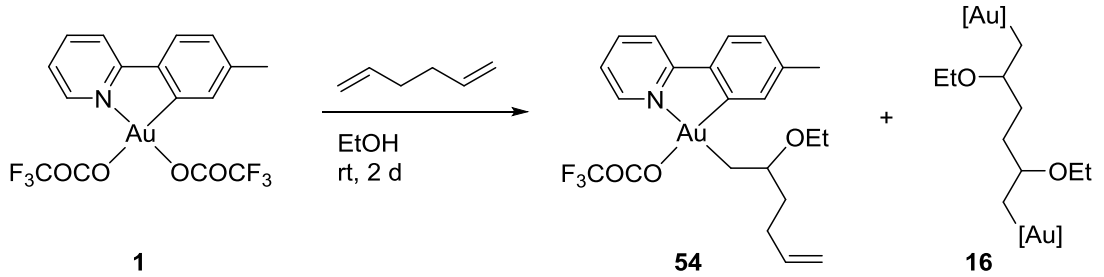

1 **54** **16**

Scheme 25: Assumed products resulting from reaction of gold(III) complex **1** with 1,5-hexadiene in EtOH. [Au]: $Au(OCOCF_3)(tpy)$.

The obtained ^{1}H-NMR spectrum shows a product mixture (Figure 26), where one product contains a double bond, showing typical shifts for vinylic protons of a terminal double bond (labeled with * in Figure 26), analogous to the reaction with 1,4-pentadiene.

Crystals suitable for single crystal X-ray analysis were obtained by vapor diffusion using CH_2Cl_2 as solvent and *n*-pentane as anti-solvent. The solid-state structure of the selected specimen verifies the dimer **16**. The argumentation regarding the recorded ^{1}H-NMR spectrum is resembling the one of 1,4-pentadiene, here two sets of triplets at 1.1 ppm are observed as well. It should be mentioned that the splitting pattern corresponding to the six-membered ring is not observed in the ^{1}H-NMR spectrum of this reaction, which indicates a higher nucleophilicity of EtOH compared to TFA and TFE.

The observations made for the reaction with 1,5-hexadiene are analogous to the ones described for the reaction with 1,4-pentadiene in EtOH and suggest a resembling reaction pathway for both dienes. It is assumed that the increased nucleophilicity of EtOH compared to trifluoroacetate allows not merely functionalization of one double bond due to a nucleophilic attack, but attack at both double bonds, hence furnishing the dimer.

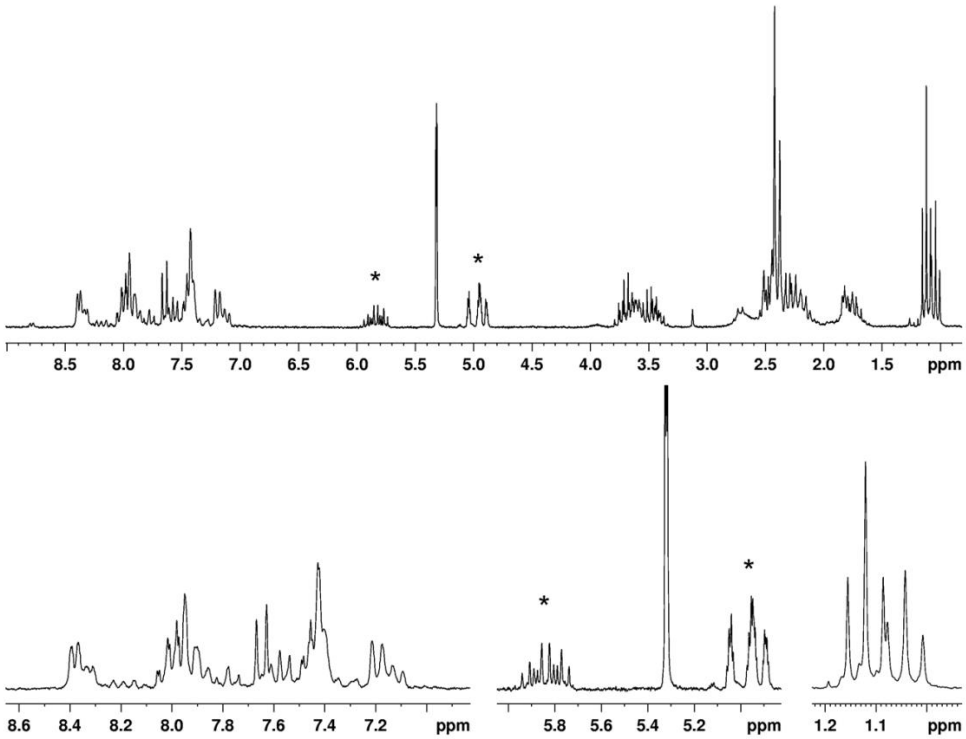

Figure 26: ^{1}H-NMR (200 MHz, CD_2Cl_2) of reaction products of gold(III) complex **1** and 1,5-hexadiene in EtOH. Close-up views in the bottom. (* indicates complex **54**).

2.4 Gold(III)-mediated Nucleophilic Attack at Alkenes – MeOH

The results of the reactions in EtOH were promising and shifted the focus of investigation towards other alcohols. As discussed before, the reversibility of these gold(III)-mediated nucleophilic additions at alkenes is assumed to be the major reason for the instability of the products. Since the methoxy group is an even poorer leaving group than the ethoxy group is, MeOH was investigated as solvent.[73]

Other group members explored reactions using simple, terminal alkenes as well as cycloalkenes.[73],[74] While most of the obtained products were instable and decomposed upon removal of the solvent when the reaction was performed in TFA, all reactions performed in MeOH were successful and yielded the expected alkyl gold(III) products, which were stable and could be isolated.[73],[74]

2.4.1 *Cis*-3-hexene

Inspired by the interesting results regarding isolation of the alkyl gold(III) complexes synthesized from the reactions in MeOH compared to the instability of the TFA analogous products, reactions in MeOH using linear internal alkenes were investigated.

The reaction of $Au(OCOCF_3)_2(tpy)$ (**1**) with *cis*-3-hexene in MeOH at room temperature gave after two days the alkyl gold(III) complex **7** in very good yields (Scheme 26).

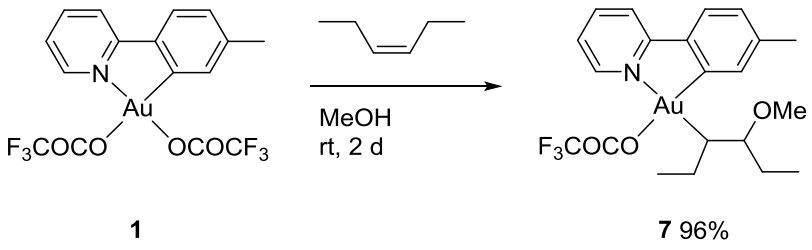

1 **7** 96%

Scheme 26: Reaction of gold(III) complex **1** with *cis*-3-hexene in MeOH.

The recorded ^{1}H-NMR spectrum shows only minor impurities, probably an isomer (Figure 27). The assignment of the peaks is straight forward with the expected peaks in the aromatic region from the tpy ligand as well as the proton peaks from the hydrogens bonded to the methine group carbons in the expected region. The hydrogen with the shift to the lower field is bonded to the same carbon as the methoxy group, while the other hydrogen is bonded to the same carbon as gold. The peak at 3.4 ppm is due to the

methoxy group. It is interesting that the ^{1}H-NMR spectrum is so clean, indicating that the reaction occurs really selective at the *cis*-isomer, allowing no or just minor scrambling.

Crystals suitable for single crystal X-ray analysis were obtained by vapor diffusion using CH_2Cl_2 as solvent and *n*-pentane as anti-solvent. The solid-state structure of the selected specimen verifies complex **7** and suggests that the nucleophilic attack occurred in an *anti* manner.

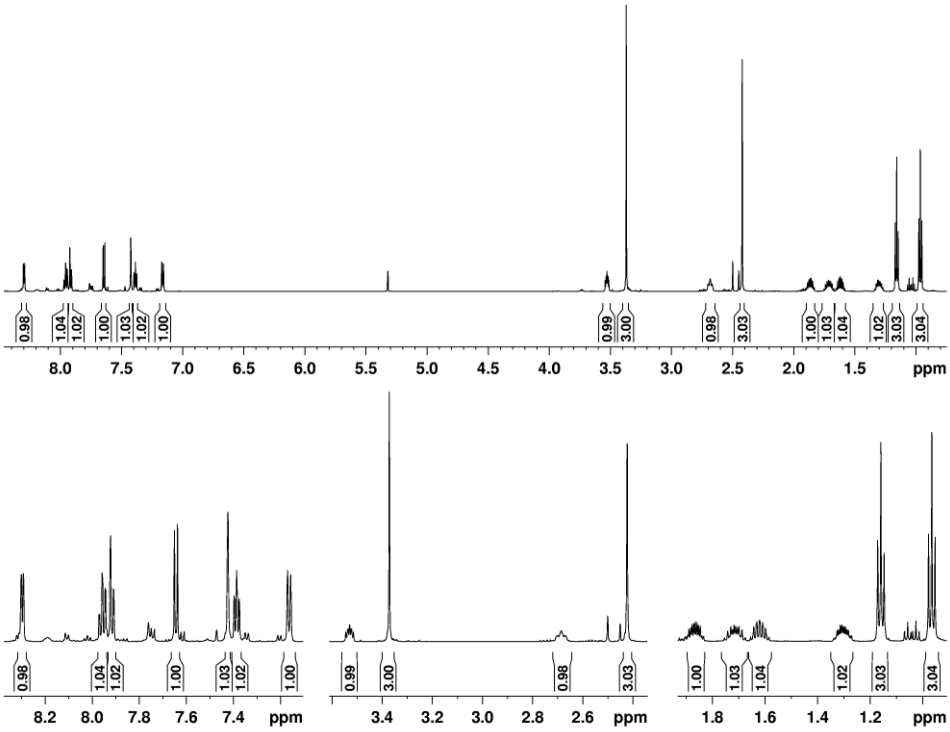

Figure 27: ^{1}H-NMR (600 MHz, CD_2Cl_2) of alkyl gold(III) complex **7**. Close-up views in the bottom.

2.4.2 *Trans*-3-hexene

The reaction of $Au(OCOCF_3)_2(tpy)$ (**1**) with *trans*-3-hexene in MeOH at room temperature yielded after two days the alkyl gold(III) complex **8** (Scheme 27). The product was not obtained entirely pure and contained approximately 15% starting material **1**.

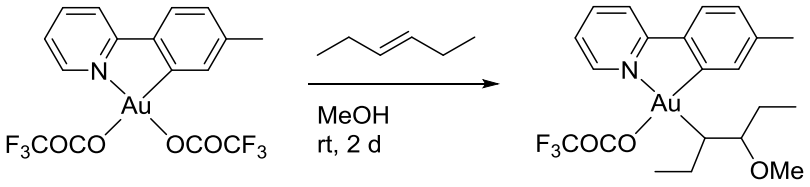

1 **8**

Scheme 27: Reaction of gold(III) complex **1** with *trans*-3-hexene in MeOH.

The recorded ^{1}H-NMR spectrum shows besides the starting material only minor impurities, probably an isomer (Figure 28). The assignment of the peaks is straight forward with the expected peaks in the aromatic region from the tpy ligand as well as the proton peaks from the hydrogens bonded to the methine group carbons in the expected region. The hydrogen with the shift to the lower field is bonded to the same carbon as the methoxy group, while the other hydrogen is bonded to the same carbon as gold. The peak at 3.4 ppm is due to the methoxy group. Corresponding with the recorded ^{1}H-NMR spectrum of complex **7**, also this spectrum is quite clean, indicating that the reaction occurs really selective at the *trans*-isomer, allowing no or just minor scrambling.

Crystals suitable for single crystal X-ray analysis were obtained by vapor diffusion using CH_2Cl_2 as solvent and *n*-pentane as anti-solvent. The solid-state structure of the selected specimen verifies complex **8** and suggests that the nucleophilic attack occurred in an *anti* manner.

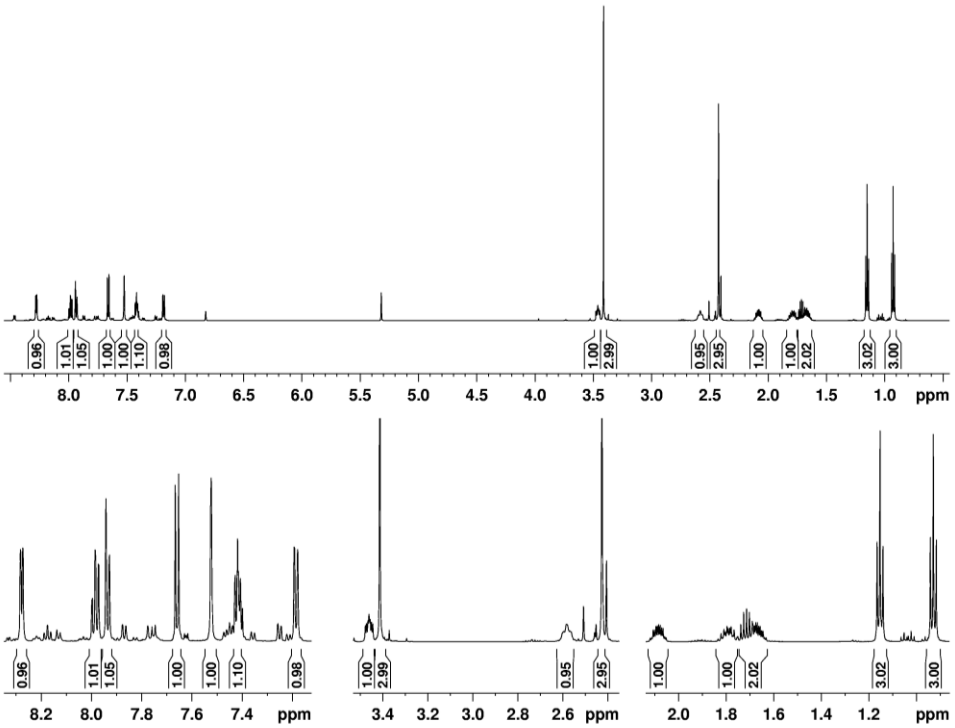

Figure 28: ^{1}H-NMR (600 MHz, CD_2Cl_2) of alkyl gold(III) complex **8**. Close-up views in the bottom.

2.4.3 *Trans*-2-hexene

To investigate if the bulkiness of the substituents at the internal alkene is influencing the preference of the position where the nucleophilic attack is taking place, the reaction with *trans*-2-hexene was explored.

The reaction of $Au(OCOCF_3)_2(tpy)$ (**1**) with *trans*-2-hexene in MeOH at room temperature gave after three days the alkyl gold(III) complexes **9** and **10** in an overall yield of 96% (Scheme 28). The product ratio of complex **9** to **10** is approximately 2:1 (Figure 29).

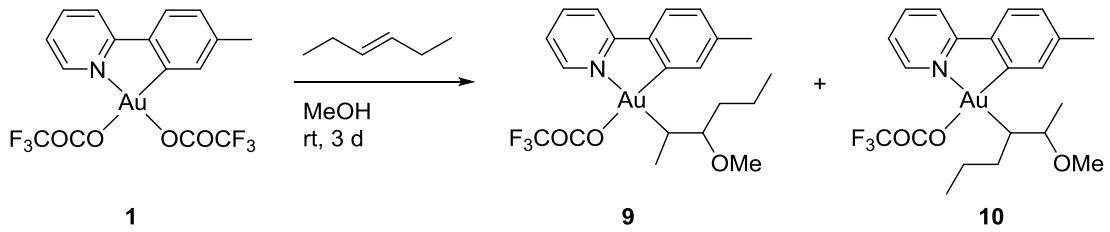

Scheme 28: Reaction of gold(III) complex **1** with *trans*-2-hexene in MeOH.

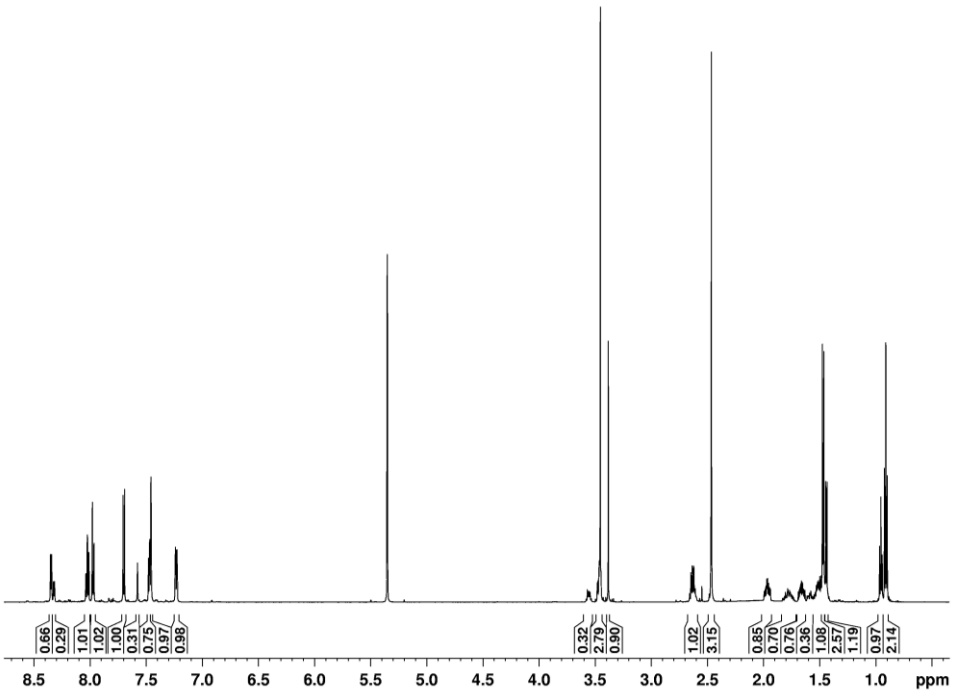

Figure 29: ^{1}H-NMR (600 MHz, CD_2Cl_2) of reaction products of gold(III) complex **1** and *trans*-2-hexene in MeOH.

The products could be isolated through crystallization of the mixture by vapor diffusion using CD_2Cl_2 as solvent and *n*-pentane as anti-solvent. It was possible to observe two kinds of crystals differing in their appearance and morphology. The solid-state structures of the selected specimen verify complexes **9** and **10**. The crystal structures suggest that the nucleophilic attack occurred in an *anti* manner. The crystals were separated by hand and new NMR spectra were recorded for each complex.

The major isomer resembles complex **9**, supported by NMR (Figure 30) as well as crystal data. The assignment of the peaks is straight forward with the expected peaks in the aromatic region from the tpy ligand as well as the proton peaks from the hydrogens of the methine groups in the expected region. The hydrogen with the shift to the lower field is bonded to the same carbon as the methoxy group, while the other hydrogen is bonded to the same carbon as gold. The peak at 3.4 ppm is due to the methoxy group.

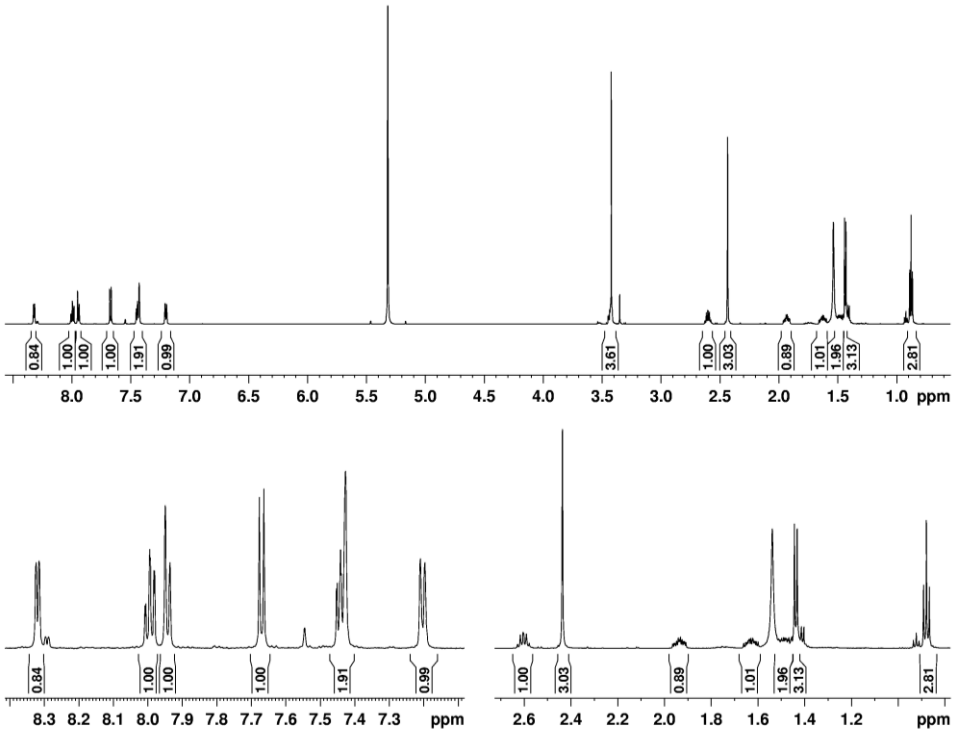

Figure 30: ^{1}H-NMR (600 MHz, CD_2Cl_2) of alkyl gold(III) complex **9**. Close-up views in the bottom. Peak at 1.5 ppm is due to water.

The minor isomer resembles complex **10**, supported by NMR (Figure 31) as well as crystal data. The assignment of the peaks of complex **10** is analogous to the assignment in complex **9**. The peak at 3.5 ppm is due to the methoxy group.

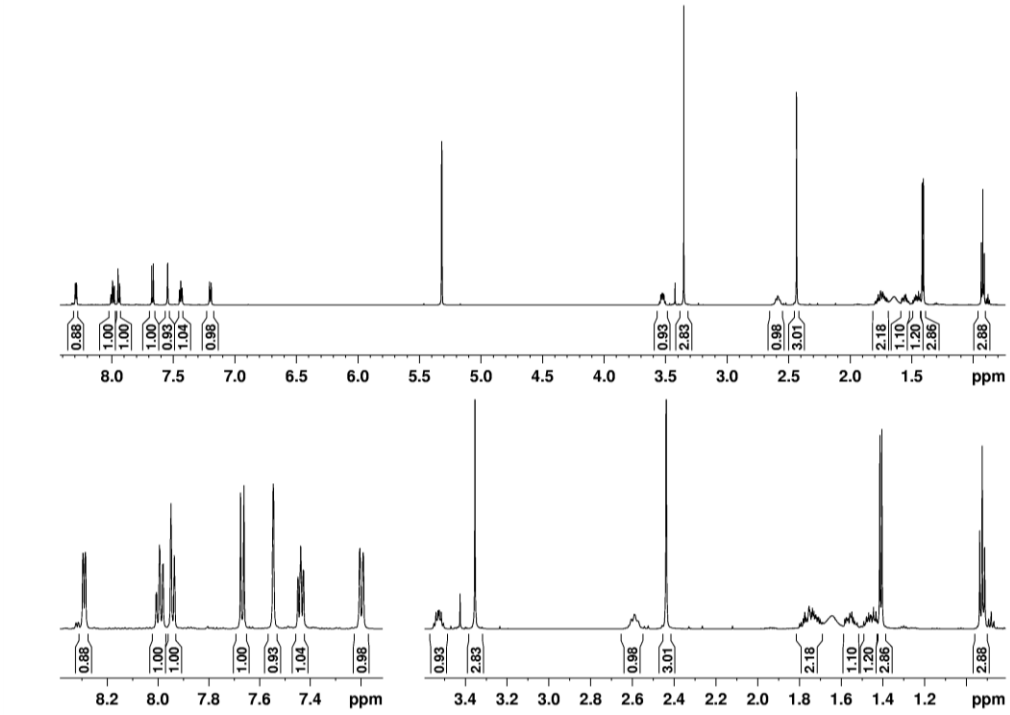

Figure 31: ^{1}H-NMR (600 MHz, CD_2Cl_2) of alkyl gold(III) complex **10**. Close-up views in the bottom. Peak at 1.6 ppm is due to water.

The ^{1}H-NMR spectra of complex **9** and **10** show both minor peaks of the other isomer. The samples were monitored by ^{1}H-NMR over a period of two weeks and no interconversion of the isomers was observed, the ratio of the peaks stayed the same in both samples. That supports the assumption that the presence of the other isomer in each sample can be ascribed due to inaccuracy in the separation by manual crystal picking. This absence of interconversion of isomers indicates a good stability of the complexes and that no reverse reaction is taking place.

Furthermore, the product ratio of approximately 2:1 for **9** to **10** suggests a preference of the nucleophilic attack occurring at the site of the double bond that is substituted with the longer alkyl chain.

2.4.4 Styrene

Styrene is of special interest because it bears the electron withdrawing phenyl group, which might open new possibilities for the investigated gold(III) mediated nucleophilic additions at alkenes. Styrene was also tested as alkene in the reaction with TFA as solvent. While styrene is not stable in pure TFA, due to polymerization, the use of solvent mixtures with different TFA/CH_2Cl_2 ratios did not result in any reaction in the presence of $Au(OCOCF_3)_2(tpy)$ (**1**). However, since the use of MeOH as solvent gave promising results for alkyl substituted alkenes the interest in the exploration of the reaction with styrene was renewed.

The reaction of $Au(OCOCF_3)_2(tpy)$ (**1**) with styrene in MeOH at room temperature gave after one day the alkyl gold(III) complex **11** in good yields (Scheme 29). Crystals suitable for single crystal X-ray analysis were obtained by vapor diffusion using CH_2Cl_2 as solvent and *n*-pentane as anti-solvent. The solid-state structure of the selected specimen verifies complex **11** and suggests that the nucleophilic attack occurred in Markovnikov manner. Furthermore, HR-MS was taken and confirmed the structure of product **11**.

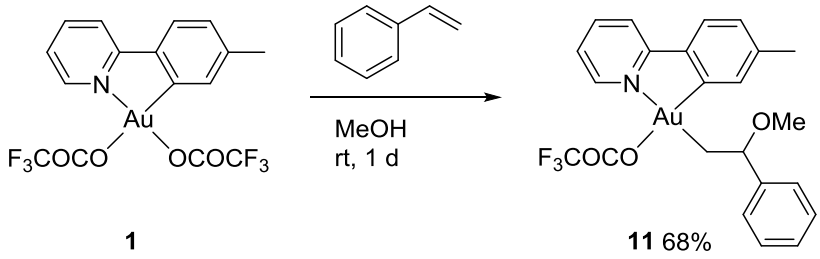

Scheme 29: Reaction of gold(III) complex **1** with styrene in MeOH.

The assignment of the peaks in the recorded ^{1}H-NMR spectrum is straight forward with the expected peaks in the aromatic region from the tpy ligand as well as the expected proton peaks from the phenyl ring of the former styrene (Figure 32). The proton peak from the hydrogen bonded to the same carbon as the methoxy group is in the expected region and the diastereotopic hydrogens that are bonded to the same carbon as gold show a reasonable splitting pattern. The peak at 3.2 ppm is due to the methoxy group.

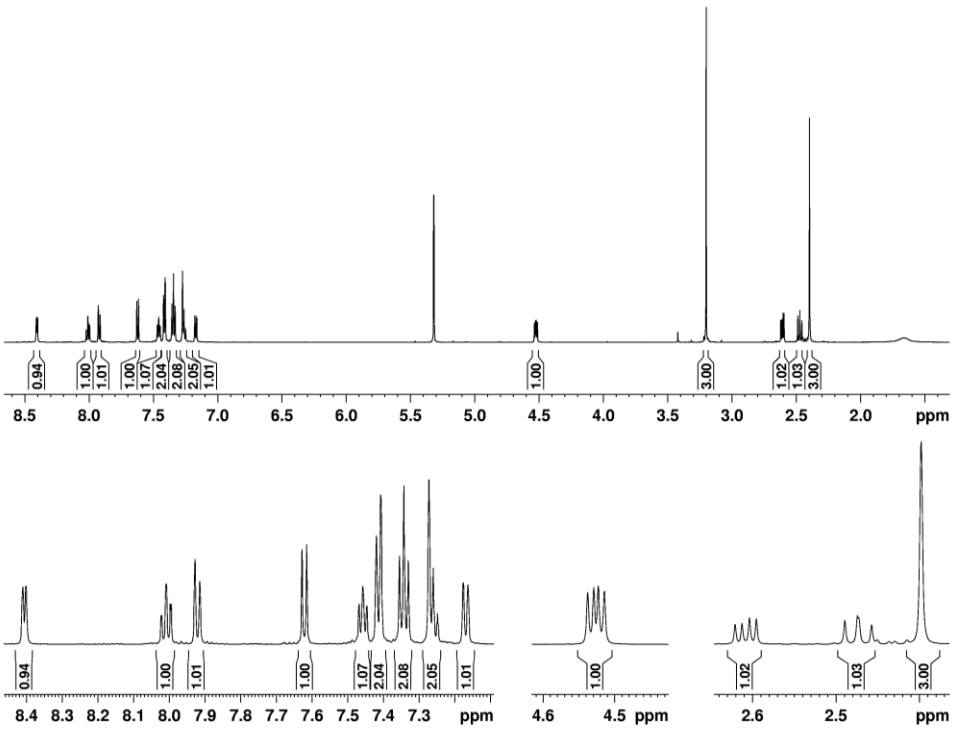

Figure 32: ^{1}H-NMR (600 MHz, CD_2Cl_2) of alkyl gold(III) complex **11**. Close-up views in the bottom. Peak at 1.6 ppm is due to water.

2.4.5 1,5-Cyclooctadiene, 1,4-Pentadiene, 1,5-Hexadiene

After obtaining informative and satisfying results regarding selectivity as well as product stability from the reactions with monoalkenes in MeOH, the investigations were focused on reactions using dienes.

The reaction of $Au(OCOCF_3)_2(tpy)$ (**1**) with 1,5-cyclooctadiene in MeOH at room temperature yielded after three hours a product mixture that could not be identified by ^{1}H-NMR and contained approximately 10% starting material **1** (Scheme 30). However, it was possible to obtain crystals suitable for X-ray analysis out of the mixture by vapor diffusion using CD_2Cl_2 as solvent and *n*-pentane as anti-solvent. The solid-state structure of the selected specimen verifies complex **12** and suggests that the nucleophilic attack occurred in an *anti* manner. Extension of the reaction time to two days led to decomposition of the complex, indicated by a golden mirror at the wall of the flask.

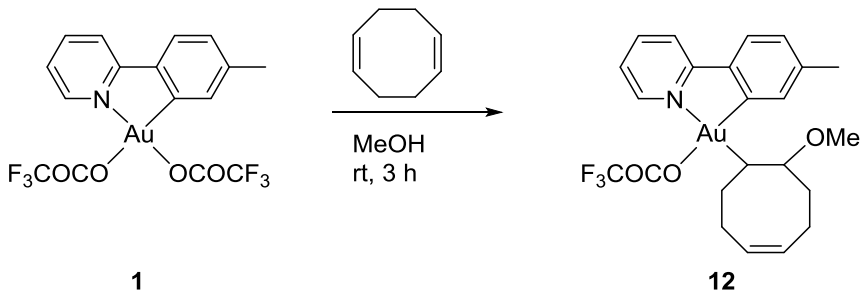

Scheme 30: One of the products obtained from the reaction of $Au(OCOCF_3)_2(tpy)$ (**1**) with 1,5-cyclooctadiene in MeOH.

The reaction of $Au(OCOCF_3)_2(tpy)$ (**1**) with 1,4-pentadiene in MeOH at room temperature yielded after one day a product mixture (Scheme 31). This mixture presumably contains, based on the recorded ^{1}H-NMR spectrum and the experience gained in the other reactions using 1,4-pentadiene, complexes **55** and **56**.

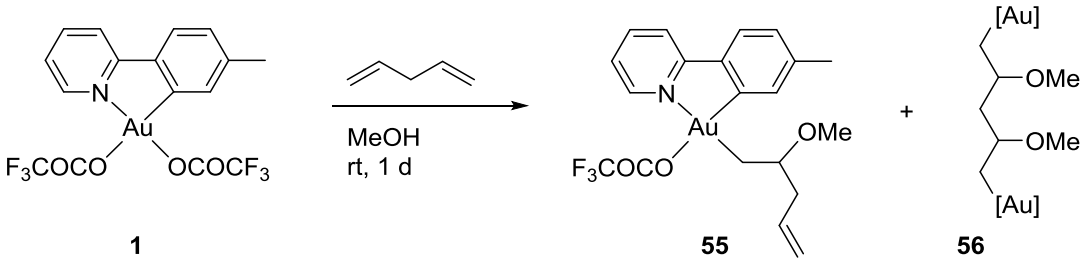

Scheme 31: Assumed products resulting from reaction of gold(III) complex **1** with 1,4-pentadiene in MeOH.

The obtained ^{1}H-NMR spectrum shows a product mixture (Figure 33), where one product contains a double bond, showing typical shifts for vinylic protons of a terminal double bond (labeled with * in Figure 33), analogous to the reaction with 1,4-pentadiene in EtOH. The recorded ^{1}H-NMR spectrum also shows two sets of singlets at 3.3 ppm. These singlets probably originate from the methoxy groups in the alkyl gold(III) complexes that have different environments. This observation of two sets of signals is analogous to the one made for the reaction in EtOH and might suggest the presence of the dimer **56**.

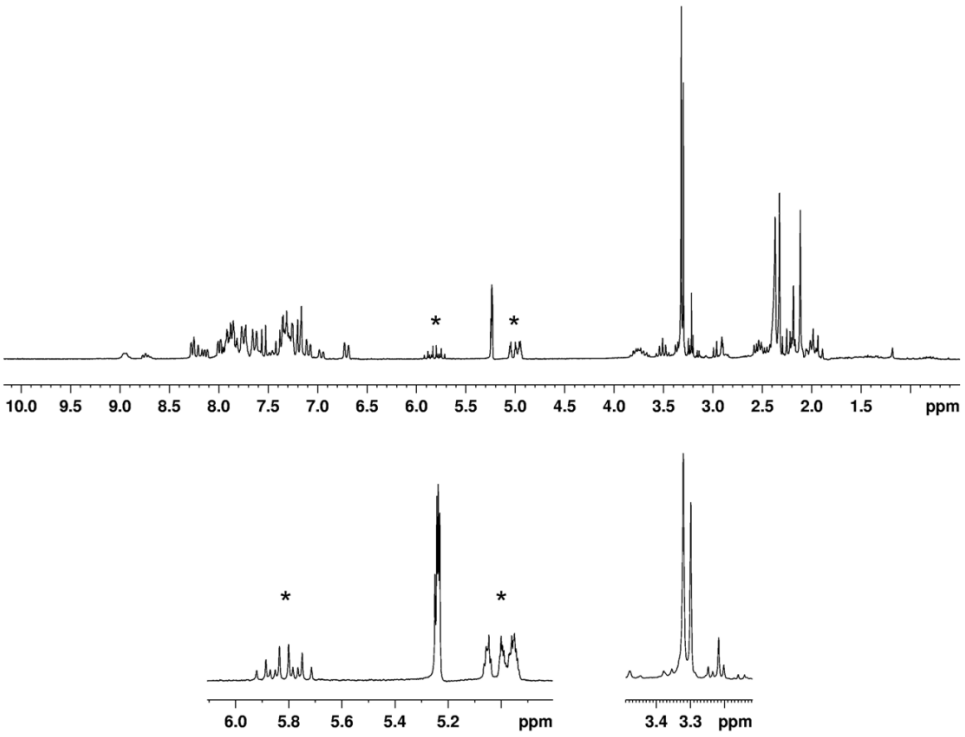

Figure 33: ^{1}H-NMR (200 MHz, CD_2Cl_2) of reaction products of gold(III) complex **1** and 1,4-pentadiene in MeOH. Close-up views in the bottom. (* indicates complex **55**)

The reaction of $Au(OCOCF_3)_2(tpy)$ (**1**) with 1,5-hexadiene in MeOH at room temperature yielded after two days a white solid, presumably the alkyl gold(III) complex **13** (Scheme 32). Observation of complex **13** indicates that the addition of the nucleophile proceeds in a Markovnikov manner, consistent with the results obtained from other reactions.

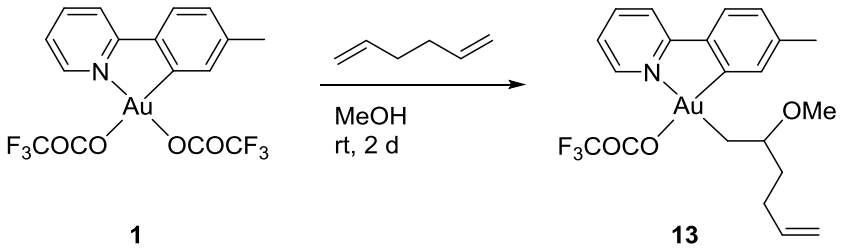

1 **13**

Scheme 32: Reaction of gold(III) complex **1** with 1,5-hexadiene in MeOH.

The white solid was only poorly soluble in standard solvents (CD_2Cl_2, MeCN, DMSO and acetone), so the obtained ^{1}H-NMR spectrum might not reflect the true nature of the product. However, the recorded ^{1}H-NMR spectrum showed next to the product **13** only minor impurities (Figure 34). The assignment of the peaks is straight forward with the

expected peaks in the aromatic region from the tpy ligand as well as the typical shifts for vinylic protons of a terminal double bond. The peak at 3.4 ppm is due to the methoxy group.

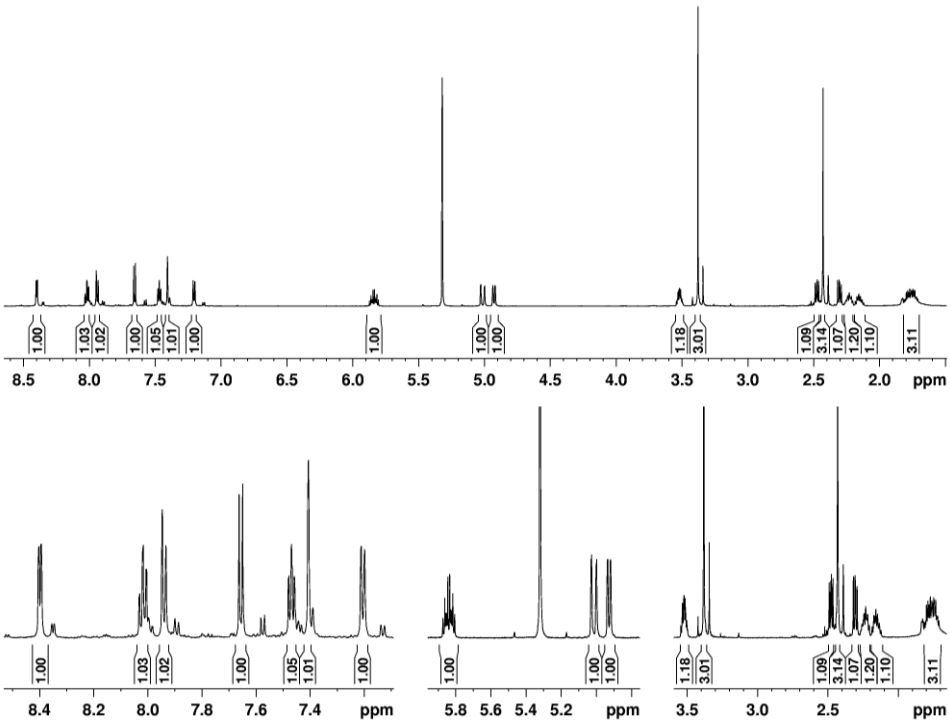

Figure 34: ^{1}H-NMR (600 MHz, CD_2Cl_2) of alkyl gold(III) complex **13**. Close-up views in the bottom.

2.5 Gold(III)-mediated Nucleophilic Attack at Alkenes – MeCN

2.5.1 Styrene

As mentioned before, the combination of styrene and $Au(OCOCF_3)_2(tpy)$ (**1**) in CH_2Cl_2/TFA solvent mixtures did not result in any reaction. In order to address this problem the solvent mixture was changed to MeCN/TFA/H_2O. In fact, upon switch of the solvent a reaction occurred but did not yield the expected alkyl gold(III) analogue.

Instead, the astonishing and unexpected alkyl gold(III) complex **14** was obtained in good yields in the reaction of $Au(OCOCF_3)_2(tpy)$ (**1**) with styrene in MeCN/TFA/H_2O at room temperature (Scheme 33). HR-MS analysis of the product shows that the cation contains one oxygen and two nitrogen atoms.

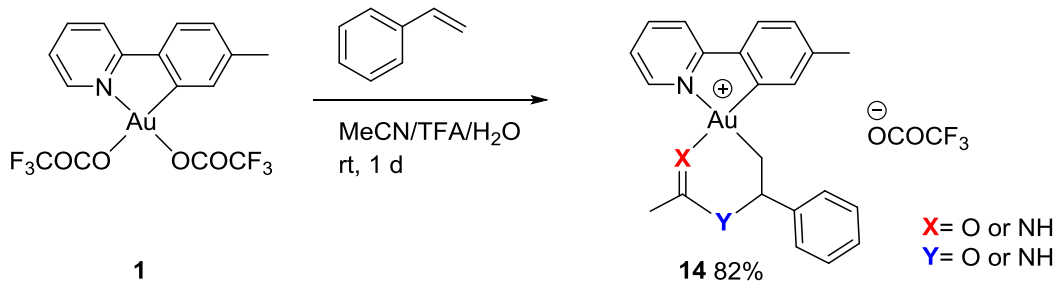

Scheme 33: Reaction of gold(III) complex **1** with styrene in MeCN/TFA/H_2O.

The recorded ^{1}H-NMR spectrum shows besides the starting material only minor impurities, probably an isomer (Figure 35). The expected peaks were observed in the aromatic region, originating from the tpy ligand as well as the phenyl ring of former styrene. The broad peak at 10.6 ppm is assigned to the hydrogen bonded to the nitrogen, which is not part of the tpy ligand. The peaks for the hydrogen atom bonded to the same carbon as the phenyl ring as well as the hydrogen atoms bonded to the same carbon as gold are broadened, which might indicate dynamic behavior. Also the peak originating from the methyl group that is not part of the tpy ligand is broadened. However, to prove this assumption of dynamic behavior further investigation is needed, for example by low-temperature NMR. Couplings observed in the COSY (Figure 36) and HSQC spectra (Figure 37) support this peak assignment. Neither the ^{1}H-^{15}N-HMBC nor the NOESY spectrum could give further information regarding the position of the NH-group. The NMR analysis needs to be redone with improved recording parameters.

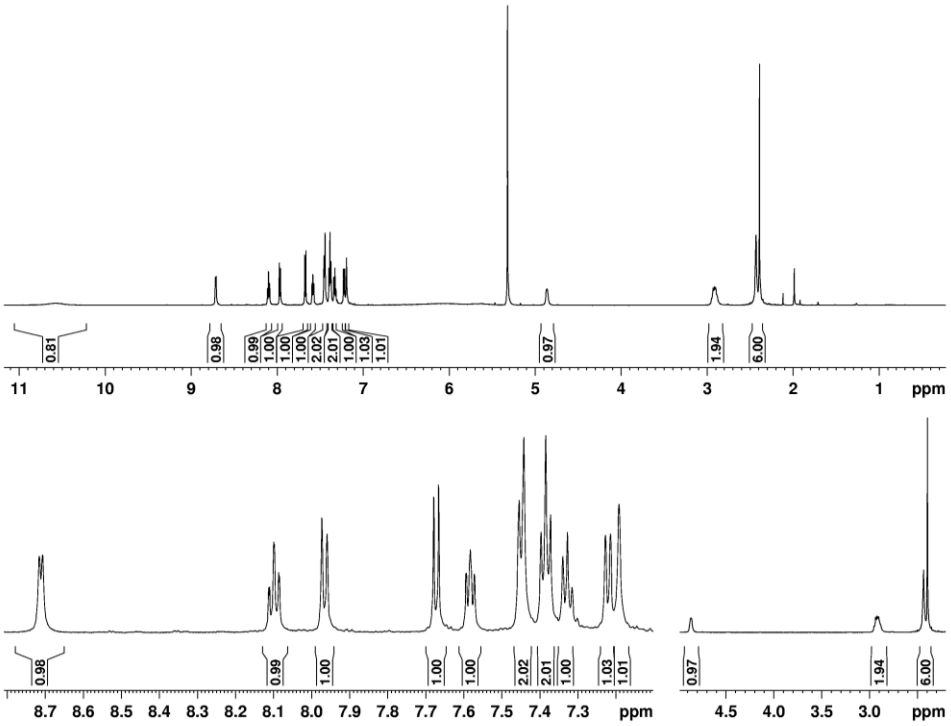

Figure 35: ^{1}H-NMR (600 MHz, CD_2Cl_2) of alkyl gold(III) complex **14**. Close-up views in the bottom.

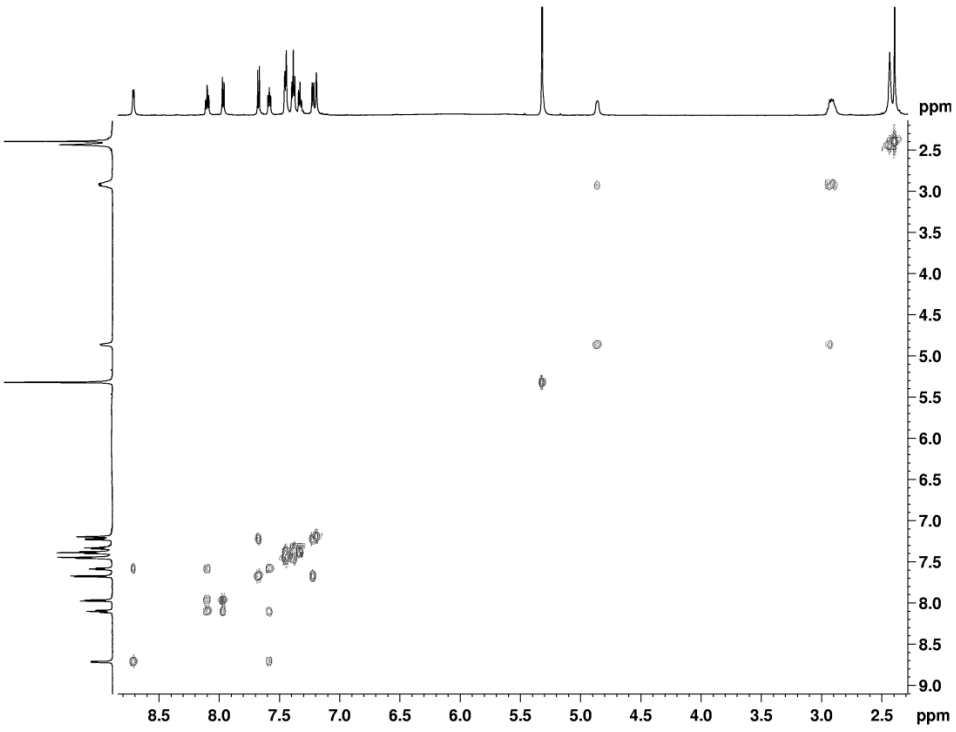

Figure 36: COSY of gold(III) complex **14**.

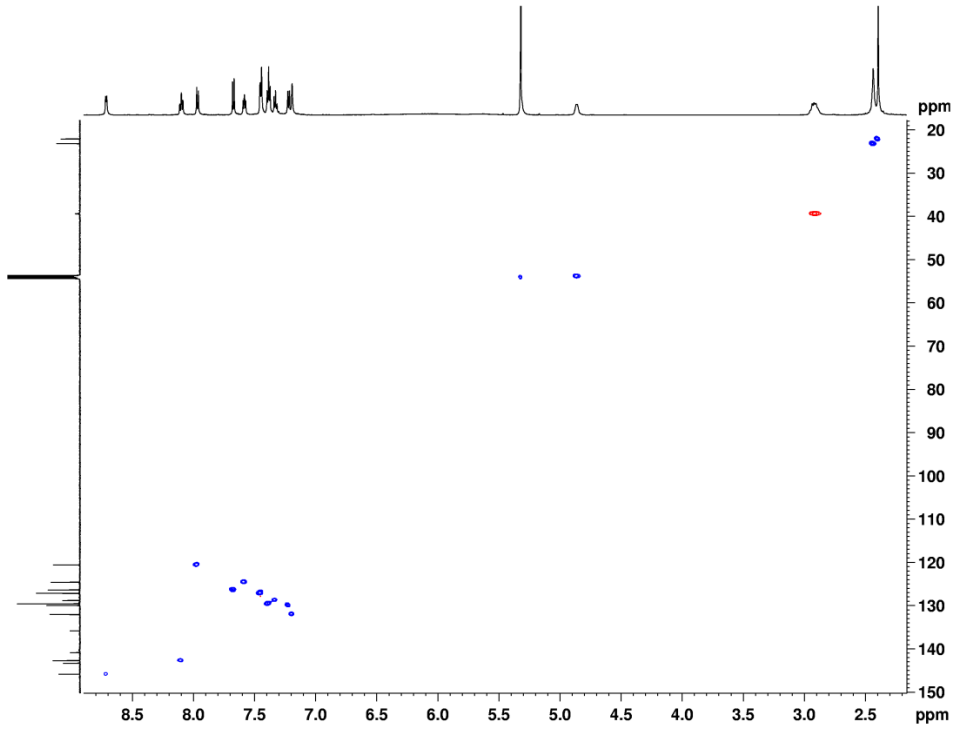

Figure 37: HSQC of gold(III) complex **14**.

Crystals suitable for single crystal X-ray analysis were obtained by vapor diffusion using CH_2Cl_2 as solvent and *n*-pentane as anti-solvent. The solid-state structure of the selected specimen verifies complex **14** and indicates that oxygen is bonded to gold (X-position) while the NH-group occupies the other position (Y-position). A detailed discussion of the crystal structure is given in the next chapter.

Interestingly, formation of a similar complex **57** was observed in the reaction of $Au(OCOCF_3)_2(tpy)$ (**1**) with ethylene in $MeCN/H_2O$ at room temperature (Scheme 34).[73]

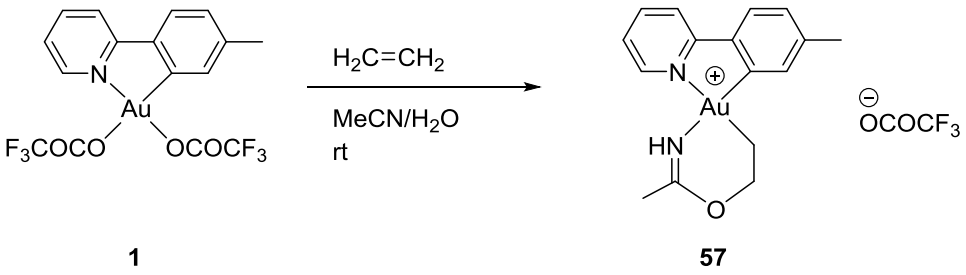

Scheme 34: Reaction of gold(III) complex **1** with styrene in $MeCN/H_2O$.[73]

The structure of complex **57** was unambiguously determined by utilization of diverse NMR techniques, HR-MS analysis and X-ray analysis.[73] The resulting complex structure

of **74** was also supported by computational data.[73] However, in product **57** the positions of the oxygen and NH-group are switched compared to the by X-ray analysis suggested structure of complex **14**.

Depicted in Scheme 35 is a proposed reaction mechanism in the reaction with ethylene. First step is the substitution of the trifluoroacetate *trans* to nitrogen by ethylene, which then gets attacked by water. In the next step substitution of the trifluoroacetate *trans* to carbon by MeCN takes place, followed by nucleophilic attack of the oxygen at the quaternary carbon of the coordinated MeCN, furnishing complex **57**.

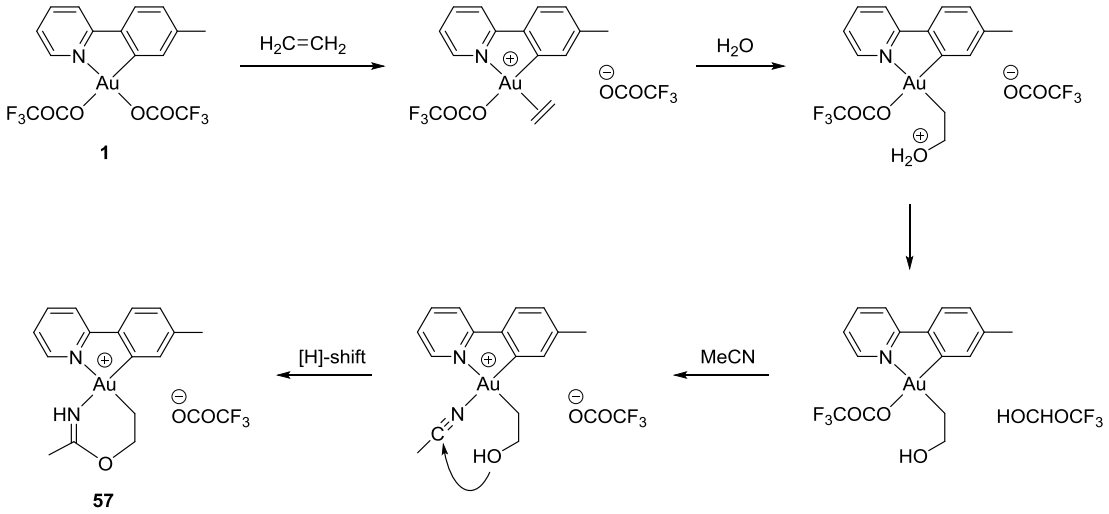

Scheme 35: Proposed reaction mechanism for formation of complex **57**.

For the reaction with styrene, however, this mechanism would not lead to the suggested structure for complex **14** with the oxygen being bonded to gold. Therefore another mechanism is proposed for the reaction with styrene (Scheme 36). It is assumed that water substitutes the trifluoroacetate *trans* to carbon. The oxygen of the water then attacks the nitrile carbon of MeCN and the nitrogen attacks the double bond, followed by binding of the coordinated styrene to gold.

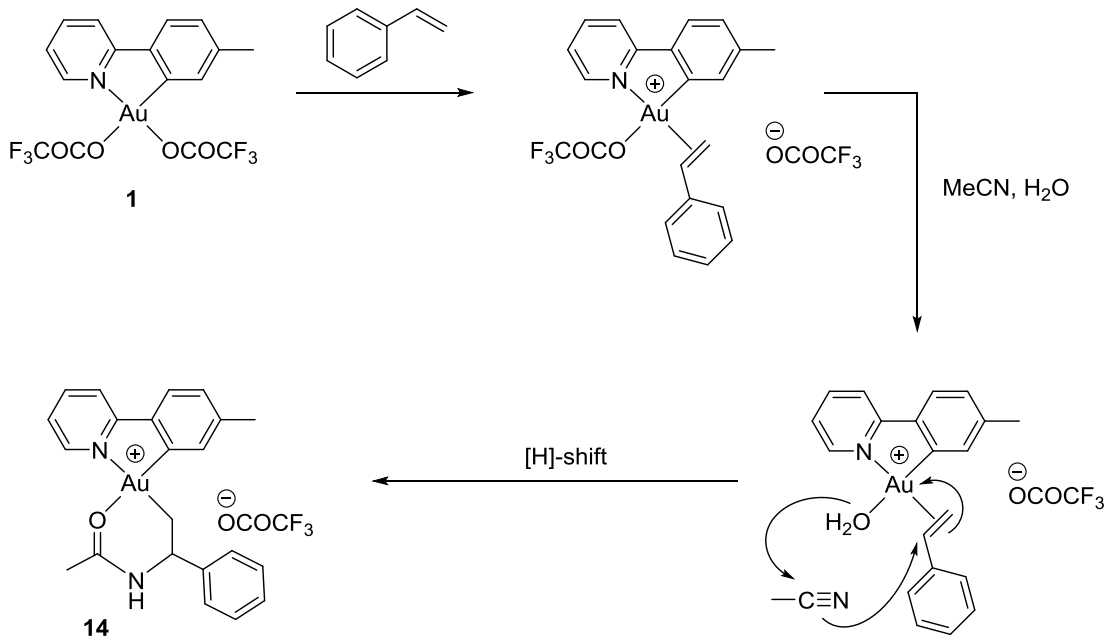

Scheme 36: Proposed reaction mechanism for formation of complex **14**.

In earlier work by the group coordination of H_2O as well as MeCN *trans* to carbon was observed.[6] It is assumed that the coordination of H_2O to gold is stronger than of MeCN to gold, which would favor the former in a competing reaction, leaving MeCN as nucleophile to attack the alkene. However, since MeCN is a weaker nucleophile than water, it cannot attack ethylene because its double bond is not activated enough. So for a reaction taking place MeCN coordinates to gold, while water attacks the alkene. That is not the case with styrene, there the double bond is activated enough due to the electron withdrawing phenyl group and nucleophilic attack by MeCN can take place.

These proposed reaction mechanisms are preliminary working hypotheses and no further evidence is given to support them.

3 Single Crystal X-Ray Diffraction Analysis of New Gold(III) Complexes

Eleven new compounds have been characterized using single crystal X-ray diffraction analysis. X-ray quality crystals were grown at about 4 °C *via* vapor diffusion using CH_2Cl_2 as solvent and *n*-pentane as anti-solvent. Data collection and refinement has been done by MSc. Sigurd Øien-Ødegaard. All of the datasets were obtained using the in-house Bruker D8 Venture instrument with Mo K_α radiation or Cu K_α radiation. All presented compounds with chiral centers are crystals of both enantiomers. The quality of the datasets is good and all structures are unambiguously determined, except the data for complex **16** being not sufficient as independent proof of structure. The crystals of complexes **15** and **16** were very disordered. The crystals of complex **8** has a twin component that is responsible for 2.5% of the diffraction pattern. This is strong enough to distort the electron density map, but too weak to integrate as a separate domain. The single crystal X-ray diffraction was not followed up by powder X-ray diffraction and no comment can be made about the overall compositions of the samples. However, in most cases the crystals resembled each other in morphology and color. The following ORTEP-plots are drawn in Diamond 4.0 with ellipsoids at the 50% level of probability. Crystallographic data can be found in the appendix.

A strong driving force for crystal growth of all shown complexes is the observed pairwise parallel displaced π-π stacking, which is a strongly attracting force, of the 2-(*p*-tolyl)pyridine ligands that was observed in all solid-state structures (Figure 38).

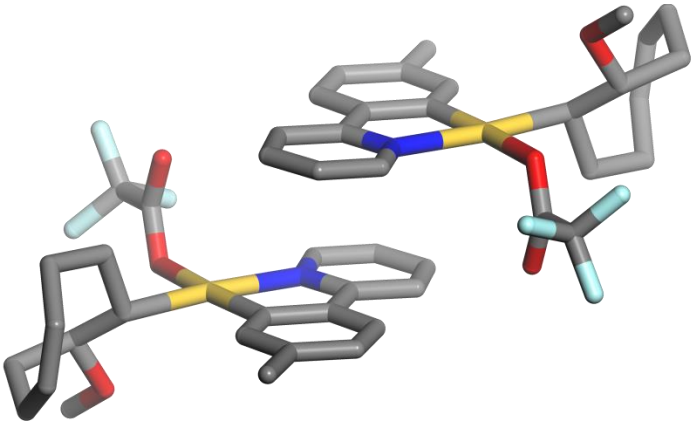

Figure 38: In Au-tpy structures commonly observed pairwise parallel displaced π-π stacking exemplified by the crystal packing of complex **6**.

3.1 Crystallographically Determined Structure of Complex 4

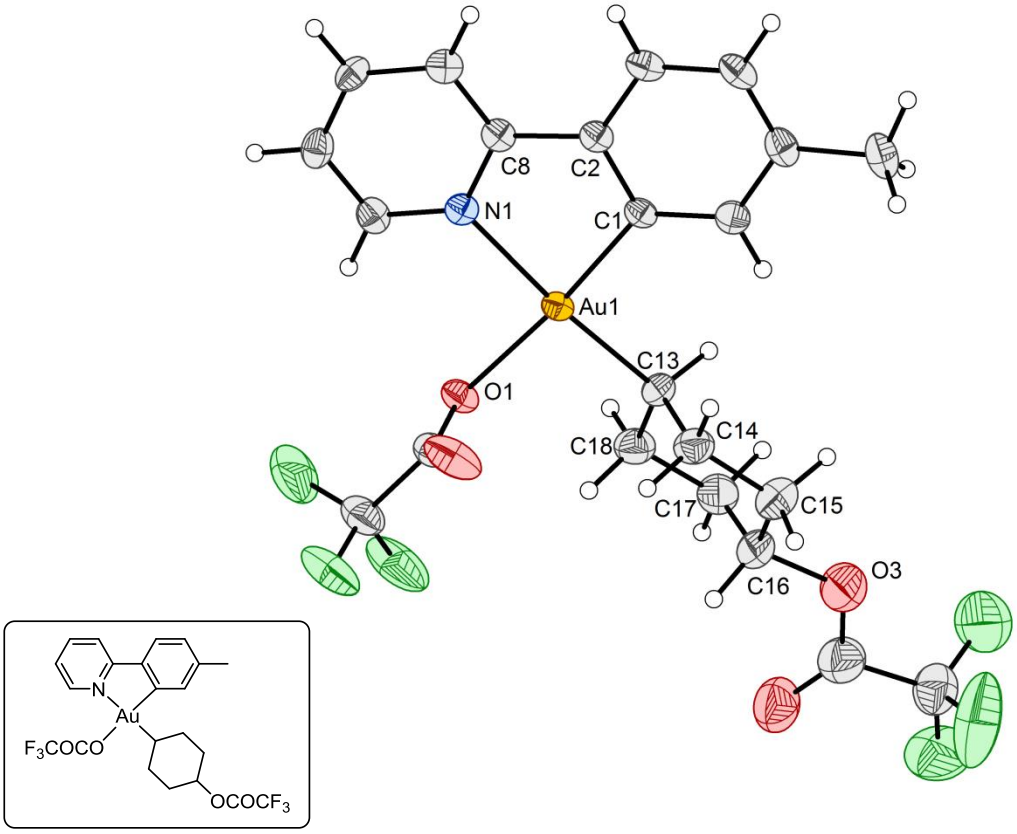

Figure 39: ORTEP view of the solid-state structure of complex **4**.

The X-ray analysis of complex **4** shows a square planar coordination geometry, as expected for gold(III) complexes, with near linear C(1)-Au(1)-O(1) and C(13)-Au(1)-N(1) angles. The bond angle described by the two non-chelating ligands is close to 90° and the chelate angle is normal for such cyclometalated species at 81.44(16)°.[7] The bond distances from gold to its neighbor atoms in complex **4** are quite similar to the corresponding distances of the already reported alkyl gold(III) complex **2**, which resulted from the reaction with ethylene.[7]

As expected, the cyclohexane segment adopted the most stable chair-conformation with the substituents in equatorial positions to achieve the least steric hindrance and avoid strains. The C-C-C bond angles of the cyclohexane ring are very close to the ideal tetrahedral angle of 109.5°.[77]

Table 5: Selected bond lengths and bond angles of complex **4**.

#	Bond	Bond length (Å)
1	Au(1)-C(1)	2.002(4)
2	Au(1)-C(13)	2.056(4)
3	Au(1)-O(1)	2.102(3)
4	Au(1)-N(1)	2.125(4)
5	O(3)-C(16)	1.499(7)
6	C(13)-C(14)	1.501(7)
7	C(13)-C(18)	1.525(7)
8	C(14)-C(15)	1.542(7)
9	C(15)-C(16)	1.536(8)
10	C(16)-C(17)	1.470(9)
11	C(17)-C(18)	1.528(7)

#	Bond	Angle (°)
1	C(1)-Au(1)-C(13)	93.74(18)
2	C(1)-Au(1)-O(1)	174.35(16)
3	C(13)-Au(1)-O(1)	91.90(16)
4	C(1)-Au(1)-N(1)	81.44(16)
5	C(13)-Au(1)-N(1)	174.43(16)
6	O(1)-Au(1)-N(1)	92.96(13)
7	C(2)-C(1)-Au(1)	112.9(3)
8	C(8)-N(1)-Au(1)	113.1(3)
9	C(13)-C(14)-C(15)	110.5(4)
10	C(13)-C(18)-C(17)	109.5(4)
11	C(16)-C(17)-C(18)	109.9(5)
12	C(16)-C(15)-C(14)	110.1(5)

3.2 Crystallographically Determined Structure of Complex 5

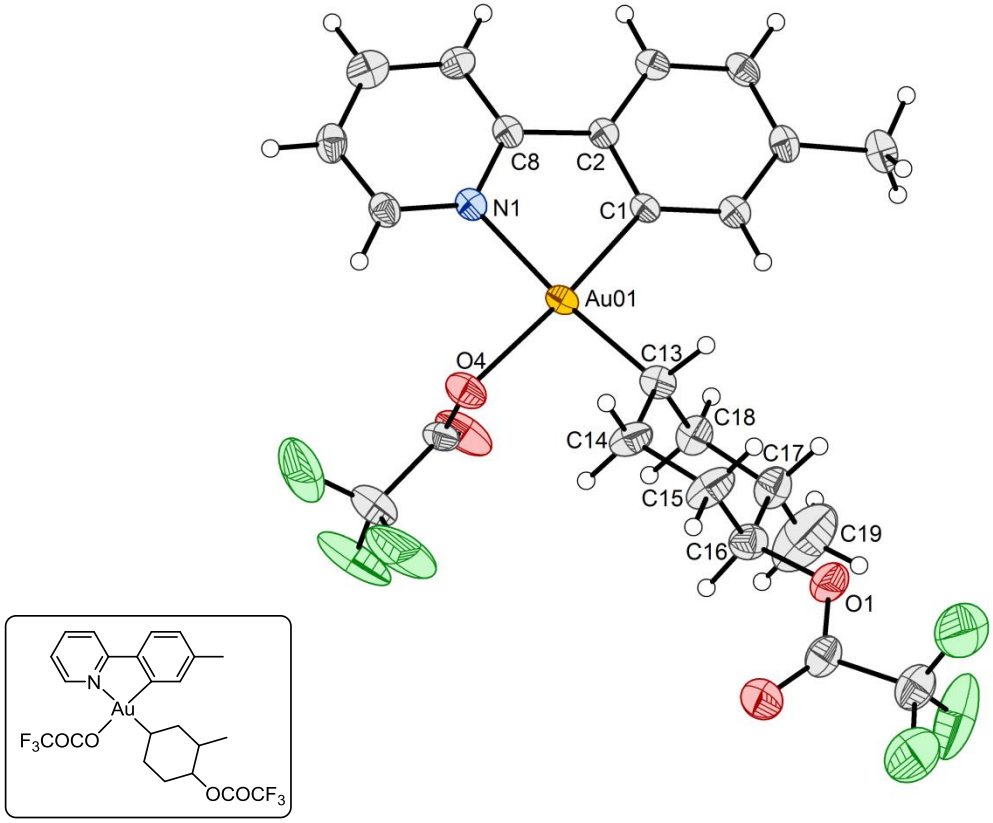

Figure 40: ORTEP view of the solid-state structure of complex **5**.

The X-ray analysis of complex **5** shows a square planar coordination geometry, as expected for gold(III) complexes, with near linear C(1)-Au(1)-O(4) and C(13)-Au(1)-N(1) angles. The bond angle described by the two non-chelating ligands is close to 90° and the chelate angle is normal for such cyclometalated species at 81.5(2)°.[7] The bond distances from gold to its neighbor atoms in complex **5** are quite similar to the corresponding distances observed in complex **4**.

Corresponding to structure **4**, the cyclohexane segment adopted the most stable chair-conformation with the substituents in equatorial positions to achieve the least steric hindrance and avoid strains. The C-C-C bond angles in the cyclohexane ring differ slightly from those in complex **4**. This could be caused by the cyclohexane ring adjusting itself in order to decrease the steric hindrance resulting from the methyl group as additional substituent. The methyl group is poorly defined, maybe due to twinning, but no twin law could be found yet. There are also some empty voids in the structure, which may contain disordered solvent molecules responsible for anomalous diffraction.

Table 6: Selected bond lengths and bond angles of complex **5**.

#	Bond	Bond length (Å)
1	Au(1)-N(1)	2.124(6)
2	Au(1)-C(1)	2.003(6)
3	Au(1)-O(4)	2.102(5)
4	Au(1)-C(13)	2.052(7)
5	O(1)-C(16)	1.483(9)
6	C(13)-C(14)	1.523(10)
7	C(13)-C(18)	1.512(10)
8	C(14)-C(15)	1.537(11)
9	C(15)-C(16)	1.541(11)
10	C(16)-C(17)	1.523(11)
11	C(17)-C(18)	1.527(11)
12	C(17)-C(19)	1.422(19)

#	Bond	Angle (°)
1	C(1)-Au(1)-N(1)	81.5(2)
2	C(1)-Au(1)-O(4)	174.3(2)
3	C(1)-Au(1)-C(13)	93.7(3)
4	O(4)-Au(1)-N(1)	93.5(2)
5	C(13)-Au(1)-N(1)	174.4(2)
6	C(13)-Au(1)-O(4)	91.5(3)
7	C(8)-N(1)-Au(1)	113.4(4)
8	C(2)-C(1)-Au(1)	112.9(4)
9	C(13)-C(14)-C(15)	109.1(7)
10	C(13)-C(18)-C(17)	111.0(6)
11	C(16)-C(15)-C(14)	108.4(7)
12	C(16)-C(17)-C(18)	109.6(7)
1	O(1)-C(16)-C(17)-C(19)	64.2(12)

3.3 Crystallographically Determined Structure of Complex 16

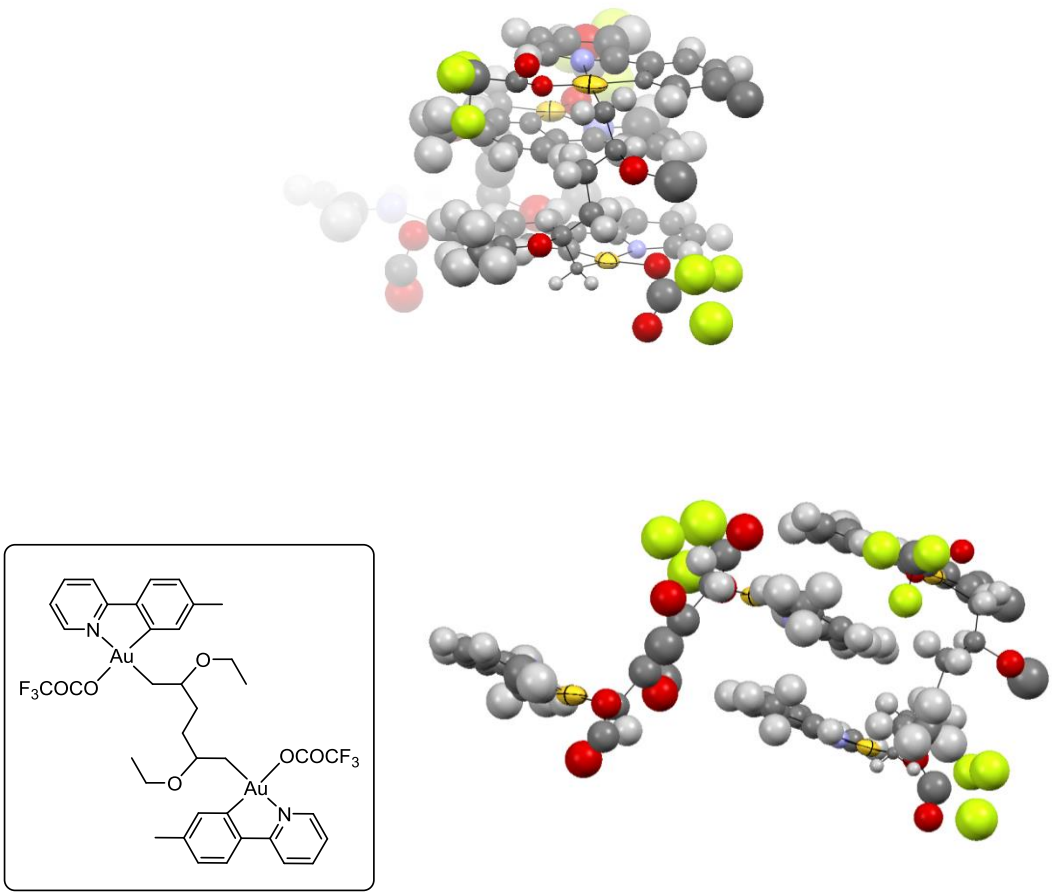

Figure 41: Crystal structure of complex **16**. Emphasizing six-membered carbon chain connecting two gold atoms in dimer (top). Emphasizing packing of dimers (bottom).

The crystal data for complex **16** is not good enough to use it as independent proof of structure. This poor data quality can be explained by the very small crystal, which results in weak diffraction and hampers the X-ray diffraction analysis, in addition to crystallographic defects. Due to the poor quality no bond lengths and bond angles were specified.

However, it clearly shows an alkyl gold(III) dimer complex and therefore corresponds with the assumption of dimer formation made based on the observed peaks in the ^{1}H-NMR spectrum. The solid-state structure also shows an interesting packing pattern of stacked dimer molecules, where one dimer is "S"-shaped and the other one "U"-shaped.

3.4 Crystallographically Determined Structure of Complex 15

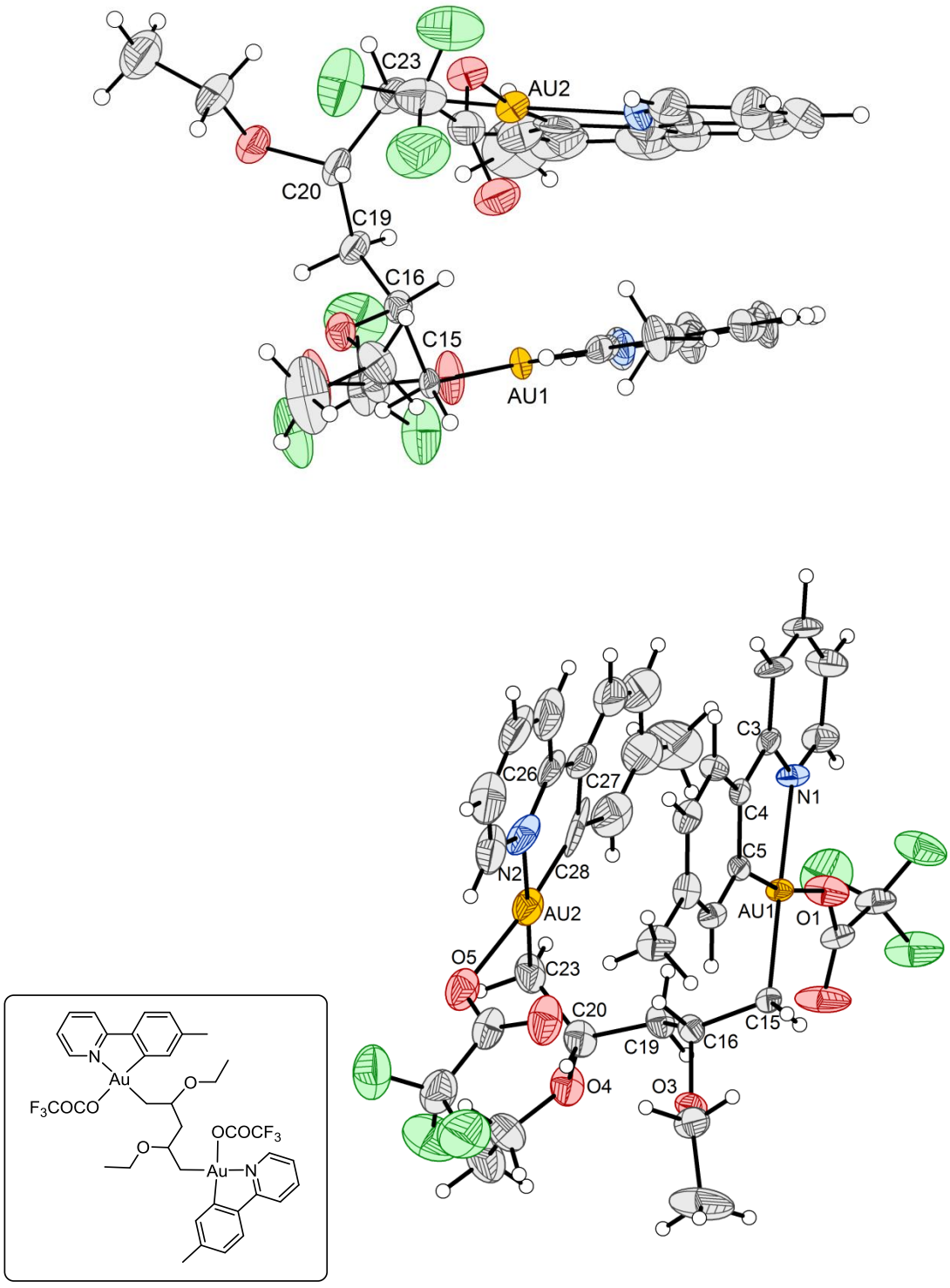

Figure 42: ORTEP view of the solid-state structure of complex **15**.

The packing diagrams show pairwise intermolecular Au(1)-Au(1)' distances of 3.4702(8) Å that are longer than the sum of van der Waals radii for two gold atoms (3.32 Å[85]), however, gold-gold attraction might still contribute to the packing of the molecules in the solid state.[86]

The X-ray analysis of complex **15** shows a square planar coordination geometry at both gold atoms, as expected for gold(III) complexes, with the angles C(5)-Au(1)-O(1) and C(15)-Au(1)-N(1) being slightly less linear than the angles C(23)-Au(2)-N(2) and C(28)-Au(2)-O(5). This deviation in planarity can be explained due to the discrepancy of the preferred distance between the tpy ligands of the dimer and the distance allowed and restricted by the strain coming from the backbone, the five-membered carbon chain. Therefore the alignment of gold atoms is a compromise and not perfectly planar. In comparison to the stacking pattern of complex **16**, the longer six-membered carbon backbone allows an external tpy ligand to stack in between the tpy ligands of the dimer to comply their preferred stacking distances.

While the chelate angles at 82.0(4)° for Au(1) and at 81.2(6)° for Au(2) are normal for such cyclometalated species, the bond angles described by the two non-chelating ligands alter in both directions from 90°, which can also be attributed to the effect of the strains coming from the backbone.[7]

Furthermore, the crystal structure of complex **15** shows that the product resulted from an addition of the nucleophile at the coordinated double bond in Markovnikov manner, corresponding with the observations made by Rezsnyak *et al.*[70]

Table 7: Selected bond lengths and bond angles of complex **15**.

#	Bond	Bond length (Å)
1	Au(1)-O(1)	2.106(8)
2	Au(1)-N(1)	2.114(9)
3	Au(1)-C(5)	1.982(10)
4	Au(1)-C(15)	2.045(10)
5	Au(2)-O(5)	2.099(10)
6	Au(2)-N(2)	2.112(10)
7	Au(2)-C(28)	1.88(2)
8	Au(2)-C(23)	2.064(12)
9	O(3)-C(16)	1.447(13)
10	O(4)-C(20)	1.434(13)
11	C(15)-C(16)	1.520(14)
12	C(16)-C(19)	1.484(14)
13	C(19)-C(20)	1.504(15)
14	C(20)-C(23)	1.517(17)

#	Bond	Angle (°)
1	O(1)-Au(1)-N(1)	86.4(3)
2	C(5)-Au(1)-O(1)	168.4(4)
3	C(5)-Au(1)-N(1)	82.0(4)
4	C(5)-Au(1)-C(15)	93.9(4)
5	C(15)-Au(1)-O(1)	97.7(4)
6	C(15)-Au(1)-N(1)	175.2(4)
7	O(5)-Au(2)-N(2)	97.5(5)
8	C(28)-Au(2)-O(5)	173.7(4)
9	C(28)-Au(2)-N(2)	81.2(6)
10	C(28)-Au(2)-C(23)	97.3(6)
11	C(23)-Au(2)-O(5)	83.7(5)
12	C(23)-Au(2)-N(2)	177.3(5)

3.5 Crystallographically Determined Structure of Complex 12

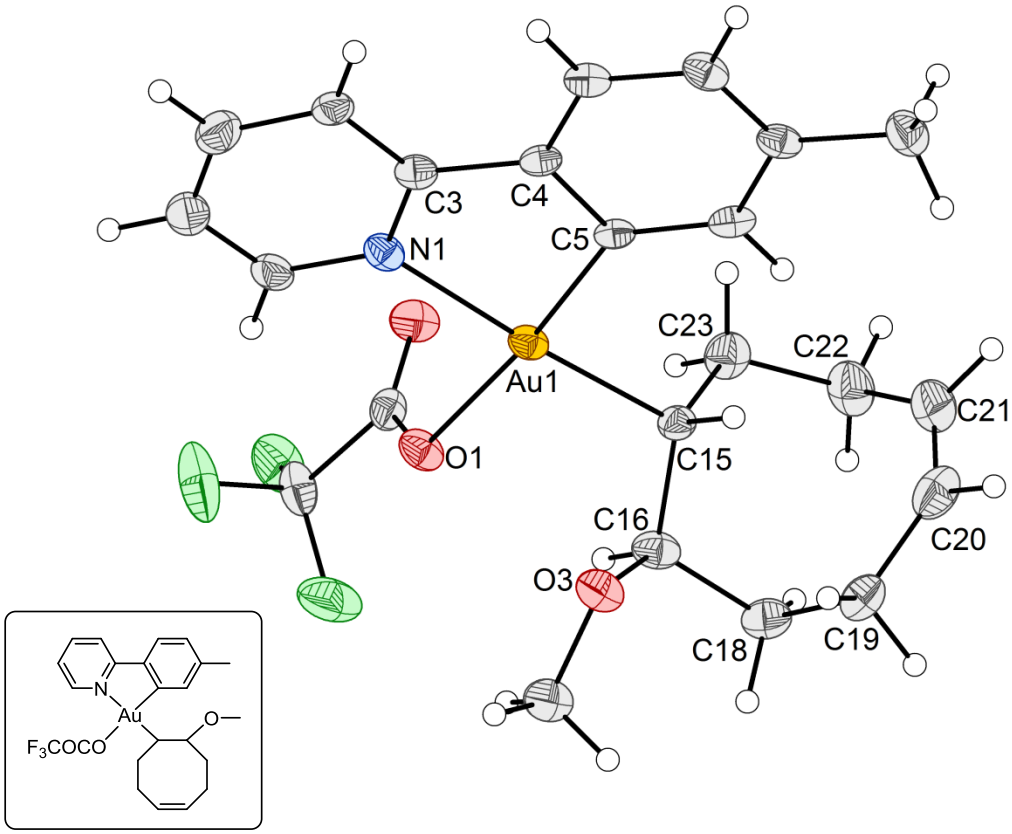

Figure 43: ORTEP view of the solid-state structure of complex **12**.

The X-ray analysis of complex **12** shows a square planar coordination geometry, as expected for gold(III) complexes, with near linear C(5)-Au(1)-O(1) and C(15)-Au(1)-N(1) angles. The bond angle described by the two non-chelating ligands is close to 90° and the chelate angle is normal for such cyclometalated species at 81.4(2)°.[7]

In the eight-membered ring all C-C bond lengths are normal for C-C single bonds and the bond length of C(20)-C(21) is with 1.337(11)Å in the range for C-C double bonds.

The crystal structure of complex **12** shows that the product resulted from *anti* addition of the nucleophile at the coordinated 1,5-cyclooctadiene, which is corresponding with the observations made for the alkyl gold(III) complex **2-d_2** resulting from the reaction of ethylene in TFA and with the observations made by Rezsnyak *et al.*[70]

Table 8: Selected bond lengths and bond angles of complex **12**.

#	Bond	Bond length (Å)
1	Au(1)-O(1)	2.109(5)
2	Au(1)-N(1)	2.150(6)
3	Au(1)-C(15)	2.068(6)
4	Au(1)-C(5)	2.004(6)
5	O(3)-C(16)	1.423(8)
6	C(15)-C(16)	1.517(9)
7	C(15)-C(23)	1.528(9)
8	C(16)-C(18)	1.534(10)
9	C(18)-C(19)	1.508(10)
10	C(19)-C(20)	1.494(11)
11	C(20)-C(21)	1.337(11)
12	C(21)-C(22)	1.489(11)
13	C(22)-C(23)	1.548(11)

#	Bond	Angle (°)
1	O(1)-Au(1)-N(1)	92.5(2)
2	C(15)-Au(1)-O(1)	93.2(2)
3	C(15)-Au(1)-N(1)	173.9(2)
4	C(5)-Au(1)-O(1)	173.9(2)
5	C(5)-Au(1)-N(1)	81.4(2)
6	C(5)-Au(1)-C(15)	92.9(3)
7	C(3)-N(1)-Au(1)	112.6(4)
8	C(4)-C(5)-Au(1)	112.5(5)

3.6 Crystallographically Determined Structure of Complexes 9 and 10

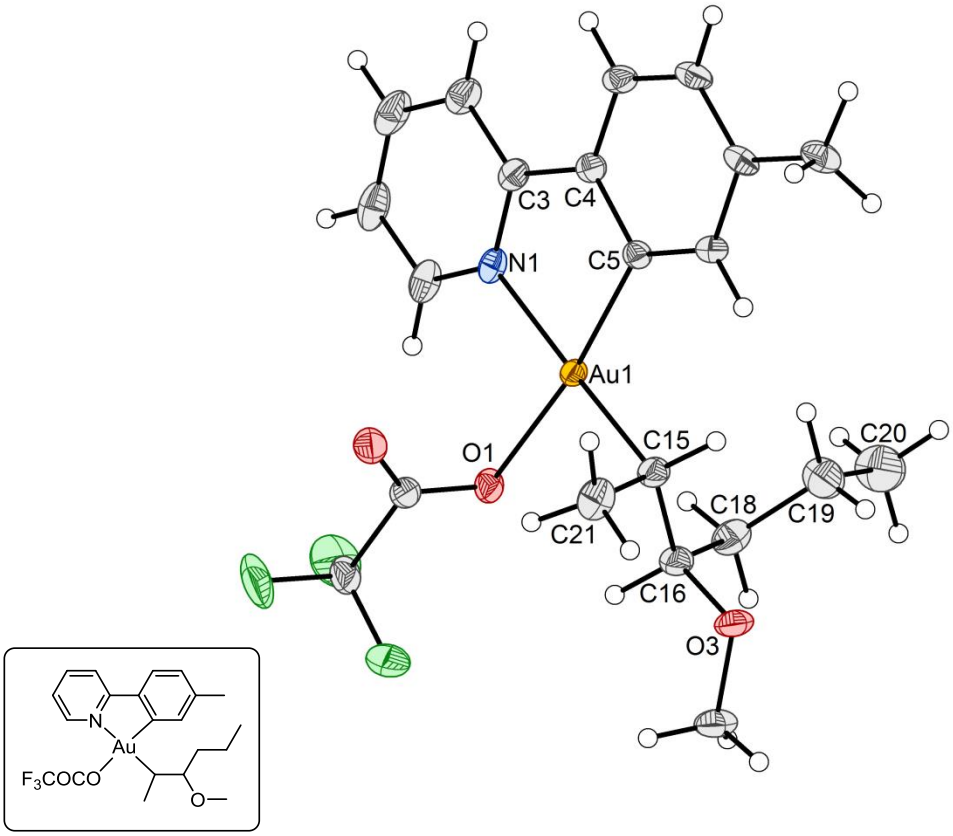

Figure 44: ORTEP view of the solid-state structure of complex **9**.

Surprisingly as well as impressively, it was possible to crystallize both isomers, which were both observed by NMR, out of the reaction mixture *via* vapor diffusion using CH_2Cl_2 as solvent and *n*-pentane as anti-solvent. It was possible to observe two kinds of crystals differing in their appearance. While complex **9** grew as big crystal rocks, the crystals formed of complex **10** were rather small.

The X-ray analysis of complex **9** shows a square planar coordination geometry, as expected for gold(III) complexes, with near linear C(5)-Au(1)-O(1) and C(15)-Au(1)-N(1) angles. The bond angle described by the two non-chelating ligands is close to 90° and the chelate angle is normal for such cyclometalated species at 81.72(10)°.[7]

Table 9: Selected bond lengths and bond angles of complex **9**.

#	Bond	Bond length (Å)
1	Au(1)-O(1)	2.110(2)
2	Au(1)-N(1)	2.131(2)
3	Au(1)-C(5)	2.007(3)
4	Au(1)-C(15)	2.069(3)
5	O(3)-C(16)	1.441(4)
6	C(15)-C(16)	1.520(4)
7	C(15)-C(21)	1.540(4)
8	C(16)-C(18)	1.536(5)
9	C(18)-C(19)	1.519(5)
10	C(19)-C(20)	1.538(5)

#	Bond	Angle (°)
1	O(1)-Au(1)-N(1)	91.92(9)
2	C(5)-Au(1)-O(1)	172.20(9)
3	C(5)-Au(1)-N(1)	81.72(10)
4	C(5)-Au(1)-C(15)	95.89(11)
5	C(15)-Au(1)-O(1)	90.39(10)
6	C(15)-Au(1)-N(1)	177.44(10)
7	C(3)-N(1)-Au(1)	112.50(19)
8	C(4)-C(5)-Au(1)	112.1(2)
1	C(21)-C(15)-C(16)-O(3)	-60.7(3)

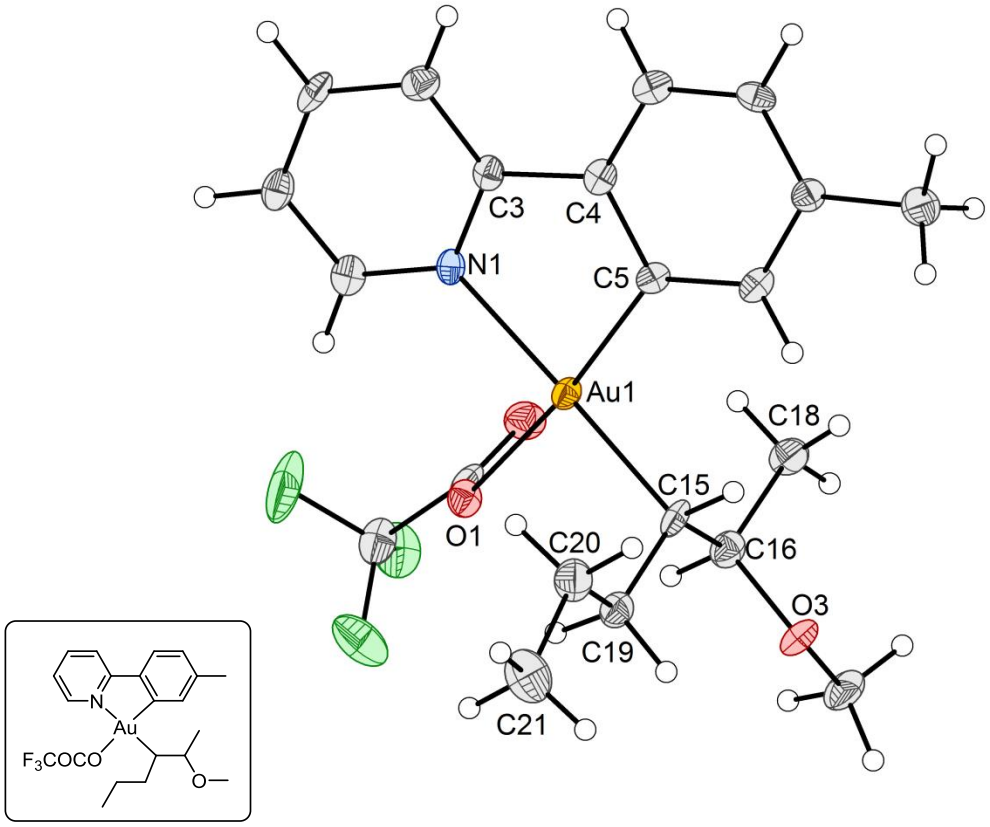

Figure 45: ORTEP view of the solid-state structure of complex **10**.

The X-ray analysis of complex **10** shows a square planar coordination geometry, as expected for gold(III) complexes, with near linear C(5)-Au(1)-O(1) and C(15)-Au(1)-N(1) angles. The bond angle described by the two non-chelating ligands is close to 90° and the chelate angle is normal for such cyclometalated species at 81.44(14)°.[7]

The crystal structures of complex **9** and **10** show that the products resulted from *anti* addition of the nucleophile at the coordinated *trans*-2-hexene, which is corresponding with the observations made for the alkyl gold(III) complex **12** and with the observations made by Rezsnyak *et al.*[70]

Table 10: Selected bond lengths and bond angles of complex **10**.

#	Bond	Bond length (Å)
1	Au(1)-O(1)	2.116(3)
2	Au(1)-N(1)	2.127(3)
3	Au(1)-C(5)	2.009(4)
4	Au(1)-C(15)	2.074(4)
5	O(3)-C(16)	1.448(5)
6	C(15)-C(16)	1.522(6)
7	C(16)-C(18)	1.518(6)
8	C(15)-C(19)	1.509(6)
9	C(19)-C(20)	1.529(6)
10	C(20)-C(21)	1.504(6)

#	Bond	Angle (°)
1	O(1)-Au(1)-N(1)	91.94(12)
2	C(5)-Au(1)-O(1)	172.51(13)
3	C(5)-Au(1)-N(1)	81.44(14)
4	C(5)-Au(1)-C(15)	96.81(16)
5	C(15)-Au(1)-O(1)	90.14(14)
6	C(15)-Au(1)-N(1)	173.79(15)
7	C(3)-N(1)-Au(1)	112.9(3)
8	C(4)-C(5)-Au(1)	112.5(3)
1	C(19)-C(15)-C(16)-O(3)	-57.3(4)

3.7 Crystallographically Determined Structure of Complex 14

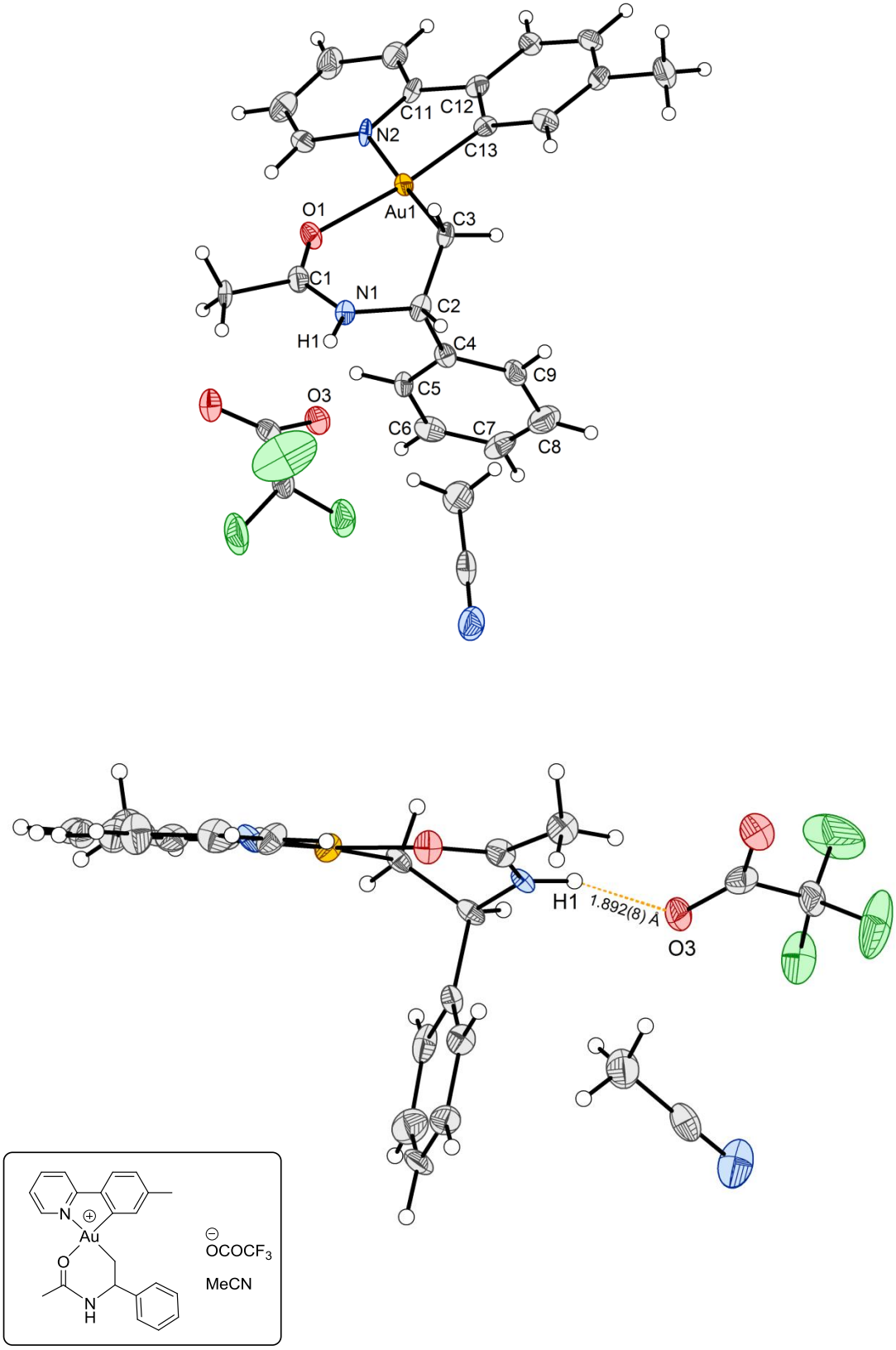

Figure 46: ORTEP view of the solid-state structure of complex **14**.

The X-ray analysis of complex **14** shows co-crystallization of complex **14** with MeCN.

The X-ray analysis of complex **14** shows a square planar coordination geometry, as expected for gold(III) complexes, with near linear C(13)-Au(1)-O(1) and C(3)-Au(1)-N(2) angles. The bond angle described by the two non-chelating ligands is close to 90° and the chelate angle is normal for such cyclometalated species at 81.7(4)°.[7]

As discussed in chapter 2.3.1, there is an uncertainty of the positions of O(1) and N(1). Since gold is a strong scatterer, and the electron densities of oxygen and nitrogen are relatively similar, also X-ray analysis cannot provide clear evidence for the positions of O(1) and N(1) in this case. However, the trifluoro acetate is quite close to N(1), which indicates positive attraction and could be explained with a N(1)-H(1)···O(1) hydrogen bond (Figure 46, bottom). If N(1) and O(1) switch positions, the adjancy of O(1) and O(3) would contrast the repulsive interactions between the oxygen atoms. Therefore, the X-ray analysis supports the assignment of the positions shown in Figure 46.

Furthermore, the crystal structure of complex **14** shows that the product resulted from an addition of the nucleophile, here acetonitrile, at the coordinated double bond in Markovnikov manner, corresponding with the observations made by Rezsnyak *et al.*[70]

Table 11: Selected bond lengths and bond angles of complex **14**.

#	Bond	Bond length (Å)
1	Au(1)-O(1)	2.083(7)
2	Au(1)-N(2)	2.107(9)
3	Au(1)-C(3)	2.034(10)
4	Au(1)-C(13)	1.997(11)
5	O(1)-C(1)	1.272(13)
6	N(1)-C(1)	1.303(13)
7	N(1)-C(2)	1.484(12)
8	C(2)-C(3)	1.511(14)
9	C(2)-C(4)	1.515(15)
10	C(4)-C(5)	1.390(14)
11	C(4)-C(9)	1.406(15)
12	C(6)-C(7)	1.399(17)
13	C(7)-C(8)	1.379(18)
14	C(5)-C(6)	1.374(15)
15	C(8)-C(9)	1.405(17)

#	Bond	Angle (°)
1	O(1)-Au(1)-N(2)	92.0(3)
2	C(3)-Au(1)-O(1)	90.4(4)
3	C(3)-Au(1)-N(2)	177.1(4)
4	C(13)-Au(1)-O(1)	172.8(4)
5	C(13)-Au(1)-N(2)	81.7(4)
6	C(13)-Au(1)-C(3)	95.9(4)
7	C(1)-O(1)-Au(1)	126.3(7)
8	C(11)-N(2)-Au(1)	113.0(7)
9	C(1)-N(1)-C(2)	127.0(9)
10	C(2)-C(3)-Au(1)	112.6(7)
11	C(12)-C(13)-Au(1)	112.5(7)
12	O(1)-C(1)-N(1)	124.4(10)

3.8 Crystallographically Determined Structure of Complex 7

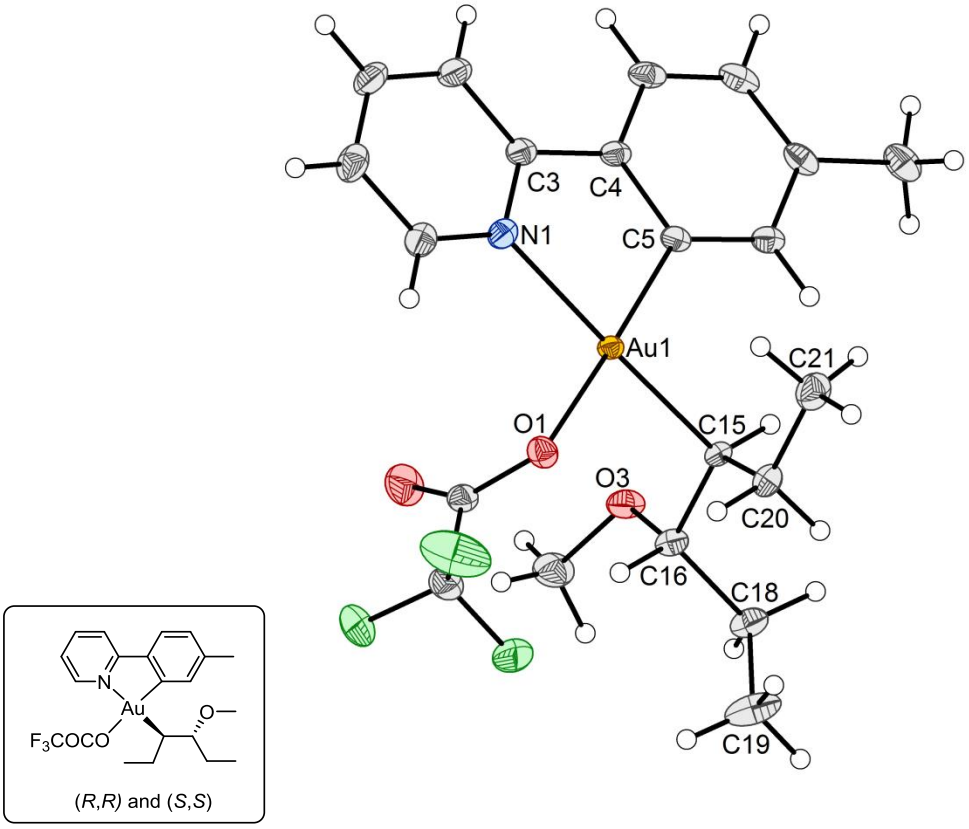

Figure 47: ORTEP view of the solid-state structure of complex **7**.

The X-ray analysis of complex **7** shows a square planar coordination geometry, as expected for gold(III) complexes, with near linear C(5)-Au(1)-O(1) and C(15)-Au(1)-N(1) angles. The bond angle described by the two non-chelating ligands is close to 90° and the chelate angle is normal for such cyclometalated species at 81.29(9)°.[7]

The crystal structure of complex **7** shows that the product resulted from *anti* addition of the nucleophile at the coordinated *cis*-3-hexene, which is corresponding with the observations made for the alkyl gold(III) complexes **9**, **10** and **12**.

Table 12: Selected bond lengths and bond angles of complex **7**.

#	Bond	Bond length (Å)
1	Au(1)-O(1)	2.0999(17)
2	Au(1)-N(1)	2.131(2)
3	Au(1)-C(15)	2.071(2)
4	Au(1)-C(5)	2.015(2)
5	O(3)-C(16)	1.436(3)
6	C(15)-C(16)	1.527(3)
7	C(15)-C(20)	1.525(3)
8	C(16)-C(18)	1.543(3)
9	C(20)-C(21)	1.526(4)
10	C(18)-C(19)	1.519(4)

#	Bond	Angle (°)
1	O(1)-Au(1)-N(1)	95.97(8)
2	C(15)-Au(1)-O(1)	86.54(8)
3	C(15)-Au(1)-N(1)	177.48(8)
4	C(5)-Au(1)-O(1)	175.11(8)
5	C(5)-Au(1)-N(1)	81.29(9)
6	C(5)-Au(1)-C(15)	96.22(10)
7	C(3)-N(1)-Au(1)	112.72(16)
8	C(4)-C(5)-Au(1)	112.36(18)
1	C(20)-C(15)-C(16)-C(18)	-61.2(3)

3.9 Crystallographically Determined Structure of Complex 8

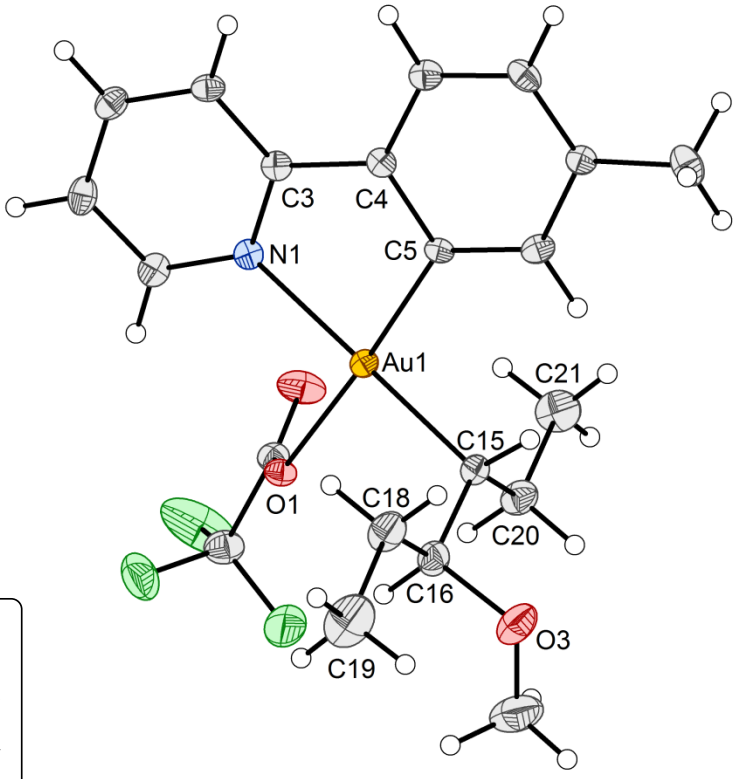

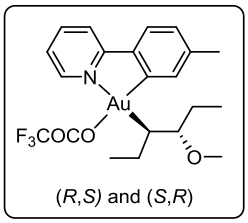

Figure 48: ORTEP view of the solid-state structure of complex **8**.

The X-ray analysis of complex **8** shows a square planar coordination geometry, as expected for gold(III) complexes, with near linear C(5)-Au(1)-O(1) and C(15)-Au(1)-N(1) angles. The bond angle described by the two non-chelating ligands is close to 90° and the chelate angle is normal for such cyclometalated species at 81.4(2)°.[7]

The crystal structure of complex **8** shows that the product resulted from *anti* addition of the nucleophile at the coordinated *trans*-3-hexene, which is corresponding with the observations made for the alkyl gold(III) complex **7**.

It is also interesting to see, when comparing complex **7** and **8**, that it is possible to draw conclusions about the former conformation of the alkene by comparing the torsion angles of the bond C(20)-C(15)-C(16)-C(18), proving that the *cis* and *trans* isomers give different products.

Table 13: Selected bond lengths and bond angles of complex **8**.

#	Bond	Bond length (Å)
1	Au(1)-O(1)	2.106(4)
2	Au(1)-N(1)	2.129(5)
3	Au(1)-C(5)	2.014(6)
4	Au(1)-C(15)	2.071(6)
5	O(3)-C(16)	1.442(8)
6	C(15)-C(20)	1.522(9)
7	C(15)-C(16)	1.526(9)
8	C(18)-C(19)	1.521(11)
9	C(16)-C(18)	1.511(10)
10	C(20)-C(21)	1.517(10)

#	Bond	Angle (°)
1	O(1)-Au(1)-N(1)	95.12(19)
2	C(5)-Au(1)-O(1)	175.3(2)
3	C(5)-Au(1)-N(1)	81.4(2)
4	C(5)-Au(1)-C(15)	96.7(2)
5	C(15)-Au(1)-O(1)	87.0(2)
6	C(15)-Au(1)-N(1)	174.8(2)
7	C(3)-N(1)-Au(1)	113.5(4)
8	C(4)-C(5)-Au(1)	112.2(4)
1	C(20)-C(15)-C(16)-C(18)	-178.4(6)

3.10 Crystallographically Determined Structure of Complex 11

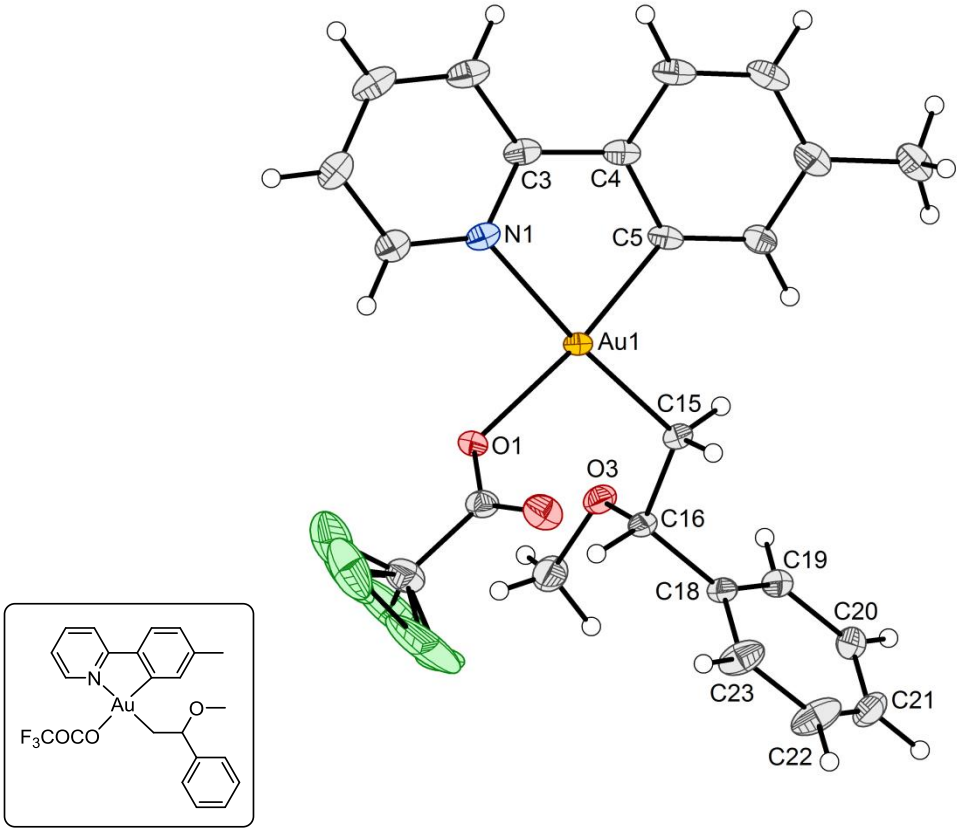

Figure 49: ORTEP view of the solid-state structure of complex **11**. The asymmetric unit of of **11** contains two complexes, but for clarity only one complex is shown.

The X-ray analysis of complex **11** shows co-crystallization of complex **11** with CH_2Cl_2 and that two molecules comprise the asymmetric unit.

The X-ray analysis of complex **11** shows a square planar coordination geometry, as expected for gold(III) complexes, with near linear C(5)-Au(1)-O(1) and C(15)-Au(1)-N(1) angles. The bond angle described by the two non-chelating ligands is close to 90° and the chelate angle is normal for such cyclometalated species at 81.44(10)° and 81.95(10)°.[7]

Furthermore, the crystal structure of complex **11** shows that the product resulted from an addition of the nucleophile at the coordinated double bond in a Markovnikov manner, corresponding with the observations made for complexes **14** and **15**.

Table 14: Selected bond lengths and bond angles of complex **11**. Complex 1 and Complex 2 denotes the two complexes which together constitute the asymmetric unit.

#	Bond	Complex 1 Bond length (Å)	Complex 2 Bond length (Å)
1	Au(1)-O(1)	2.1159(17)	2.1022(18)
2	Au(1)-N(1)	2.126(2)	2.113(2)
3	Au(1)-C(5)	2.010(2)	2.002(2)
4	Au(1)-C(15)	2.054(2)	2.044(3)
5	O(3)-C(16)	1.425(3)	1.424(3)
6	C(15)-C(16)	1.523(3)	1.513(3)
7	C(16)-C(18)	1.517(3)	1.515(4)
8	C(18)-C(19)	1.381(4)	1.393(4)
9	C(18)-C(23)	1.389(4)	1.394(4)
10	C(19)-C(20)	1.393(4)	1.382(4)
11	C(20)-C(21)	1.381(4)	1.386(5)
12	C(21)-C(22)	1.368(5)	1.376(5)
13	C(22)-C(23)	1.395(4)	1.384(4)

#	Bond	Complex 1 Angle (°)	Complex 2 Angle (°)
1	O(1)-Au(1)-N(1)	91.20(8)	88.90(8)
2	C(5)-Au(1)-O(1)	172.50(9)	170.84(10)
3	C(5)-Au(1)-N(1)	81.44(10)	81.95(10)
4	C(5)-Au(1)-C(15)	92.8(1)	94.07(11)
5	C(15)-Au(1)-O(1)	94.63(9)	95.09(9)
6	C(15)-Au(1)-N(1)	173.14(9)	175.07(10)
7	C(3)-N(1)-Au(1)	112.86(18)	113.01(18)
8	C(4)-C(5)-Au(1)	112.45(19)	112.4(2)

4 Conclusion and Future Prospects

Gold(III)-mediated nucleophilic addition reactions to alkenes have been investigated, testing several different nucleophiles as well as a wide variety of alkenes. A number of novel alkyl gold(III) complexes have been synthesized and characterized by NMR spectroscopy, mass spectrometry and X-ray crystallography and studied by computational methods. The reaction of $Au(OCOCF_3)_2(tpy)$ with 1,5-hexadiene in TFA yielded an especially intriguing and unexpected product due to the formation of a six-membered ring. This observation could underline the special properties of gold(III) complexes, since formation of a six-membered ring was never observed upon reaction of 1,5-hexadiene with other metal compounds like Ni(II) or Pt(II) complexes.

However, the products obtained from the reactions in TFA were unstable and could not be isolated, but changing the solvent to MeOH increased the product stability immensely. It is assumed that the methoxy group is a worse leaving group than trifluoroacetate and therefore hinders the reverse reaction of the nucleophilic attack, leading to more stable alkyl gold(III) complexes.

Also the use of MeCN as solvent led to unexpected products. A preliminary reaction mechanism was proposed but is still object of further investigations.

One major goal for future work is the achievement of a catalytic reaction. The main issue that needs to be addressed is that the protonation of $C(sp^2)$ is favored over $C(sp^3)$. Therefore the tpy ligand will be cleaved off upon protonation before the alkene can be released. A possible solution would be the adjustment of the gold(III) complex, so that the gold atom is also bonded to a $C(sp^3)$ atom of the ligand. Until now, there are only few examples reported for this kind of complexes, which offers a lot of opportunities for further development.[87],[88]

Last but not least, expanding the scope of investigated alkenes and nucleophiles is anticipated for the future. Exploration of reactions using nitrogen nucleophiles or alkenes containing hetero atoms, like allyl vinyl ether, to name just a few, present interesting targets.

5 Experimental Section

All reagents, unless specified, were used without further purification as purchased from commercial suppliers. $Au(OAc)_3$ was purchased from Alfa Aesar and ABCR. All alkenes were purchased from Sigma Aldrich. Dry CH_2Cl_2 and MeCN were dried by use of the MB SPS-800 Solvent Purification System from MBraun. MeOH was dried over molecular sieves. Distilled water was used and aqueous solutions were prepared on site. Argon gas was used to perform reactions under inert atmosphere. Vacuum line (1×10^{-3} mbar) was used for removal of solvents unless otherwise noted. All reactions were shielded from light using aluminum foil.

The microwave synthesis was performed using a microwave oven of the type Milestone MicroSYNTH with a rotor of the type SK-10.

^1H, ^{13}C, ^1H-^1H COSY, NOESY, HSQC and HMBC NMR experiments were recorded in CD_2Cl_2, CD_3CN, TFA-*d* or DMSO-d_6 using either a Bruker Avance DPX200, AVII400, DRX500, AV600 or AVII600 instrument with residual solvent peaks as references (CHD_2CN (δH = 1.94 ppm), $CHDCl_2$ (δH = 5.32 ppm), TFA-*d* (δC = 116.6 ppm, 164.2 ppm), DMSO-d_6 (δC = 39.5 ppm) or CD_2Cl_2 (δC = 54.0 ppm) as an internal standard). Chemical shifts (δ) are given in parts per million (ppm) and coupling constants (*J*) are given in Hertz (Hz). Multiplicities are abbreviated as: s - singlet; d - doublet; t - triplet; dd - doublet of doublets; dt - doublet of triplets; td - triplet of doublets; ddt - doublet of doublets of triplets; m - multiplet; br. - broad.

Mass spectra were obtained on a Micromass QTOF II spectrometer (ESI) by Osamu Sekiguchi.

5.1 Synthesis of $Au(OCOCF_3)_2(tpy)$ (1)[2]

A solution of $Au(OAc)_3$ (384 mg, 1.03 mmol, 1.0 eq.) and 2-(*p*-tolyl)pyridine (186 µl, 1.09 mmol, 1.06 eq.) in 30 ml H_2O/TFA (1:1) was heated up in a microwave oven for 30 min at 120 °C. The mixture was filtered after cooling down for 30 min at room temperature. By addition of 30 ml H_2O to the filtrate and cooling down to 0 °C the product precipitated. It was collected in a fine frit, washed with H_2O (3 x 5 ml) and diethyl ether (5 ml), and dried under a stream of air for 1 h. The product was obtained as a pale yellow solid (582 mg, 0.99 mmol, 96%). Spectroscopic data was in agreement with reported literature data.

^{1}H-NMR: (200 MHz, CD_3CN) δ[ppm] = 8.44 (d, *J* = 6.0 Hz, 1 H, H-1), 8.24 (t, *J* = 8.1 Hz, 1 H, H-3), 7.99 (d, *J* = 8.2 Hz, 1 H, H-4), 7.60-7.47 (m, 2 H, H-2,5), 7.28 (d, *J* = 7.9 Hz, 1 H, H-6), 6.76 (s, 1 H, H-8), 2.38 (s, 3 H, H-7).

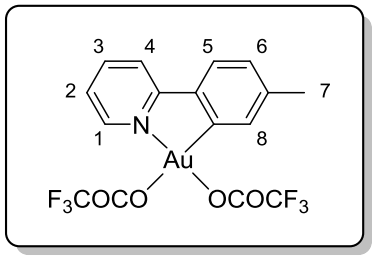

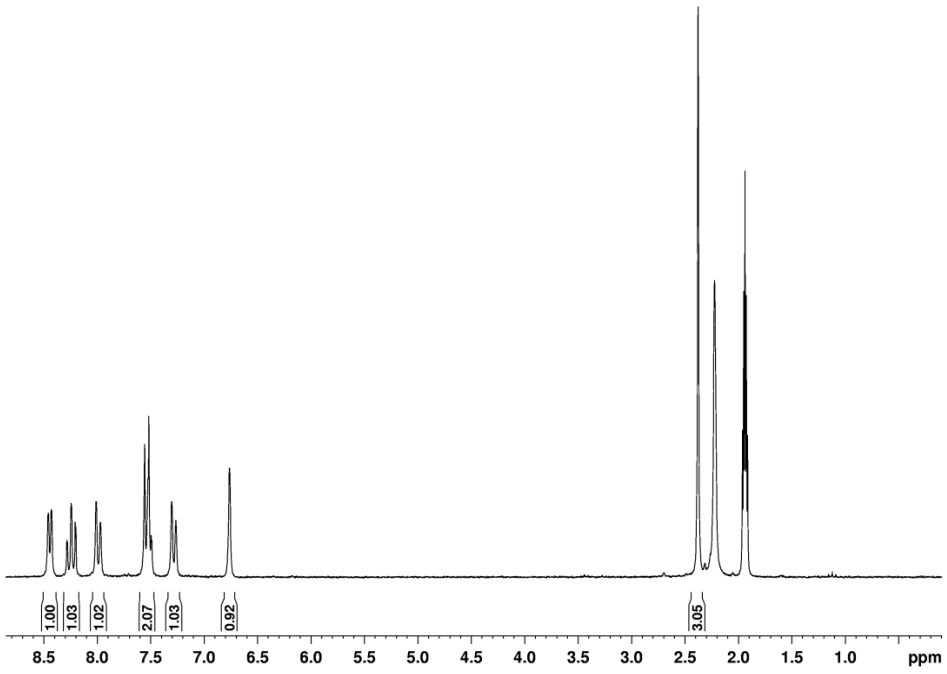

Figure 50: ^{1}H NMR (200 MHz, CD_3CN) of compound **1**.

5.2 Synthesis of Complex 2[7]

A solution of $Au(OCOCF_3)_2(tpy)$ (**1**, 100 mg, 0.17 mmol, 1.0 eq.) and 5 ml TFA in a flask capped with a septum and equipped with a vent needle was bubbled through by ethylene gas for 2 h at room temperature. The solvent was removed *in vacuo* to yield a pale yellow solid (70.7 mg, 0.11 mmol, 68%). Spectroscopic data was in agreement with reported literature data.

^{1}H-NMR: (200 MHz, CD_2Cl_2) δ[ppm] = 8.41 (d, *J* = 5.8 Hz, 1 H, H-1), 8.06 (t, *J* = 7.6 Hz, 1 H, H-3), 7.94 (d, *J* = 8.0 Hz, 1 H, H-4), 7.65 (d, *J* = 7.9 Hz, 1 H, H-5), 7.50 (t, *J* = 6.5 Hz, 1 H, H-2), 7.39 (s, 1 H, H-8), 7.23 (d, *J* = 7.9 Hz, 1 H, H-6), 4.82-4.73 (m, 2 H, H-10), 2.46 (s, 3 H, H-7), 2.47-2.39 (m, 2 H, H-9).

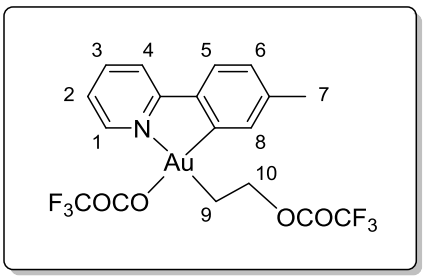

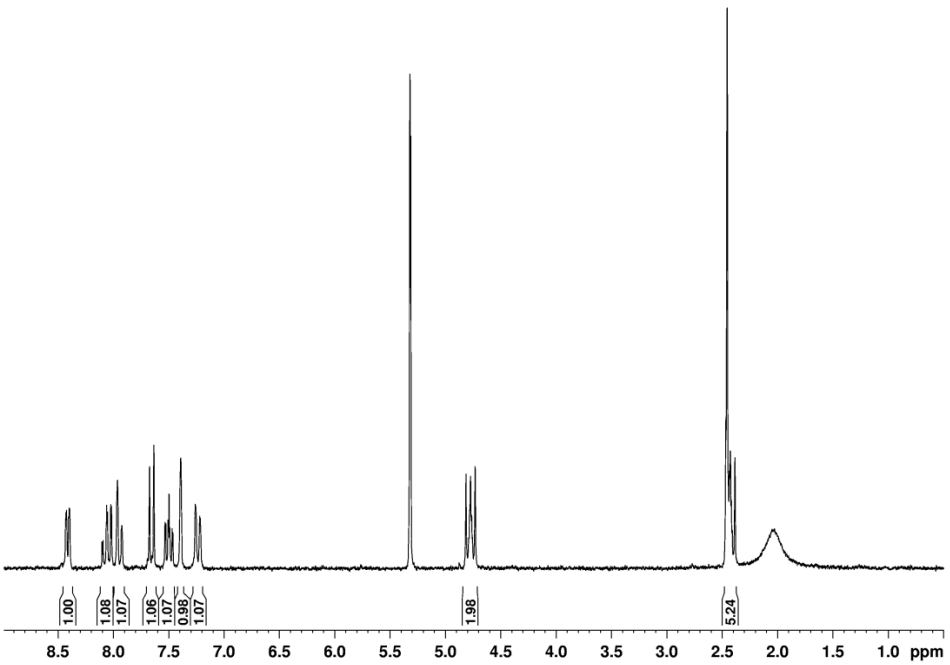

Figure 51: ^{1}H NMR (200 MHz, CD_2Cl_2) of compound **2**. Peak at 2.39 ppm is due to TFA residue.

5.3 Synthesis of Complex 3

1,4-Pentadiene (10.5 µl, 0.102 mmol, 1.2 eq.) was added to a solution of $Au(OCOCF_3)_2(tpy)$ (**1**, 50.0 mg, 0.085 mmol, 1.0 eq.) in 3 ml TFA. After 2 h reaction time the reaction was completed under full conversion of starting material **1**. The product could not be isolated since it is only stable in solution and decomposes upon removal of the solvent.

^{1}H-NMR: (400 MHz, CD_2Cl_2) δ[ppm] = 8.32 (d, *J* = 4.9 Hz, 1 H, H-1), 8.05 (td, *J* = 7.9 Hz, *J* = 1.5 Hz, 1 H, H-3), 7.94 (d, *J* = 8.2 Hz, 1 H, H-4), 7.63 (d, *J* = 7.9 Hz, 1 H, H-7), 7.49 (t, *J* = 6.5 Hz, 1 H, H-2), 7.39 (s, 1 H, H-11), 7.23 (d, *J* = 7.9 Hz, 1 H, H-8), 5.82 (ddt, *J* = 17.2 Hz, *J* = 10.2 Hz, *J* = 7.0 Hz, 1 H, H-16), 5.46-5.38 (m, 1 H, H-14), 5.24-5.12 (m, 2 H, H-17), 2.75-2.57 (m, 2 H, H-15), 2.47-2.39 (m, 5 H, H-10,13).

^{13}C-NMR: (100 MHz, CD_2Cl_2) δ[ppm] = 160.9 (C-5), 157.7 (q, *J* = 42 Hz, **C**O), 146.6 (C-1), 143.6 (C-12), 142.5 (C-3), 140.7 (C-9), 136.1 (C-6), 133.1 (C-16), 132.5 (C-11), 130.0 (C-8), 126.3 (C-7), 124.8 (C-2), 120.7 (C-4), 119.7 (C-17), 115.1 (q, *J* = 286 Hz, **C**F_3), 80.3 (C-14), 41.0 (C-15), 33.0 (C-13), 22.0 (C-10). The missing carbons from the $COCF_3$ groups were not observed.

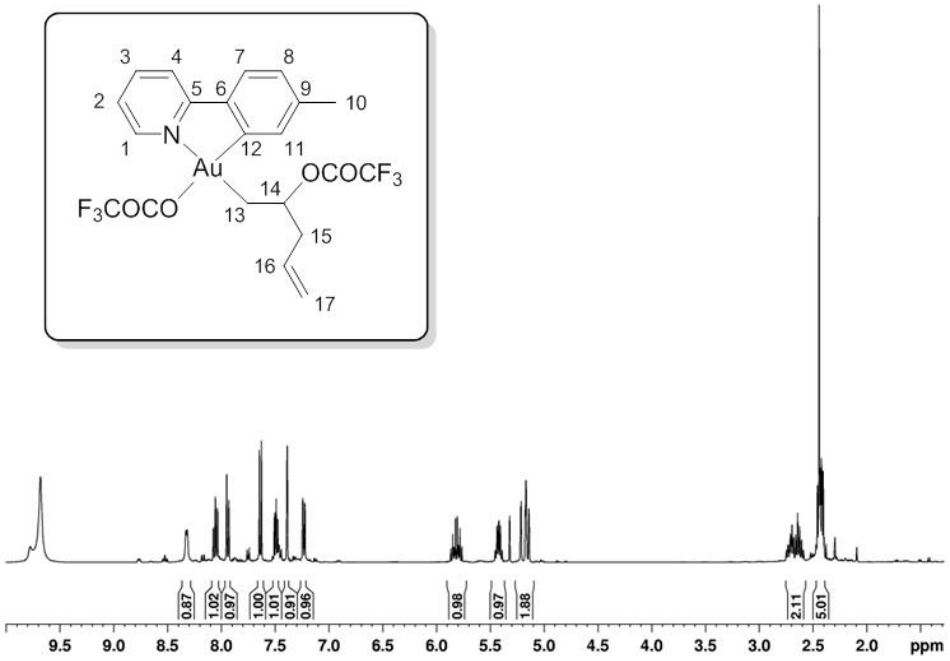

Figure 52: ^{1}H NMR (400 MHz, CD_2Cl_2) of compound **3**.

5.4 Synthesis of Complex 4

1,5-Hexadiene (12.1 µl, 0.102 mmol, 1.2 eq.) was added to a solution of $Au(OCOCF_3)_2(tpy)$ (**1**, 50.0 mg, 0.085 mmol, 1.0 eq.) in 5 ml TFA. After 1.5 h reaction time the reaction was completed under full conversion of starting material **1**. The product could not be isolated since it is only stable in solution and decomposes upon removal of the solvent.

^{1}H-NMR: (400 MHz, CD_2Cl_2) δ[ppm] = 8.32 (d, *J* = 5.5 Hz, 1 H, H-1), 8.00 (td, *J* = 7.7 Hz, *J* = 1.5 Hz, 1 H, H-3), 7.94 (d, *J* = 8.0 Hz, 1 H, H-4), 7.68 (d, *J* = 7.9 Hz, 1 H, H-7), 7.45 (t, *J* = 6.4 Hz, 1 H, H-2), 7,29 (s, 1 H, H-11), 7.22 (d, *J* = 7.9 Hz, 1 H, H-8), 4.99 (tt, *J* = 11.4 Hz, *J* = 4.7 Hz, 1 H, H-16), 2.54-2.43 (m, 4 H, H-10,13), 2.36-2.25 (m, 2 H, H-14eq), 2.24-2.11 (m, 2 H, H-15eq), 2.06-1.94 (m, 2 H, H-14ax), 1.78-1.65 (m, 2 H, H-15ax).

^{13}C-NMR: (100 MHz, CD_2Cl_2) δ[ppm] = 146.7 (C-1), 141.9 (C-3), 131.0 (C-11), 129.6 (C-8), 126.0 (C-7), 124.5 (C-2), 120.5 (C-4), 78.5 (C-16), 53.0 (C-13), 34.1 (C-15), 31.4 (C-14), 22.4 (C-10). Quaternary carbons were not observed.

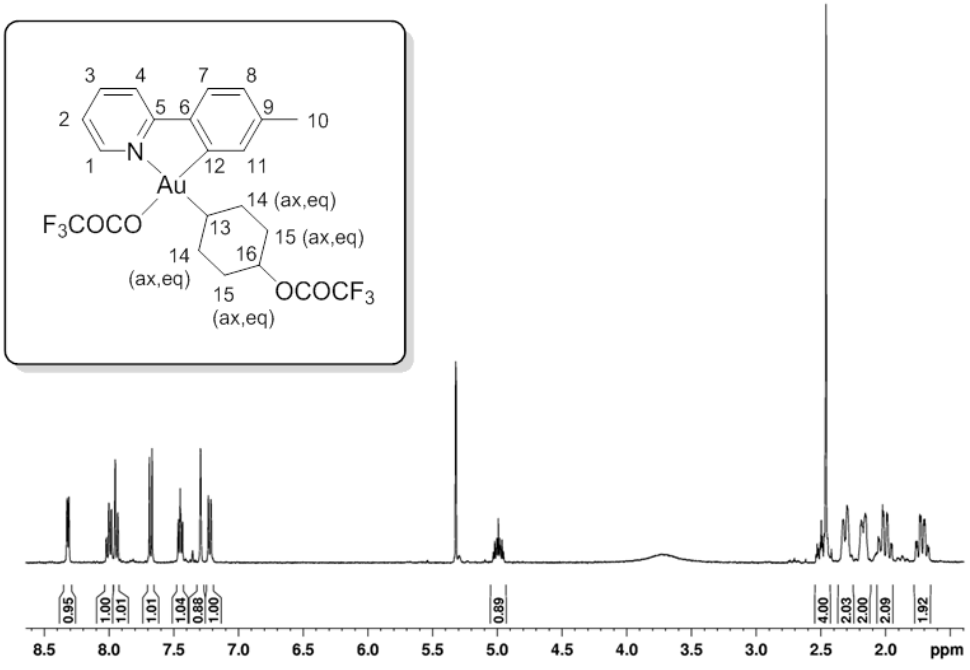

Figure 53: ^{1}H NMR (400 MHz, CD_2Cl_2) of compound **4**.

5.5 Synthesis of Complexes 5 and 57

1,5-Heptadiene (13.6 µl, 0.102 mmol, 1.2 eq.) was added to a solution of $Au(OCOCF_3)_2(tpy)$ (**1**, 50.0 mg, 0.085 mmol, 1.0 eq.) in 5 ml TFA. After 1 h reaction time the reaction was completed under full conversion of starting material **1**. The NMR shows isomers. It was not possible to separate them. The products could not be isolated since they are only stable in solution and decompose upon removal of the solvent.

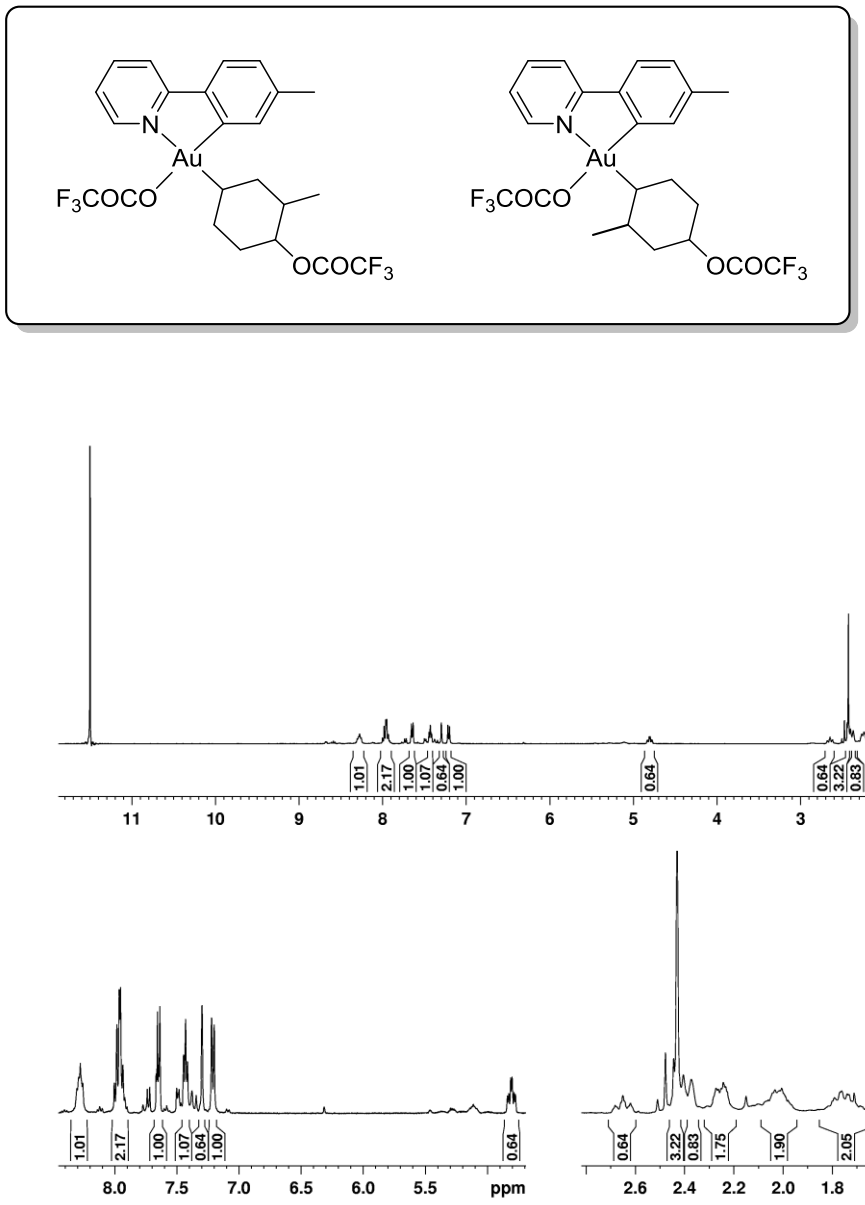

Figure 54: ^{1}H NMR (400 MHz, TFA-*d*) of reaction of gold(III) complex **1** with 1,5-heptadiene. Close-up views in the bottom.

5.6 Synthesis of Complex 6

1,5-Cyclooctadiene (4.0 µl, 0.042 mmol, 1.7 eq.) was added to a solution of $Au(OCOCF_3)_2(tpy)$ (**1**, 15.0 mg, 0.025 mmol, 1.0 eq.) in 0.5 ml CH_2Cl_2 and 0.5 ml TFA. After 30 min reaction time the reaction was completed under full conversion of starting material **1**. The product could not be isolated since it is only stable in solution and decomposes upon removal of the solvent.

^{1}H-NMR: (600 MHz, CD_2Cl_2) δ[ppm] = 8.40 (d, *J* = 5.4 Hz, 1 H, H-1), 8.17 (t, *J* = 7.9 Hz, 1 H, H-3), 8.06 (d, *J* = 8.2 Hz, 1 H, H-4), 7.77 (d, *J* = 7.9 Hz, 1 H, H-7), 7.73 (s, 1 H, H-11), 7.62 (t, *J* = 6.5 Hz, 1 H, H-2), 7.36 (d, *J* = 7.9 Hz, 1 H, H-8), 6.95-6.88 (m, 1 H, H-18), 6.86-6.80 (m, 1 H, H-17), 5.69 (dt, *J* = 11.6 Hz, *J* = 4.3 Hz, 1 H, H-14), 3.28-3.18 (m, 2 H, H-13,16a), 2.97-2.85 (m, 2 H, H-16b,19a), 2.81-2.72 (m, 1 H, H-15a), 2.71-2.59 (m, 3 H, H-19b,20), 2.48 (s, 3 H, H-10), 2.34-2.28 (m, 1 H, H-15b).

^{13}C-NMR: (151 MHz, TFA-*d*) δ[ppm] = 147.5 (C-1), 143.5 (C-3), 135.1 (C-18), 133.0 (C-17), 132.9 (C-11), 131.6 (C-8), 127.1 (C-7), 126.2 (C-2), 121.9 (C-4), 79.6 (C-14), 56.9 (C-13), 35.2 (C-20), 29.3 (C-15), 29.2 (C-16), 25.2 (C-19), 22.1 (C-10). Quaternary carbons were not observed.

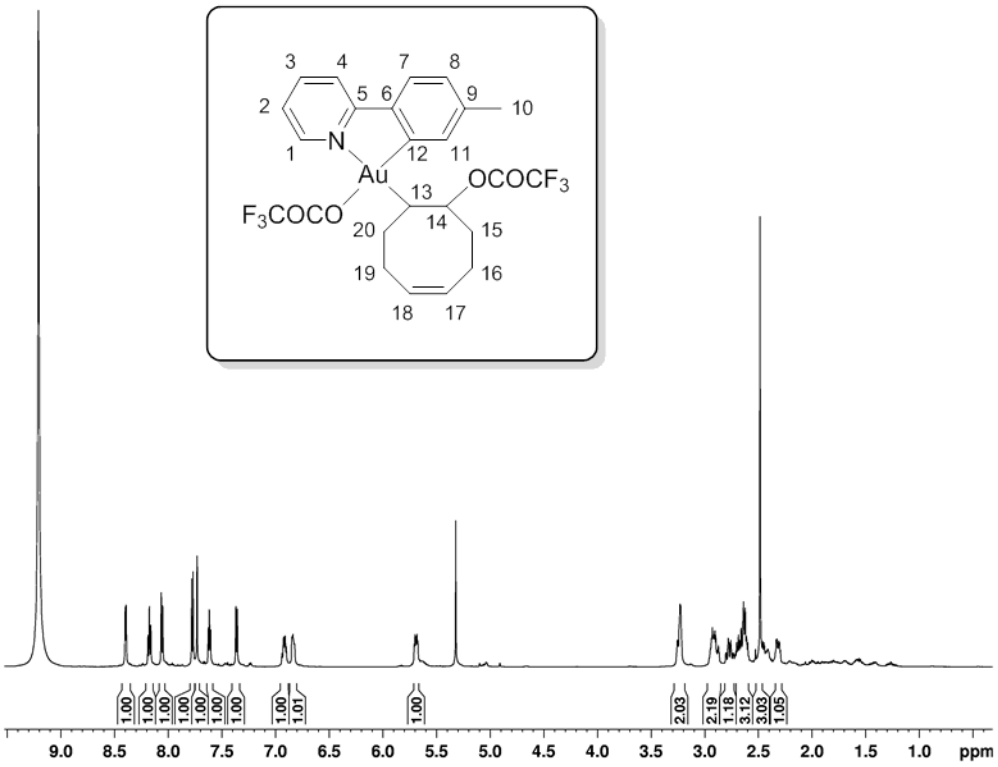

Figure 55: ^{1}H NMR (600 MHz, CD_2Cl_2) of compound **6**.

5.7 Synthesis of Complex 7

Cis-3-hexene (12.5 µl, 0.102 mmol, 1.2 eq.) was added to a solution of $Au(OCOCF_3)_2(tpy)$ (**1**, 50.0 mg, 0.085 mmol, 1.0 eq.) in 3 ml MeOH. After 2 days reaction time the solvent was removed *in vacuo* to yield a yellow solid (48.3 mg, 0.081 mmol, 96%).

^{1}H-NMR: (600 MHz, CD_2Cl_2) δ[ppm] = 8.30 (d, *J* = 5.4 Hz, 1 H, H-1), 7.96 (t, *J* = 7.8 Hz, 1 H, H-3), 7.91 (d, *J* = 8.1 Hz, 1 H, H-4), 7.64 (d, *J* = 7.9 Hz, 1 H, H-7), 7.42 (s, 1 H, H-11), 7.39 (t, *J* = 6.4 Hz, 1 H, H-2), 7.16 (d, *J* = 7.9 Hz, 1 H, H-8), 3.56-3.50 (m, 1 H, H-16), 3.37 (s, 3 H, OC**H$_3$**), 2.71-2.64 (m, 1 H, H-15), 2.42 (s, 3 H, H-10), 1.89-1.83 (d, *J* = 8.1 Hz, 1 H, H-17a), 1.76-1.67 (m, 1 H, H-14a), 1.66-1.58 (m, 1 H, H-17b), 1.35-1.27 (m, 1 H, H-14b), 1.16 (t, *J* = 7.3 Hz, 3 H, H-13), 0.96 (t, *J* = 7.5 Hz, 3 H, H-18).

^{13}C-NMR: (151 MHz, CD_2Cl_2) δ[ppm] = 161.4 (q, *J* = 37 Hz, **C**O), 160.7 (C-5), 147.1 (C-1), 142.1 (C-12), 141.5 (2 C, C-3,9), 137.2 (C-6), 132.3 (C-11), 129.2 (C-8), 126.0 (C-7), 124.3 (C-2), 120.3 (C-4), 118.7 (q, *J* = 290 Hz, **C**F_3), 85.1 (C-16), 65.8 (C-15), 56.9 (O**C**H_3), 25.9 (C-14), 24.7 (C-17), 22.3 (C-10), 15.9 (C-13), 8.7 (C-18).

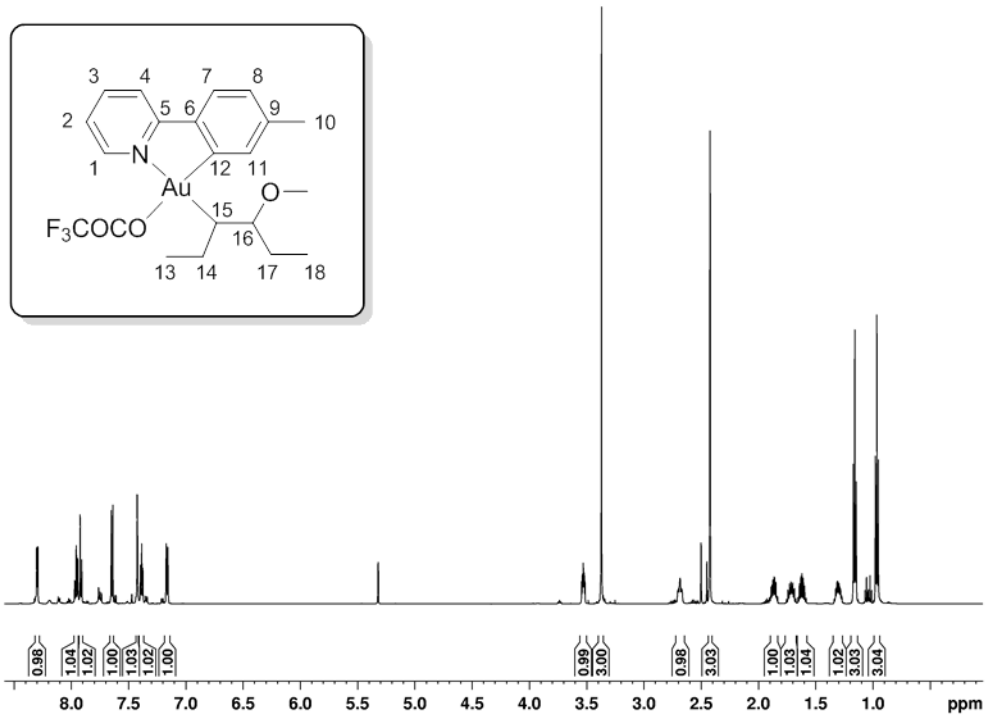

Figure 56: ^{1}H NMR (600 MHz, CD_2Cl_2) of compound **7**.

5.8 Synthesis of Complex 8

Trans-3-hexene (12.6 µl, 0.102 mmol, 1.2 eq.) was added to a solution of $Au(OCOCF_3)_2(tpy)$ (**1**, 50.0 mg, 0.085 mmol, 1.0 eq.) in 3 ml MeOH. After 3 days reaction time the solvent was removed *in vacuo* to yield a colorless oil. The product could not be obtained entirely pure and contained approximately 15% starting material **1**.

^{1}H-NMR: (600 MHz, CD_2Cl_2) δ[ppm] = 8.28 (d, *J* = 5.5 Hz, 1 H, H-1), 7.98 (t, *J* = 7.8 Hz, 1 H, H-3), 7.93 (d, *J* = 8.1 Hz, 1 H, H-4), 7.66 (d, *J* = 7.9 Hz, 1 H, H-7), 7.52 (m, 1 H, H-10), 7.43-7.40 (m, 1 H, H-2), 7.19 (d, *J* = 7.9 Hz, 1 H, H-8), 3.49-3.44 (m, 1 H, H-16), 3.41 (s, 3 H, OC**H$_3$**), 2.62-2.55 (m, 1 H, H-15), 2.43 (s, 3 H, H-10), 2.13-2.04 (m, 1 H, H-17a), 1.84-1.75 (m, 1 H, H-14a), 1.74-1.63 (m, 2 H, H-17b,14b), 1.15 (t, *J* = 7.4 Hz, 3 H, H-13), 0.93 (t, *J* = 7.4 Hz, 3 H, H-18).

^{13}C-NMR: (151 MHz, CD_2Cl_2) δ[ppm] = 147.0 (C-1), 141.7 (C-3), 133.0 (C-11), 129.3 (C-8), 126.1 (C-7), 124.4 (C-2), 120.3 (C-4), 85.1 (C-16), 67.7 (C-15), 58.9 (O**C**H$_3$), 29.1 (C-17), 26.6 (C-14), 22.3 (C-10), 16.1 (C-13), 9.8 (C-18). Quaternary carbons were not observed.

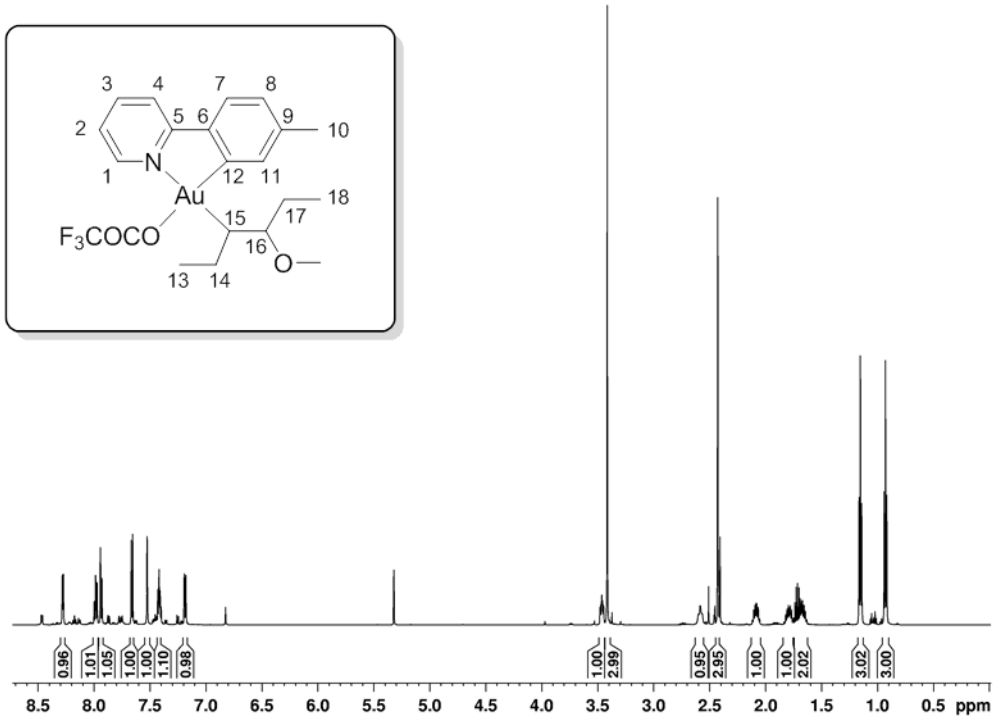

Figure 57: ^{1}H NMR (600 MHz, CD_2Cl_2) of compound **8**.

5.9 Synthesis of Complexes 9 and 10

Trans-2-hexene (12.8 µl, 0.102 mmol, 1.2 eq.) was added to a solution of $Au(OCOCF_3)_2(tpy)$ (**1**, 50.0 mg, 0.085 mmol, 1.0 eq.) in 3 ml MeOH. After 3 days reaction time the solvent was removed *in vacuo* to yield a white solid as product mixture of **9** and **10** in an approximate ratio of 2:1 (48.1 mg, 0.081 mmol, 96%). It was possible to isolate each product through crystallization of the mixture by vapor diffusion using CD_2Cl_2 as solvent and *n*-pentane as anti-solvent.

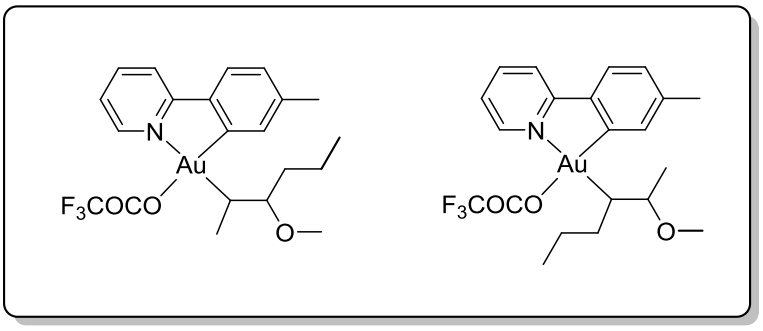

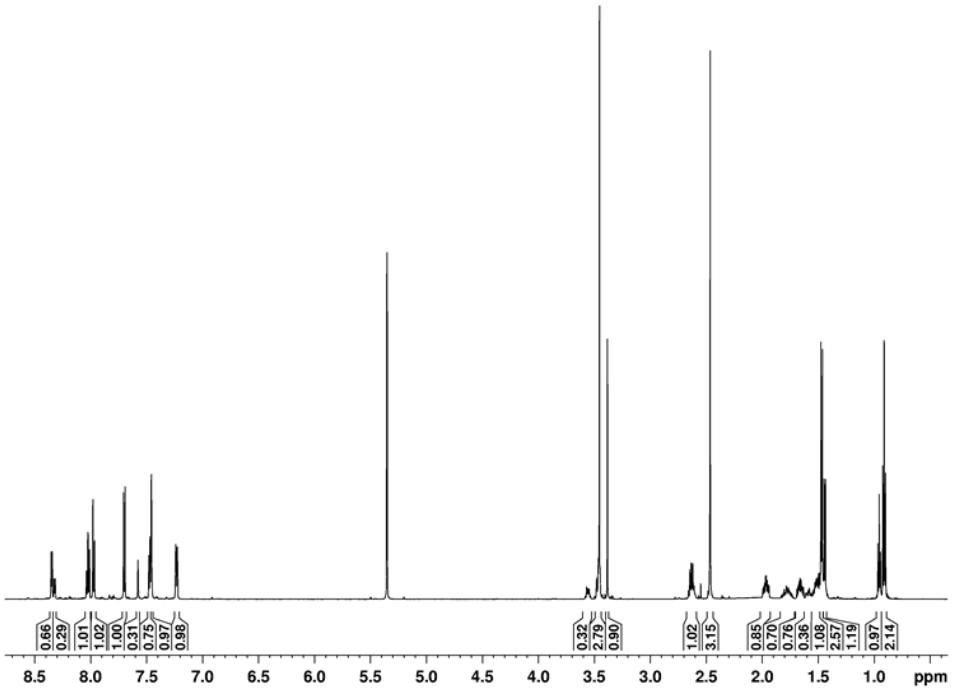

Figure 58: ^1H NMR (600 MHz, CD_2Cl_2) of product mixture **9** and **10**.

*Major isomer **9**:*

^{1}H-NMR: (600 MHz, CD_2Cl_2) δ[ppm] = 8.32 (d, *J* = 5.5 Hz, 1 H, H-1), 7.99 (t, *J* = 7.8 Hz, 1 H, H-3), 7.94 (d, *J* = 8.1 Hz, 1 H, H-4), 7.67 (d, *J* = 7.9 Hz, 1 H, H-7), 7.47-7.40 (m, 2 H, H-2,11), 7.20 (d, *J* = 7.9 Hz, 1 H, H-8), 3.48-3.39 (m, 4 H, H-15,OC**H**$_3$), 2.65-2.57 (m, 1 H, H-14), 2.44 (s, 3 H, H-10), 1.97-1.90 (m, 1 H, H-16a), 1.68-1.59 (m, 1 H, H-16b), 1.52-1.45 (m, 2 H, H-17), 1.44 (d, *J* = 7.0 Hz, 3 H, H-13), 0.88 (t, *J* = 7.4 Hz, 1 H, H-18).

^{13}C-NMR: (151 MHz, CD_2Cl_2) δ[ppm] = 161.4 (q, *J* = 37 Hz, **C**O), 160.7 (C-5), 147.0 (C-1), 142.6 (C-12), 141.6 (C-3), 141.2 (C-9), 137.9 (C-6), 132.0 (C-11), 129.3 (C-8), 125.9 (C-7), 124.4 (C-2), 120.4 (C-4), 84.3 (C-15), 59.2 (O**C**H$_3$), 56.2 (C-14), 39.0 (C-16), 22.2 (C-10), 19.2 (C-17), 18.3 (C-13), 14.6 (C-18). The carbon from the CF_3 group were not observed.

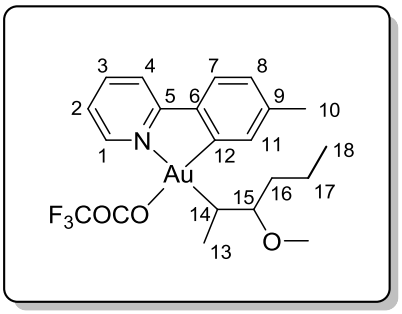

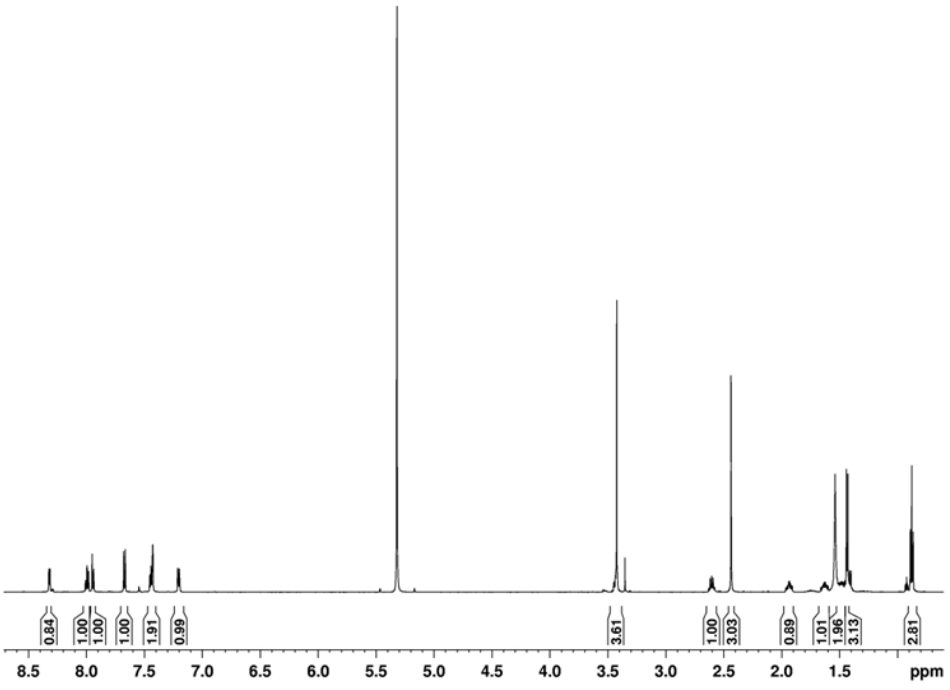

Figure 59: ^{1}H NMR (600 MHz, CD_2Cl_2) of **9**. The peak at 1.54 ppm is due to water.

*Minor isomer **10**:*

^{1}H-NMR: (600 MHz, CD_2Cl_2) δ[ppm] = 8.29 (d, *J* = 5.4 Hz, 1 H, H-1), 7.99 (t, *J* = 7.8 Hz, 1 H, H-3), 7.94 (d, *J* = 8.2 Hz, 1 H, H-4), 7.67 (d, *J* = 8.0 Hz, 1 H, H-7), 7.55 (s, 1 H, H-11), 7.44 (t, *J* = 6.4 Hz, 1 H, H-2), 7.20 (d, *J* = 7.9 Hz, 1 H, H-8), 3.57-3.49 (m, 1 H, H-17), 3.35 (s, 3 H, OC**H**$_3$), 2.65-2.55 (m, 1 H, H-16), 2.44 (s, 3 H, H-10), 1.81-1.69 (m, 2 H, H-14a,15a), 1.59-1.52 (m, 1 H, H-15b), 1.49-1.43 (m, 1 H, H-14b), 1.41 (d, *J* = 6.1 Hz, 3 H, H-18), 0.92 (t, *J* = 7.2 Hz, 3 H, H-13).

^{13}C-NMR: (151 MHz, CD_2Cl_2) δ[ppm] = 161.4 (q, *J* = 37 Hz, **C**O), 160.7 (C-5), 147.0 (C-1), 142.4 (C-12), 141.7 (C-3), 141.4 (C-9), 137.2 (C-6), 133.2 (C-11), 129.3 (C-8), 126.0 (C-7), 124.5 (C-2), 120.4 (C-4), 118.6 (q, *J* = 289 Hz, **C**F_3), 80.1 (C-17), 57.3 (O**C**H_3), 56.2 (C-16), 35.9 (C-15), 24.8 (C-14), 22.2 (C-10), 21.7 (C-18), 14.7 (C-13).

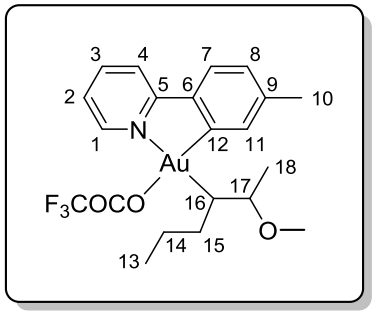

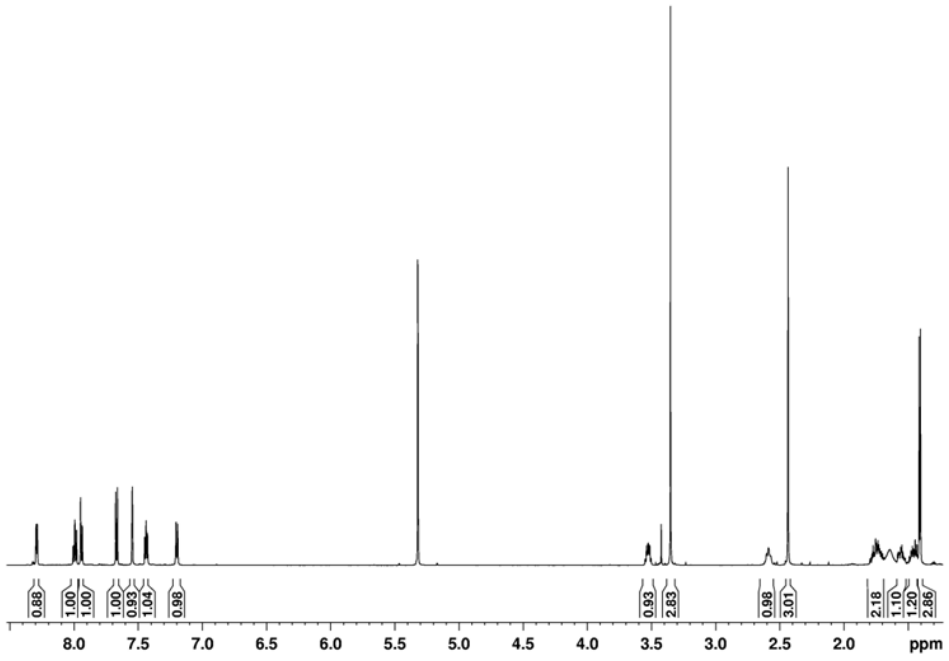

Figure 60: ^{1}H NMR (600 MHz, CD_2Cl_2) of **10**. The peak at 1.64 ppm is due to water.

5.10 Synthesis of Complex 11

Styrene (11.7 µl, 0.102 mmol, 1.2 eq.) was added to a solution of $Au(OCOCF_3)_2(tpy)$ (**1**, 50.0 mg, 0.085 mmol, 1.0 eq.) in 3 ml MeOH. After 23 h reaction time the solvent was removed *in vacuo*, the pale blue solid dissolved in CH_2Cl_2 and filtered afterwards. The solvent was removed *in vacuo* to yield a white solid (35.5 mg, 0.058 mmol, 68%).

^{1}H-NMR: (600 MHz, CD_2Cl_2) δ[ppm] = 8.41 (d, *J* = 5.4 Hz, 1 H, H-1), 8.01 (t, *J* = 7.8 Hz, 1 H, H-3), 7.92 (d, *J* = 8.1 Hz, 1 H, H-4), 7.62 (d, *J* = 7.8 Hz, 1 H, H-7), 7.46 (t, *J* = 6.5 Hz, 1 H, H-2), 7.41 (d, *J* = 7.5 Hz, 2 H, H-16), 7.34 (t, *J* = 7.5 Hz, 2 H, H-17), 7.29-7.24 (m, 2 H, H-11,18), 7.17 (d, *J* = 7.8 Hz, 1 H, H-8), 4.53 (dd, *J* = 8.9 Hz, *J* = 5.1 Hz, 1 H, H-14), 3.20 (s, 3 H, OC**H$_3$**), 2.61 (dd, *J* = 10.4 Hz, *J* = 5.1 Hz, 1 H, H-13a), 2.50-2.45 (m, 1 H, H-13b), 2.40 (m, 3 H, H-10).

^{13}C-NMR: (151 MHz, CD_2Cl_2) δ[ppm] = 161.4 (q, *J* = 37 Hz, **C**O), 160.8 (C-5), 146.7 (C-1), 143.7 (C-15), 142.5 (C-12), 141.9 (C-3), 141.0 (C-9), 136.9 (C-6), 132.7 (C-11), 129.3 (C-8), 129.0 (C-17), 128.0 (C-18), 127.2 (C-16), 125.9 (C-7), 124.4 (C-2), 120.5 (C-4), 118.5 (q, *J* = 290 Hz, **C**F_3), 84.1 (C-14), 57.0 (O**C**H_3), 41.3 (C-13), 22.2 (C-10).

MS (ESI, MeCN) m/z (rel %): 1113(100), 1045(36), 636($M{\cdot}Na^+$, 2), 500(M^+-$OCOCF_3$, 78).

HR-MS (MeCN): 636.1031, calculated for $C_{23}H_{21}NO_3F_3AuNa$: 636.1036 (-0.0005 ppm).

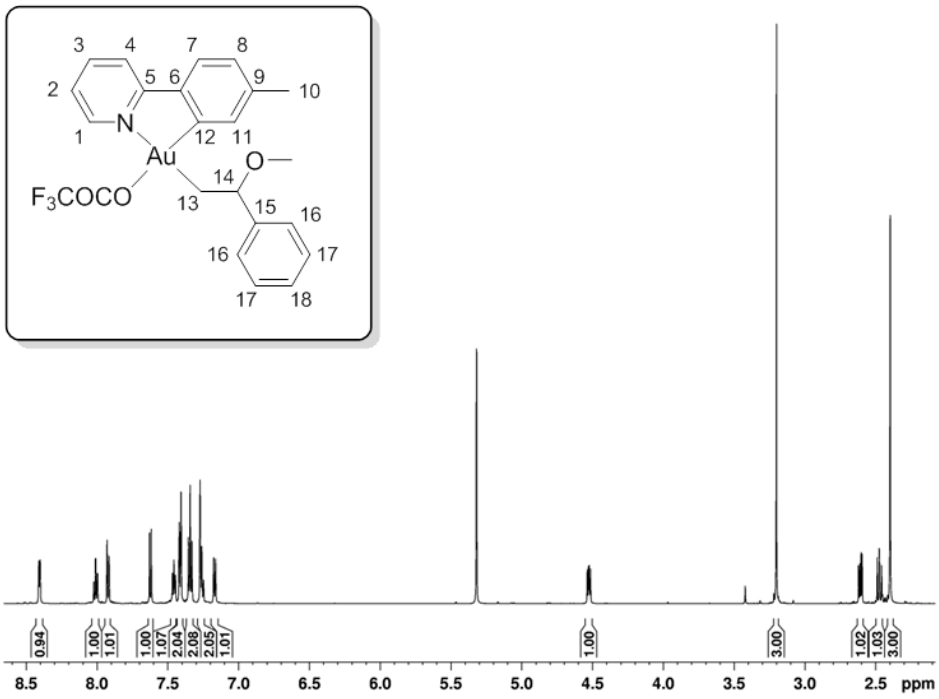

Figure 61: ^{1}H NMR (600 MHz, CD_2Cl_2) of compound **11**.

5.11 Synthesis of Complex 12

This reaction was carried out under varying conditions, however, none yielded clean product. The tested experimental procedures are described below.

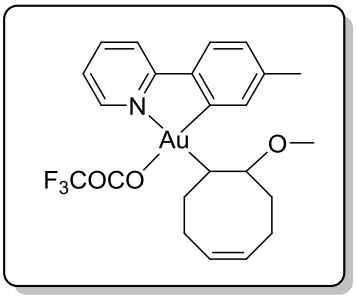

Method 1:

1,5-Cyclooctadiene (12.5 µl, 0.102 mmol, 1.2 eq.) was added to a solution of $Au(OCOCF_3)_2(tpy)$ (**1**, 50.0 mg, 0.085 mmol, 1.0 eq.) in 3 ml MeOH. After 1 h reaction time the solvent was removed *in vacuo*. The product could not be obtained pure and contained approximately 40% starting material **1**. However, crystals suitable for X-ray analysis were obtained through crystallization by vapor diffusion using CD_2Cl_2 as solvent and *n*-pentane as anti-solvent.

Method 2:

1,5-Cyclooctadiene (12.5 µl, 0.102 mmol, 1.2 eq.) was added to a solution of $Au(OCOCF_3)_2(tpy)$ (**1**, 50.0 mg, 0.085 mmol, 1.0 eq.) in 3 ml MeOH. After 3 h reaction time the solvent was removed *in vacuo*. The product could not be obtained pure and contained approximately 10% starting material **1**.

Method 3:

1,5-Cyclooctadiene (12.5 µl, 0.102 mmol, 1.2 eq.) was added to a solution of $Au(OCOCF_3)_2(tpy)$ (**1**, 50.0 mg, 0.085 mmol, 1.0 eq.) in 3 ml MeOH. After 2 days reaction time the solvent was removed *in vacuo*. The observed product was mainly free ligand.

5.12 Synthesis of Complex 13

1,5-Hexadiene (12.1 µl, 0.102 mmol, 1.2 eq.) was added to a solution of $Au(OCOCF_3)_2(tpy)$ (**1**, 50.0 mg, 0.085 mmol, 1.0 eq.) in 3 ml MeOH. After 2 days reaction time the solvent was removed *in vacuo* yielding a grey solid. The product was only poorly soluble in standard solvents (CD_2Cl_2, MeCN, DMSO, and acetone), so the obtained NMR spectra might not reflect the true nature of the product.

^{1}H-NMR: (600 MHz, CD_2Cl_2) δ[ppm] = 8.40 (d, *J* = 5.5 Hz, 1 H, H-1), 8.02 (t, *J* = 7.9 Hz, 1 H, H-3), 7.94 (d, *J* = 8.0 Hz, 1 H, H-4), 7.66 (d, *J* = 7.9 Hz, 1 H, H-7), 7.47 (t, *J* = 6.5 Hz, 1 H, H-2), 7.41 (s, 1 H, H-11), 7.20 (d, *J* = 7.9 Hz, 1 H, H-8), 5.84 (ddt, *J* = 17.2 Hz, *J* = 10.3 Hz, *J* = 6.6 Hz, 1 H, H-17), 5.01 (t, *J* = 17.2 Hz, 1 H, H-18$_{trans}$), 4.93 (t, *J* = 10.3 Hz, 1 H, H-18$_{cis}$), 3.55-3.49 (m, 1 H, H-14), 3.38 (s, 3 H, OC**H**$_3$), 2.48 (dd, *J* = 10.1 Hz, *J* = 6.4 Hz, 1 H, H-13a), 2.43 (s, 3 H, H-10), 2.30 (dd, *J* = 10.1 Hz, *J* = 7.1 Hz, 1 H, H-13a), 2.27-2.20 (m, 1 H, H-16a), 2.19-2.11 (m, 1 H, H-16b), 1.82-1.70 (m, 2 H, H-15).

^{13}C-NMR: (151 MHz, DMSO-d_6) δ[ppm] = 159.1 (C-5), 145.8 (C-1), 142.6 (C-12), 141.7 (C-3), 140.5 (C-9), 138.5 (C-17), 135.3 (C-6), 131.7 (C-11), 129.0 (C-8), 126.4 (C-7), 124.9 (C-2), 120.7 (C-4), 114.7 (C-18), 79.9 (C-14), 56.1 (O**C**H$_3$), 36.9 (C-13), 35.2 (C-15), 29.5 (C-16), 21.4 (C-10). The carbons from the $COCF_3$ groups were not observed.

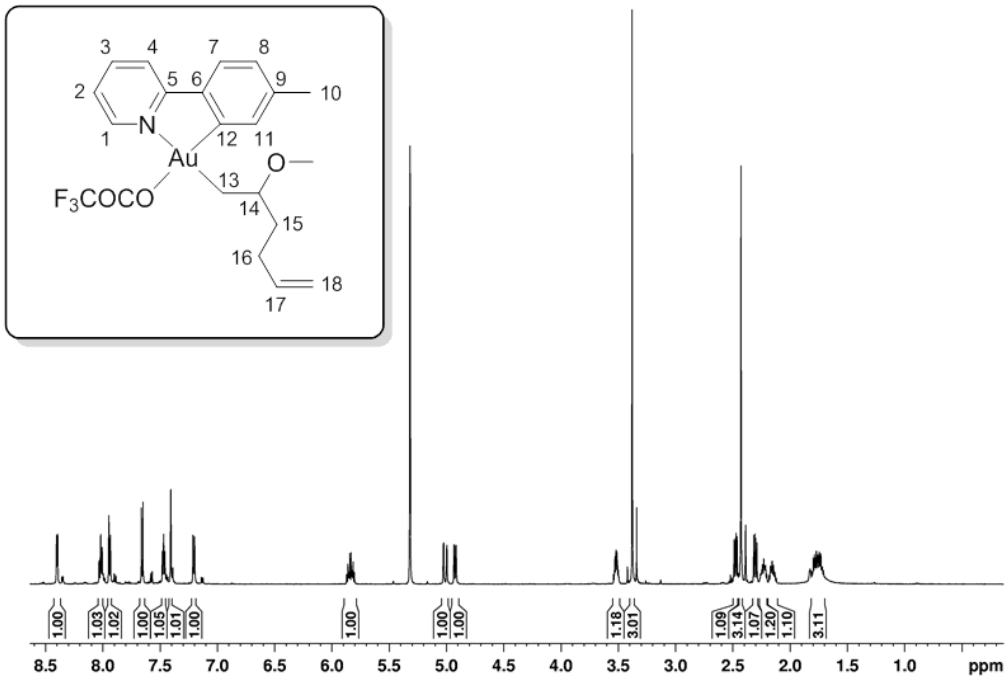

Figure 62: ^{1}H NMR (600 MHz, CD_2Cl_2) of compound **13**.

5.13 Synthesis of Complex 14

Styrene (11.7 µl, 0.102 mmol, 1.2 eq.) was added to a solution of $Au(OCOCF_3)_2(tpy)$ (**1**, 50.0 mg, 0.085 mmol, 1.0 eq.) in 4.00 ml MeCN, 0.50 ml TFA and 0.05 ml H_2O. After 21 h reaction time the solvent was removed *in vacuo*, the purple solid was dissolved in CH_2Cl_2 and filtered afterwards. The solvent was removed *in vacuo* to yield a yellow solid (36.5 mg, 0.692 mmol, 82%).

^{1}H-NMR: (600 MHz, CD_2Cl_2) δ[ppm] = 11.05-10.22 (br., 1 H, N**H**), 8.71 (d, *J* = 5.1 Hz, 1 H, H-1), 8.10 (t, *J* = 7.9 Hz, 1 H, H-3), 7.97 (d, *J* = 8.1 Hz, 1 H, H-4), 7.67 (d, *J* = 7.9 Hz, 1 H, H-7), 7.58 (t, *J* = 6.5 Hz, 1 H, H-2), 7.45 (d, *J* = 7.3 Hz, 2 H, H-16), 7.38 (t, *J* = 7.4 Hz, 2 H, H-17), 7.33 (t, *J* = 7.3 Hz, 1 H, H-18), 7.22 (d, *J* = 7.9 Hz, 1 H, H-8), 7.19 (s, 1 H, H-11), 4.91-4.81 (br., 1 H, H-14), 2.98-2.84 (br., 1 H, H-13), 2.47-2.41 (br., 3 H, H-20), 2.39 (s, 3 H, H-10).

^{13}C-NMR: (151 MHz, CD_2Cl_2) δ[ppm] = 175.7 (C-19), 160.8 (C-5), 145.9 (C-1), 143.3 (C-12), 142.7 (C-3), 140.9 (C-9), 135.8 (C-6), 132.0 (C-11), 130.0 (C-8), 129.6 (C-17), 128.8 (C-18), 127.2 (C-16), 126.4 (C-7), 124.6 (C-2), 120.6 (C-4), 54.0 (C-14), 39.4 (C-13), 23.2 (C-20), 22.1 (C-10).

MS (ESI, MeCN) m/z (rel %): 1129(4), 576(10), 527(M^+, 100).

HR-MS (MeCN): 527.1378, calculated for $C_{22}H_{22}N_2OAu$: 527.1397 (-3.74 ppm).

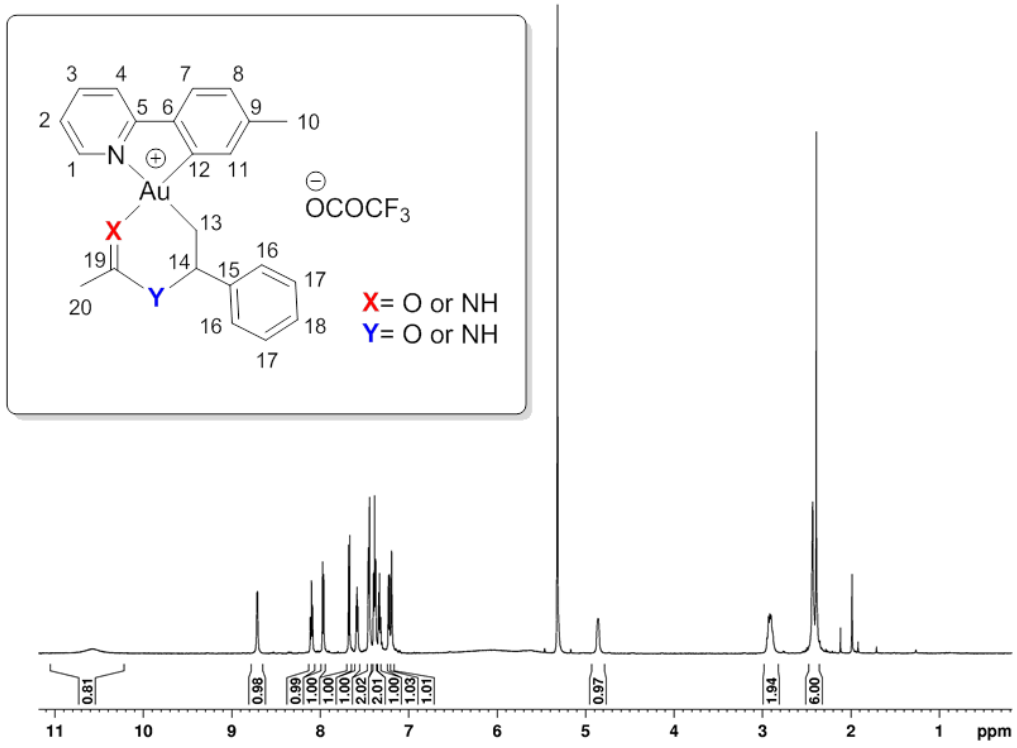

Figure 63: ^{1}H NMR (600 MHz, CD_2Cl_2) of compound **14**.

5.14 Reaction of $Au(OCOCF_3)_2(tpy)$ (1) with Internal Alkenes in TFA-*d*

$Au(OCOCF_3)_2(tpy)$ (**1**, 5 mg, 0.01 mmol, 1.0 eq.) was added to a solution of *cis*-3-hexene (1.3 µl, 0.01 mmol, 1.0 eq.) in 0.45 ml TFA-*d* and 0.5 µl 1,2-dichloroethane. After 60 min no full conversion was observed, so more *cis*-3-hexene (1.5 µl, 0.01 mmol, 1.0 eq.) was added, yielding free ligand as main product after another 30 min.

$Au(OCOCF_3)_2(tpy)$ (**1**, 5 mg, 0.01 mmol, 1.0 eq.) was added to a solution of *trans*-3-hexene (1.3 µl, 0.01 mmol, 1.0 eq.) in 0.45 ml TFA-*d* and 0.5 µl 1,2-dichloroethane. After 40 min no full conversion was observed, so more *trans*-3-hexene (2.0 µl, 0.02 mmol, 1.9 eq.) was added, yielding free ligand as main product after another 20 min.

$Au(OCOCF_3)_2(tpy)$ (**1**, 5 mg, 0.01 mmol, 1.0 eq.) was added to a solution of *trans*-2-hexene (1.3 µl, 0.01 mmol, 1.0 eq.) in 0.45 ml TFA-*d* and 0.5 µl 1,2-dichloroethane. After 45 min no full conversion was observed, so more *trans*-2-hexene (3.0 µl, 0.02 mmol, 2.8 eq.) was added, yielding free ligand as main product after another 3 h.

5.15 Reaction of $Au(OCOCF_3)_2(tpy)$ (1) with 1,5-Hexadiene in TFE

1,5-Hexadiene (12.1 µl, 0.102 mmol, 1.2 eq.) was added to a solution of $Au(OCOCF_3)_2(tpy)$ (**1**, 50.0 mg, 0.085 mmol, 1.0 eq.) in 3 ml TFE. After 2 h reaction time the reaction mixture was cannula filtrated, yielding a white precipitate. The white solid was only poorly soluble in standard solvents (CD_2Cl_2, MeCN, DMSO, and acetone). The obtained NMR spectrum showed product mixture.

5.16 Reaction of $Au(OCOCF_3)_2(tpy)$ (1) with 1,4-Pentadiene in EtOH

1,4-pentadiene (10 µl, 0.10 mmol, 1.2 eq.) was added to a solution of $Au(OCOCF_3)_2(tpy)$ (**1**, 50.0 mg, 0.085 mmol, 1.0 eq.) in 3 ml EtOH. After 1 day reaction time the solvent was removed *in vacuo* yielding a purple solid. The obtained NMR spectrum showed product mixture.

5.17 Reaction of $Au(OCOCF_3)_2(tpy)$ (1) with 1,5-Hexadiene in EtOH

1,5-Hexadiene (12.1 µl, 0.102 mmol, 1.2 eq.) was added to a solution of $Au(OCOCF_3)_2(tpy)$ (**1**, 50.0 mg, 0.085 mmol, 1.0 eq.) in 3 ml EtOH. After 2 days reaction time the solvent was removed *in vacuo* yielding an air-sensitive purple solid. The obtained NMR spectrum showed product mixture.

5.18 Reaction of $Au(OCOCF_3)_2(tpy)$ (1) with 1,4-Pentadiene in MeOH

1,4-pentadiene (10 µl, 0.10 mmol, 1.2 eq.) was added to a solution of $Au(OCOCF_3)_2(tpy)$ (**1**, 50.0 mg, 0.085 mmol, 1.0 eq.) in 3 ml MeOH. After 1 day reaction time the solvent was removed *in vacuo* yielding a black solid. The obtained NMR spectrum showed product mixture.

5.19 Reaction of Complex 2 with Bu_4NCl

A solution of $Au(OCOCF_3)_2(tpy)$ (**1**, 6 mg, 0.01 mmol, 1.0 eq.) and 0.45 µl TFA-*d* in a NMR-tube was bubbled through by ethylene gas for 1 min at room temperature. Bu_4NCl (5 mg, 0.02 mmol, 2.0 eq.) was added, then the solvent removed *in vacuo* yielding a yellow solid.

6 Appendix

6.1 Complex 1[2]

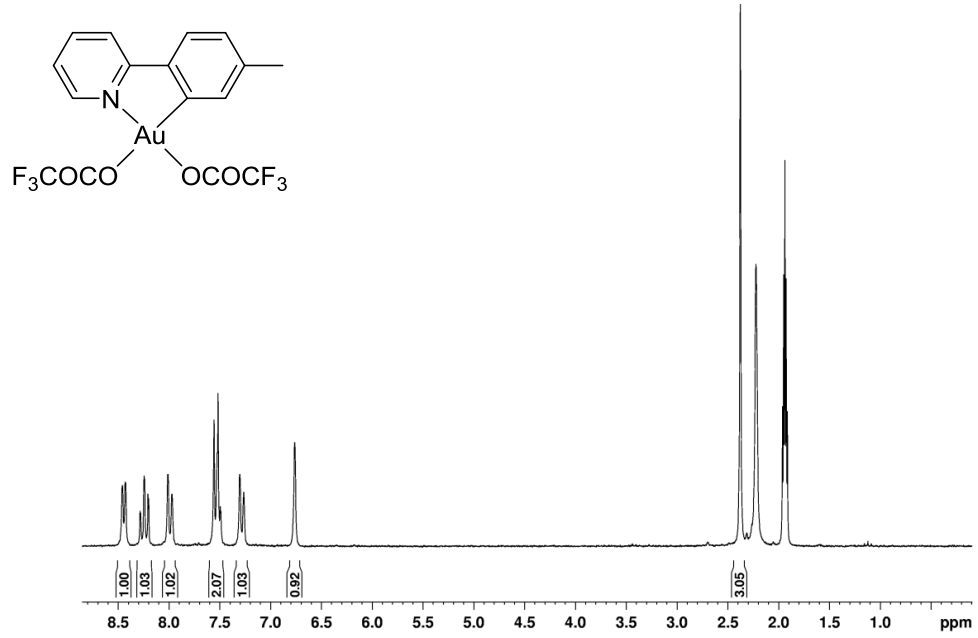

Figure 64: ^{1}H NMR (200 MHz, CD_3CN) of compound **1**.

6.2 Complex 2[7]

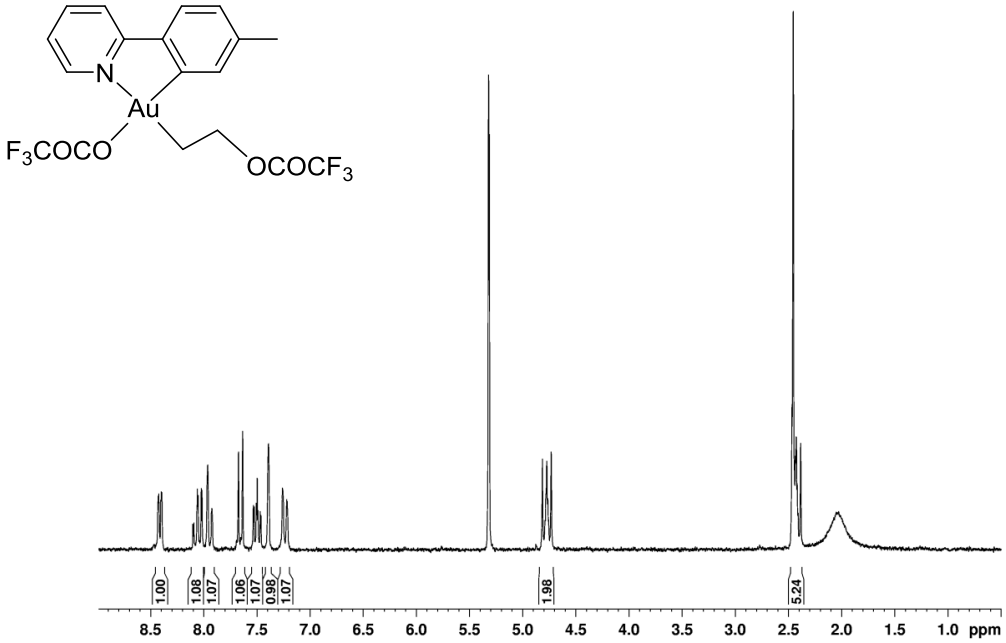

Figure 65: ^{1}H NMR (200 MHz, CD_2Cl_2) of compound **2**. Peak at 2.39 ppm is due to TFA residue.

6.3 Complex 3

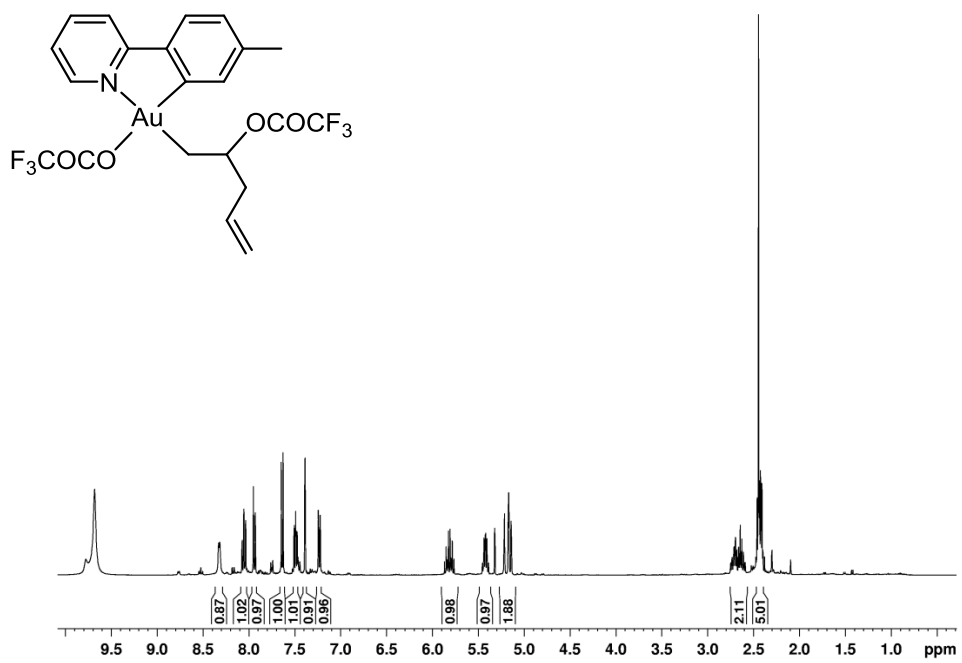

Figure 66: ^{1}H NMR (400 MHz, CD_2Cl_2) of compound **3**. Peak at 9.7 ppm is due to TFA residue.

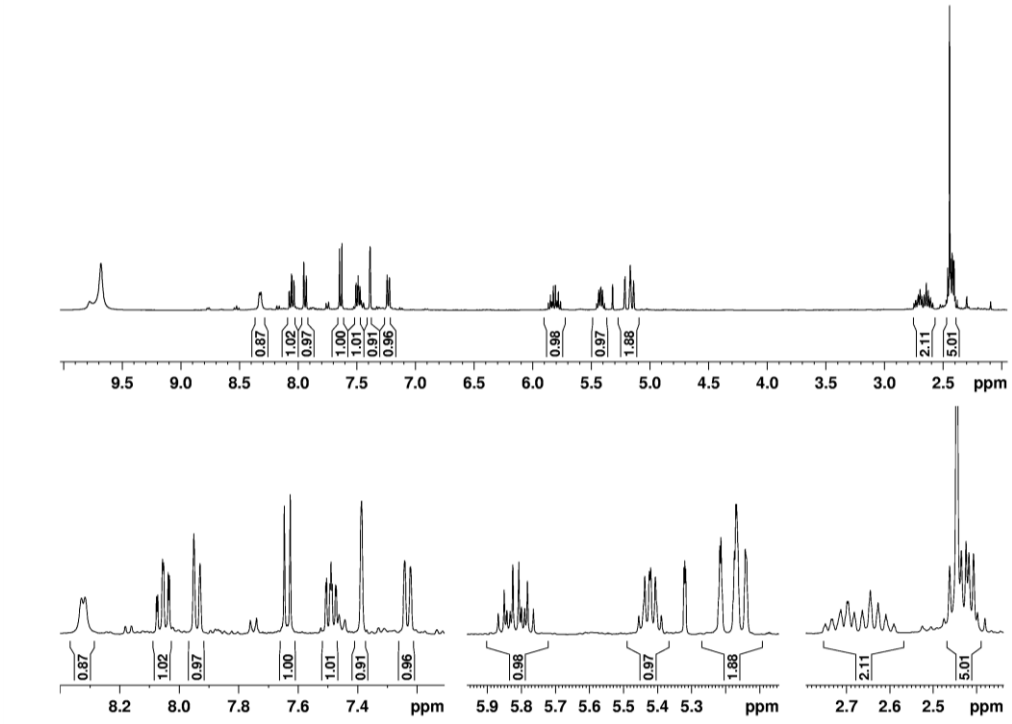

Figure 67: ^{1}H-NMR (400 MHz, CD_2Cl_2) of alkyl gold(III) complex **3**. Close-up views in the bottom. Peak at 9.7 ppm is due to TFA residue.

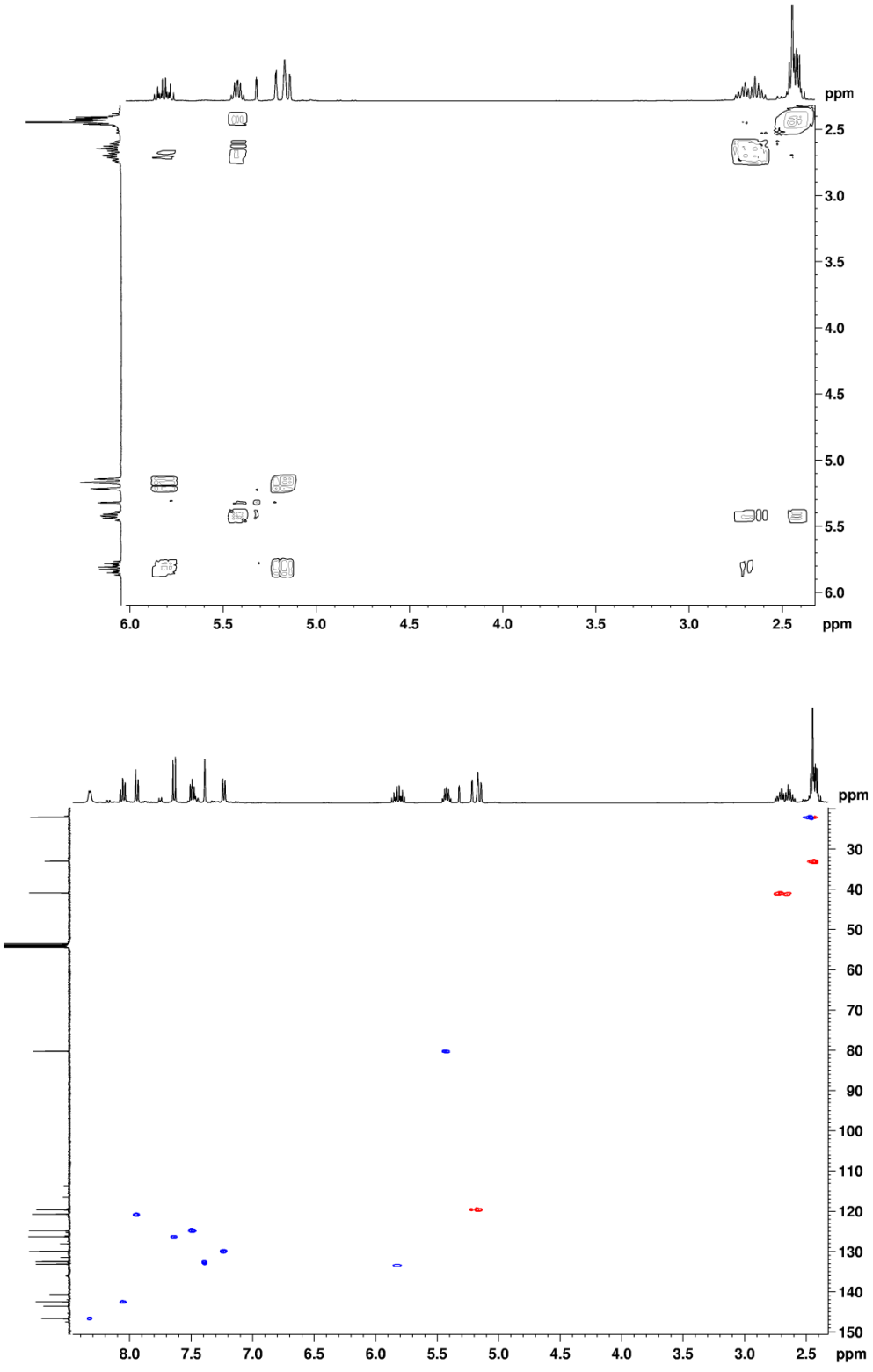

Figure 68: (400 MHz, CD_2Cl_2) Close-up view of COSY (top) and HSQC (bottom) of complex **3**.

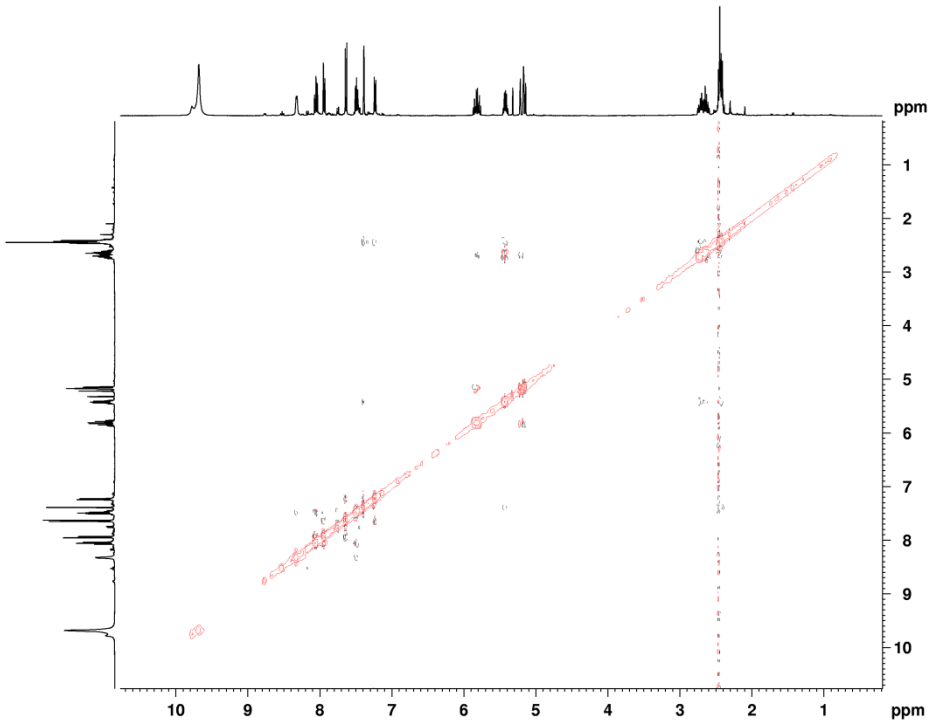

Figure 69: NOESY (400 MHz, CD_2Cl_2) of complex **3**.

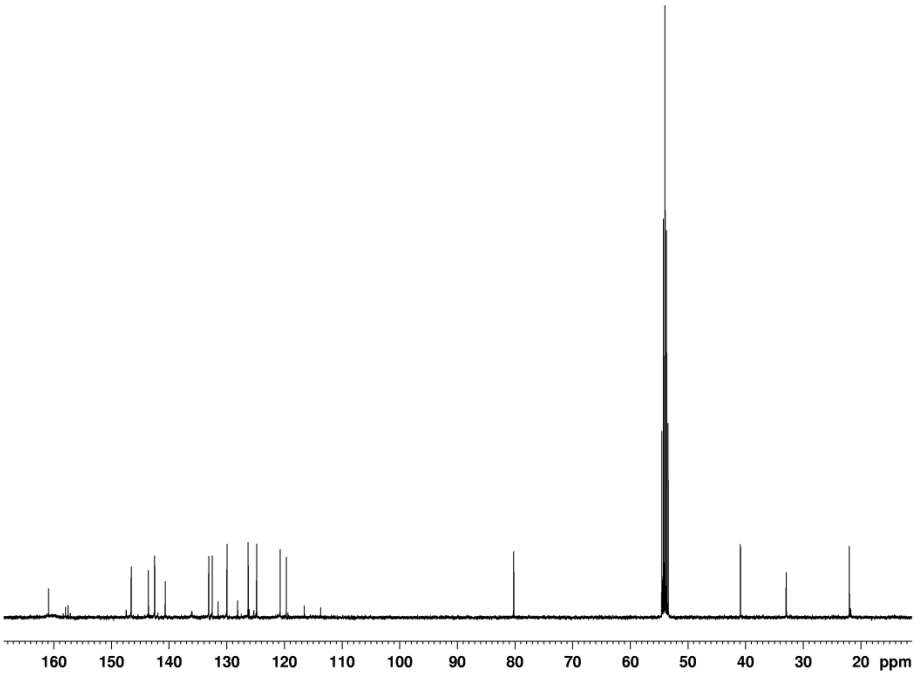

Figure 70: ^{13}C-NMR (100 MHz, CD_2Cl_2) of complex **3**.

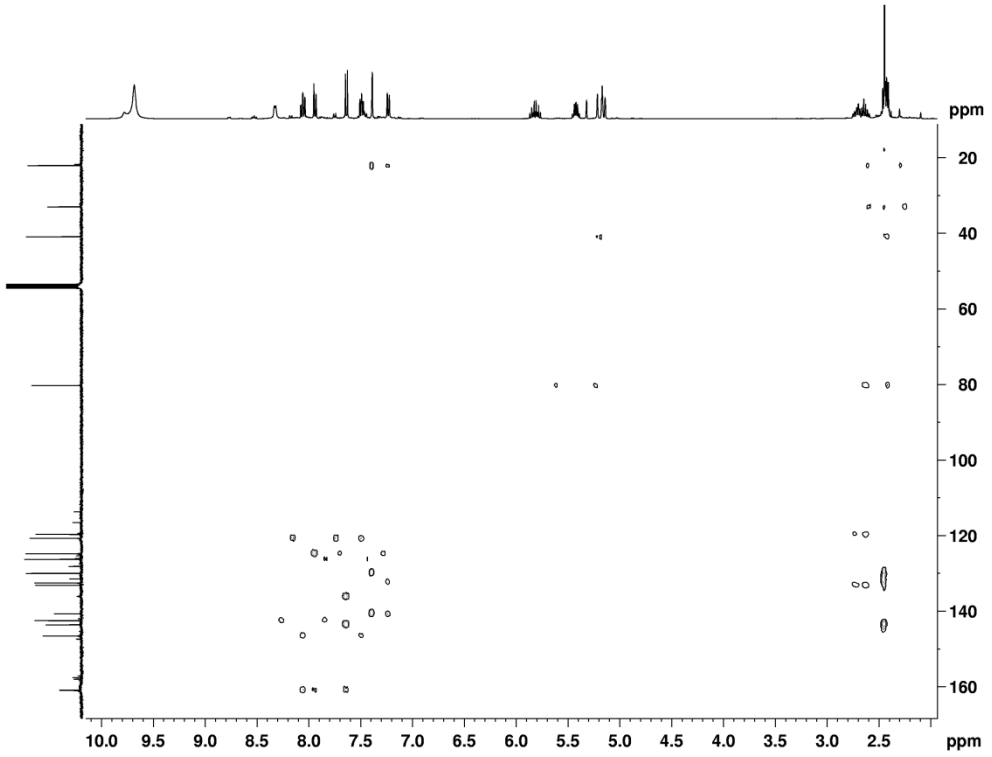

Figure 71: HMBC (400 MHz, CD_2Cl_2) of complex **3**.

6.4 Complex 4

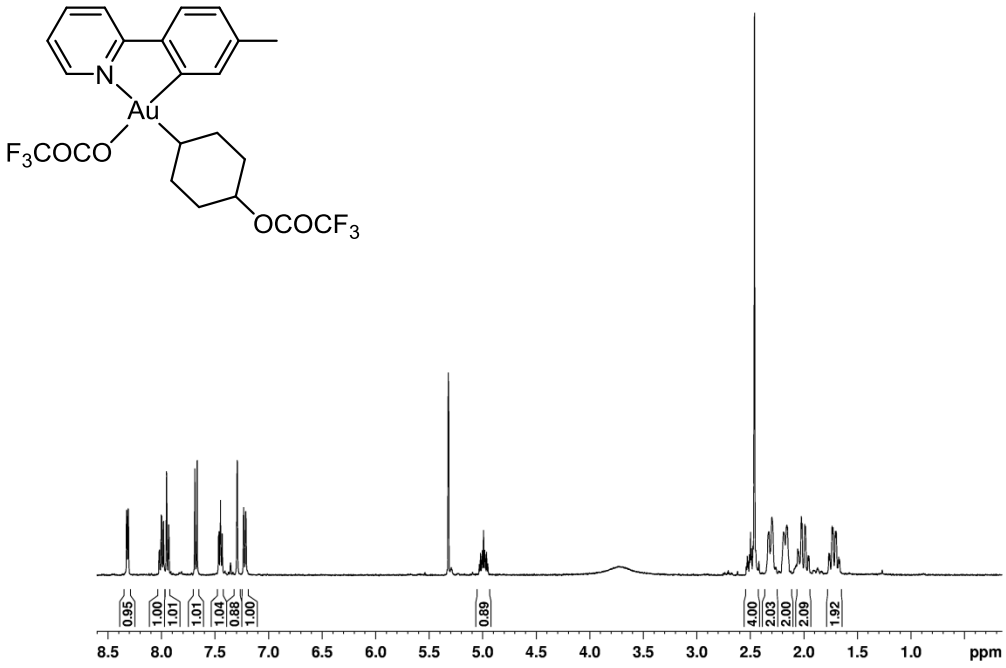

Figure 72: ^{1}H NMR (400 MHz, CD_2Cl_2) of compound **4**. Peak at 3.7 ppm is due to TFA residue.

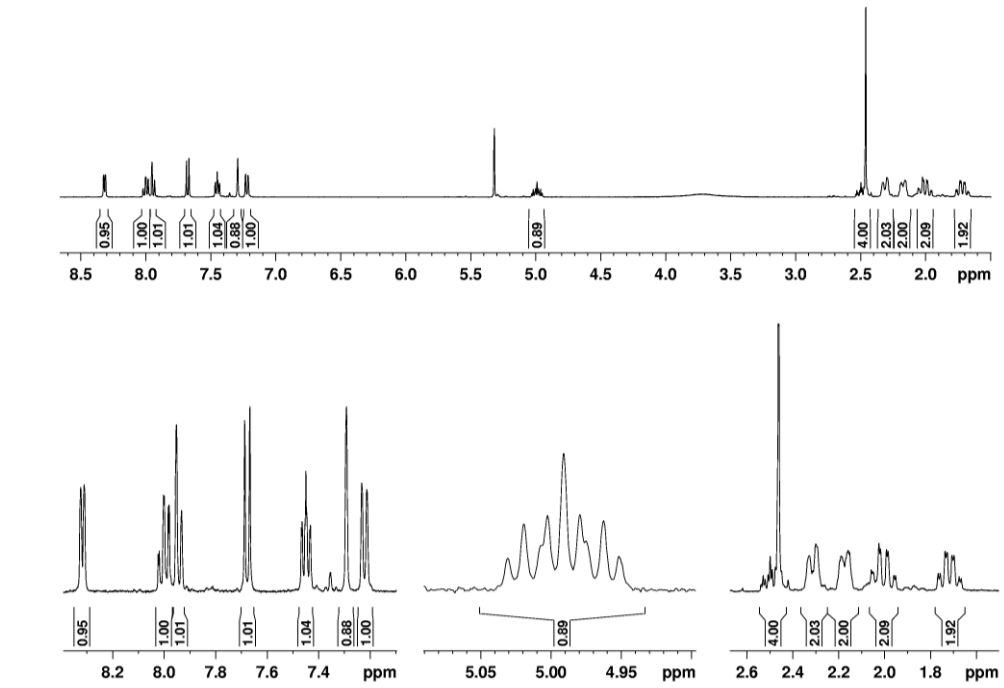

Figure 73: ^{1}H-NMR (400 MHz, CD_2Cl_2) of alkyl gold(III) complex **4**. Close-up views in the bottom. Peak at 3.7 ppm is due to TFA residue.

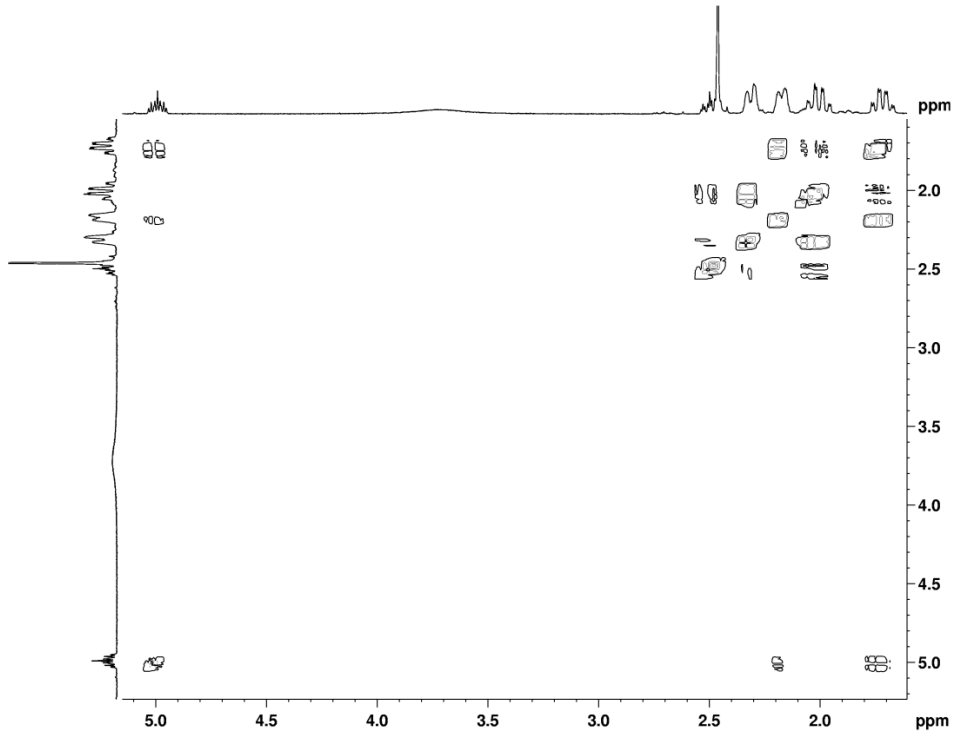

Figure 74: Close-up view of COSY (400 MHz, CD_2Cl_2) of complex **4**.

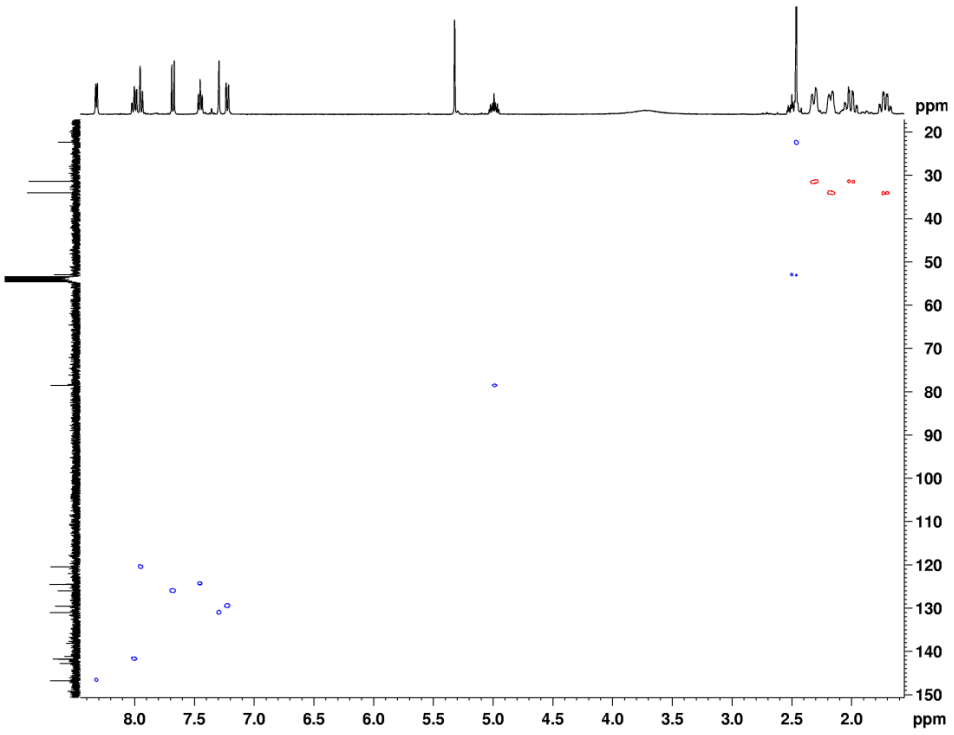

Figure 75: HSQC (400 MHz, CD_2Cl_2) of complex **4**.

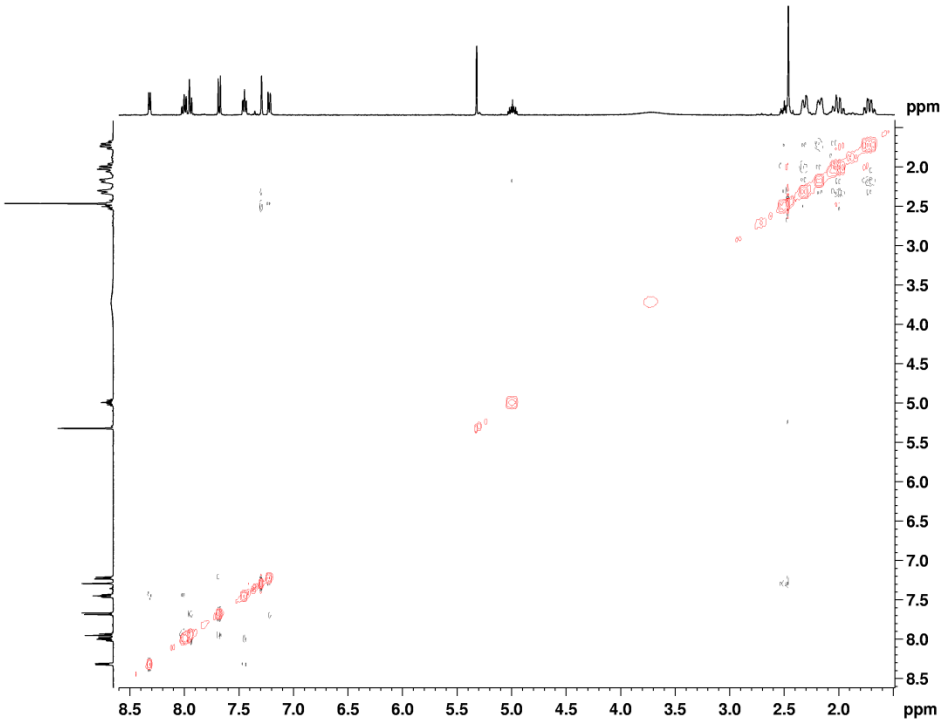

Figure 76: NOESY(400 MHz, CD_2Cl_2) of complex **4**.

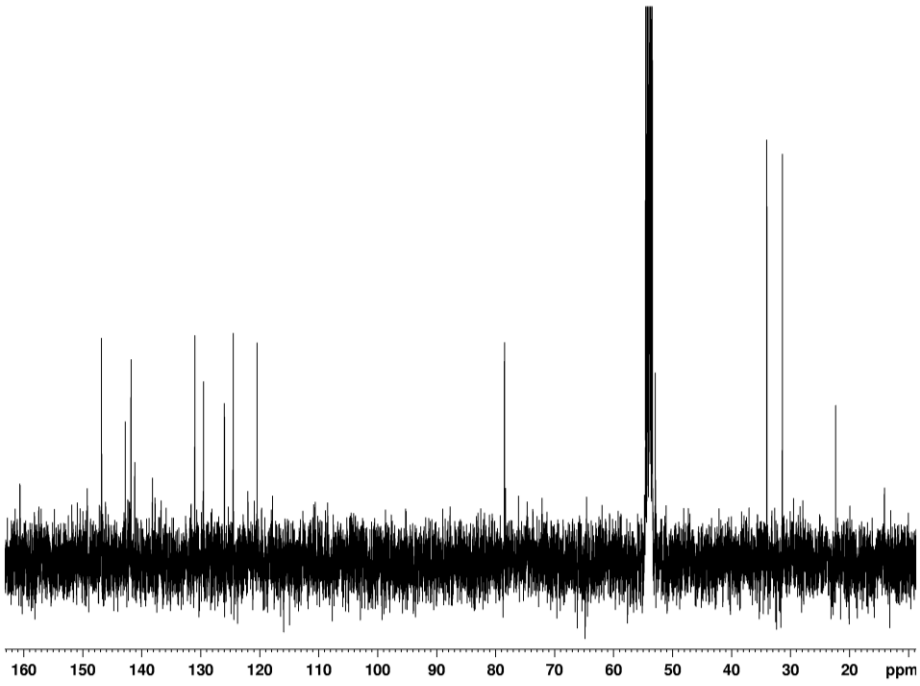

Figure 77: ^{13}C-NMR (100 MHz, CD_2Cl_2) of complex **4**.

6.5 Complex 6

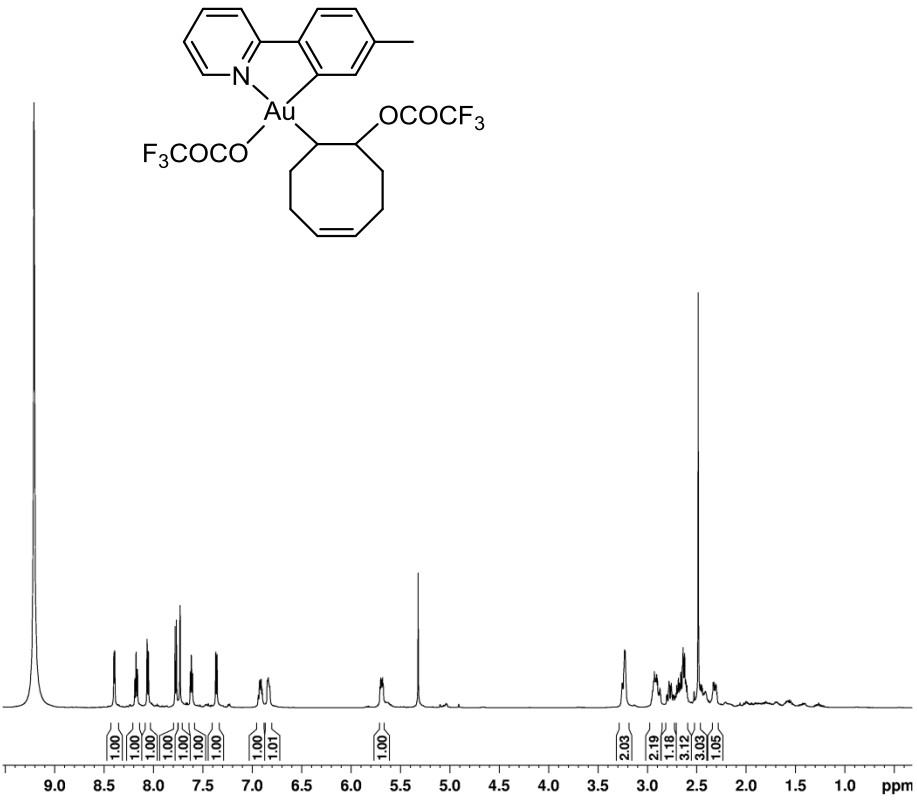

Figure 78: ^{1}H NMR (600 MHz, CD_2Cl_2) of compound **6**.

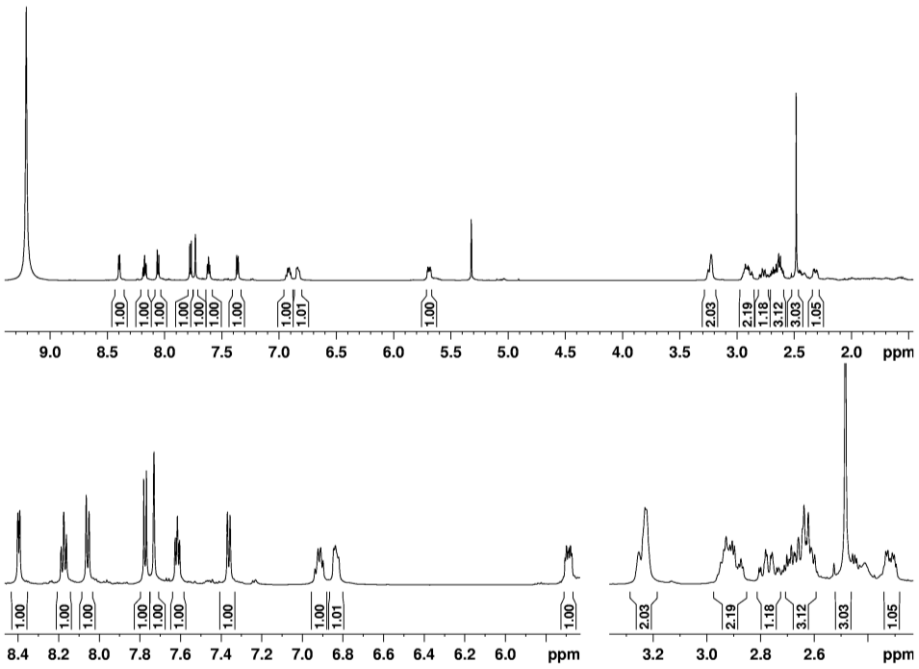

Figure 79: ^{1}H-NMR (600 MHz, CD_2Cl_2) of alkyl gold(III) complex **6**. Close-up views in the bottom. Peak at 9.2 ppm is due to TFA residue.

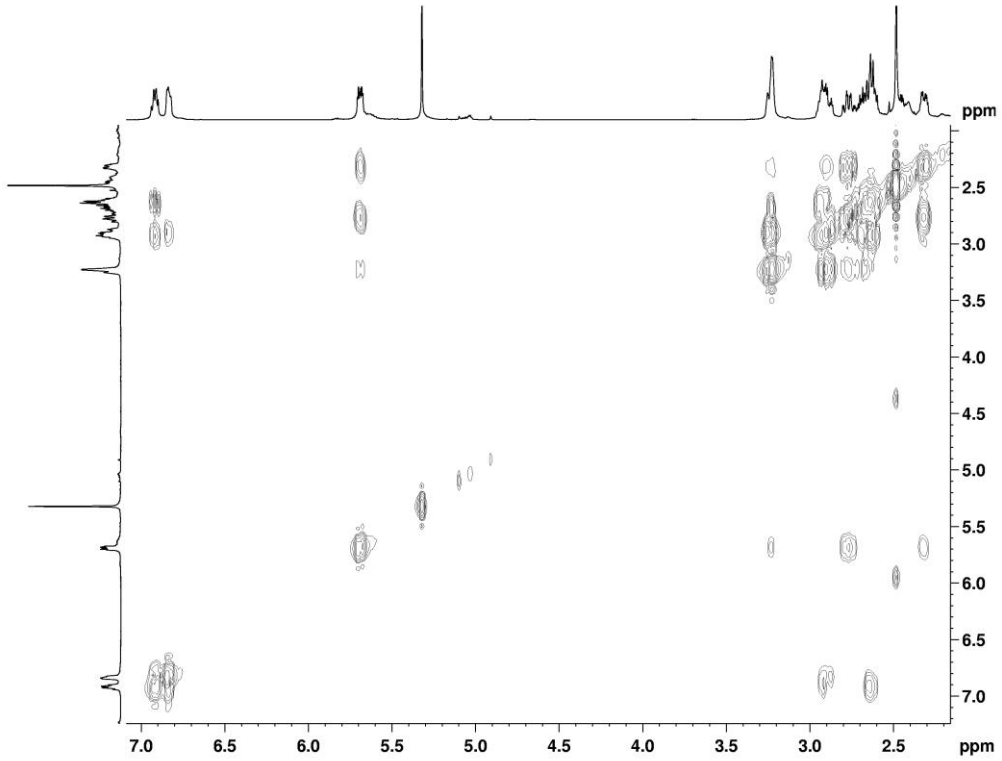

Figure 80: Close-up view of COSY (600 MHz, CD_2Cl_2)of complex **6**.

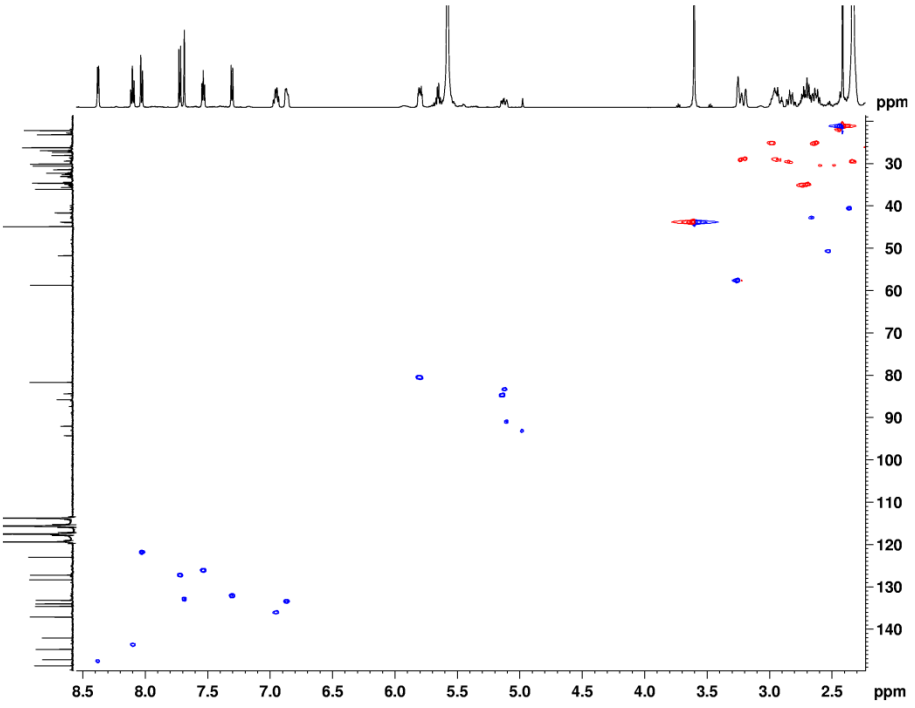

Figure 81: HSQC (600 MHz, TFA-*d*) obtained from small scale experiment yielding complex **6**, therefore additional peaks from starting material and internal standard.

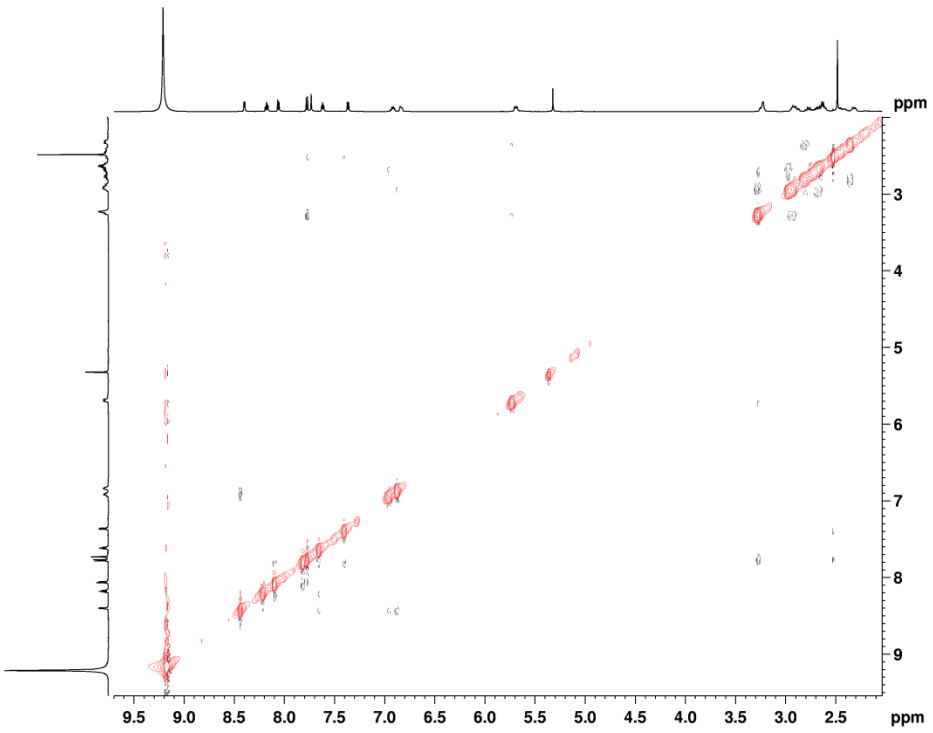

Figure 82: NOESY (600 MHz, CD_2Cl_2)of complex **6**.

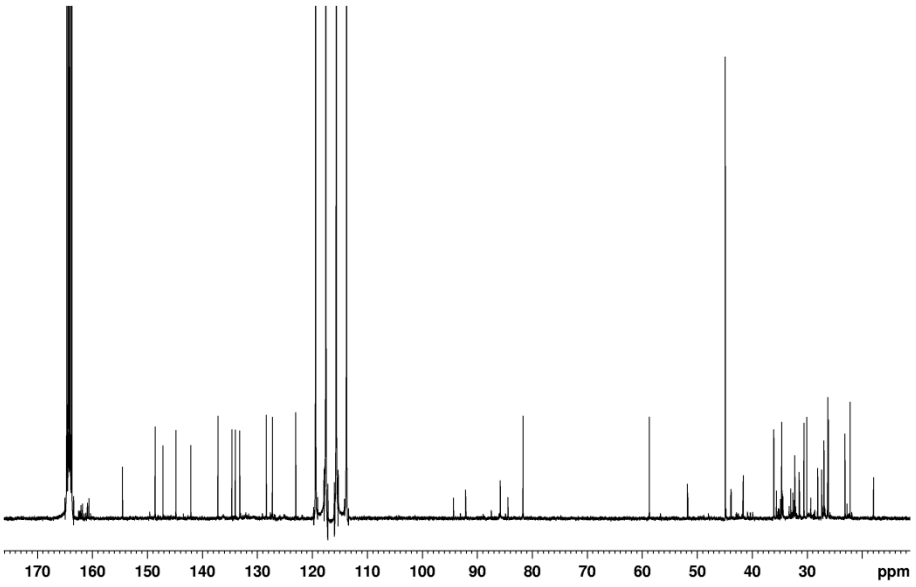

Figure 83: ^{13}C-NMR (151 MHz, TFA-*d*) obtained from small scale experiment yielding complex **6**, therefore additional peaks from starting material and internal standard.

6.6 Complex 7

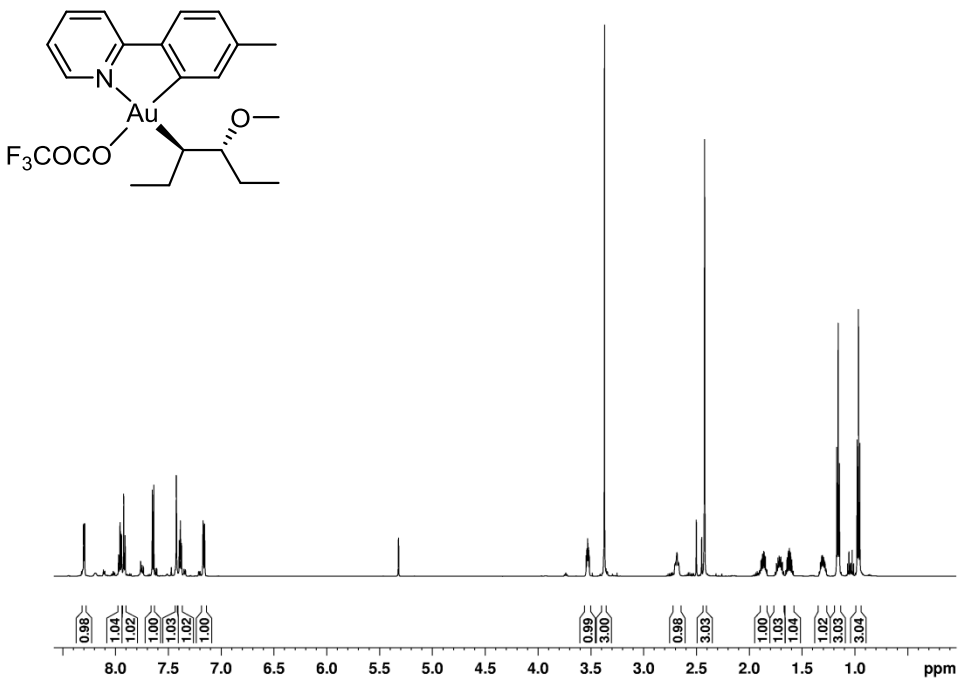

Figure 84: ^{1}H NMR (600 MHz, CD_2Cl_2) of compound **7**.

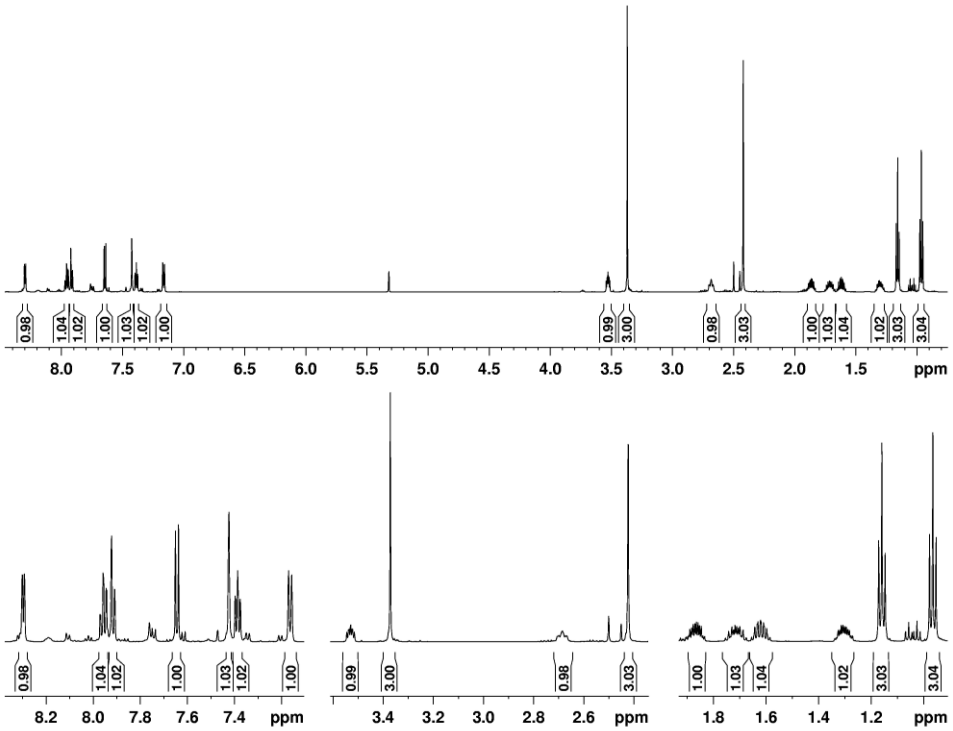

Figure 85: ^{1}H-NMR (600 MHz, CD_2Cl_2) of alkyl gold(III) complex **7**. Close-up views in the bottom.

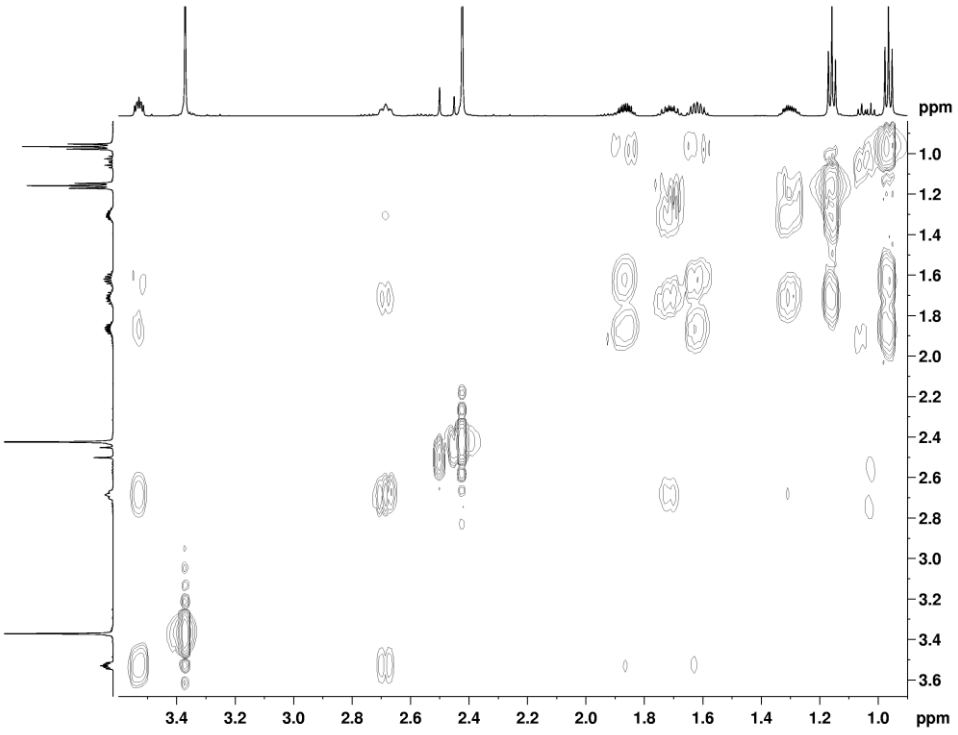

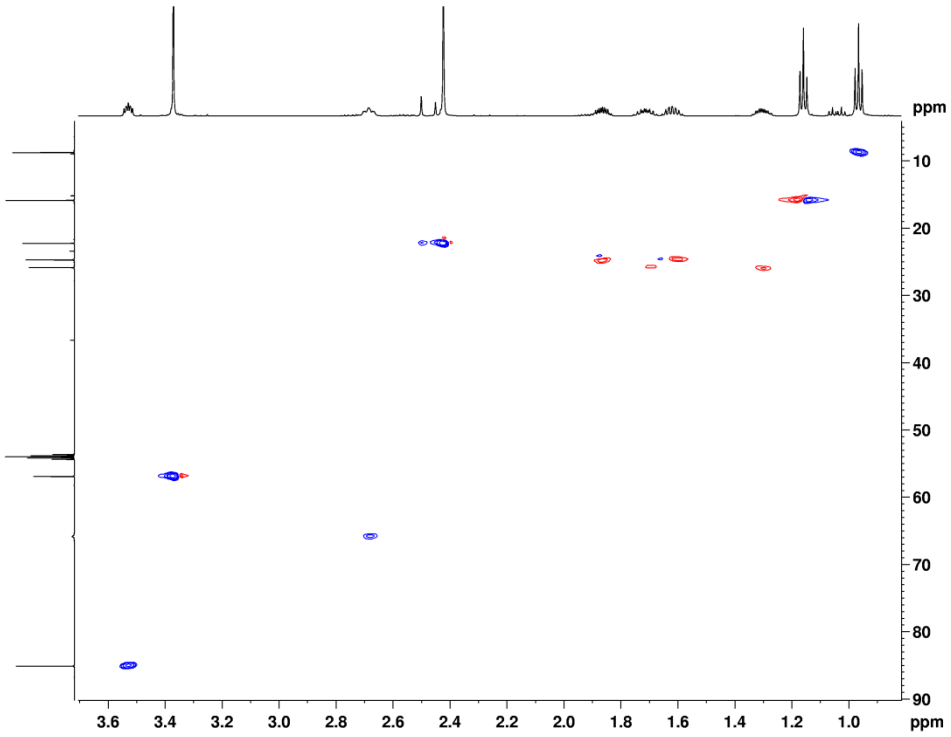

Figure 86: (600 MHz, CD_2Cl_2). Close-up view of COSY (top) and HSQC (bottom) of complex **7**.

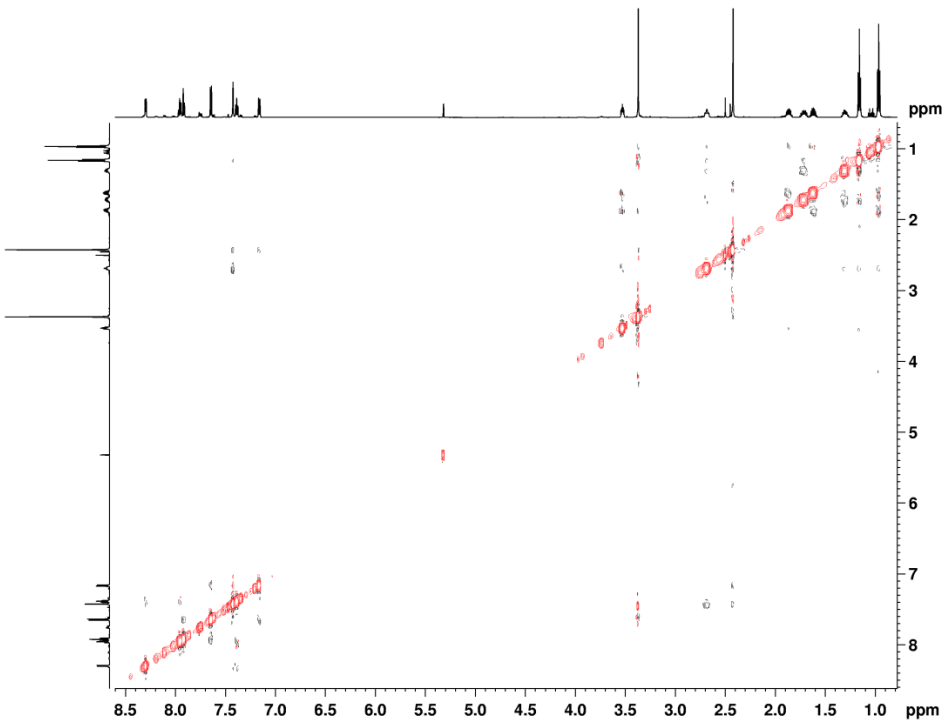

Figure 87: NOESY (600 MHz, CD_2Cl_2) of complex **7**.

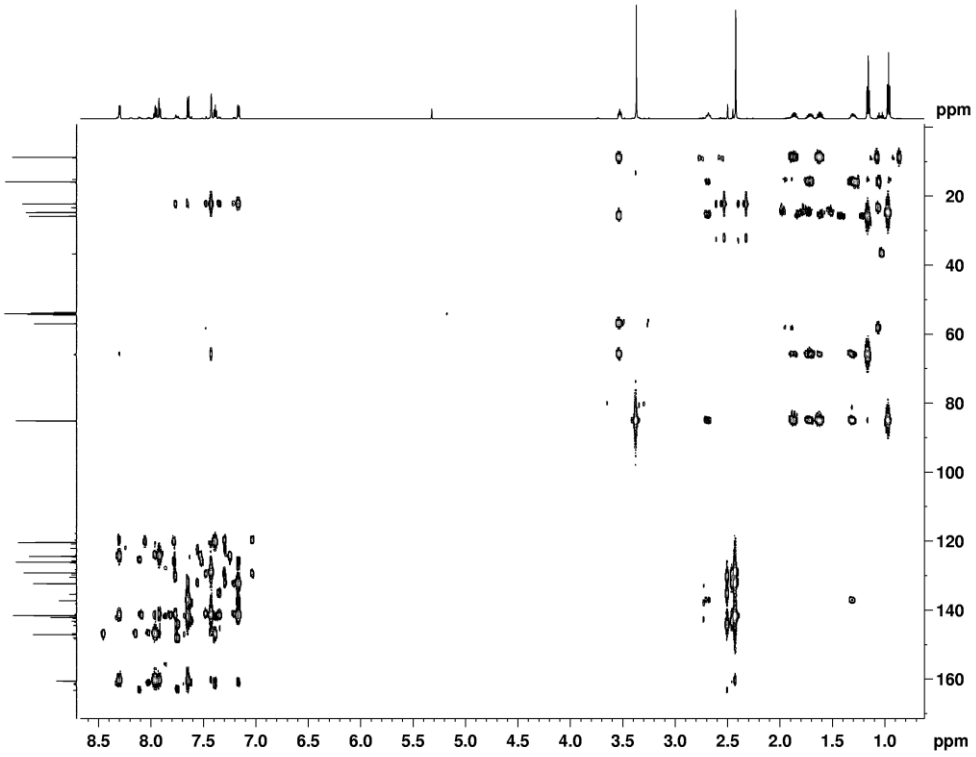

Figure 88: HMBC (600 MHz, CD_2Cl_2) of complex **7**.

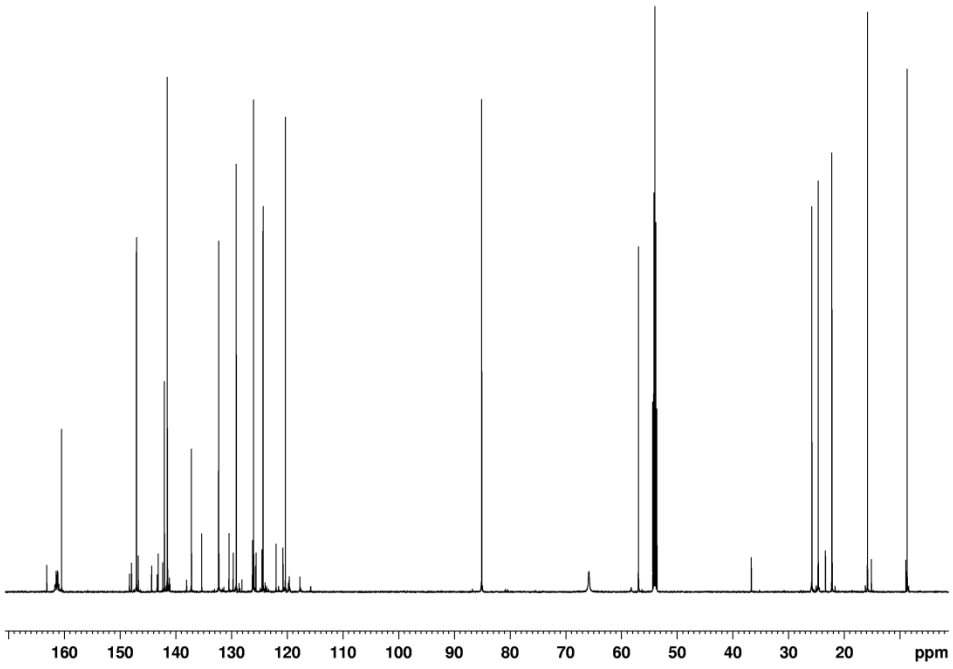

Figure 89: ^{13}C-NMR (151 MHz, CD_2Cl_2) of complex **7**.

6.7 Complex 8

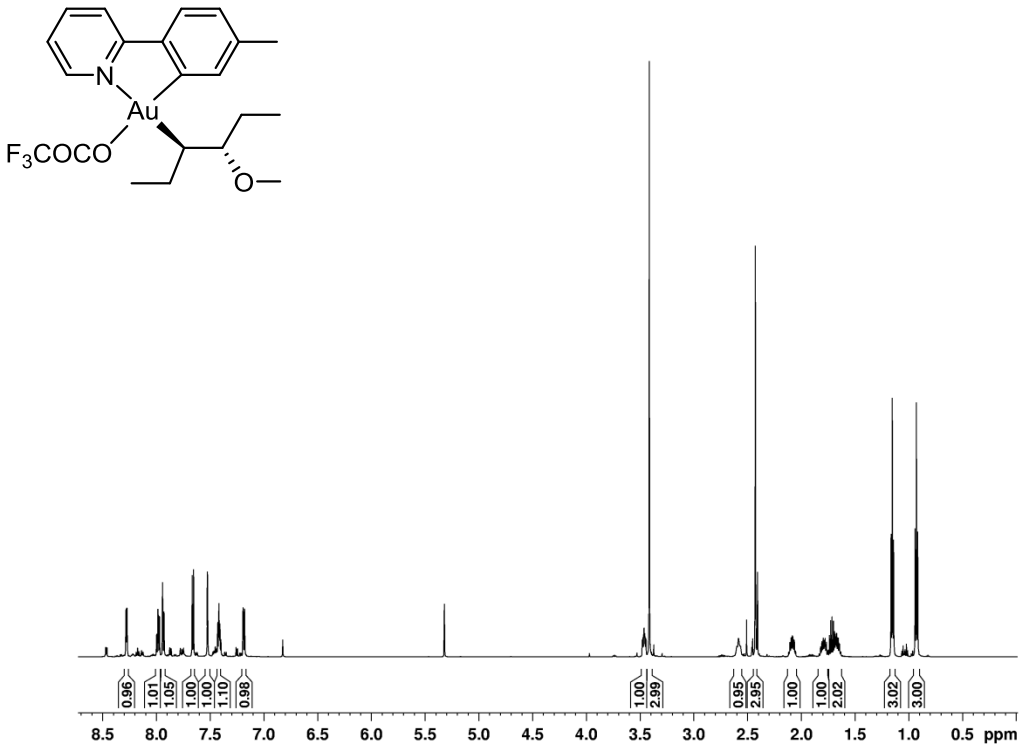

Figure 90: ^{1}H NMR (600 MHz, CD_2Cl_2) of compound **8**.

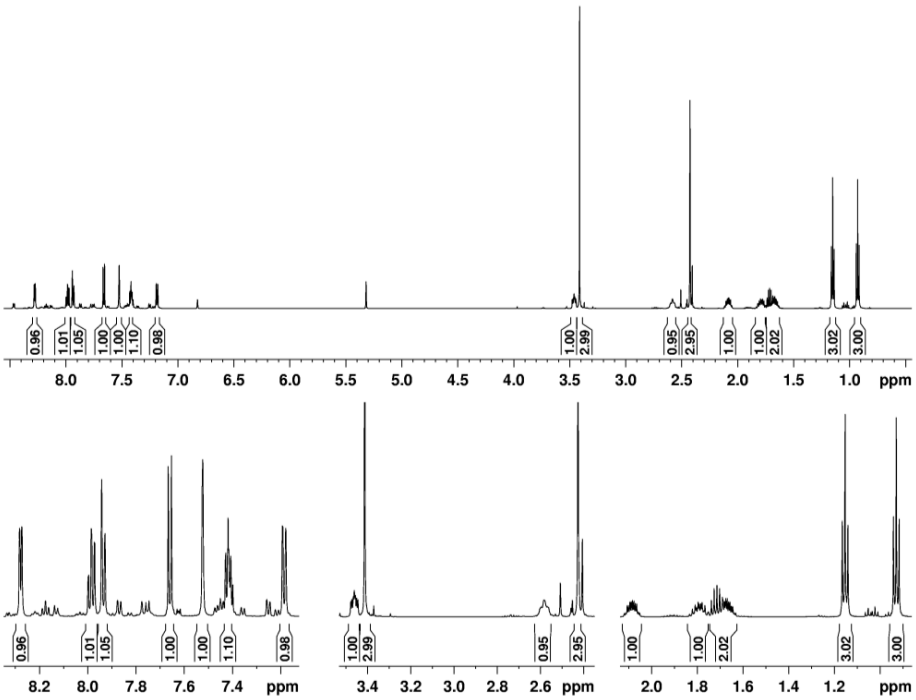

Figure 91: ^{1}H-NMR (600 MHz, CD_2Cl_2) of alkyl gold(III) complex **8**. Close-up views in the bottom.

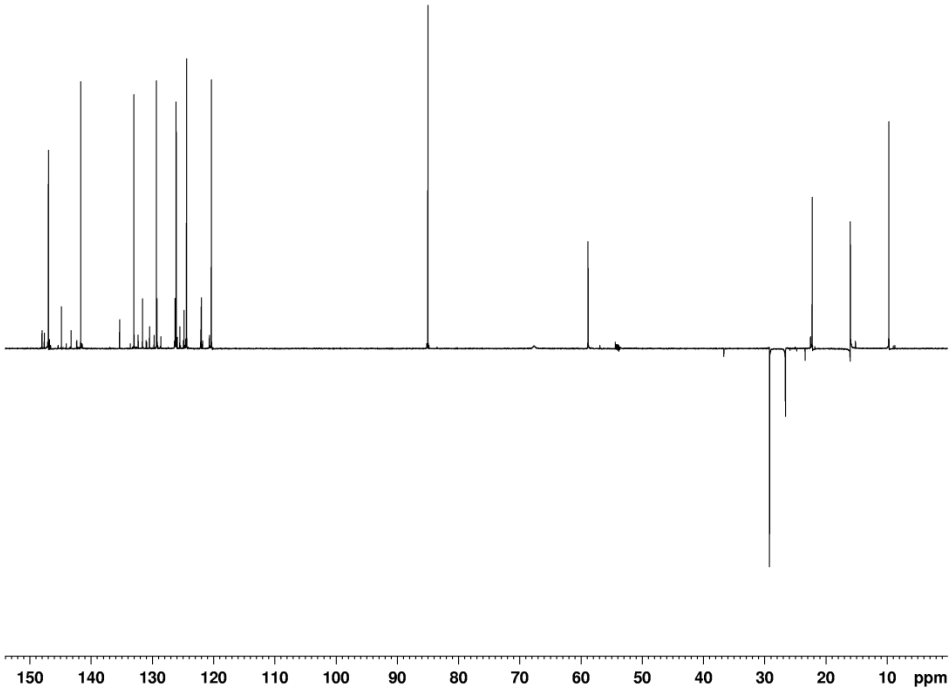

Figure 92: DEPT135 (151MHz, CD_2Cl_2) of alkyl gold(III) complex **8**.

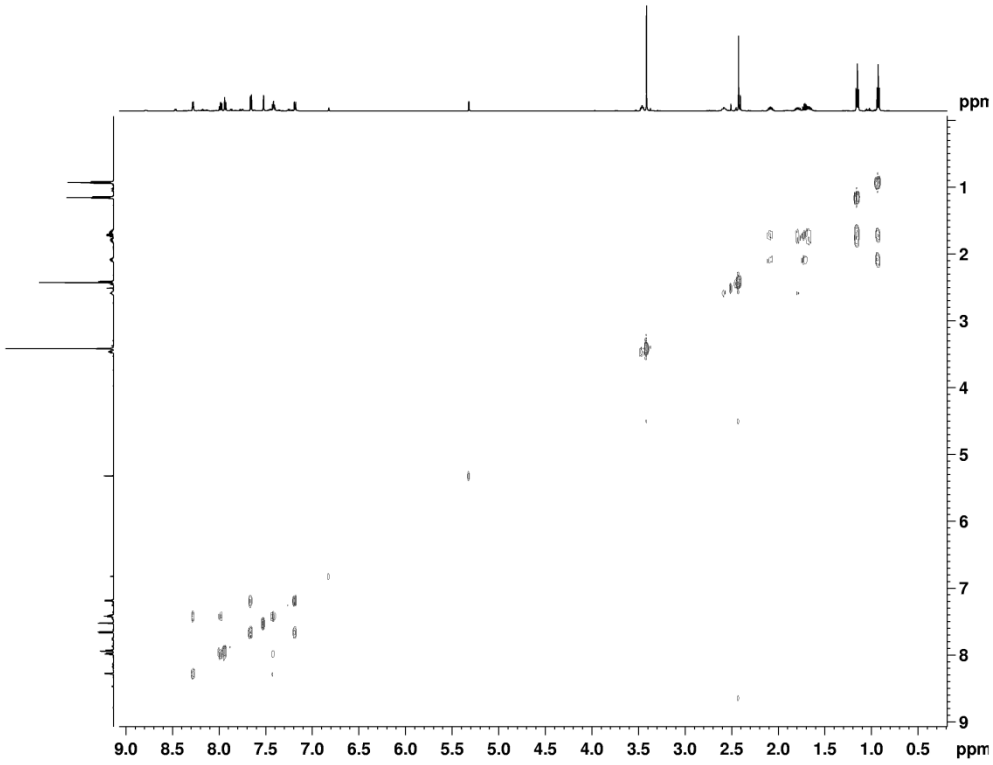

Figure 93: COSY (600 MHz, CD_2Cl_2)of complex **8**.

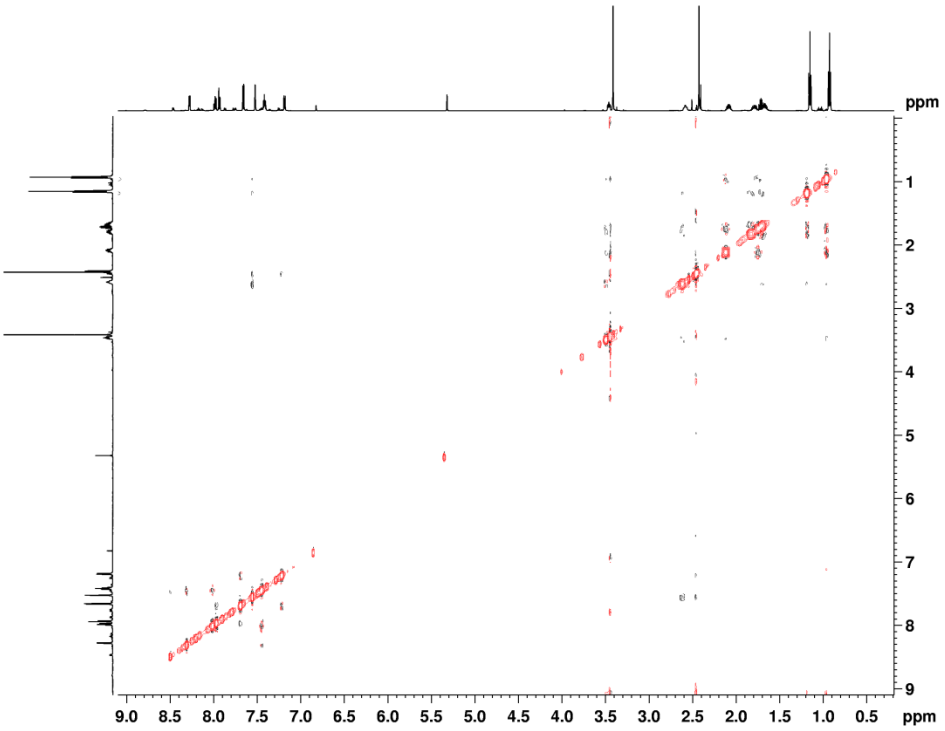

Figure 94: NOESY (600 MHz, CD_2Cl_2)of complex **8**.

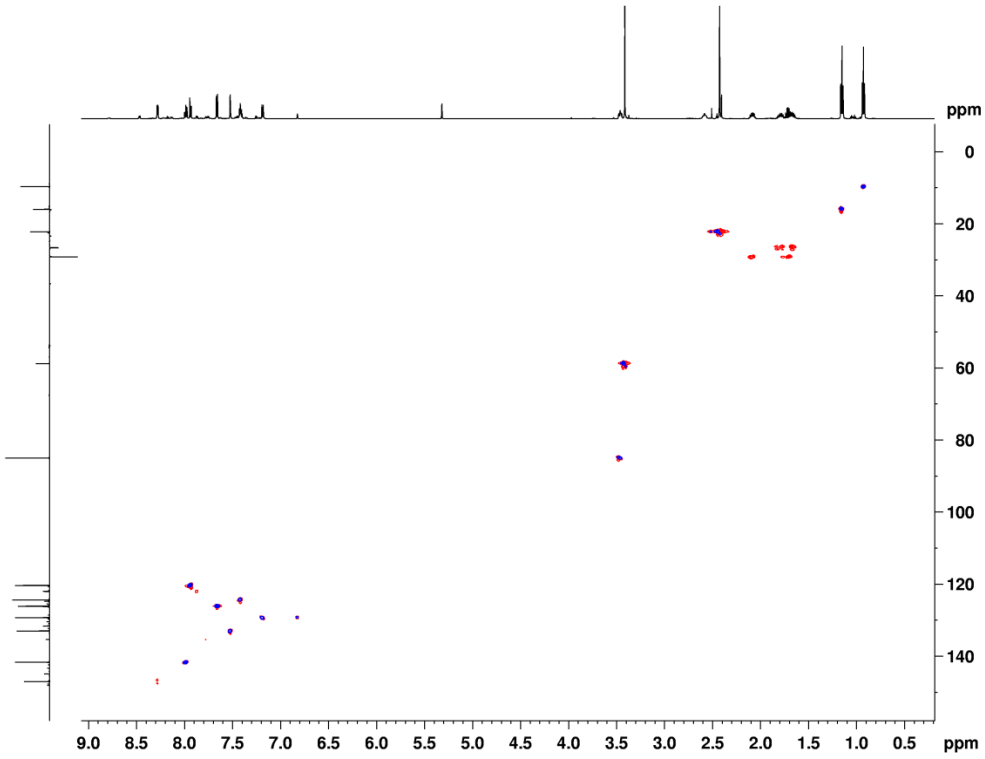

Figure 95: HSQC (600 MHz, CD_2Cl_2)of complex **8**.

6.8 Complex 9

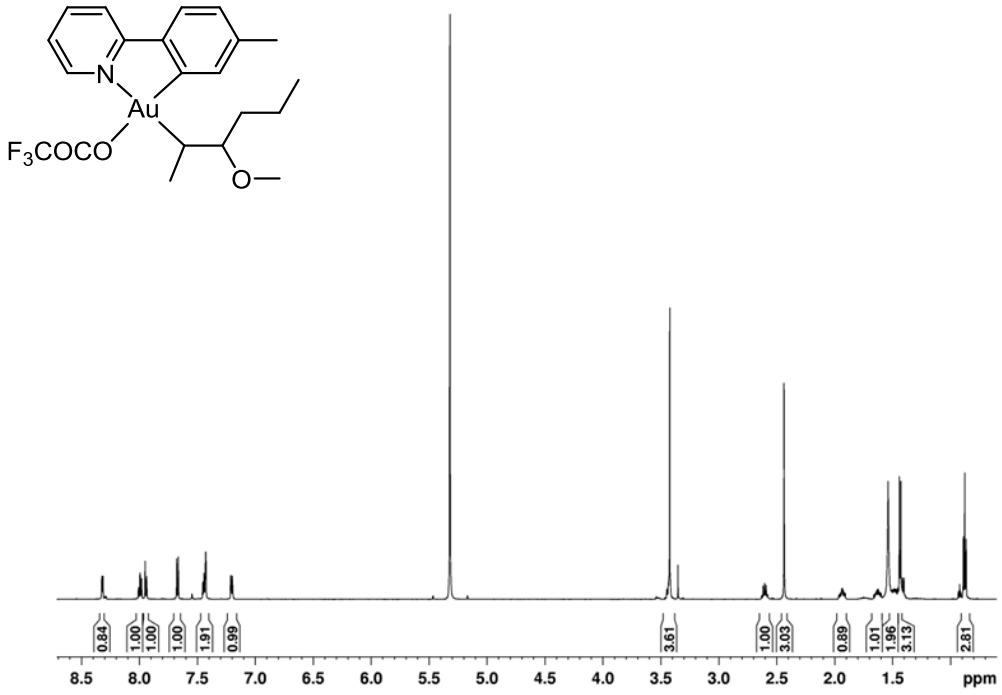

Figure 96: ^{1}H NMR (600 MHz, CD_2Cl_2) of **9**. The peak at 1.54 ppm is due to water.

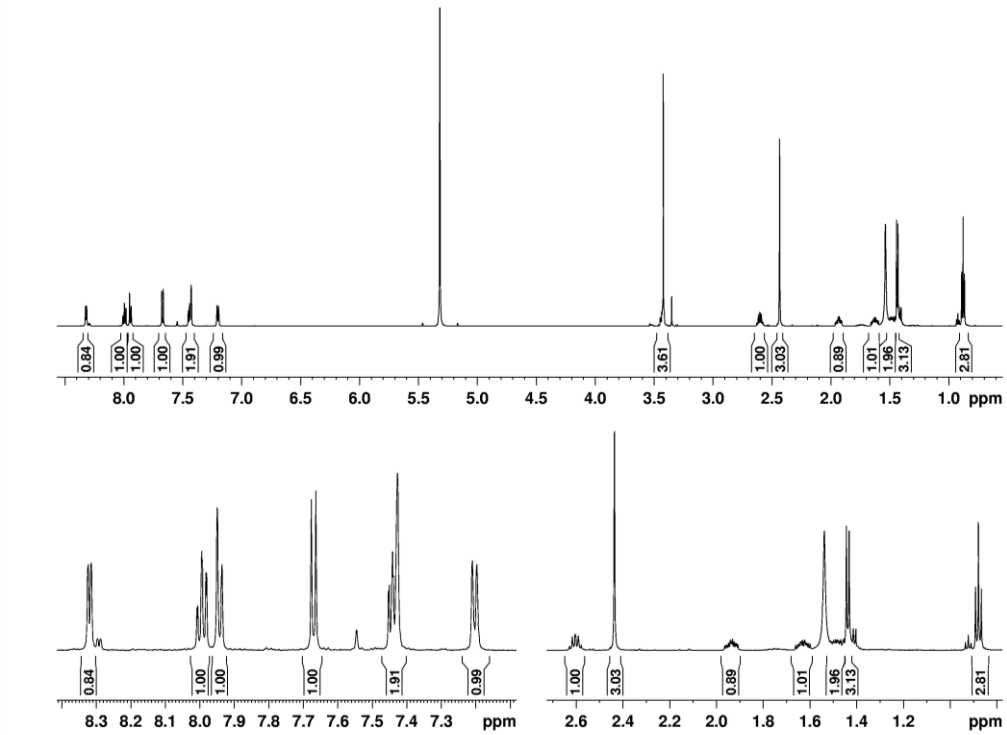

Figure 97: ^{1}H-NMR (600 MHz, CD_2Cl_2) of alkyl gold(III) complex **9**. Close-up views in the bottom. Peak at 1.5 ppm is due to water.

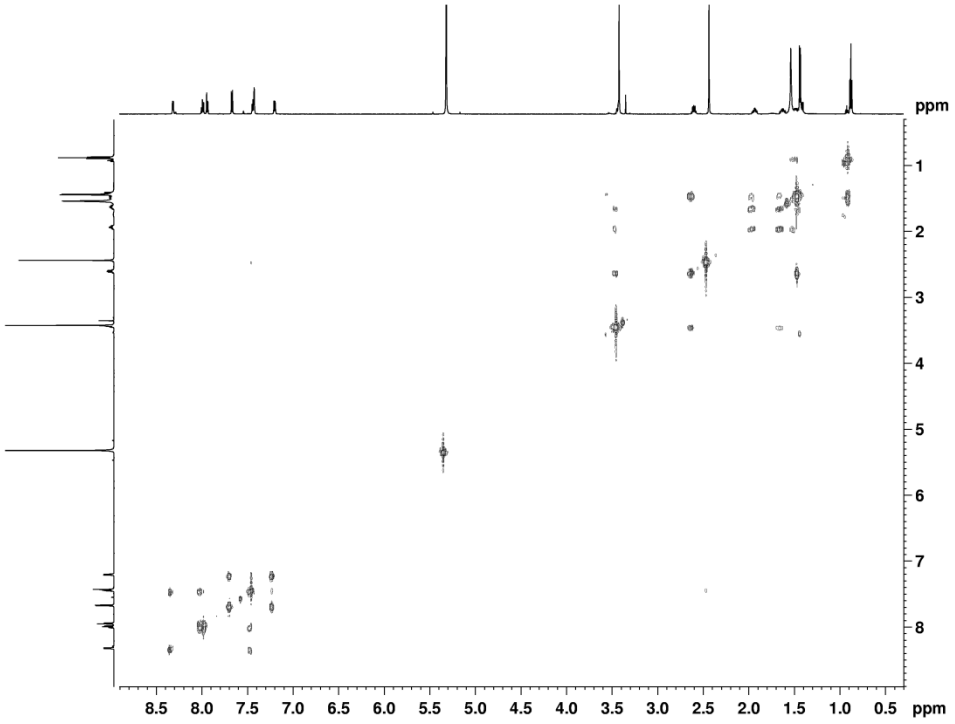

Figure 98: COSY (600 MHz, CD_2Cl_2) of alkyl gold(III) complex **9**.

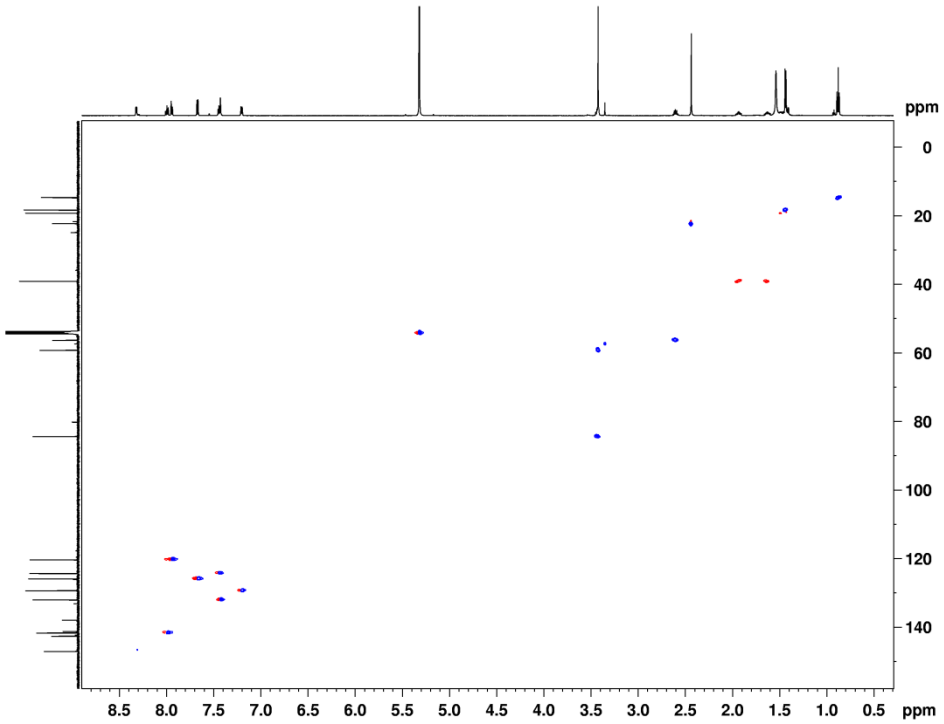

Figure 99: HSQC (600 MHz, CD_2Cl_2) of alkyl gold(III) complex **9**.

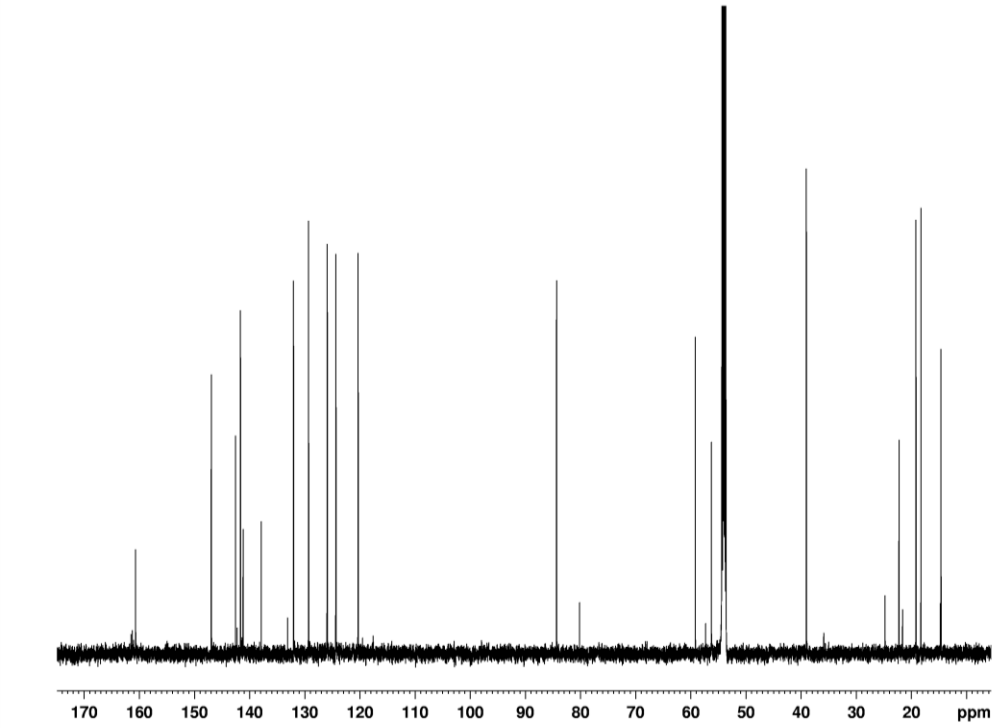

Figure 100: ^{13}C-NMR (151 MHz, CD_2Cl_2) of alkyl gold(III) complex **9**.

6.9 Complex 10

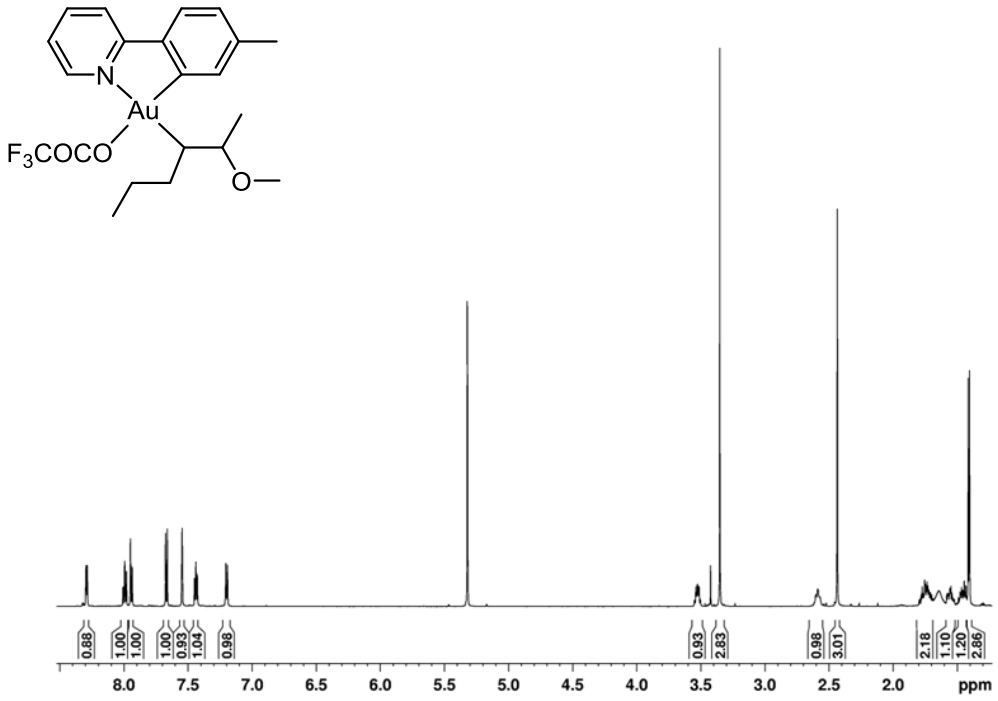

Figure 101: ^{1}H NMR (600 MHz, CD_2Cl_2) of **10**. The peak at 1.64 ppm is due to water.

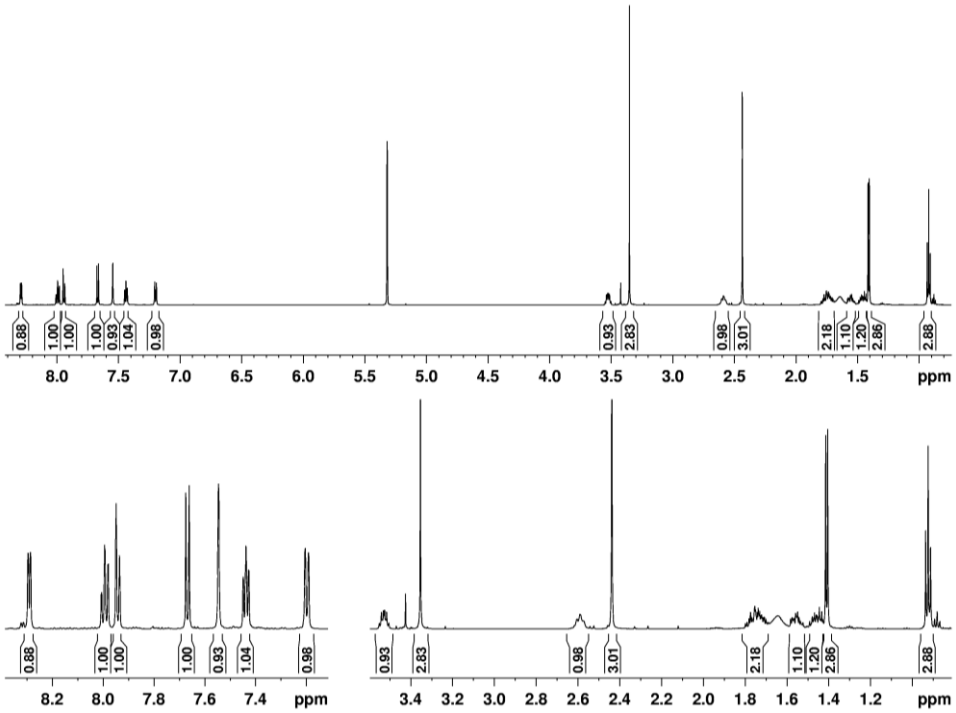

Figure 102: ^{1}H-NMR (600 MHz, CD_2Cl_2) of alkyl gold(III) complex **10**. Close-up views in the bottom. Peak at 1.6 ppm is due to water.

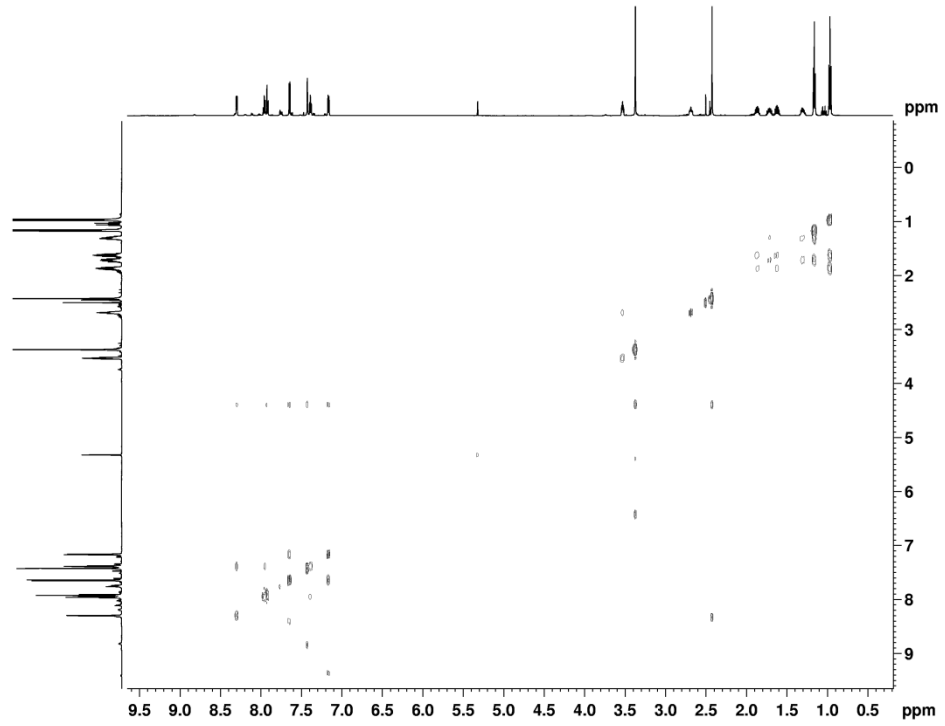

Figure 103: COSY (600 MHz, CD_2Cl_2) of alkyl gold(III) complex **10**.

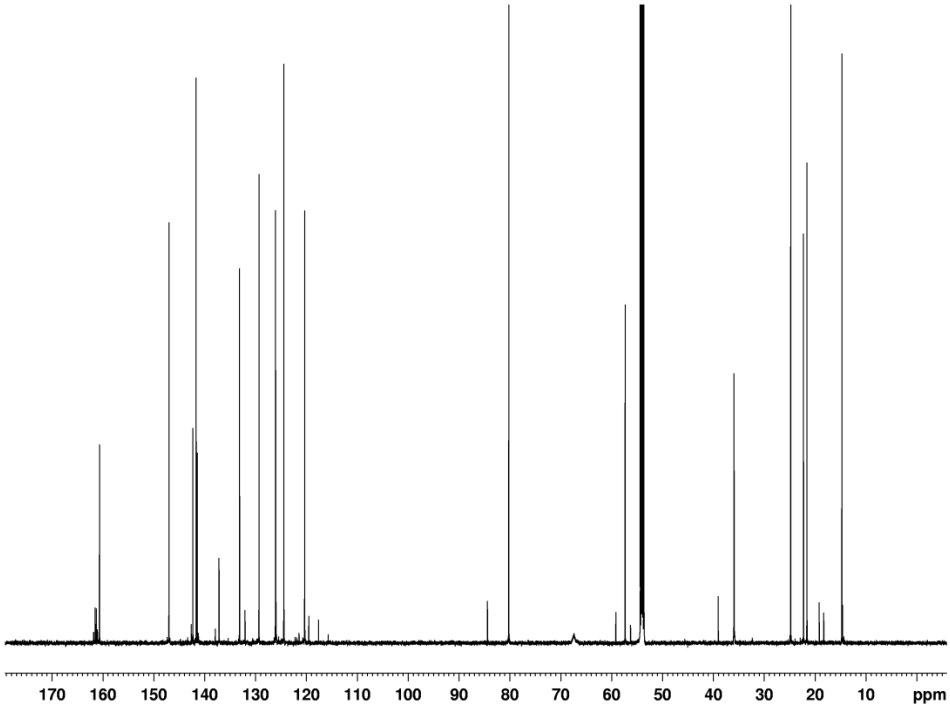

Figure 104: ^{13}C-NMR (151 MHz, CD_2Cl_2) of alkyl gold(III) complex **10**.

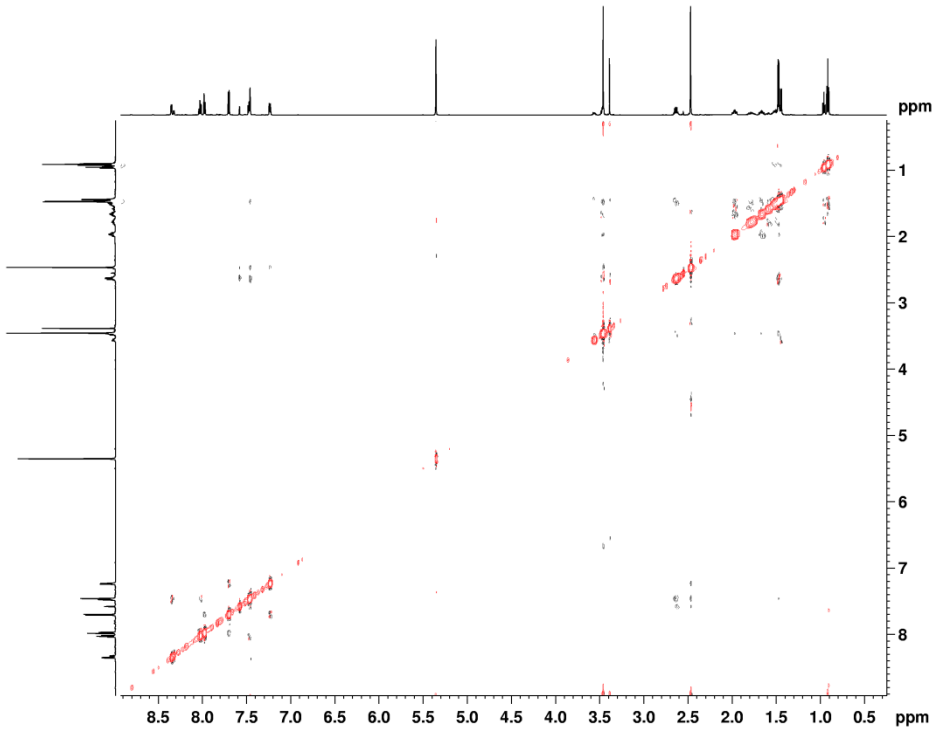

Figure 105: NOESY (600 MHz, CD_2Cl_2) of alkyl gold(III) complex **9** and **10**.

6.10 Complex 11

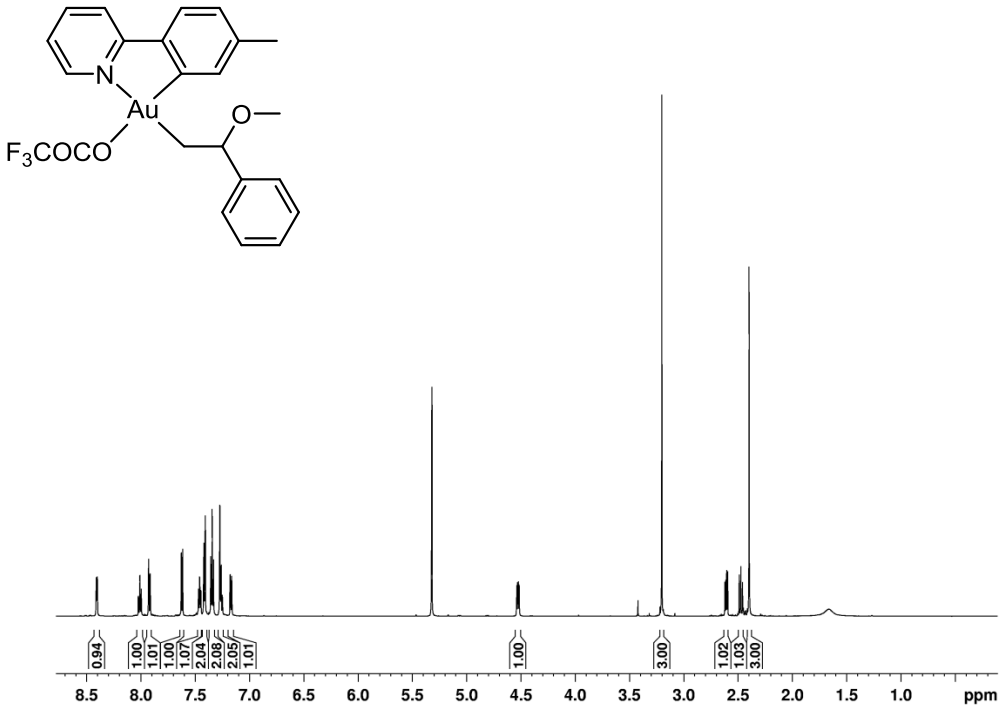

Figure 106: ^{1}H NMR (600 MHz, CD_2Cl_2) of compound **11**.

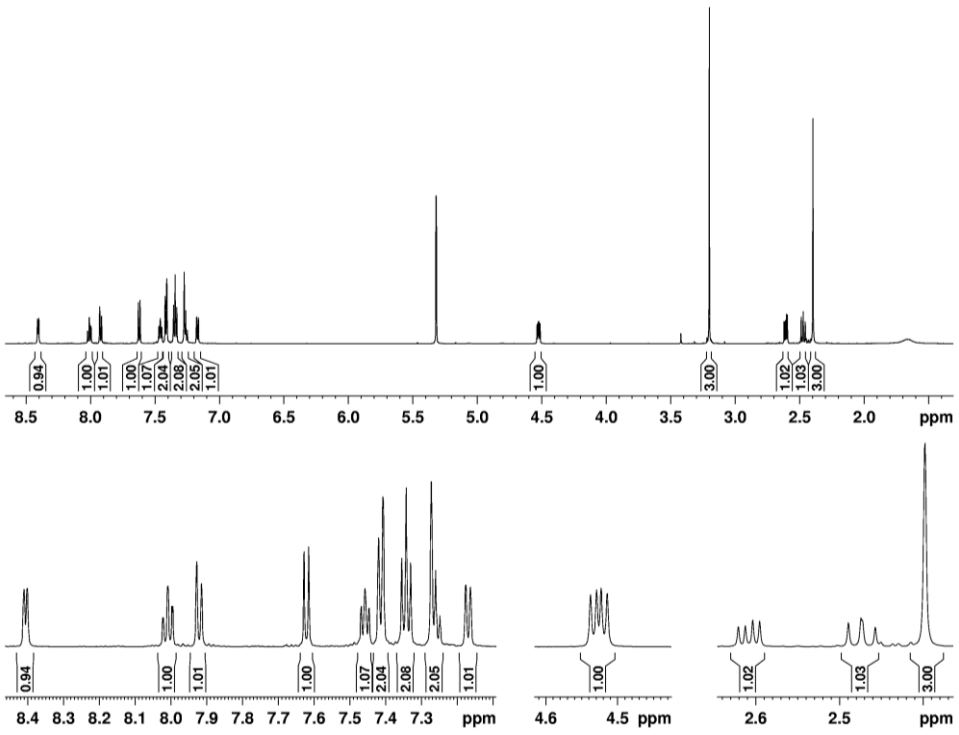

Figure 107: ^{1}H NMR (600 MHz, CD_2Cl_2) of compound **11**. Close-up view in the bottom.

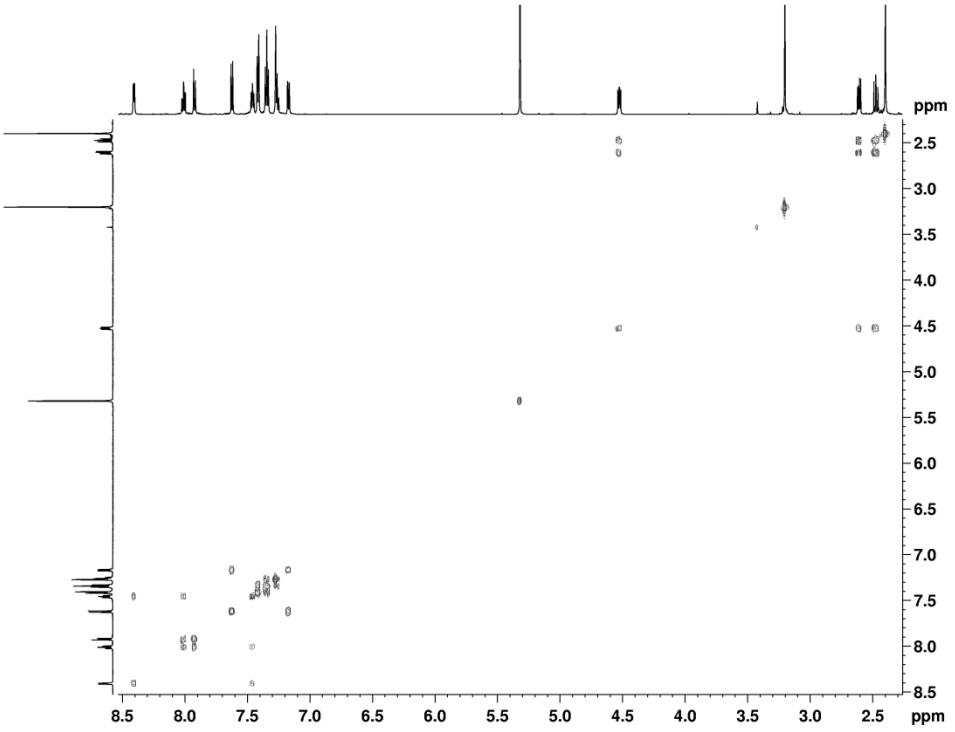

Figure 108: COSY (600 MHz, CD_2Cl_2) of compound **11**.

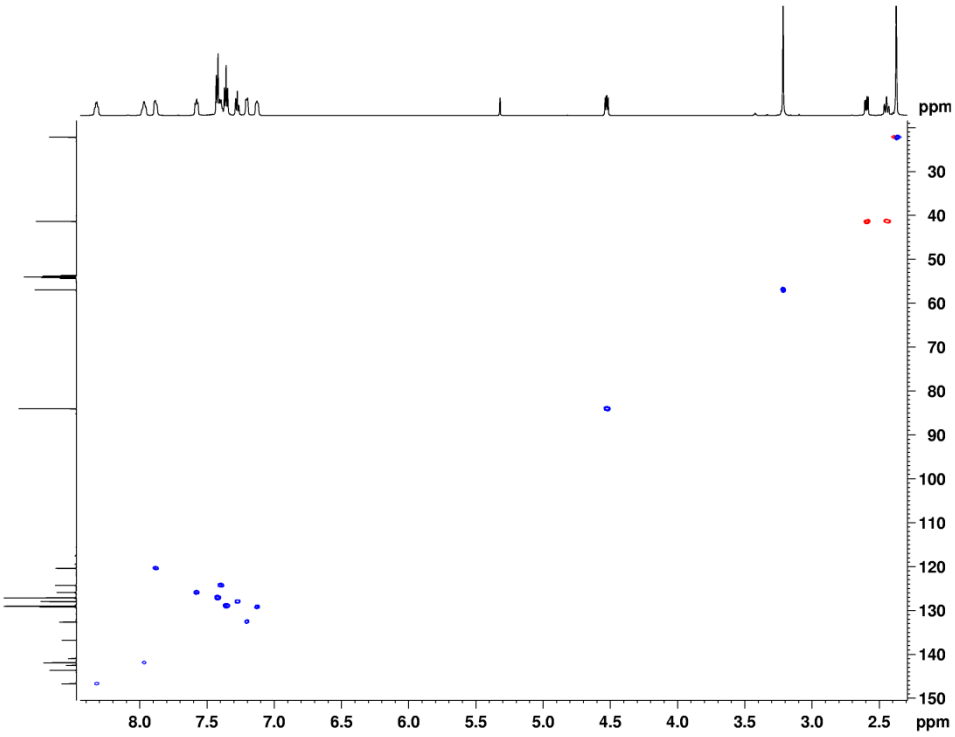

Figure 109: HSQC (600 MHz, CD_2Cl_2) of compound **11**.

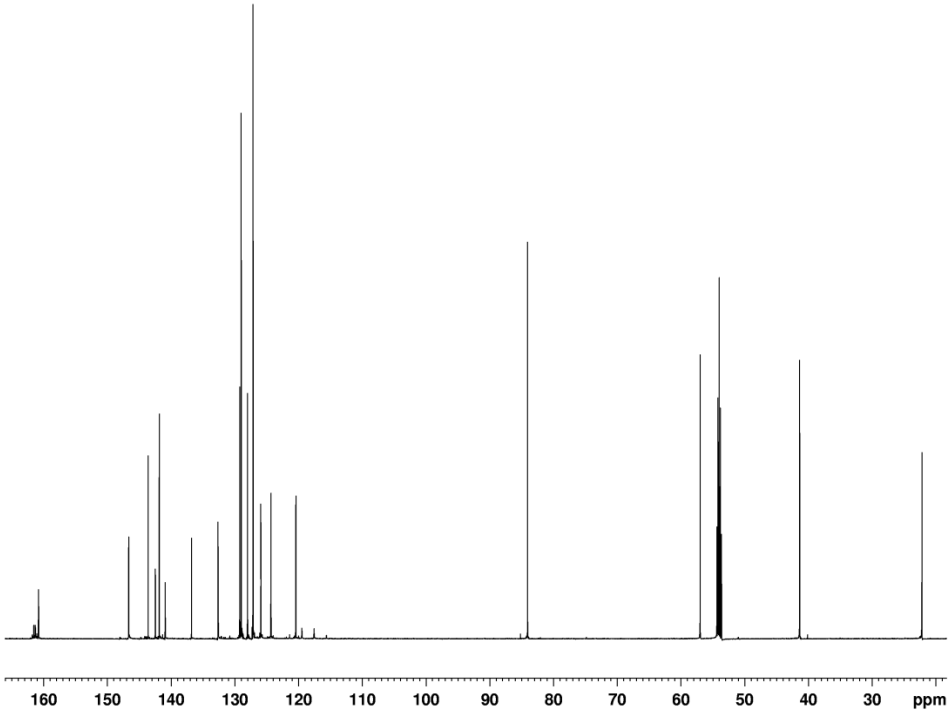

Figure 110: ^{13}C-NMR (151 MHz, CD_2Cl_2) of compound **11**.

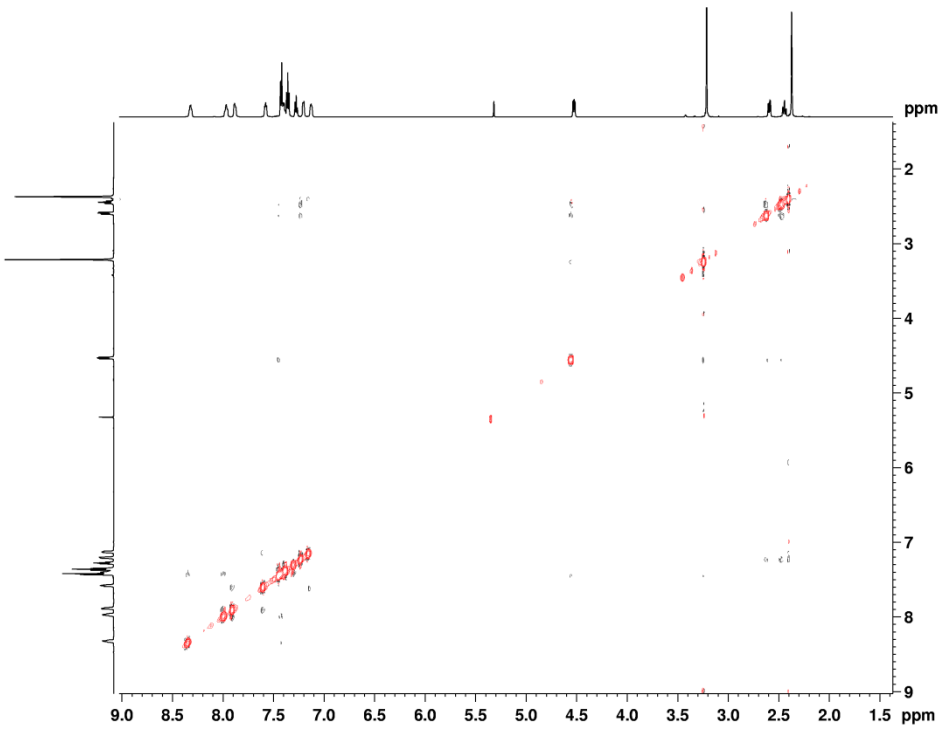

Figure 111: NOESY (600 MHz, CD_2Cl_2) of compound **11**.

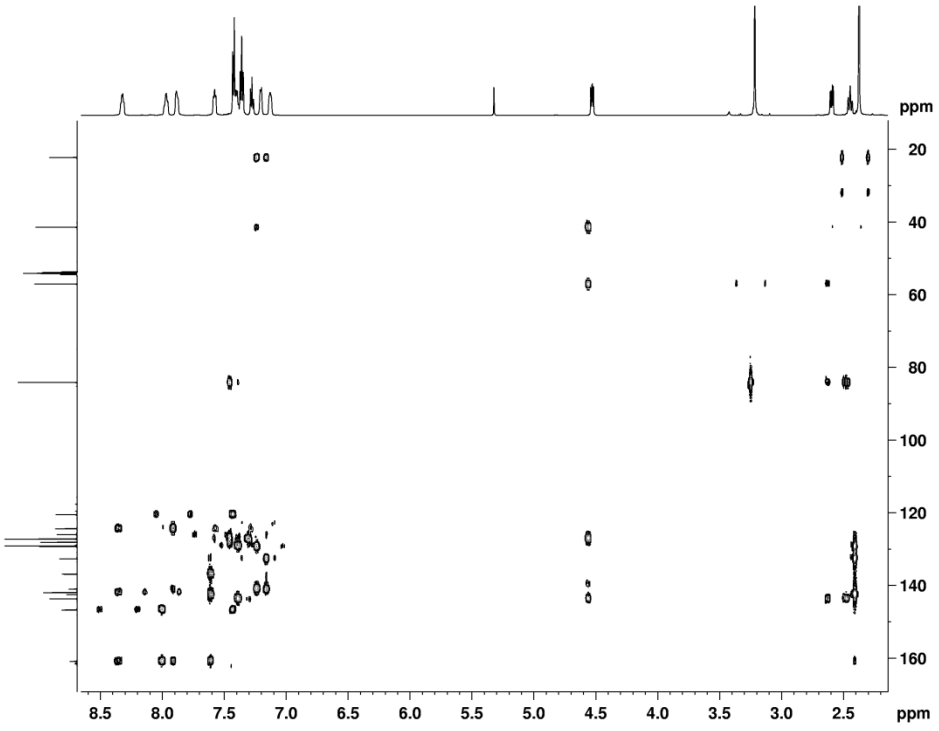

Figure 112: HMBC (600 MHz, CD_2Cl_2) of compound **11**.

6.11 Complex 13

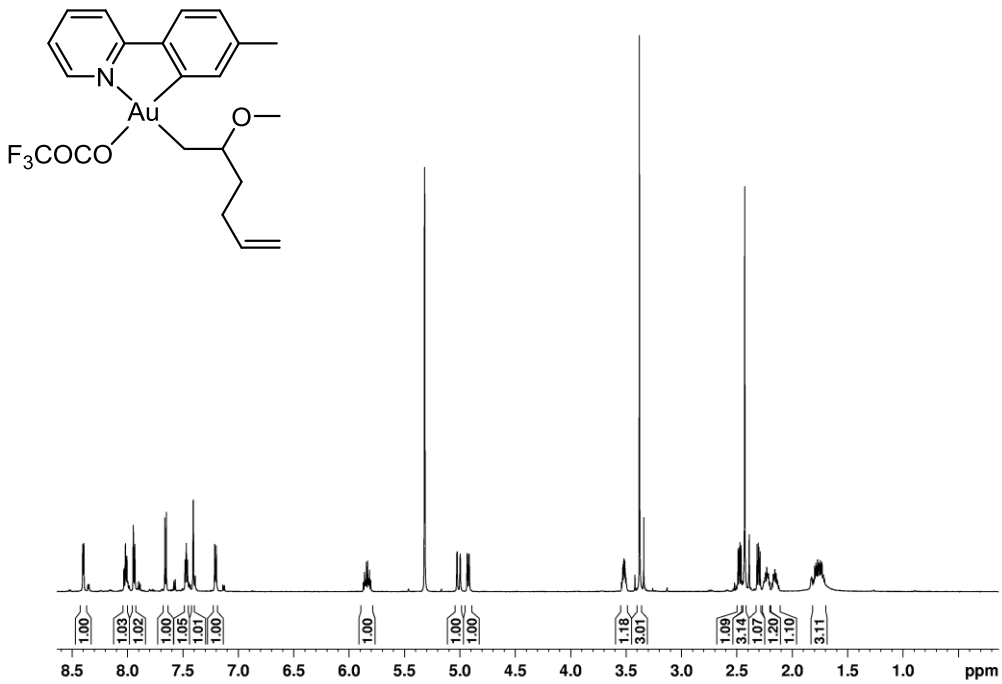

Figure 113: ^{1}H NMR (600 MHz, CD_2Cl_2) of compound **13**.

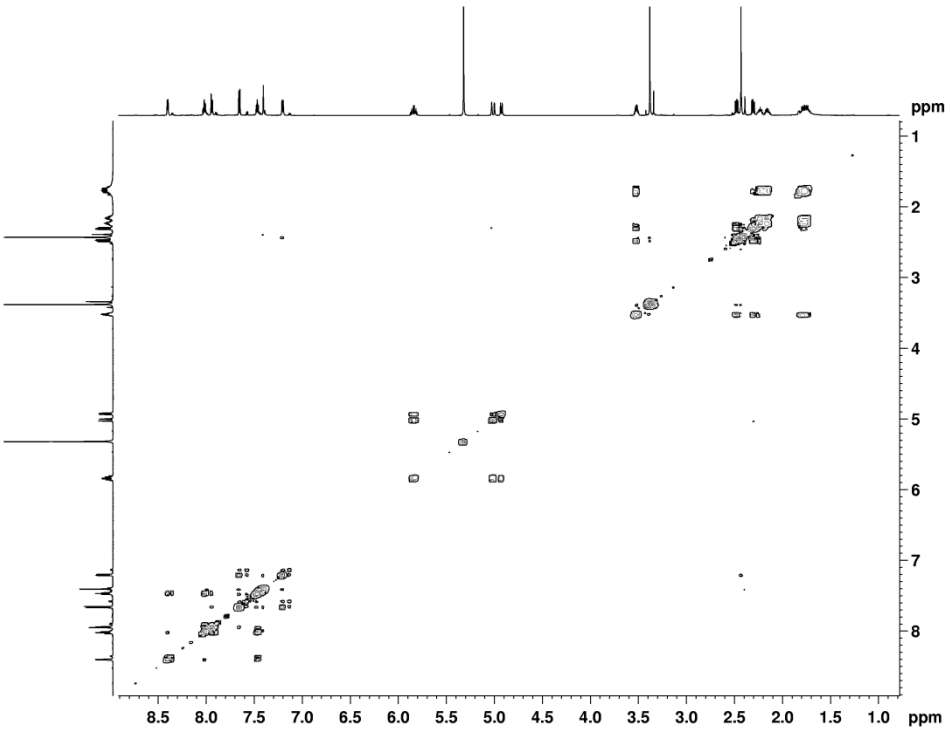

Figure 114: COSY (600 MHz, CD_2Cl_2) of compound **13**.

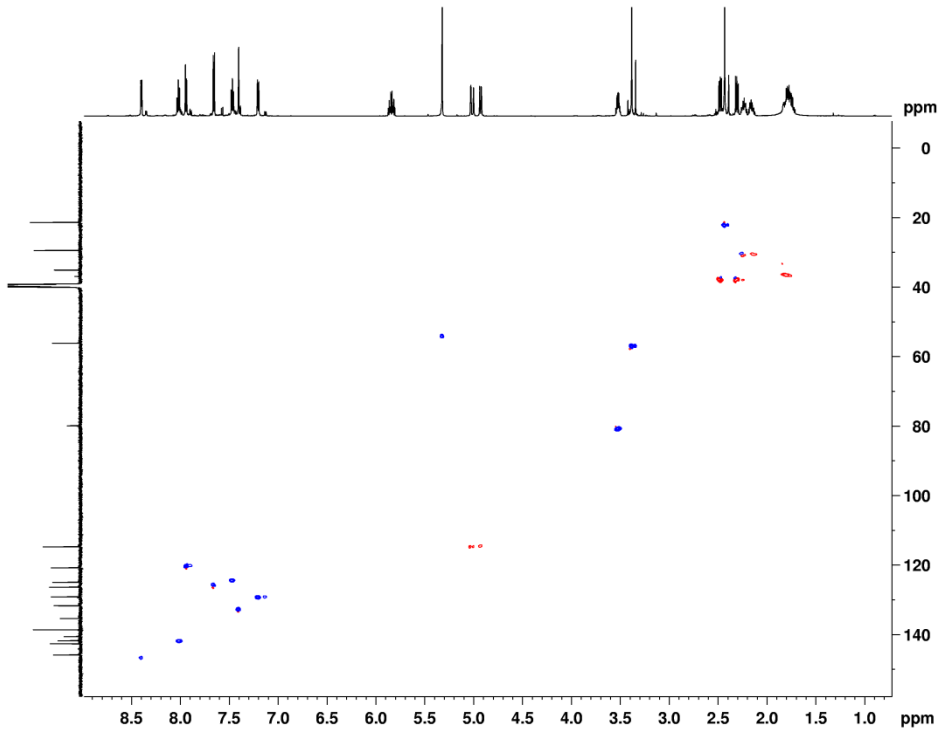

Figure 115: HSQC (600 MHz, CD_2Cl_2) of compound **13**.

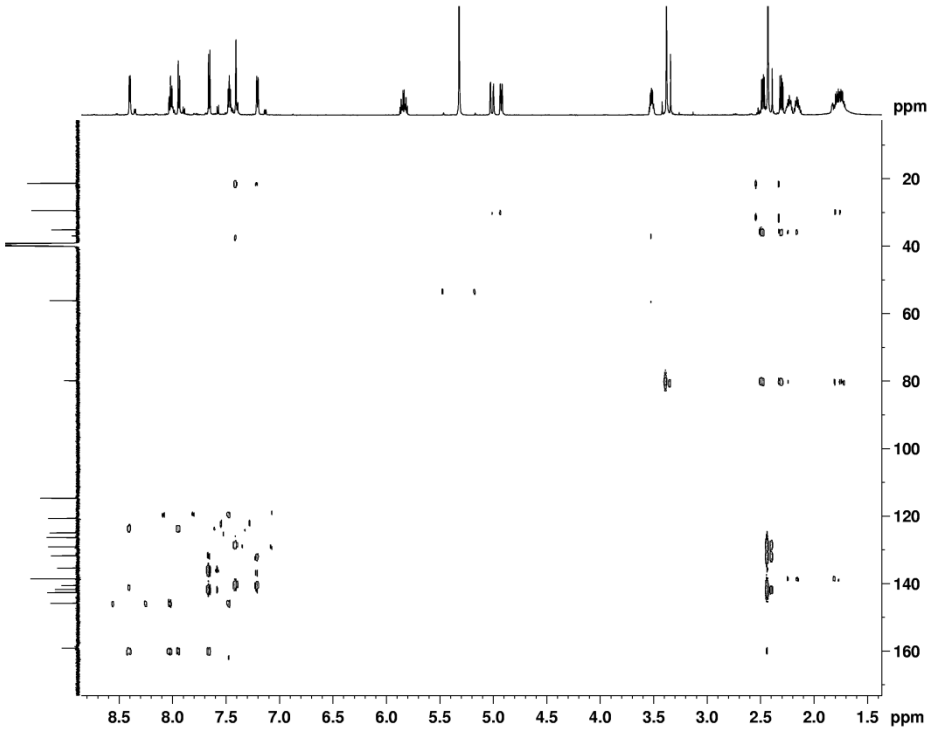

Figure 116: HMBC (600 MHz, CD_2Cl_2) of compound **13**.

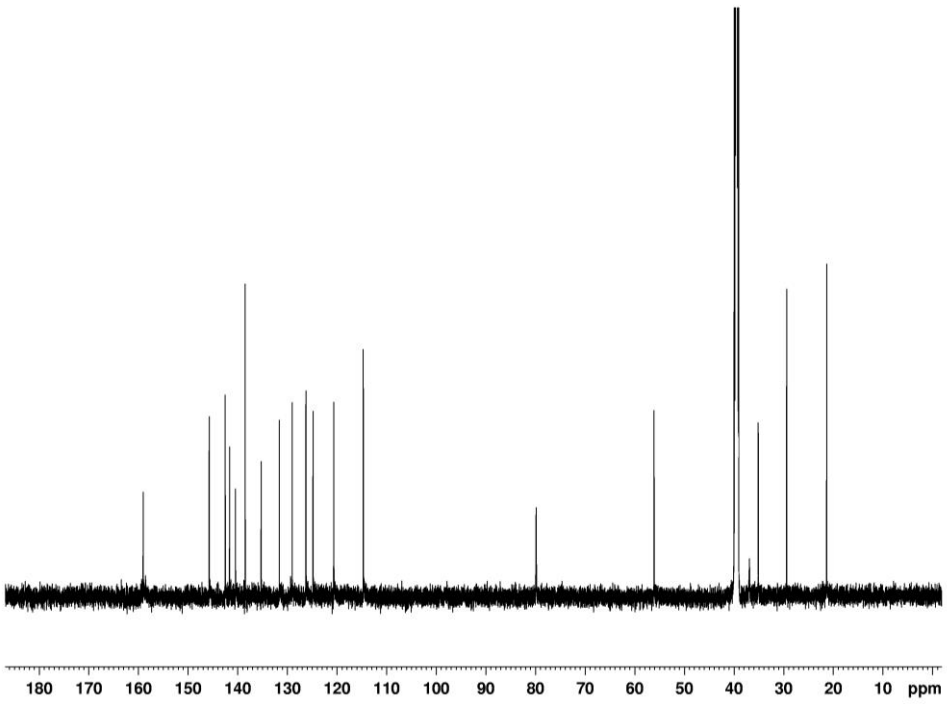

Figure 117: ^{13}C (151 MHz, CD_2Cl_2) of compound **13**.

6.12 Complex 14

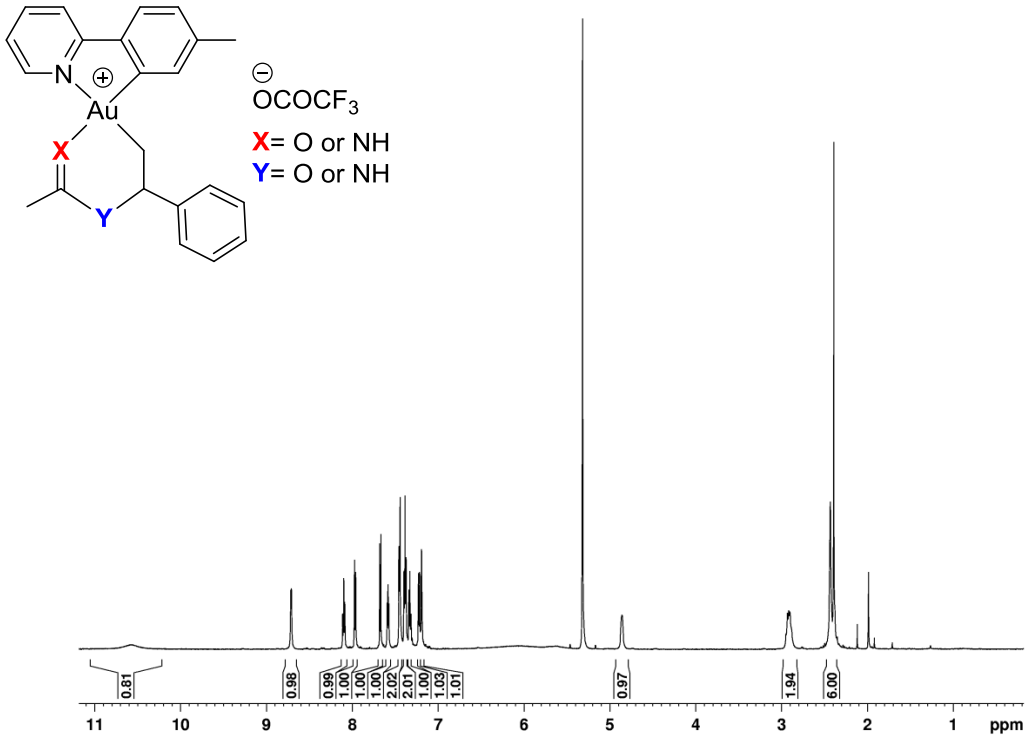

Figure 118: ^{1}H NMR (600 MHz, CD_2Cl_2) of compound **14**.

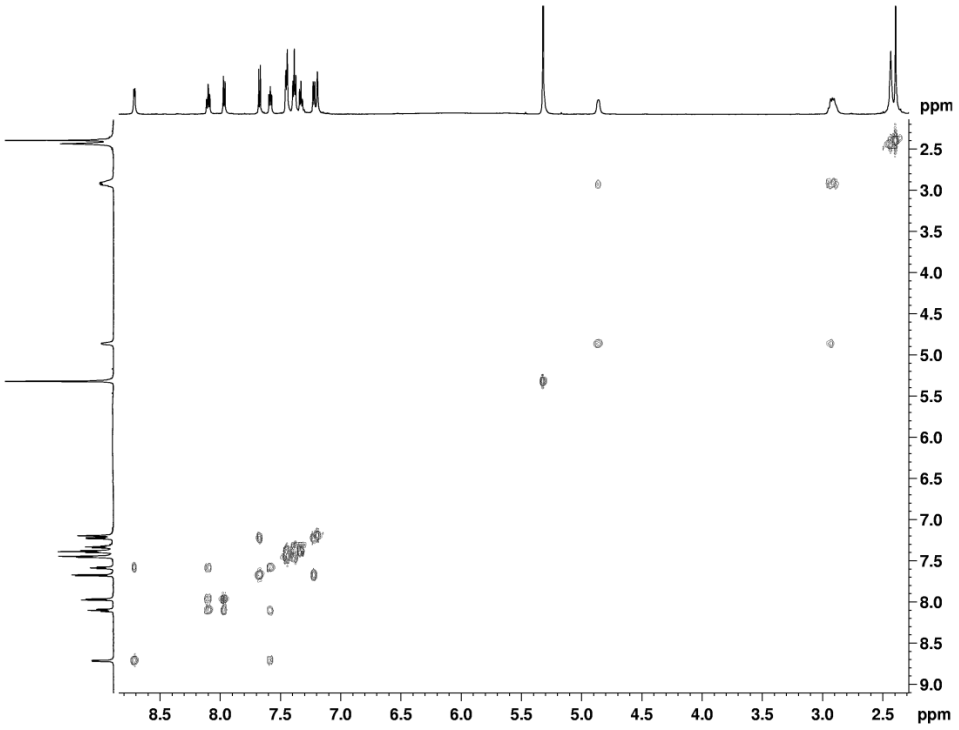

Figure 119: COSY (600 MHz, CD_2Cl_2) of compound **14**.

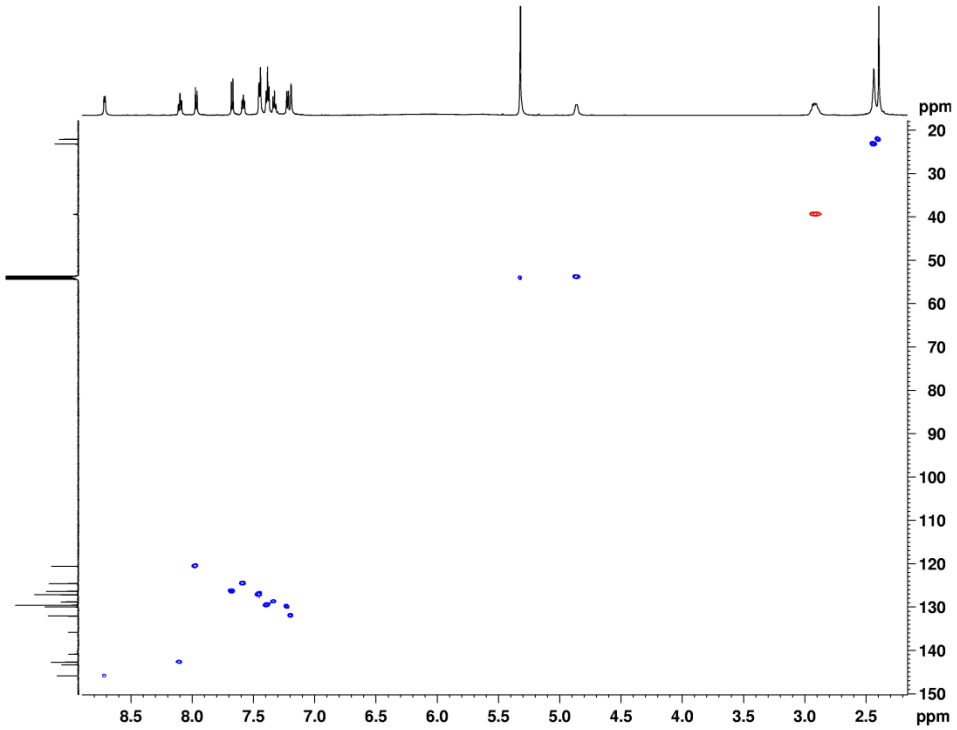

Figure 120: HSQC (600 MHz, CD_2Cl_2) of compound **14**.

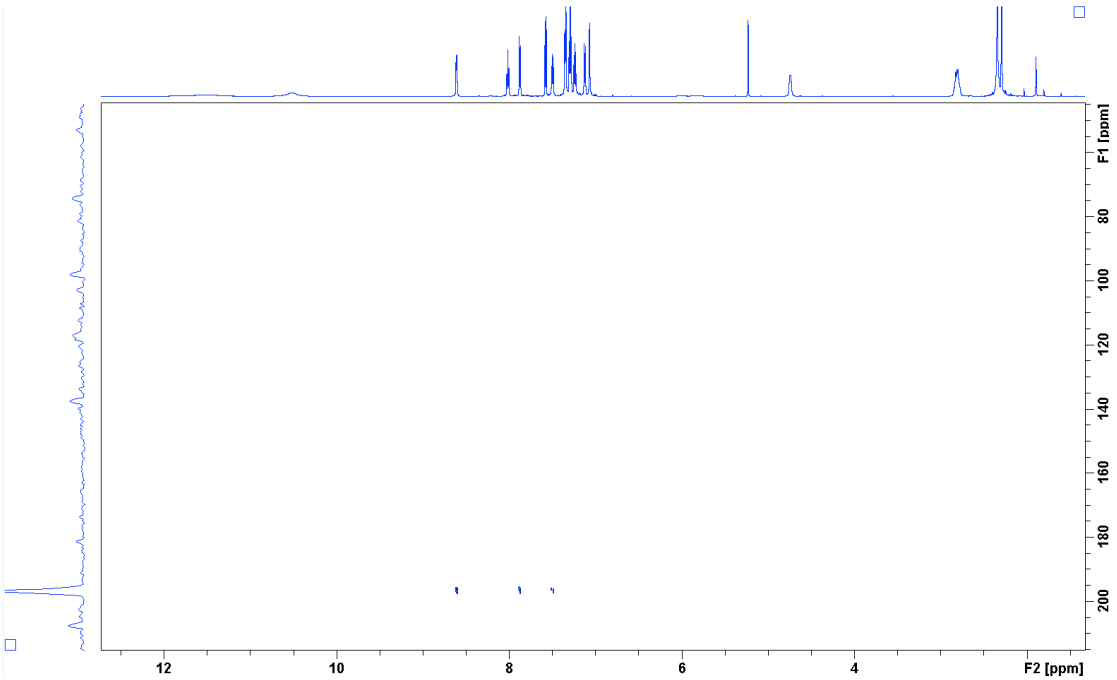

Figure 121: ^{1}H-^{15}N-HMBC of compound **14**.

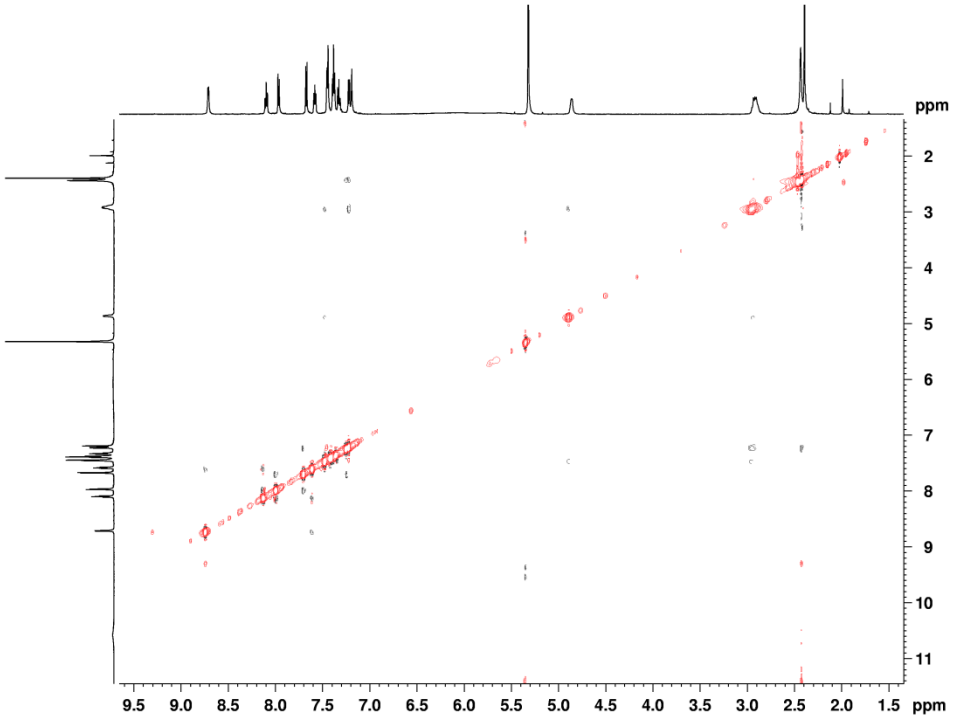

Figure 122: NOESY (600 MHz, CD_2Cl_2) of compound **14**.

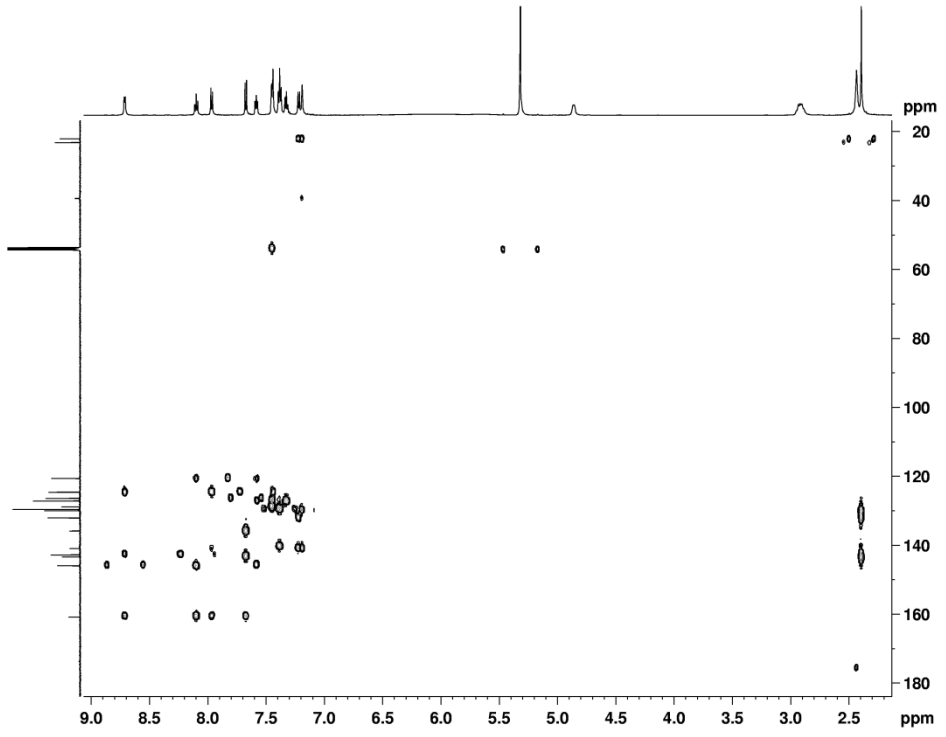

Figure 123: HMBC (600 MHz, CD_2Cl_2) of compound **14**.

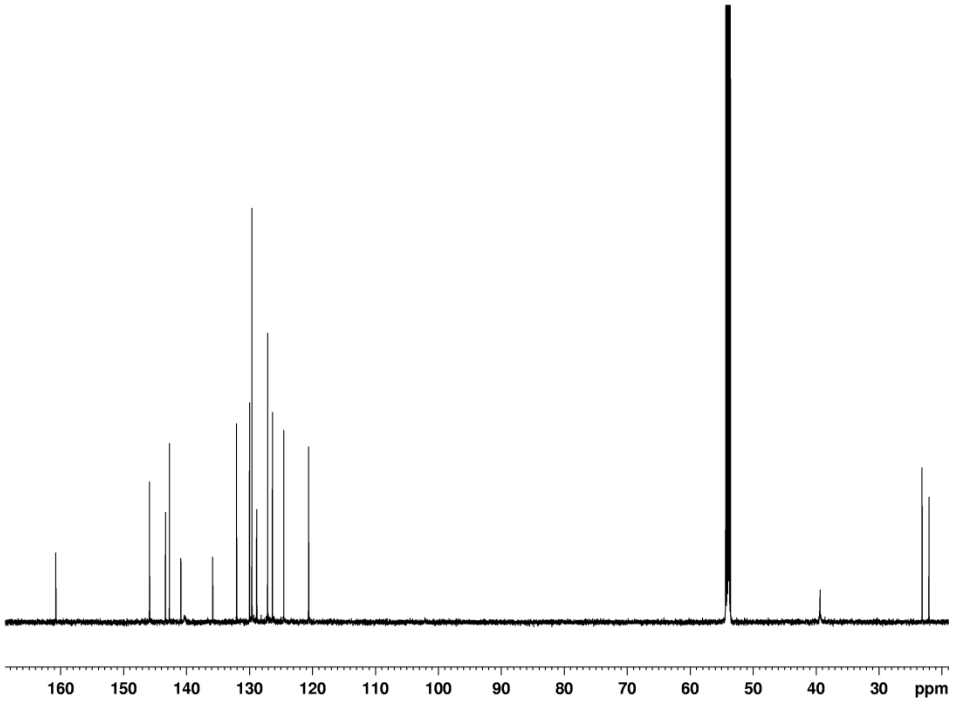

Figure 124: ^{13}C-NMR (151 MHz, CD_2Cl_2) of compound **14**.

Complex 7

Table 1 Crystal data and structure refinement for FI-85new_a_pl.

Identification code	FI-85new_a_pl
Empirical formula	$C_{21}H_{25}AuF_3NO_3$
Formula weight	593.39
Temperature/K	100.15
Crystal system	triclinic
Space group	P-1
a/Å	7.6029(7)
b/Å	10.2775(9)
c/Å	13.8220(12)
α/°	78.224(2)
β/°	86.720(2)
γ/°	77.086(2)
Volume/Å^3	1030.48(16)
Z	2
ϱ_{calc}g/cm^3	1.912
μ/mm^{-1}	7.187
F(000)	576.0
Crystal size/mm^3	0.31 × 0.28 × 0.06
Radiation	MoKα (λ = 0.71073)
2Θ range for data collection/°	4.62 to 56.596
Index ranges	-10 ≤ h ≤ 10, -13 ≤ k ≤ 13, -18 ≤ l ≤ 18
Reflections collected	14141
Independent reflections	5103 [R_{int} = 0.0265, R_{sigma} = 0.0268]
Data/restraints/parameters	5103/0/266
Goodness-of-fit on F^2	1.263
Final R indexes [I>=2σ (I)]	R_1 = 0.0172, wR_2 = 0.0474
Final R indexes [all data]	R_1 = 0.0189, wR_2 = 0.0579
Largest diff. peak/hole / e Å^{-3}	0.80/-1.67

Complex 8

Table 1 Crystal data and structure refinement for FI-91-ignoretwin_a_pl.

Identification code	FI-91-ignoretwin_a_pl
Empirical formula	$C_{21}H_{25}AuF_3NO_3$
Formula weight	593.39
Temperature/K	100.15
Crystal system	monoclinic
Space group	$P2_1/c$
a/Å	7.4994(5)
b/Å	30.2042(18)
c/Å	9.5331(6)
α/°	90
β/°	99.9490(10)
γ/°	90
Volume/Å^3	2126.9(2)
Z	4
ϱ_{calc}g/cm^3	1.853
μ/mm^{-1}	6.964
F(000)	1152.0
Crystal size/mm^3	0.20 × 0.16 × 0.15
Radiation	MoKα (λ = 0.71073)
2Θ range for data collection/°	5.678 to 61.162
Index ranges	-10 ≤ h ≤ 10, -36 ≤ k ≤ 43, -13 ≤ l ≤ 13
Reflections collected	21881
Independent reflections	6491 [R_{int} = 0.0222, R_{sigma} = 0.0218]
Data/restraints/parameters	6491/6/266
Goodness-of-fit on F^2	1.615
Final R indexes [I>=2σ (I)]	R_1 = 0.0508, wR_2 = 0.1101
Final R indexes [all data]	R_1 = 0.0523, wR_2 = 0.1105
Largest diff. peak/hole / e Å^{-3}	3.08/-4.31

Complex 9

Table 1 Crystal data and structure refinement for FI-083_a_pl.

Identification code	FI-083_a_pl
Empirical formula	$C_{21}H_{25}AuF_3NO_3$
Formula weight	593.39
Temperature/K	100.15
Crystal system	monoclinic
Space group	C2/c
a/Å	31.585(3)
b/Å	10.7421(12)
c/Å	13.1516(14)
α/°	90
β/°	109.409(2)
γ/°	90
Volume/Å^3	4208.6(8)
Z	8
ρ_{calc}g/cm^3	1.873
μ/mm^{-1}	7.039
F(000)	2304.0
Crystal size/mm^3	0.37 × 0.17 × 0.12
Radiation	MoKα (λ = 0.71073)
2Θ range for data collection/°	4.904 to 63.336
Index ranges	-46 ≤ h ≤ 41, -15 ≤ k ≤ 15, -19 ≤ l ≤ 19
Reflections collected	33617
Independent reflections	7074 [R_{int} = 0.0358, R_{sigma} = 0.0290]
Data/restraints/parameters	7074/0/266
Goodness-of-fit on F^2	1.177
Final R indexes [I>=2σ (I)]	R_1 = 0.0257, wR_2 = 0.0620
Final R indexes [all data]	R_1 = 0.0351, wR_2 = 0.0724
Largest diff. peak/hole / e Å^{-3}	1.76/-1.63

Complex 10

Table 1 Crystal data and structure refinement for FI-083tiny_a_pl.

Identification code	FI-083tiny_a_pl
Empirical formula	$C_{21}H_{25}AuF_3NO_3$
Formula weight	593.39
Temperature/K	100.15
Crystal system	triclinic
Space group	P-1
a/Å	8.6722(9)
b/Å	10.9879(11)
c/Å	12.6673(13)
α/°	114.020(3)
β/°	102.946(3)
γ/°	94.562(3)
Volume/Å^3	1054.56(19)
Z	2
ϱ_{calc}g/cm^3	1.869
μ/mm^{-1}	7.023
F(000)	576.0
Crystal size/mm^3	0.06 × 0.04 × 0.03
Radiation	MoKα (λ = 0.71073)
2Θ range for data collection/°	4.91 to 54.354
Index ranges	-11 ≤ h ≤ 11, -14 ≤ k ≤ 14, -16 ≤ l ≤ 16
Reflections collected	12911
Independent reflections	4670 [R_{int} = 0.0409, R_{sigma} = 0.0547]
Data/restraints/parameters	4670/0/266
Goodness-of-fit on F^2	1.033
Final R indexes [I>=2σ (I)]	R_1 = 0.0293, wR_2 = 0.0514
Final R indexes [all data]	R_1 = 0.0409, wR_2 = 0.0541
Largest diff. peak/hole / e Å^{-3}	2.63/-1.09

Complex 11

Table 1 Crystal data and structure refinement for Fi-92_a_pl.

Identification code	Fi-92_a_pl
Empirical formula	$C_{47}H_{44}Au_2Cl_2F_6N_2O_6$
Formula weight	1311.68
Temperature/K	100.15
Crystal system	monoclinic
Space group	$P2_1/n$
a/Å	9.0549(5)
b/Å	23.7874(14)
c/Å	21.0134(12)
α/°	90
β/°	99.6010(10)
γ/°	90
Volume/Å^3	4462.7(4)
Z	4
ϱ_{calc}g/cm^3	1.952
μ/mm^{-1}	6.764
F(000)	2536.0
Crystal size/mm^3	0.33 × 0.16 × 0.07
Radiation	MoKα (λ = 0.71073)
2Θ range for data collection/°	4.288 to 64.134
Index ranges	-13 ≤ h ≤ 13, -35 ≤ k ≤ 35, -31 ≤ l ≤ 31
Reflections collected	76829
Independent reflections	15566 [R_{int} = 0.0363, R_{sigma} = 0.0297]
Data/restraints/parameters	15566/0/617
Goodness-of-fit on F^2	1.020
Final R indexes [I>=2σ (I)]	R_1 = 0.0262, wR_2 = 0.0475
Final R indexes [all data]	R_1 = 0.0390, wR_2 = 0.0507
Largest diff. peak/hole / e Å^{-3}	1.50/-1.30

Complex 12

Table 1 Crystal data and structure refinement for FI-80_a_pl.

Identification code	FI-80_a_pl
Empirical formula	$C_{23}H_{25}AuF_3NO_3$
Formula weight	617.41
Temperature/K	100.15
Crystal system	monoclinic
Space group	$P2_1/c$
a/Å	8.6597(9)
b/Å	25.737(3)
c/Å	9.7108(10)
α/°	90
β/°	99.250(3)
γ/°	90
Volume/Å^3	2136.1(4)
Z	4
ϱ_{calc}g/cm^3	1.920
μ/mm^{-1}	6.938
F(000)	1200.0
Crystal size/mm^3	0.07 × 0.07 × 0.02
Radiation	MoKα (λ = 0.71073)
2Θ range for data collection/°	4.534 to 56.742
Index ranges	-11 ≤ h ≤ 11, -34 ≤ k ≤ 34, -12 ≤ l ≤ 12
Reflections collected	39145
Independent reflections	5331 [R_{int} = 0.0463, R_{sigma} = 0.0306]
Data/restraints/parameters	5331/0/282
Goodness-of-fit on F^2	1.329
Final R indexes [I>=2σ (I)]	R_1 = 0.0484, wR_2 = 0.0868
Final R indexes [all data]	R_1 = 0.0599, wR_2 = 0.0895
Largest diff. peak/hole / e Å^{-3}	3.13/-2.88

Complex 14

Table 1 Crystal data and structure refinement for FI-72-new_a_pl.

Identification code	FI-72-new_a_pl
Empirical formula	$C_{26}H_{25}AuF_3N_3O_3$
Formula weight	681.46
Temperature/K	100.15
Crystal system	monoclinic
Space group	$P2_1/n$
a/Å	7.7466(11)
b/Å	12.1649(16)
c/Å	27.101(4)
α/°	90
β/°	98.153(4)
γ/°	90
Volume/Å^3	2528.1(6)
Z	4
ρ_{calc}g/cm^3	1.790
μ/mm^{-1}	5.874
F(000)	1328.0
Crystal size/mm^3	0.21 × 0.04 × 0.01
Radiation	MoKα (λ = 0.71073)
2Θ range for data collection/°	4.52 to 50.754
Index ranges	$-9 \leq h \leq 9$, $-14 \leq k \leq 14$, $-32 \leq l \leq 32$
Reflections collected	39829
Independent reflections	4633 [R_{int} = 0.1008, R_{sigma} = 0.0659]
Data/restraints/parameters	4633/24/328
Goodness-of-fit on F^2	1.397
Final R indexes [I>=2σ (I)]	R_1 = 0.0674, wR_2 = 0.1163
Final R indexes [all data]	R_1 = 0.0893, wR_2 = 0.1205
Largest diff. peak/hole / e Å^{-3}	1.87/-3.43

Complex 15

Table 1 Crystal data and structure refinement for FI-70a_a_pl.

Identification code	FI-70a_a_pl
Empirical formula	$C_{24.67}H_{25.33}Au_{1.33}F_4N_{1.33}O_4$
Formula weight	743.09
Temperature/K	100.15
Crystal system	monoclinic
Space group	P2/c
a/Å	15.1382(8)
b/Å	12.1805(7)
c/Å	20.0502(11)
α/°	90
β/°	98.109(2)
γ/°	90
Volume/Å^3	3660.1(3)
Z	6
ϱ_{calc}g/cm^3	2.023
μ/mm^{-1}	8.086
F(000)	2136.0
Crystal size/mm^3	0.06 × 0.04 × 0.03
Radiation	MoKα (λ = 0.71073)
2Θ range for data collection/°	4.31 to 50.274
Index ranges	-18 ≤ h ≤ 18, -14 ≤ k ≤ 14, -23 ≤ l ≤ 23
Reflections collected	67318
Independent reflections	6519 [R_{int} = 0.0736, R_{sigma} = 0.0418]
Data/restraints/parameters	6519/0/482
Goodness-of-fit on F^2	1.143
Final R indexes [I>=2σ (I)]	R_1 = 0.0536, wR_2 = 0.1059
Final R indexes [all data]	R_1 = 0.0750, wR_2 = 0.1123
Largest diff. peak/hole / e Å^{-3}	3.32/-3.02

Complex 16

Table 1 Crystal data and structure refinement for FI-69-Cu_a_pl.

Identification code	FI-69-Cu_a_pl
Empirical formula	$C_{105}H_{86}Au_6F_{18}N_6O_{18}$
Formula weight	3243.62
Temperature/K	293(2)
Crystal system	monoclinic
Space group	$P2_1/c$
a/Å	10.2796(9)
b/Å	34.310(3)
c/Å	18.9669(19)
α/°	90
β/°	100.311(5)
γ/°	90
Volume/Å^3	6581.5(11)
Z	2
ϱ_{calc}g/cm^3	1.637
μ/mm^{-1}	12.957
F(000)	3075.0
Crystal size/mm^3	0.05 × 0.05 × 0.02
Radiation	CuKα (λ = 1.54178)
2Θ range for data collection/°	5.39 to 73.644
Index ranges	$-7 \leq h \leq 7$, $-26 \leq k \leq 26$, $-14 \leq l \leq 14$
Reflections collected	22031
Independent reflections	3152 [R_{int} = 0.0962, R_{sigma} = 0.0593]
Data/restraints/parameters	3152/0/324
Goodness-of-fit on F^2	1.112
Final R indexes [I>=2σ (I)]	R_1 = 0.1222, wR_2 = 0.3383
Final R indexes [all data]	R_1 = 0.1434, wR_2 = 0.3530
Largest diff. peak/hole / e Å^{-3}	1.62/-1.03

7 Bibliography

[1] A. P. Shaw, M. Tilset, R. H. Heyn, S. Jakobsen, *J. Coord. Chem.* **2011**, *64*, 38-47.
[2] E. Langseth, C. H. Gørbitz, R. H. Heyn, M. Tilset, *Organometallics* **2012**, *31*, 6567-6571.
[3] E. Langseth, M. L. Scheuermann, D. Balcells, W. Kaminsky, K. I. Goldberg, O. Eisenstein, R. H. Heyn, M. Tilset, *Angew. Chem., Int. Ed.* **2013**, *52*, 1660-1663.
[4] H. Schmidbaur, A. Schier, *Arabian J. Sci. Eng.* **2012**, *37*, 1187-1225.
[5] E. Langseth, PhD Thesis, University of Oslo **2014**.
[6] E. A. Tråseth, Master's Thesis, University of Oslo **2014**.
[7] E. Langseth, A. Nova, E. A. Tråseth, F. Rise, S. Øien, R. H. Heyn, M. Tilset, *J. Am. Chem. Soc.* **2014**, *136*, 10104-10115.
[8] K. Kenison Falkner, J. M. Edmond, *Earth and Planetary Science Letters* **1990**, *98*, 208-221.
[9] E. Riedel, C. Janiak, *Anorganische Chemie*, 7 ed., Walter de Gruyter, Berlin, **2007**.
[10] A. F. Holleman, E. Wiberg, N. Wiberg, *Lehrbuch der Anorganischen Chemie*, 102 ed., Walter de Gruyter, Berlin, **2007**.
[11] Y. Okinaka, M. Hoshino, *Gold Bull.* **1998**, *31*, 3-13.
[12] C. F. Shaw, III, *Chem. Rev.* **1999**, *99*, 2589-2600.
[13] I. Kostova, *Anti-Cancer Agents Med. Chem.* **2006**, *6*, 19-32.
[14] W. F. Kean, L. Hart, W. W. Buchanan, *Br. J. Rheumatol.* **1997**, *36*, 560-572.
[15] E. R. T. Tiekink, *Inflammopharmacology* **2008**, *16*, 138-142.
[16] D. Fan, C.-T. Yang, J. D. Ranford, J. J. Vittal, P. F. Lee, *Dalton Trans.* **2003**, 3376-3381.
[17] A. Casini, M. A. Cinellu, G. Minghetti, C. Gabbiani, M. Coronnello, E. Mini, L. Messori, *J. Med. Chem.* **2006**, *49*, 5524-5531.
[18] C. Bronner, O. S. Wenger, *Dalton Trans.* **2011**, *40*, 12409-12420.
[19] A. Stephen, K. Hashmi, G. J. Hutchings, *Angew. Chem., Int. Ed.* **2006**, *45*, 7896-7936.
[20] B. S. Takale, M. Bao, Y. Yamamoto, *Org. Biomol. Chem.* **2014**, *12*, 2005-2027.
[21] A. S. K. Hashmi, *Chem. Rev.* **2007**, *107*, 3180-3211.
[22] A. Arcadi, *Chem. Rev.* **2008**, *108*, 3266-3325.
[23] N. D. Shapiro, F. D. Toste, *Synlett* **2010**, 675-691.
[24] R. Skouta, C.-J. Li, *Tetrahedron* **2008**, *64*, 4917-4938.
[25] X. Zhang, F. X. Llabres i. Xamena, A. Corma, *J. Catal.* **2009**, *265*, 155-160.
[26] M. S. Kharasch, H. S. Isbell, *J. Am. Chem. Soc.* **1931**, *53*, 3053-3059.
[27] A. S. K. Hashmi, L. Schwarz, J.-H. Choi, T. M. Frost, *Angew. Chem., Int. Ed.* **2000**, *39*, 2285-2288.
[28] A. S. K. Hashmi, M. Rudolph, *Chem. Soc. Rev.* **2008**, *37*, 1766-1775.
[29] Y.-M. Wang, A. D. Lackner, F. D. Toste, *Acc. Chem. Res.* **2014**, *47*, 889-901.
[30] Z. Li, C. Brouwer, C. He, *Chem. Rev.* **2008**, *108*, 3239-3265.
[31] R. E. M. Brooner, R. A. Widenhoefer, *Angew. Chem., Int. Ed.* **2013**, *52*, 11714-11724.
[32] A. Corma, A. Leyva-Perez, M. J. Sabater, *Chem. Rev.* **2011**, *111*, 1657-1712.
[33] M. A. Cinellu, G. Minghetti, F. Cocco, S. Stoccoro, A. Zucca, M. Manassero, *Angew. Chem., Int. Ed.* **2005**, *44*, 6892-6895.
[34] M. Joost, L. Estevez, S. Mallet-Ladeira, K. Miqueu, A. Amgoune, D. Bourissou, *J. Am. Chem. Soc.* **2014**, *136*, 10373-10382.
[35] Y. Fukuda, K. Utimoto, *J. Org. Chem.* **1991**, *56*, 3729-3731.

[36] H. C. Shen, *Tetrahedron* **2008**, *64*, 3885-3903.
[37] M. Jia, M. Bandini, *ACS Catal.* **2015**, *5*, 1638-1652.
[38] S. Zhang, F. Wei, C. Song, J. Jia, Z. Xu, *Chin. J. Chem.* **2014**, *32*, 937-956.
[39] D. Wang, R. Cai, S. Sharma, J. Jirak, S. K. Thummanapelli, N. G. Akhmedov, H. Zhang, X. Liu, J. L. Petersen, X. Shi, *J. Am. Chem. Soc.* **2012**, *134*, 9012-9019.
[40] Y. Zhu, C. S. Day, L. Zhang, K. J. Hauser, A. C. Jones, *Chem. - Eur. J.* **2013**, *19*, 12264-12271.
[41] C. Obradors, A. M. Echavarren, *Chem. Commun.* **2014**, *50*, 16-28.
[42] S. Gaillard, J. Bosson, R. S. Ramon, P. Nun, A. M. Z. Slawin, S. P. Nolan, *Chem. - Eur. J.* **2010**, *16*, 13729-13740.
[43] C.-Y. Wu, T. Horibe, C. B. Jacobsen, F. D. Toste, *Nature* **2015**, *517*, 449-454.
[44] C.-Y. Zhou, P. W. H. Chan, C.-M. Che, *Org. Lett.* **2006**, *8*, 325-328.
[45] S. Trofimenko, *Inorg. Chem.* **1973**, *12*, 1215-1221.
[46] M. I. Bruce, *Angew. Chem.* **1977**, *89*, 75-89.
[47] J. Vicente, M. T. Chicote, M. D. Bermudez, *J. Organomet. Chem.* **1984**, *268*, 191-195.
[48] J. Vicente, M. T. Chicote, M. D. Bermudez, *Inorg. Chim. Acta* **1982**, *63*, 35-39.
[49] P. A. Bonnardel, R. V. Parish, R. G. Pritchard, *J. Chem. Soc., Dalton Trans.* **1996**, 3185-3193.
[50] W. Henderson, *Adv. Organomet. Chem.* **2006**, *54*, 207-265.
[51] M. Horvat, in *Trace Element Speciation for Environment, Food and Health*, Royal Society of Chemistry, **2001**.
[52] E. C. Constable, T. A. Leese, *J. Organomet. Chem.* **1989**, *363*, 419-424.
[53] A. P. Shaw, *Unpublished results*.
[54] M. A. Mansour, R. J. Lachicotte, H. J. Gysling, R. Eisenberg, *Inorg. Chem.* **1998**, *37*, 4625-4632.
[55] W. Henderson, B. K. Nicholson, S. J. Faville, D. Fan, J. D. Ranford, *J. Organomet. Chem.* **2001**, *631*, 41-46.
[56] J. Zhao, W. Yan, **2011**, 173-195.
[57] S. Caddick, R. Fitzmaurice, *Tetrahedron* **2009**, *65*, 3325-3355.
[58] M. A. Herrero, J. M. Kremsner, C. O. Kappe, *J. Org. Chem.* **2008**, *73*, 36-47.
[59] P. Lidstrom, J. Tierney, B. Wathey, J. Westman, *Tetrahedron* **2001**, *57*, 9225-9283.
[60] M. Larhed, C. Moberg, A. Hallberg, *Acc. Chem. Res.* **2002**, *35*, 717-727.
[61] S. M. Garringer, A. J. Hesse, J. R. Magers, K. R. Pugh, S. A. O'Reilly, A. M. Wilson, *Organometallics* **2009**, *28*, 6841-6844.
[62] N. Godbert, T. Pugliese, I. Aiello, A. Bellusci, A. Crispini, M. Ghedini, *Eur. J. Inorg. Chem.* **2007**, 5105-5111.
[63] A. Basak, K. Chakrabarty, A. Ghosh, G. K. Das, *J. Org. Chem.* **2013**, *78*, 9715-9724.
[64] R. Fang, L. Yang, Y. Wang, *Org. Biomol. Chem.* **2011**, *9*, 2760-2770.
[65] L.-P. Liu, G. B. Hammond, *Chem. Soc. Rev.* **2012**, *41*, 3129-3139.
[66] aD. Belli Dell'Amico, F. Calderazzo, R. Dantona, J. Straehle, H. Weiss, *Organometallics* **1987**, *6*, 1207-1210; bJ. A. Flores, H. V. R. Dias, *Inorg. Chem.* **2008**, *47*, 4448-4450; cT. N. Hooper, M. Green, J. E. McGrady, J. R. Patel, C. A. Russell, *Chem. Commun.* **2009**, 3877-3879; dT. J. Brown, B. D. Robertson, R. A. Widenhoefer, *J. Organomet. Chem.* **2014**, *758*, 25-28.
[67] H. Schmidbaur, A. Schier, *Organometallics* **2010**, *29*, 2-23.
[68] N. Savjani, D.-A. Rosca, M. Schormann, M. Bochmann, *Angew. Chem., Int. Ed.* **2013**, *52*, 874-877.
[69] M. Chiarucci, M. Bandini, *Beilstein J. Org. Chem.* **2013**, *9*, 2586-2614.

[70] C. E. Rezsnyak, J. Autschbach, J. D. Atwood, S. Moncho, *J. Coord. Chem.* **2013**, *66*, 1153-1165.
[71] R. L. La Londe, W. E. Brenzovich, Jr., D. Benitez, E. Tkatchouk, K. Kelley, W. A. Goddard, III, F. D. Toste, *Chem. Sci.* **2010**, *1*, 226-233.
[72] F. Rekhroukh, R. Brousses, A. Amgoune, D. Bourissou, *Angew. Chem., Int. Ed.* **2015**, *54*, 1266-1269.
[73] M. S. Holmsen, *Unpublished results* **2014**.
[74] Y. Wencke, *Unpublished results* **2014**.
[75] D. Walther, T. Dohler, K. Heubach, O. Klobes, B. Schweder, H. Gorls, *Z. Anorg. Allg. Chem.* **1999**, *625*, 923-932.
[76] A. Behr, U. Freudenberg, W. Keim, *J. Mol. Catal.* **1986**, *35*, 9-17.
[77] J. Clayden, N. Greeves, S. Warren, P. Wothers, *Organic Chemistry*, 1 ed., Oxford University Press, New York, **2001**.
[78] D. L. Pavia, G. M. Lampman, G. S. Kriz, J. A. Vyvyan, *Introduction to Spectroscopy*, 4 ed., Brooks/Cole, Belmont, **2009**.
[79] M. J. Frisch, G. W. Trucks, H. B. Schlegel, G. E. Scuseria, M. A. Robb, J. R. Cheeseman, G. Scalmani, V. Barone, B. Mennucci, G. A. Petersson, H. Nakatsuji, M. Caricato, X. Li, H. P. Hratchian, A. F. Izmaylov, G. Z. J. Bloino, J. L. Sonnenberg, M. E. M. Hada, K. Toyota, R. Fukuda, J. Hasegawa, M. Ishida, T. Nakajima, Y. Honda, O. Kitao, H. Nakai, T. Vreven, J. J. A. Montgomery, J. E. Peralta, F. Ogliaro, M. Bearpark, J. J. Heyd, E. Brothers, K. N. Kudin, V. N. Staroverov, R. Kobayashi, J. Normand, K. Raghavachari, A. Rendell, J. C. Burant, S. S. Iyengar, J. Tomasi, M. Cossi, N. Rega, J. M. Millam, M. Klene, J. E. Knox, J. B. Cross, V. Bakken, C. Adamo, J. Jaramillo, R. Gomperts, R. E. Stratmann, O. Yazyev, A. J. Austin, R. Cammi, C. Pomelli, J. W. Ochterski, R. L. Martin, K. Morokuma, V. G. Zakrzewski, P. S. G. A. Voth, J. J. Dannenberg, S. Dapprich, A. D. Daniels, Ö. Farkas, J. B. Foresman, J. V. Ortiz, J. Cioslowski, D. J. Fox, in *Gaussian 09, Revision D.01*, Gaussian, Inc., Wallingford CT, **2009**.
[80] This work was performed on the Abel Cluster, owned by the University of Oslo and the Norwegian metacenter for High Performance Computing (NOTUR), and operated by the Research Computing Services group at USIT, the University of Oslo IT-department. http://www.hpc.uio.no/.
[81] A. D. McLean, G. S. Chandler, *J. Chem. Phys.* **1980**, *72*, 5639-5648.
[82] R. Krishnan, J. S. Binkley, R. Seeger, J. A. Pople, *J. Chem. Phys.* **1980**, *72*, 650-654.
[83] D. Figgen, G. Rauhut, M. Dolg, H. Stoll, *Chem. Phys.* **2005**, *311*, 227-244.
[84] W. Koch, M. C. Holthausen, *A Chemist's Guide to Density Functional Theory*, Wiley-VCH Verlag GmbH, **2001**.
[85] A. Bondi, *J. Phys. Chem.* **1964**, *68*, 441-451.
[86] P. De Frémont, N. M. Scott, E. D. Stevens, S. P. Nolan, *Organometallics* **2005**, *24*, 2411-2418.
[87] J. Vicente, M. T. Chicote, M. I. Lozano, S. Huertas, *Organometallics* **1999**, *18*, 753-757.
[88] M. A. Cinellu, F. Cocco, G. Minghetti, S. Stoccoro, A. Zucca, M. Manassero, *J. Organomet. Chem.* **2009**, *694*, 2949-2955.